2014

The odd power of dispersion

Peng Xu
Iowa State University

The odd power of dispersion

by

Peng Xu

A dissertation submitted to the graduate faculty

in partial fulfillment of the requirements for the degree of

DOCTOR OF PHILOSOPHY

Major: Physical Chemistry

Program of Study Committee:
Mark S. Gordon, Major Professor
Theresa L. Windus
Jacob W. Petrich
Klaus Schmidt-Rohr
Monica H. Lamm

Iowa State University

Ames, Iowa

2014

Dedicated to my parents,

Ziming and Lingling,

and to my love, Dapeng Jing

TABLE OF CONTENTS

CHAPTER 1 GENERAL INTRODUCTION

Overview

In ancient China, water has been regarded as one of the five vital components of life. It has been observed that water has many fascinating properties: water is 'soft' yet it can penetrate a hard rock; water is 'pure' yet it can tolerate other beings. Because of its unique properties, water is often associated with good quality and has been given the highest praise by Laozi in his book *Tao Te Ching* saying: the highest/best quality that one can have is being like water. However, little did people understand why and how water possesses such fascinating properties.

Modern scientific developments made people realize that the macroscopic liquid water is made of a large number of water molecules held together via a network of hydrogen bonds. And those wonderful properties of water are merely the macroscopic manifestations of the interactions between water molecules and other molecules. For example, the dissolving ability of water is due to the fact that the interaction between a water molecule and the other molecular species is stronger than the interactions among their own molecular species. In fact the interactions between any two molecules are governed by the same physics and are termed intermolecular interaction (or intermolecular forces in some literature, although technically 'force' is incorrect usage here).

Although the very existence of the intermolecular interactions is easily proved, e.g. the mere presence of the solid phase of matter, and scientists today have recognized

that the seemingly weak intermolecular interactions essentially hold the world together through a delicate and cooperative process, the theoretical understanding of various intermolecular interactions is still far from satisfactory. On the practical side, theoreticians need to balance computational cost and accuracy. Because of the relatively small magnitudes of the intermolecular interactions, errors that appear tiny compared to the usual chemical (covalent) bonding may change conclusions qualitatively. High-level *ab initio* methods including explicit description of electron correlation can achieve the desired accuracy at very high computational cost. (Chapter 5 and 6) However the cooperative network of hundreds of thousands of molecules that reflects the true power of intermolecular interactions cannot be modeled easily by *ab initio* methods. Deeper understanding of intermolecular interactions yields better theoretical models; better theoretical models facilitate and even deepen the understanding of intermolecular interactions. With the aforementioned motivation in mind, a significant portion of this dissertation is dedicated to developing a method to describe the intermolecular interactions accurately with affordable computational resources. (Chapter 2-4)

Dissertation Organization

This introduction chapter builds the foundation of *ab initio* methods and briefly describes the theoretical methods employed in the following chapters including an overview of the effective fragment potential method (EFP). Chapter 2 presents the development and implementation of using the valence virtual orbitals (VVOs) in place of canonical virtual orbitals for the charge transfer interaction and its gradient between two EFP fragments (EFP-EFP). Chapter 3 provides a detailed derivation and implementation of the R^{-7} term of the dispersion energy expansion using dipole-dipole and dipole-

quadrupole localized molecular orbital (LMO) dynamic polarizabilities over the imaginary frequency range in the framework of EFP. Chapter 4 derives the fully analytic gradient of the approximated QM-EFP exchange repulsion energy between the *ab initio* molecule and EFP fragment (QM-EFP). Extensive code modification on the previous implementation of QM-EFP exchange repulsion Fock operator and energy is made to allow the presence of multiple EFP fragments. Chapter 5 explores the application of a local correlation coupled cluster approach, cluster-in-molecules (CIM) to study the anionic water clusters in the range of 4 – 20 water molecules. Chapter 6 studies the temperature effect on the binding enthalpies between SiH_4 and three boron containing compounds and realizes the importance of outer core correlation in obtaining accurate energies and structures.

Theoretical Background

Time-Dependent Schrödinger Equation

Quantum mechanics provides the laws of motion for microscopic particles. Schrödinger postulated the dynamical equation that governs the time evolution of the system in 1926, known as the time-dependent Schrödinger equation[1–5].

$$-\frac{\hbar}{i}\frac{\partial \Psi(\mathbf{r},t)}{\partial t} = \hat{\mathrm{H}}\Psi(\mathbf{r},t) = (\mathbf{T}+\mathbf{V})\Psi(\mathbf{r},t) \qquad (1)$$

The Hamiltonian operator **H** is given as a sum of kinetic and potential energy operators (for low-velocity particles, i.e. non-relativistic). The solution of the time-dependent Schrödinger equation is a function of time and position called a wave function. The wave function Ψ contains all of the information about the system. The probability of observing a particle at position **r** and time t is given as the square of the wave function.

This is a fundamental difference between classical mechanics and quantum mechanics, because classical mechanics is deterministic while quantum mechanics is probabilistic.

For systems in which the potential energy operator is time-independent, the Hamiltonian becomes time-independent. When acting on the wave function, the Hamiltonian yields the total energy of the system.

$$\hat{\mathrm{H}}\Psi(\mathbf{r},t) = \mathrm{E}\Psi(\mathbf{r},t) = -\frac{\hbar}{i}\frac{\partial\Psi(\mathbf{r},t)}{\partial t} \qquad (2)$$

Time-Independent Schrödinger Equation

The non-relativistic, time-independent Schrödinger Equation can be written as

$$\hat{\mathrm{H}}\Phi(\mathbf{r}) = \mathrm{E}\Phi(\mathbf{r}) \qquad (3)$$

where $\hat{\mathrm{H}}$ is the Hamiltonian operator. In atomic units, it is defined as

$$H = -\sum_{A=1}^{M}\frac{1}{2M_A}\nabla_A^2 - \sum_{i=1}^{N}\frac{1}{2}\nabla_i^2 - \sum_{i=1}^{N}\sum_{A=1}^{M}\frac{Z_A}{r_{iA}} + \sum_{i=1}^{N}\sum_{j>i}^{N}\frac{1}{r_{ij}} + \sum_{A=1}^{M}\sum_{B>A}^{M}\frac{Z_A Z_B}{R_{AB}} \qquad (4)$$

Where M_A is the ratio of the mass of nucleus A to the mass of an electron and Z_A is the atomic number of the nucleus A. The systems of electrons and nuclei are described by their position vectors $\mathbf{r}_i$ and $\mathbf{R}_A$, respectively. Then the distance between electron i and nucleus A is $r_{iA} = |\mathbf{r}_i - \mathbf{R}_A|$, the distance between electrons i and j is $r_{ij} = |\mathbf{r}_i - \mathbf{r}_j|$ and the distance between nuclei A and B is $R_{AB} = |\mathbf{R}_A - \mathbf{R}_B|$. The first two terms in Eq. (4) represent the operators for the kinetic energy of the nuclei and electrons, respectively. The third term is the Coulomb attraction between nuclei and electrons. The last two terms represent the repulsion between electrons and between nuclei, respectively. Φ is the total wave function describing a collection of charged particles, nuclei and electrons. It is a

function of electronic and nuclear coordinates, $\Phi\left(\{\mathbf{r}_i\},\{\mathbf{R}_A\}\right)$, where $\{\mathbf{r}_i\}$ and $\{\mathbf{R}_A\}$ represent the collection of electronic and nuclear coordinates in the system, respectively.

Born-Oppenheimer Approximation[6]

Since nuclei are so much heavier than electrons, the nuclei move much slower than electrons. To a good approximation, electrons can be considered to move in a field of fixed nuclei. Two consequences immediately follow: the nuclear kinetic energy is zero and the repulsion energy between the nuclei is a constant. The remaining terms in Eq. (4) are defined as the electronic Hamiltonian.

$$\hat{H}_{elec} = -\sum_{i=1}^{N}\frac{1}{2}\nabla_i^2 - \sum_{i=1}^{N}\sum_{A=1}^{M}\frac{Z_A}{r_{iA}} + \sum_{i=1}^{N}\sum_{j>i}^{N}\frac{1}{r_{ij}} \qquad (5)$$

The eigenvalue solution to the electronic Hamiltonian is the electronic wave function, which describes the motion of electrons for a fixed nuclear configuration.

$$\hat{H}_{elec}\,\Phi_{elec}\left(\{\mathbf{r}_i\};\{\mathbf{R}_A\}\right) = E_{elec}\Phi_{elec}\left(\{\mathbf{r}_i\};\{\mathbf{R}_A\}\right) \qquad (6)$$

The electronic wave functions obtained by solving Eq. (6) depend explicitly on the electronic coordinates and parametrically on the nuclear coordinates.

Invoking the same approximation, one could solve the nuclear wave function: since electrons move so much faster than the nuclei, the nuclei "feel" the electrons in an averaged field. The nuclear Hamiltonian then becomes

$$\begin{aligned} H &= -\sum_{A=1}^{M}\frac{1}{2M_A}\nabla_A^2 + \left\langle -\sum_{i=1}^{N}\frac{1}{2}\nabla_i^2 - \sum_{i=1}^{N}\sum_{A=1}^{M}\frac{Z_A}{r_{iA}} + \sum_{i=1}^{N}\sum_{j>i}^{N}\frac{1}{r_{ij}}\right\rangle + \sum_{A=1}^{M}\sum_{B>A}^{M}\frac{Z_A Z_B}{R_{AB}} \\ &= -\sum_{A=1}^{M}\frac{1}{2M_A}\nabla_A^2 + E_{elec}\left(\{\mathbf{R}_A\}\right) + \sum_{A=1}^{M}\sum_{B>A}^{M}\frac{Z_A Z_B}{R_{AB}} \end{aligned} \qquad (7)$$

The second and third terms of Eq. (7) together constitute the potential energy operator for the nuclei. This is a significant consequence of Born-Oppenheimer approximation: it is possible to define the "shape" of a molecule and describe how the energy of the molecule changes as the shape of the molecule changes, i.e. moving on a potential energy surface. The concepts of equilibrium geometries such as minima and transition states become meaningful.

By solving the nuclear Schrödinger equation,

$$\hat{H}_{nuc}\,\Phi_{nuc}\left(\{\mathbf{R}_A\}\right) = E_{nuc}\Phi_{nuc}\left(\{\mathbf{R}_A\}\right) \qquad (8)$$

the motions of the nuclei, vibration and rotation, can be described.

Under the premise of the Born-Oppenheimer approximation, the problem of solving the Schrödinger equation is reduced to solving the electronic Schrödinger equation for a fixed nuclear configuration and is what all the *ab initio* methods described below aim for.

For systems with more than one electron an exact analytic solution of the Schrödinger equation is not possible because the electron-electron repulsion term is inseparable. Various approximations must be made to get around this problem.

Variational Theorem

Another important theorem is the variational theorem, which states that for a system whose Hamiltonian is time-independent and whose lowest-energy eigenvalue is E_0, if Φ is any normalized, well-behaved function that satisfies the appropriate boundary conditions, then

$$\int \Phi^{*}\,\hat{H}\,\Phi\,d\tau \geq E_0 \qquad (9)$$

The integral in Eq. (9) is called the variational integral. The better the trial function is, the lower the values of the variational integral and closer to the true ground state energy E_0.

Antisymmetry Principle

Electrons are fermions, hence they obey antisymmetry principle, which states that a many-electron wave function must be antisymmetric with respect to interchange of any two electrons. The simplest example would be a two-electron system and, to satisfy antisymmetry principle, the total wave function Φ, expressed in terms of one-electron wave functions ψ, is in the form,

$$\Phi(\mathbf{r}_1, \mathbf{r}_2) = 2^{-1/2}\left[\psi_1(\mathbf{r}_1)\psi_2(\mathbf{r}_2) - \psi_1(\mathbf{r}_2)\psi_2(\mathbf{r}_1)\right] \qquad (10)$$

Eq. (10) can be cast into a determinant called a Slater determinant, and this can be generalized to an N-electron wave function. This single determinant wave function is an approximation to the exact wave function.

Hartree-Fock Method

The Hartree-Fock (HF) method[7–10] is (for closed shell species) a single determinant method that solves the approximate time-independent Schrödinger equation in a self-consistent manner. The approximate wave function is the single determinant formed from a set of occupied spin orbitals, χ_i

$$\Phi = |\chi_1\chi_2\cdots\chi_N\rangle \qquad (11)$$

The energy of this approximate wave function is calculated as the expectation value of the Hamiltonian operator, provided the wave function is normalized.

$$E = \langle\Phi|H|\Phi\rangle \qquad (12)$$

The determinantal form of the wave function gives rise to an exchange term in the energy expression,

$$E = \sum_{i}^{N} h_i + \frac{1}{2}\sum_{i}^{N}\sum_{j}^{N}\left(J_{ij} - K_{ij}\right) + V_{NN} \tag{13}$$

where i and j run over all of the electrons in the system, and the factor of 1/2 accounts for the double counting of electron pairs. The variational theorem tells us that the "best" wave function, or the best set of occupied MOs is the one that makes the energy a minimum, that is, the variation of the energy with respect to a change in the MOs is zero, with the constraint that the MOs remain orthonormal. Such a constrained optimization can be facilitated by the Lagrange method of undetermined multipliers.

$$\begin{aligned} L &= \langle \Phi \mid H \mid \Phi \rangle - \sum_{ij}^{N} \varepsilon_{ij}\left[\left(\chi_i \mid \chi_j\right) - \delta_{ij}\right] \\ &= E_0\left[\{\chi_i\}\right] - \sum_{ij}^{N} \varepsilon_{ij}\left[\left(\chi_i \mid \chi_j\right) - \delta_{ij}\right] \end{aligned} \tag{14}$$

where $\Phi = \left|\chi_1\chi_2\cdots\chi_i\chi_j\cdots\chi_N\right\rangle$ is the single determinant formed from N occupied spin orbitals. The energy $E_0 = \langle \Phi \mid H \mid \Phi \rangle$ is a functional of the spin orbitals $\{\chi_i\}$. ε_{ij} is the Lagrange multiplier. This procedure leads to the HF equations

$$f(1)\chi_i(1) = \varepsilon_i \chi_i(1) \tag{15}$$

where ε is the orbital energy and f is the Fock operator, which (for closed shells) is defined (in terms of spin orbitals) to be

$$f(1) = h(1) + v^{HF}(1) = h(1) + \sum_{j=1}^{N}\left[J(1) - K(1)\right] \tag{16}$$

The Fock operator is an effective one-electron energy operator, with $h(1)$ describing the kinetic energy of an electron and its attraction to the nuclei, and $v^{HF}(1)$ describing the repulsion to all the other electrons in an averaged way. J and K are the Coulomb and exchange operators, respectively. Their effects when operating on a spin orbital are

$$J_j(1)\chi_i(1) = \left[\int d\mathbf{r}_2 \chi_j^*(2) r_{12}^{-1} \chi_j(2)\right]\chi_i(1) \tag{17}$$

$$K_j(1)\chi_i(1) = \left[\int d\mathbf{r}_2 \chi_j^*(2) r_{12}^{-1} \chi_i(2)\right]\chi_j(1) \tag{18}$$

where the spin orbital takes the form $\chi(\mathbf{r},\omega) = \varphi(\mathbf{r})\alpha(\omega) or \varphi(\mathbf{r})\beta(\omega)$. Note that the Coulomb and exchange operators have a functional dependence on the solutions of the Fock operator and hence Eq. (15) is nonlinear and must be solved iteratively.

LCAO-MO approximation (Basis Set approximation)

A set of basis functions is introduced to expand the spin orbitals.

$$\chi_i = \sum_\mu C_{\mu i}\phi_\mu \tag{19}$$

This turns solving the HF equation into solving a matrix equation for the expansion coefficients. The spin orbital χ_i would be exactly represented by the expansion of Eq. (19) if the basis set was complete (infinite in dimension). The energy obtained would then be the HF limit. In practice, a calculation can utilize only a finite number of basis functions. Typically, the larger the basis set, the better the trial wave function as it has more flexibility during the self-consistent iterations.

At the beginning of self-consistent iterations, an initial guess of orbitals is made from which the density is obtained. The Fock matrix is formed from the core-

Hamiltonian matrix and the two-electron integral matrix. Diagonalization of the Fock matrix leads to a new set of orbitals. The process repeats until the density obtained from new orbitals agrees with the previous density within a certain threshold.

The general HF equation is written in terms of molecular spin orbitals that contain a spin function and a spatial orbital. Restricted HF (RHF) wave functions contain pairs of electrons, and each pair has the same spatial part but opposite spin functions. RHF is used for closed-shell system. For open-shell systems, the restricted open-shell HF (ROHF) method forces the spatial part of the doubly occupied orbitals to be the same. If there is no restriction on the spatial orbitals that are occupied by electrons of different spins, the trial wave function is an unrestricted HF (UHF) wave function.

By using a single determinant form of the wave function, the instantaneous electron-electron repulsion is replaced by an average interaction. The missing electron correlation energy, although small (~1% of the total energy), is extremely important for describing chemical phenomena. In addition, the restricted form of the wave function simply cannot describe the dissociation process into open-shell fragments while the unrestricted wave function does not produce accurate results. Despite its limitations, the HF wave function is the best single-determinant trial wave function within a given basis set and is the starting point for more accurate approximations.

Post-Hartree Fock methods

Various methods have been developed in an effort of recovering the dynamic correlation energy. Although the configuration interaction method is not used in this thesis, it is briefly mentioned in order to define the correlation energy.

Configuration Interaction (CI)[11,12]

The HF wave function, the determinant formed from the N lowest-energy orbitals, is the simplest electronic representation of the ground state wave function that is antisymmetric. Other so-called excited determinants that are formed from the solutions of the HF equation represent the configurations with promotion of electrons from some occupied to virtual orbitals. Conceptually, the true wave function is likely to result from the interaction of several electronic configurations and mixing those excited determinants allows more variational flexibility in the wave function. The set of HF determinants and all the excited determinants can serve as a basis to expand the exact ground state many-electron wave function, Φ_0.

$$\left|\Phi_0\right\rangle = c_0\left|\Psi_0\right\rangle + \sum_{ar} c_a^r \left|\Psi_a^r\right\rangle + \sum_{\substack{a<b \\ r<s}} c_{ab}^{rs}\left|\Psi_{ab}^{rs}\right\rangle + \sum_{\substack{a<b<c \\ r<s<t}} c_{abc}^{rst}\left|\Psi_{abc}^{rst}\right\rangle + \ldots \qquad (20)$$

This is the form of the full CI ground state wave function. Here a, b, c etc. denote occupied orbitals and r, s, t etc. denote virtual orbitals. Ψ_0 is the HF determinant, and Ψ_a^r is a singly excited determinant differing from Ψ_0 by exciting the electron in ψ_a to ψ_r. The restriction on the summation ensures that each excited determinant is included only once.

If the AO basis is complete, so is the basis of determinants. Then full CI would give the exact energies of all the electronic states. At finite basis, full CI provides the upper bound for that basis. The (dynamic) correlation energy is defined as the difference between the exact energy and the HF energy

$$E_{corr} = E_{FCI} - E_{HF} \qquad (21)$$

Except for a few very small systems, full CI is practically intractable. Therefore truncation at single and double excitation in Eq. (20) is common.

Perturbation Theory

The basic idea behind perturbation theory is that knowing how to treat a simple system and given that the real system is not too different from the simple system, one can treat the real/more complex system mathematically as a perturbed simple system. The commonly used second-order Möller-Plesset perturbation theory (MP2) is the application of a more general formalism called Rayleigh-Schrödinger perturbation theory (RSPT) to many-body systems. Since the Effective Fragment Potential Method (which constitutes the bulk of this thesis) is formulated in the framework of Rayleigh-Schrödinger perturbation theory (RSPT), RSPT will be briefly mentioned for later discussion.

Rayleigh-Schrödinger Perturbation Theory (RSPT)

The full Hamiltonian H is the sum of the unperturbed Hamiltonian H_0 and the perturbation V, where the solution to H_0 is known: $H_0|\Psi_i\rangle = E_i^{(0)}|\Psi_i\rangle$. To solve the eigenvalue problem $H|\Phi_i\rangle = E_i|\Phi_i\rangle$, one introduces an ordering parameter λ and expands the eigenvalues and eigenfunctions in terms of $E_i^{(n)}$ and $\Psi_i^{(n)}$ in a Taylor series of λ.

$$E_i = E_i^{(0)} + \lambda E_i^{(1)} + \lambda^2 E_i^{(2)} + \ldots \quad (22)$$

$$|\Phi_i\rangle = |\Psi_i^{(0)}\rangle + \lambda|\Psi_i^{(1)}\rangle + \lambda^2|\Psi_i^{(2)}\rangle + \ldots \quad (23)$$

$E_i^{(n)}$ and $|\Psi_i^{(n)}\rangle$ are called the n-th order energy and n-th order wave function, respectively.

By choosing intermediate normalization, $\left\langle \Psi_i^{(0)} \middle| \Phi_i \right\rangle = 1$, and expanding $\left| \Psi_i^{(1)} \right\rangle$ in the basis of the eigenfunctions of H_0, $\left| \Psi_i^{(1)} \right\rangle = \sum_n c_n^{(1)} \left| \Psi_n^{(0)} \right\rangle$, the first three order of energies can be expressed as:

$$E_i^{(0)} = \left\langle \Psi_i^{(0)} \middle| H_0 \middle| \Psi_i^{(0)} \right\rangle \tag{24}$$

$$E_i^{(1)} = \left\langle \Psi_i^{(0)} \middle| V \middle| \Psi_i^{(0)} \right\rangle \tag{25}$$

$$E_i^{(2)} = \left\langle \Psi_i^{(0)} \middle| V \middle| \Psi_i^{(1)} \right\rangle = \sum_{n \neq i} \frac{\left\langle \Psi_i^{(0)} \middle| V \middle| \Psi_n^{(0)} \right\rangle \left\langle \Psi_n^{(0)} \middle| V \middle| \Psi_i^{(0)} \right\rangle}{E_i^{(0)} - E_n^{(0)}} \tag{26}$$

Möller-Plesset Perturbation Theory (MPPT)[13]

MPPT is the application of RSPT to the many-body problem. H_0 is a sum of the Fock operators

$$H_0 = \sum_i f_i = \sum_i \left(h(i) + v^{HF}(i) \right) \tag{27}$$

In Eq. (27), i sums over the electrons in the system. Hence the perturbation V is

$$V = \sum_{i<j} r_{ij}^{-1} - \sum_i v^{HF}(i) \tag{28}$$

When the HF wave function is used as the zeroth order wave function, E^0+E^1 recovers the HF energy. The correction to the HF energy starts at the second-order, MP2. MP2 typically accounts for 80-90% of the correlation energy and is widely used for its efficiency and adaptivity on parallel computer systems. Since the Hamiltonian used is not exact, perturbation theory is not variational. Hence higher order energy corrections do not always guarantee a lowering of the energy.

Coupled-Cluster Theory (CC)[14–16]

Like configuration interaction (CI), CC expresses the wave function as a sum of the HF determinant and all other excited determinants. This correlated wave function is obtained by allowing a series of excitation operators T_n to act on the HF wave function.

$$\Phi = \left(1 + T + \frac{T^2}{2!} + \frac{T^3}{3!} + ...\right)\Psi^{HF} = e^T \Psi^{HF} \tag{29}$$

And the cluster operator T is

$$T = T_1 + T_2 + T_3 + ... + T_n \tag{30}$$

where T_1 is the single electron excitation operator and T_2 is the double electron excitation operator, and so on. When T_i acts on an HF reference wave function, all excited determinants are generated.

$$T_1 \Psi^{HF} = \sum_{i}^{occ} \sum_{a}^{vir} t_i^a \Psi_i^a \tag{31}$$

$$T_2 \Psi^{HF} = \sum_{i<j}^{occ} \sum_{a<b}^{vir} t_{ij}^{ab} \Psi_{ij}^{ab} \tag{32}$$

where the expansion coefficients t are called amplitudes.

If all of the cluster operators up to T_n are included in T, the CC wave function will be equivalent to full CI. A full CC computation is impossible except for very small systems. It is therefore common to use a truncated cluster operator that includes only singles and doubles (CCSD) and the triples contribution computed by perturbation theory (CCSD(T)).

Solvation Method

The aforementioned *ab initio* methods become computationally intractable when dealing with the solvation problem due to steep scaling with the system size. Two classes of approaches have been developed to circumvent this problem. One class is called the continuum or implicit solvation. These methods represent the bulk solvent by some dielectric parameters and interact with the solute via this pre-defined electric field. The advantage of such methods is that they attempt to describe the bulk solvation in a computationally inexpensive manner. However they lack the explicit solvent-solute interactions. Insightful understanding of structures, properties and reaction mechanism relies on accurate description of solvent-solute interaction. The other class of methods called the discrete or explicit solvation methods are developed for this reason. Note that all the *ab initio* methods treat solvent molecules explicitly. However the explicit solvation methods usually refer to those that approximate each solvent molecule as a perturbative potential for the solute molecules. Most explicit solvent methods contain some parameters that are obtained by fitting to experiment or high-level *ab initio* calculation; TIP3P would be an example of such potential[17].

Effective Fragment Potential Method (EFP)

The Effective Fragment Potential method (EFP) has been developed by Gordon and coworkers for the past two decades or so to study intermolecular interactions, including solvation. The EFP method is designed to accurately and efficiently describe the interaction between molecules. Detailed descriptions of EFP can be found in many papers[18–23] (including Chapters 2-4 in this dissertation). The following paragraphs present the framework within which EFP is built.

Consider a system of two weakly interacting molecules ($A \cdots B$), the unperturbed Hamiltonian is the sum of the individual Hamiltonian.

$$H_0 = H_A + H_B \tag{33}$$

Assuming the electron densities of the two molecules do not overlap, the 0th order wave function is the Hartree product of the wave functions of isolated A and B. This is the so-called long-range approximation.

$$\Psi^{(0)} = \Psi_0^A \Psi_0^B \tag{34}$$

The perturbation V is the electronic interaction between the electrons and nuclei in the two molecules. Then the zeroth order energy is just the sum of the energies of isolated A and B. Three types of intermolecular interaction arises as the first and second order perturbation energy:

$$E^{(1)} = \left\langle \Psi^{(0)} \middle| V \middle| \Psi^{(0)} \right\rangle = \left\langle \Psi_0^A \middle| \left\langle \Psi_0^B \middle| V \middle| \Psi_0^A \right\rangle \middle| \Psi_0^B \right\rangle \tag{35}$$

$$\begin{aligned} E^{(2)} = & \sum_{m\neq 0} \frac{\left\langle \Psi_0^A \middle| \left\langle \Psi_0^B \middle| V \middle| \Psi_m^A \right\rangle \middle| \Psi_0^B \right\rangle}{\left(E_0^A + E_0^B\right) - \left(E_m^A + E_0^B\right)} + \sum_{n\neq 0} \frac{\left\langle \Psi_0^A \middle| \left\langle \Psi_0^B \middle| V \middle| \Psi_0^A \right\rangle \middle| \Psi_n^B \right\rangle}{\left(E_0^A + E_0^B\right) - \left(E_0^A + E_n^B\right)} \\ & + \sum_{m\neq 0} \sum_{n\neq 0} \frac{\left\langle \Psi_0^A \middle| \left\langle \Psi_0^B \middle| V \middle| \Psi_m^A \right\rangle \middle| \Psi_n^B \right\rangle}{\left(E_0^A + E_0^B\right) - \left(E_m^A + E_n^B\right)} \end{aligned} \tag{36}$$

Eq. (35) is just the classical coulomb interaction. The first two terms of the 2nd-order perturbation energy gives the induction/polarization energy, arising from promoting molecule A to excited state m **or** promoting molecule B to excited state n. The last term corresponds to the dispersion energy when both A and B are excited. Since the overlap between the two molecules is assumed to be negligible, the excited states of individual molecules result from mixing their own virtual orbitals. The interaction operator V can be

represented as multipole-multipole interactions. In EFP, distributed multipole expansions developed by Stone [24,25] are used.

As two molecules approach, the long-range approximation starts to break down. Instead of reformulating all three above-mentioned interactions, damping functions have been developed as short-range corrections for these three interactions. In addition, two types of interaction arise at short range. Exchange repulsion and charge transfer interaction emerge as additional first- and second-order interactions, respectively, when using antisymmetrized product of wave functions for the cluster AB.

The initial implementation of EFP is for water only (EFP1)[18]. The intermolecular interaction between molecules is partitioned into three components: Coulomb interaction, induction and a remainder repulsive term. The Coulomb interaction is computed according to Stone's distributed multipole analysis[24,25], with the expansion truncated at octopole and the expansion centers at the atom centers and bond midpoints. The induction term is computed using the static anisotropic localized molecular orbital (LMO) dipole polarizability tensor. The dipole induced by the total electric field of all other molecules/fragments is iterated to self-consistency, incorporating many-body effect into the model. The remainder term is determined by fitting to water potential calculated either with Hartree-Fock or density functional theory (B3LYP functional[26,27]). This empirically determined remainder term prevents EFP1 from easy generalization to other solvent types.

The second implementation, EFP2, also known in the literature as the general effective fragment potential method has been developed for any closed-shell molecule. The interaction between molecules in EFP2 is partitioned into five terms: Coulomb

interaction, polarization, dispersion, exchange repulsion and charge transfer. The coulomb and polarization terms are identical to EFP1. The dispersion is modeled using the dynamic dipole polarizability tensor over imaginary frequency range. In this dissertation, R^{-7} dispersion interaction is developed using the dynamic anisotropic dipole-quadrupole polarizability tensor over the imaginary frequency range. The exchange repulsion is derived from a power expansion of the intermolecular overlap truncated at the second order. The charge transfer interaction is obtained from a second-order perturbative treatment, using the same power expansion of the intermolecular overlap but truncated at the first order.

References

(1) Schrodinger, E. Quantisation as an Eigen Value Problem. *Ann. Phys.* **1926**, *79*, 361.

(2) Schrodinger, E. Quantisation as an Eigen-Value Problem. *Ann. Phys.* **1926**, *79*, 489–527.

(3) Schrodinger, E. On the Connection of Heisenberg-Born-Jordan's Quantum Mechanics with Mine. *Ann. Phys.* **1926**, *79*, 734–756.

(4) Schrodinger, E. Quantification of the Eigen Value Problem. *Ann. Phys.* **1926**, *80*, 437–490.

(5) Schrodinger, E. Quantization as a Problem of Eigenvalue. *Ann. Phys.* **1926**, *81*, 109.

(6) Born, M.; Oppenheimer, R. Quantum Theory of the Molecules. *Ann. der Phys. (Berlin, Ger.* **1927**, *84*, 457–484.

(7) Hartree, D. R. The Wave Mechanics of an Atom with a Non-Coulomb Central Field. I. Theory and Methods. *Proc. Camb. Philol. Soc.* **1928**, *24*, 89–110.

(8) Hartree, D. R. The Wave Mechanics of an Atom with a Non-Coulomb Central Field. II. Some Results and Discussion. *Proc. Camb. Philol. Soc.* **1928**, *24*, 111–132.

(9) Hartree, D. R. Wave Mechanics of an Atom with a Non-Coulomb Central Field. III. Term Values and Intensities in Series in Optical Spectra. *Proc. Camb. Philol. Soc.* **1928**, *24*, 426–437.

(10) Fock, V. "Self-Consistent Field" with Interchange for Sodium. *Zeitschrift fuer Phys.* **1930**, *62*, 795–805.

(11) Shavitt, I. The Method of Configuration Interaction. *Mod. Theor. Chem.* **1977**, *3*, 189–275.

(12) Sherrill, C. D.; Schaefer III., H. F. The Configuration Interaction Method: Advances in Highly Correlated Approaches. *Adv. Quantum Chem.* **1999**, *34*, 143–269.

(13) Moller, C.; Plesset, M. S. Note on the Approximation Treatment for Many-Electron Systems. *Phys. Rev.* **1934**, *46*, 618–622.

(14) Raghavachari, K.; Trucks, G. W.; Pople, J. A.; Head-Gordon, M. A Fifth-Order Perturbation Comparison of Electron Correlation Theories. *Chem. Phys. Lett.* **1989**, *157*, 479–483.

(15) Piecuch, P.; Kucharski, S. A.; Kowalski, K.; Musial, M. Efficient Computer Implementation of the Renormalized Coupled-Cluster Methods: The R-CCSD[T], R-CCSD(T), CR-CCSD[T], and CR-CCSD(T) Approaches. *Comput. Phys. Commun.* **2002**, *149*, 71–96.

(16) Wloch, M.; Gour, J. R.; Piecuch, P. Extension of the Renormalized Coupled-Cluster Methods Exploiting Left Eigenstates of the Similarity-Transformed Hamiltonian to Open-Shell Systems: A Benchmark Study. *J. Phys. Chem. A* **2007**, *111*, 11359–11382.

(17) Jorgensen, W. L.; Chandrasekhar, J.; Madura, J. D.; Impey, R. W.; Klein, M. L. Comparison of Simple Potential Functions for Simulating Liquid Water. *J. Chem. Phys.* **1983**, *79*, 926–935.

(18) Day, P. N.; Jensen, J. H.; Gordon, M. S.; Webb, S. P.; Stevens, W. J.; Krauss, M.; Garmer, D.; Basch, H.; Cohen, D. An Effective Fragment Method for Modeling Solvent Effects in Quantum Mechanical Calculations. *J. Chem. Phys.* **1996**, *105*, 1968–1986.

(19) Jensen, J. H.; Gordon, M. S. An Approximate Formula for the Intermolecular Pauli Repulsion between Closed Shell Molecules. *Mol. Phys.* **1996**, *89*, 1313–1325.

(20) Adamovic, I.; Gordon, M. S. Dynamic Polarizability, Dispersion Coefficient C6 and Dispersion Energy in the Effective Fragment Potential Method. *Mol. Phys.* **2005**, *103*, 379–387.

(21) Li, H.; Gordon, M. S.; Jensen, J. H. Charge Transfer Interaction in the Effective Fragment Potential Method. *J. Chem. Phys.* **2006**, *124*, 214108/1–214108/16.

(22) Smith, Q. A.; Ruedenberg, K.; Gordon, M. S.; Slipchenko, L. V. The Dispersion Interaction between Quantum Mechanics and Effective Fragment Potential Molecules. *J. Chem. Phys.* **2012**, *136*, 244107/1–244107/12.

(23) Xu, P.; Gordon, M. S. Charge Transfer Interaction Using Quasiatomic Minimal-Basis Orbitals in the Effective Fragment Potential Method. *J. Chem. Phys.* **2013**, *139*, 194104/1–194104/11.

(24) Stone, A. J. Distributed Multipole Analysis, or How to Describe a Molecular Charge Distribution. *Chem. Phys. Lett.* **1981**, *83*, 233–239.

(25) Stone, A. J.; Alderton, M. Distributed Multipole Analysis Methods and Applications. *Mol. Phys.* **1985**, *56*, 1047–1064.

(26) Lee, C.; Yang, W.; Parr, R. G. Development of the Colle-Salvetti Correlation-Energy Formula into a Functional of the Electron Density. *Phys. Rev. B Condens. Matter Mater. Phys.* **1988**, *37*, 785–789.

(27) Becke, A. D. Density-Functional Thermochemistry. III. The Role of Exact Exchange. *J. Chem. Phys.* **1993**, *98*, 5648–5652.

CHAPTER 2 CHARGE TRANSFER INTERACTION USING QUASIATOMIC MINIMAL-BASIS ORBITALS IN THE EFFECTIVE FRAGMENT POTENTIAL METHOD

A paper published in

Journal of Chemical Physics **2013**, *139*, 194104

Peng Xu and Mark S. Gordon

Abstract

The charge transfer (CT) interaction, the most time-consuming term in the general effective fragment potential (EFP) method, is made much more computationally efficient. This is accomplished by the projection of the quasiatomic minimal-basis-set orbitals (QUAMBOs) as the atomic basis onto the self-consistent field (SCF) virtual molecular orbital (MO) space to select a subspace of the full virtual space called the valence virtual space. The diagonalization of the Fock matrix in terms of QUAMBOs recovers the canonical occupied orbitals and more importantly, gives rise to the valence virtual orbitals (VVOs). The CT energies obtained using VVOs are generally as accurate as those obtained with the full virtual space canonical MOs because the QUAMBOs span the valence part of the virtual space, which can generally be regarded as 'chemically important'. The number of QUAMBOs is the same as the number of minimal-basis molecular orbitals (MOs) of a molecule. Therefore, the number of VVOs is significantly

smaller than the number of canonical virtual MOs, especially for large atomic basis sets. This leads to a dramatic decrease in the computational cost.

Introduction

Modeling intermolecular interactions accurately and efficiently has been a target of computational chemistry for decades. Intermolecular interactions play an important role in determining the structures and consequently the properties of molecular systems that have physical, chemical, and biological significance. For example it is essentially the hydrogen-bonding pattern between the nucleotide bases that enables the correct transcription and translation processes in expressing a protein.[1] The dispersion interaction among the stacking nucleotide bases provides a significant portion of the stabilization.[2,3] Protein structures are ultimately the result of chemical and intermolecular interactions between the amino acids.[1] High-level *ab initio* methods that include dynamic electron correlation can provide accurate descriptions of all of the contributions to intermolecular interactions, including Coulomb, induction/polarization, exchange repulsion, dispersion, and charge transfer interactions. Unfortunately, such correlated methods are very computationally demanding. For example, second order perturbation theory (MP2) and coupled cluster theory with singe, double, and perturbative triple excitations, CCSD(T), scale as N^5 and N^7, respectively, where N is the number of basis functions. Consequently, such methods quickly become prohibitive for large systems, unless approximations are introduced.

Chemistry is often carried out in a solvent. A fundamental understanding of how solvent molecules interact with solutes and with each other can provide molecular-level insights about how chemical phenomena occur. In order to capture explicit solvent effects

one frequently needs to include a large number of solvent molecules, more than is practicable for correlated *ab initio* methods. One therefore needs to develop methods that are more efficient and at the same time retain the accuracy of the correlated methods. Implicit solvent methods circumvent these scaling problems, but at the expense of omitting explicit solute-solvent interactions, such as hydrogen bonding.

The effective fragment potential (EFP) method is an explicit solvent method[4,5]. The original EFP implementation, called EFP1,[5] was designed solely for water. The components of the EFP1 potential are the Coulomb interaction, the induction/polarization interaction, and a remainder term. The Coulomb interaction is modeled using the Stone distributed multipole analysis (DMA) method [6,] expanded through octopoles, where the expansion points are the atom centers and the bond midpoints. The polarization interaction is modeled with localized molecular orbital (LMO) polarizability tensors on individual bonds and lone pairs of electrons and is iterated to self-consistency. The iterative process incorporates many-body effects into the model. The remainder term is fitted to the water dimer potential calculated either with Hartree-Fock (HF) or density functional theory (DFT, with the B3LYP functional[7]). For EFP1/HF, the remainder term includes exchange repulsion and charge transfer. In the EFP1/DFT method the remainder term also includes some correlation effects.

The general EFP implementation, often called EFP2, has no empirically fitted parameters and is therefore applicable to any (closed shell) molecular species. The components of the EFP2 method are: Coulomb, induction/polarization, dispersion, exchange repulsion and charge transfer. Each of these intermolecular interactions is derived from first principles, based on truncated expansions. The Coulomb and induction

interactions are the same as in EFP1. The exchange repulsion interaction is derived from a power expansion in the intermolecular overlap, truncated at the second order, expressed in terms of LMOs.[8] The dispersion interaction is modeled with LMO dynamic (imaginary frequency) polarizability tensors obtained from time-dependent Hartree-Fock calculations.[9] The charge transfer interaction term is obtained using a second-order perturbative treatment, and is also derived based on an expansion in the intermolecular overlap, neglecting second and higher order terms.[10] All of the required EFP2 input parameters are generated in one *ab initio* preparative calculation on the isolated individual molecule. There is no empirical parameterization and EFP2 can be systematically improved by including higher order terms in the expansions. In the following, EFP2 will be called, simply, EFP.

The charge transfer (CT) interaction may be defined as the energy stabilization due to the mixing of the occupied orbitals of one molecule with the virtual orbitals of another molecule. The CT interaction can be important in ionic and polar molecular systems such as water.[11] Previously the CT energy and gradient between two EFP fragments were derived and implemented using a perturbative approach with SCF canonical molecular orbitals (CMOs) (both occupied and virtual orbitals).[10] The CT interaction is the most time-consuming part of an EFP calculation, mainly due to the large number of canonical virtual orbitals when reliable basis sets are used. The goal of the present work is to present a new implementation that decreases the number of virtual orbitals used in the calculation, while retaining the accuracy of the original method. This goal is accomplished by making use of the quasiatomic minimal-basis-set orbitals (QUAMBOs), a localized orbital-based method developed by Ruedenberg and co-

workers.[12] QUAMBOs may be thought of as the virtual orbital complement of the valence occupied space of a molecule. They therefore provide a natural set of virtual orbitals with which to determine the majority of the charge transfer interaction energy.

The reduced variational space (RVS) method is an energy decomposition analysis algorithm proposed by Stevens and Fink[13] which is closely related to the commonly used Kitaura-Morokuma (KM) energy decompoisition analysis (EDA)[14]. Both analyses partition the interaction energy, at the Hartree-Fock level of theory, into electrostatic/Coulomb, polarization, exchange and charge transfer components. It has been demonstrated that the RVS interaction energy components are better behaved than their counterparts in the KM analysis when the orbital interactions are strong.[13] This is because the corresponding wave function from which the RVS component energies are obtained is antisymmetrized. Since the EFP-EFP CT formula is also derived using the antisymmetrized wave function as the zeroth order wave function, the numerical results from EFP and RVS are comparable. RVS CT results serve as benchmark numbers in this study.

This paper is organized as follows. The derivation of the EFP charge transfer energy and gradients has been described in a previous paper in detail[10] and is only briefly summarized here in Sec. II A. The formulation of QUAMBOs is also detailed in another paper[12] and is only briefly described in Sec II B. The computational methodology used in this study is summarized in Sec. III A. Numerical results are discussed in Sec III B. Conclusions are drawn in Sec IV.

Theory

A. EFP2 Charge transfer interaction

The detailed derivation of the EFP-EFP charge transfer energy and gradient was presented in a previous paper[10] using a second-order perturbative treatment with CMOs. The key steps and important approximations in the derivation are summarized here.

The starting point is the expression for the energy of a closed-shell molecule M with nonorthogonal molecular orbitals:

$$E_M = 2\sum_{i}^{occM}\sum_{k}^{occM} h_{ik}S^{-1}_{ik} + \sum_{i}^{occM}\sum_{k}^{occM} S^{-1}_{ik}\sum_{r}^{occM}\sum_{s}^{occM}(2\langle ik|rs\rangle - \langle ir|ks\rangle)S^{-1}_{rs} + E^{nuc} \qquad (1)$$

where i, k, r and s are the occupied orbitals of molecule M (thus, the upper limit occM on the summations). h_{ik} is a one-electron integral, 2<ik|rs>-<ir|ks> are the two-electron integrals, S is the matrix of overlap integrals, and E^{nuc} is the nuclear repulsion energy. The molecular orbitals can be non-orthogonal and non-normalized but they are linearly independent.

Next, using the definition[15]

$$S^{-1} = I - P \qquad (2)$$

and substituting Eq (2) into Eq (1), one obtains

$$\begin{aligned} E_M &= 2\sum_{i}^{occM}\sum_{k}^{occM} h_{ik}\left(\delta_{ik} - P^M_{ik}\right) \\ &+ \sum_{i}^{occM}\sum_{k}^{occM}\left(\delta_{ik} - P^M_{ik}\right)\times\sum_{r}^{occM}\sum_{s}^{occM}\left(2\langle ik|rs\rangle - \langle ir|ks\rangle\right)\left(\delta_{rs} - P^M_{rs}\right) + E^{nuc} \end{aligned} \qquad (3)$$

Now, to approach the intermolecular interaction in a perturbative manner, suppose two weakly interacting molecules A and B form a supermolecule; then the zero-order

wave function, $\Psi^{(0)}$, for the supermolecule is the antisymmetrized product wave function formed from wave functions that describe A and B.

Let H be the full Hamiltonian, including the perturbation. Then the zeroth + first order energy is:

$$\begin{aligned} E_{AB}^{(0)} + E_{AB}^{(1)} &= \left\langle \Psi^{(0)} \middle| H \middle| \Psi^{(0)} \right\rangle \\ &= 2\sum_{i}^{occAB}\sum_{k}^{occAB} h_{ik}^{AB}\left(\delta_{ik} - P_{ik}^{AB}\right) \\ &+ \sum_{i}^{occAB}\sum_{k}^{occAB}\left(\delta_{ik} - P_{ik}^{AB}\right)\sum_{r}^{occAB}\sum_{s}^{occAB}\left(2\langle ik|rs\rangle - \langle ir|ks\rangle\right)\left(\delta_{rs} - P_{rs}^{AB}\right) + E^{nuc} \end{aligned} \tag{4}$$

where the indices i, k, r and s represent the occupied MOs of isolated A and B.

$E_{AB}^{(0)}$ and $E_{AB}^{(1)}$ are the zeroth- and first-order energies of the system. h^{AB} includes the electron kinetic energy plus the electron-nuclear attraction from both molecules:

$$h^{AB} = T + V^{nucA} + V^{nucB} \tag{5}$$

The superscript AB on P means that the overlap matrix used to define the P matrix is the overlap matrix of the supermolecule AB. If the orbitals are normalized, the diagonal elements of the overlap matrix are unity and one can separate the off-diagonal part of the matrix:

$$\tilde{S} = S - I \tag{6}$$

Then, the P matrix can be expanded in terms of $\tilde{S}$:

$$P = I - S^{-1} = I - (I + \tilde{S})^{-1} = I - (I - \tilde{S} + \tilde{S}^2 - \tilde{S}^3 + \ldots) = \tilde{S} - \tilde{S}^2 + \tilde{S}^3 - \ldots \tag{7}$$

For those off-diagonal elements in which both orbitals belong to the same molecule, the leading term in the expansion is the quadratic power of S because the orbitals within the same molecule are orthogonal. Suppose both i and k are MOs on atom A,

$$P_{ik}^{AB} = \tilde{S}_{ik} - (\tilde{S}^2)_{ik} + (\tilde{S}^3)_{ik} - \ldots \approx -(\tilde{S}^2)_{ik} = -\sum_r^{occA} \tilde{S}_{ir}\tilde{S}_{rk} - \sum_j^{occB} \tilde{S}_{ij}\tilde{S}_{jk}$$
$$= -\sum_j^{occB} \tilde{S}_{ij}\tilde{S}_{jk} = -\sum_j^{occB} (S_{ij} - I_{ij})(S_{jk} - I_{jk}) \qquad (8)$$
$$= -\sum_j^{occB} S_{ij}S_{jk}$$

If the two indices are from different molecules, the leading term of P contains the first power of S.

$$P_{ij}^{AB} = \tilde{S}_{ij} - (\tilde{S}^2)_{ij} + (\tilde{S}^3)_{ij} - \ldots \approx \tilde{S}_{ij} - \sum_k^{occA} \tilde{S}_{ik}\tilde{S}_{kj} - \sum_l^{occB} \tilde{S}_{il}\tilde{S}_{lj}$$
$$= \tilde{S}_{ij} = (S_{ij} - I_{ij}) = S_{ij} \qquad (9)$$

The original EFP charge transfer formula resulted from truncating the 2nd and higher order powers of S in the expansion of P.

Now, let i, k, r and s be the occupied MOs of A and j, l, t and w be the occupied MOs of B. Substituting Eqs (8) and (9) into Eq (4) gives

$$E_{AB}^{(0)} + E_{AB}^{(1)} \approx 2\sum_i^{occA}\sum_k^{occA} h_{ik}^{AB}\delta_{ik} - 2\sum_i^{occA}\sum_j^{occB} h_{ij}^{AB}S_{ij} - 2\sum_j^{occB}\sum_k^{occA} h_{jk}^{AB}S_{jk} + 2\sum_j^{occB}\sum_l^{occB} h_{jl}^{AB}\delta_{jl}$$
$$+\sum_i^{occA}\sum_k^{occA}\delta_{ik}\left[\begin{array}{l}\sum_r^{occA}\sum_s^{occA}\left(2\langle ik|rs\rangle - \langle ir|ks\rangle\right)\delta_{rs} + \sum_t^{occB}\sum_w^{occB}\left(2\langle ik|tw\rangle - \langle it|kw\rangle\right)\delta_{tw} \\ -\sum_r^{occA}\sum_w^{occB}\left(2\langle ik|rw\rangle - \langle ir|kw\rangle\right)S_{rw} - \sum_t^{occB}\sum_s^{occA}\left(2\langle ik|ts\rangle - \langle it|ks\rangle\right)S_{ts}\end{array}\right]$$
$$+\sum_j^{occB}\sum_l^{occB}\delta_{jl}\left[\begin{array}{l}\sum_r^{occA}\sum_s^{occA}\left(2\langle jl|rs\rangle - \langle jr|ls\rangle\right)\delta_{rs} + \sum_t^{occB}\sum_w^{occB}\left(2\langle jl|tw\rangle - \langle jt|lw\rangle\right)\delta_{tw} \\ -\sum_r^{occA}\sum_w^{occB}\left(2\langle jl|rw\rangle - \langle jr|lw\rangle\right)S_{rw} - \sum_t^{occB}\sum_s^{occA}\left(2\langle jl|ts\rangle - \langle jt|ls\rangle\right)S_{ts}\end{array}\right]$$
$$-\sum_i^{occA}\sum_l^{occB} S_{il}\left[\sum_r^{occA}\sum_s^{occA}\left(2\langle il|rs\rangle - \langle ir|ls\rangle\right)\delta_{rs} + \sum_t^{occB}\sum_w^{occB}\left(2\langle il|tw\rangle - \langle it|lw\rangle\right)\delta_{tw}\right]$$
$$-\sum_j^{occB}\sum_k^{occA} S_{jk}\left[\sum_r^{occA}\sum_s^{occA}\left(2\langle jk|rs\rangle - \langle jr|ks\rangle\right)\delta_{rs} + \sum_t^{occB}\sum_w^{occB}\left(2\langle jk|tw\rangle - \langle jt|kw\rangle\right)\delta_{tw}\right] + E^{nuc}$$

(10)

Let $\Psi^{(1)} = \Psi^{(0)} + \Psi'$ where Ψ' is the first order correction to the zeroth order wavefunction $\Psi^{(0)}$:

The second order perturbation energy is then obtained as

$$E_{AB}^{(2)} = \left\langle \Psi^{(0)} \middle| H \middle| \Psi^{(1)} \right\rangle - \left\langle \Psi^{(0)} \middle| H \middle| \Psi^{(0)} \right\rangle \quad (11)$$

By definition, the energy lowering when the occupied MOs of A mix with the virtual MOs of B is referred to as the charge transfer energy of A due to B. The first-order perturbed wavefunction of one molecule is obtained by mixing in the virtual MOs of the other molecule. For example, the first-order perturbed MO i on molecule A is

$$\Psi_i^{A(1)} = \Psi_i^{A(0)} + \sum_n^{virB} U_{in} \Psi_n^{B(0)} \quad (12)$$

where U is the mixing coefficient matrix.

Substituting Eq (12) into Eq (10) and collecting the energy changes due to the mixing from virtual orbitals of B, one obtains the change transfer energy of A due to B. Note that if both the bra and ket wavefunctions are from molecule A, only one of them is perturbed (e.g., see Eq. 11). In this paper, $\Psi_i^{A(0)}$ and $\Psi_r^{A(0)}$ are conveniently chosen to be perturbed to $\Psi_i^{A(1)}$ and $\Psi_r^{A(1)}$. $\Psi_k^{A(0)}$ and $\Psi_s^{A(0)}$ are unperturbed.

Combining the contributions to the energy change from each term in Eq. (10) and splitting the one-electron operator h^{AB} into the kinetic energy operator and the nuclear attraction operators from A and B, the CT energy of molecule A due to the presence of B is

$$CT^{A(B)} = 2\sum_{i}^{occA}\sum_{n}^{virB} U_{in}\left[T_{in} + V_{in}^{nucA} + \sum_{k}^{occA}\left(2\langle in|kk\rangle - \langle ik|nk\rangle\right) + V_{in}^{nucB} + \sum_{j}^{occB}\left(2\langle in|jj\rangle - \langle ij|nj\rangle\right)\right]$$
$$-2\sum_{i}^{occA}\sum_{n}^{virB} U_{in}\sum_{j}^{occB}\left[T_{nj} + V_{nj}^{nucB} + \sum_{l}^{occB}\left(2\langle nj|ll\rangle - \langle nl|jl\rangle\right) + V_{nj}^{nucA} + \sum_{k}^{occA}\left(2\langle nj|kk\rangle - \langle nk|jk\rangle\right)\right]S_{ij} \tag{13}$$

Further simplification includes

$$T_{nj} + V_{nj}^{nucB} + \sum_{l}^{occB}\left(2\langle nj|ll\rangle - \langle nl|jl\rangle\right) = F_{nj}^{B} = 0, \quad n \in virB,\ j \in occB \tag{14}$$

where n and j belong to the virtual and occupied orbitals of molecule B, respectively. This is because, for CMOs, the off-diagonal elements of the Fock operator are zero. Likewise,

$$T_{in} + V_{in}^{nucA} + \sum_{k}^{occA}\left(2\langle in|kk\rangle - \langle ik|nk\rangle\right) = F_{in}^{A} = 0, \quad i \in occA,\ n \in virB \tag{15}$$

In Eq. (15), i is an index for the MOs of A and $\Psi_n^{B(0)}$ is assumed to be orthogonal to all the MOs of A. This is enforced by the following approximate orthonormalization procedure

$$\Phi_n^{B(0)} = \frac{1}{\sqrt{1-\sum_{m}^{allA}\left(S_{nm}\right)^2}}\left(\Psi_n^{B(0)} - \sum_{m}^{allA} S_{nm}\Psi_m^{A(0)}\right), \quad n \in virB \tag{16}$$

where Φ is the MO after orthonormalization. To simplify Eq. (14) further, two sets of approximations can be applied. The first set [Eqs. (17) and (18)] neglects the exchange integrals and approximates the Coulomb integrals with the multipole expansion as the electrostatic potential of the molecule, truncated at the quadrupole:

$$V_{in}^{nucB} + \sum_{j}^{occB}\left(2\langle in|jj\rangle - \langle ij|nj\rangle\right) \approx V_{in}^{nucB} + \sum_{j}^{occB} 2\langle in|jj\rangle \approx V_{in}^{EFB}, \quad i \in occA,\ n \in virB \tag{17}$$

$$V_{nj}^{nucA} + \sum_{k}^{occA}\left(2\langle nj|kk\rangle - \langle nk|jk\rangle\right) \approx V_{nj}^{nucA} + \sum_{k}^{occA} 2\langle nj|kk\rangle \approx V_{nj}^{EFA}, \quad n \in virB,\ j \in occB \tag{18}$$

The superscripts EFA and EFB represent the potentials of molecules A and B, respectively, described by a distributed multipole expansion. The other possible set of approximations [Eqs.(19) and (20)] set the Fock matrix to zero if the two indices are either from different molecules (Eq. (19)) or from the occupied and virtual orbitals of the same molecule (Eq. (20)).

$$V_{in}^{nucB} + \sum_{j}^{occB} \left(2\langle in|jj\rangle - \langle ij|nj\rangle \right) = F_{in}^{B} - T_{in} \approx -T_{in}, \quad i \in occA,\ n \in virB \tag{19}$$

$$V_{nj}^{nucA} + \sum_{k}^{occA} \left(2\langle nj|kk\rangle - \langle nk|jk\rangle \right) = F_{nj}^{A} - T_{nj} \approx -T_{nj}, \quad n \in virB,\ j \in occB \tag{20}$$

Different combinations of Eqs (17)-(20) can result in four possible formulae (see Appendix). Previously, it was demonstrated that the combination of Eqs (17) and (20) gives the most accurate numerical results when compared with values obtained from a reduced variational space (RVS) analysis.[10,13] When the valence virtual orbitals (see Section IIB) are used, numerical tests show that this combination still gives the best results (see Appendix).

Applying Eqs. (17) and (20) to Eq. (13) results in

$$CT^{A(B)} = 2\sum_{i}^{occA}\sum_{n}^{virB} U_{in}\left(V_{in}^{EFB} + \sum_{j}^{occB} T_{nj} S_{ij} \right) \tag{21}$$

The mixing coefficient matrix element U_{in} is approximated as[10]

$$U_{in} \approx \frac{\left\langle \Psi_i^{A(0)} \middle| V^{EFB} \middle| \Psi_n^{B(0)} \right\rangle}{\varepsilon_i^A - \varepsilon_n^A} = \frac{\left\langle \Psi_i^{A(0)} \middle| V^{EFB} \middle| \Psi_n^{B(0)} \right\rangle}{F_{ii}^A - F_{nn}^A}, \quad i \in occA,\ n \in virB \tag{22}$$

In Eq. (22) V^{EFB} is the multipole potential defined in Eq (17). ε_i^A is the orbital energy of Ψ_i^A, which equals the corresponding diagonal element of the Fock matrix, F_{ii}^A. ε_n^A, on

the other hand, is the orbital energy of Ψ_n^B when it is assumed to be orthonormal to the virtual MOs of molecule A (enforced by Eq. (16)). ε_n^A can also be written as a Fock matrix element, F_{nn}^A, in an analogous manner:

$$F_{nn}^A = T_{nn} + V_{nn}^{nucA} + \sum_i^{occA} \left(2\langle nn|ii\rangle - \langle ni|ni\rangle \right) = T_{nn} + V_{nn}^{EFA} - \sum_i^{occA} \langle ni|ni\rangle, \quad n \in vir.\, B \tag{23}$$

The last equality in Eq. (23) is obtained using Eq. (18). It is important to realize that F_{nn}^A is not related to F_{nn}^B. The latter is the orbital energy of ψ_n^B determined by diagonalizing the Fock matrix of isolated B. Therefore F_{nn}^A is not a quantity that can be obtained from the preparative *ab initio* calculation on the isolated molecule that is used to construct an EFP. Since ψ_n and ψ_i are from different molecules, the exchange term $\langle ni|ni\rangle$ and the potential energy due to the multipole charge distribution on fragment A, V_{nn}^{EFA}, in Eq. (23) are relatively small and can be neglected. ($F_{nn}^A \approx T_{nn}$) Numerical tests were done previously to justify this approximation.[10] Hence the final form for the mixing coefficient matrix U is

$$U_{in} \approx \frac{V_{in}^{EFB}}{F_{ii}^A - T_{nn}} \tag{24}$$

Combining Eqs. (21) and (24) and replacing ψ_n^B with Eq. (16), one obtains the final form of the charge transfer energy expression as

$$CT^{A(B)} = 2\sum_i^{occA}\sum_n^{virB} \frac{1}{1-\sum_m^{allA}(S_{nm})^2} \times \frac{V_{in}^{EFB} - \sum_m^{allA} S_{nm} V_{im}^{EFB}}{\left(F_{ii}^A - T_{nn}\right)} \times \left[V_{in}^{EFB} - \sum_m^{allA} S_{nm} V_{im}^{EFB} + \sum_j^{occB} S_{ij} \left(T_{nj} - \sum_m^{allA} S_{nm} T_{mj} \right) \right] \tag{25}$$

where $CT^{A(B)}$ is the CT energy of A induced by B.

Similarly, the CT energy of B induced by A is

$$CT^{B(A)} = 2\sum_{j}^{occB}\sum_{m}^{virA}\frac{1}{1-\sum_{n}^{allB}\left(S_{nm}\right)^2}\times\frac{V_{jm}^{EFA}-\sum_{n}^{allB}S_{nm}V_{jn}^{EFA}}{\left(F_{jj}^{B}-T_{mm}\right)} \times\left[V_{jm}^{EFA}-\sum_{n}^{allB}S_{nm}V_{jn}^{EFA}+\sum_{i}^{occA}S_{ij}\left(T_{mi}-\sum_{n}^{allB}S_{nm}T_{ni}\right)\right] \quad (26)$$

Since the final CT energy formulation is unaltered by the use of the quasiatomic minimal-basis-set orbitals, the expression for the gradient remains unchanged from the one that was derived previously.[10]

B. QUAMBOs and Valence Virtual Orbitals (VVOs)

Quasiatomic minimal-basis-set orbitals (QUAMBOs), developed by Ruedenberg and coworkers,[12] have the following attributes: (i) the number of QUAMBOs equals the number of minimal basis set molecular orbitals for the system. (ii) the QUAMBOs deviate minimally from the minimal basis set orbitals of the corresponding free atoms of that system. Thus QUAMBOs can be viewed as slightly deformed minimal basis atomic orbitals. (iii) The formulation of QUAMBOs is independent of the atomic basis sets used.

The projection of the QUAMBOs onto the SCF virtual space selects a subspace, called the virtual valence space, which yields a good approximation to the most important correlating orbitals. The most time-consuming part of an EFP CT calculation is the computation of the one-electron potential terms. Fundamentally, the bottleneck is the huge number of canonical virtual orbitals compared to the number of occupied orbitals. Hence, the motivation for using QUAMBOs as the basis for EFP-EFP charge transfer calculations is the expectation that the dramatically reduced number of virtual orbitals

will diminish the cost of a CT calculation significantly while these chemically important "valence virtual orbitals" (VVOs) can capture most of the CT interaction.

The full description of QUAMBOs is given in reference 12. A summary of how QUAMBOs are constructed is given here.

The free-atom minimal basis atomic orbital A_j^* can be expressed in terms of the occupied and virtual SCF MOs:

$$A_j^* = \sum_n^{occ} \phi_n a_{nj}^* + \sum_v^{vir} \phi_v a_{vj}^* \tag{27}$$

where $a_{nj}^* = \langle \phi_n | A_j^* \rangle$ and $a_{vj}^* = \langle \phi_v | A_j^* \rangle$

Note that the * here does not represent complex conjugate, but is merely a symbol to distinguish the free-atom minimal basis atomic orbitals from QUAMBOs.

The QUAMBO A_j can be similarly expanded as

$$A_j = \sum_n^{occ} \phi_n a_{nj} + \sum_v^{vir} \phi_v a_{vj} \tag{28}$$

$$\text{with } a_{nj} = \langle \phi_n | A_j \rangle \text{ and } a_{vj} = \langle \phi_v | A_j \rangle . \tag{29}$$

For both the free-atom minimal basis orbitals, A_j^* and QUAMBOs, A_j, the index j runs from 1 to M, with M being the total number of minimal basis set valence atomic orbitals in the molecule. One can write M = N + P, where P is the number of virtual valence orbitals. The M-dimensional space spanned by the QUAMBOs must also be spanned by the N occupied SCF MOs plus the appropriate number (P) of orbitals in the V-dimensional SCF virtual space. Calling these virtual orbitals φ_p, QUAMBO A_j can be expressed in terms of the SCF occupied MOs and these φ_p:

$$A_j = \sum_{n}^{occ} \phi_n a_{nj} + \sum_{p}^{val.vir} \varphi_p b_{pj} \tag{30}$$

and

$$\varphi_p = \sum_{v}^{vir} \phi_v T_{vp} \tag{31}$$

In Eq. (30) p goes up to the number of minimal basis set virtual orbitals, which equals the number of the VVO, P.

The QUAMBO A_j is constructed in such a way that it deviates as little as possible from the free-atom minimal basis atomic orbital A_j^*. This corresponds to minimizing the square deviation[12]

$$\left\langle A_j - A_j^* \middle| A_j - A_j^* \right\rangle = 2\left[1 - \left\langle A_j \middle| A_j^* \right\rangle\right] = 2\left[1 - \left(D_j\right)^{1/2}\right] \tag{32}$$

where $D_j = \sum_{n}^{occ} \left\langle \phi_n \middle| A_j^* \right\rangle^2 + \sum_{p}^{val.vir} \left\langle \varphi_p \middle| A_j^* \right\rangle^2$ (33)

with the normalization condition $\left\langle A_j \middle| A_j \right\rangle = 1$ and $\left\langle A_j^* \middle| A_j^* \right\rangle = 1$

A constrained Lagrange minimization leads to

$$A_j = D_j^{-1/2} \left\{ \sum_{n}^{occ} \phi_n \left\langle \phi_n \middle| A_j^* \right\rangle + \sum_{p}^{val.vir} \varphi_p \left\langle \varphi_p \middle| A_j^* \right\rangle \right\} \tag{34}$$

So, the QUAMBOs are the normalized projection of the free-atom minimal-basis atomic orbitals A^* onto the space spanned by the SCF MOs. Combining Eqs. (34), (29) and (31), one obtains

$$\begin{aligned} A_j &= \sum_{n=1}^{occ} (D_j^{-1/2} \left\langle \phi_n \middle| A_j^* \right\rangle) \phi_n + \sum_{p=1}^{val.vir} D_j^{-1/2} \sum_{v}^{vir} \phi_v T_{vp} \left\langle \sum_{w}^{vir} \phi_w T_{wp} \middle| A_j^* \right\rangle \\ &= \sum\nolimits_n \left(D_j^{-1/2} a_{nj}^* \right) \phi_n + \sum\nolimits_v \sum\nolimits_w \left(\sum\nolimits_p D_j^{-1/2} T_{vp} T_{wp} \right) \left\langle \phi_w \middle| A_j^* \right\rangle \phi_v \\ &= \sum\nolimits_n a_{nj}^{'} \phi_n + \sum\nolimits_v a_{vj}^{'} \phi_v \end{aligned} \tag{35}$$

To find a'_{nj} and a'_{vj} requires the determination of the expansion coefficient matrix T. The simultaneous minimization of the quantity in Eq (32) for all QUAMBOs is equivalent to maximizing the sum

$$\sum_{j}^{\min basis} D_j = \sum_j \left[\sum_{n}^{occ} \left\langle \phi_n \middle| A_j^* \right\rangle^2 + \sum_{p}^{val.vir} \left\langle \varphi_p \middle| A_j^* \right\rangle^2 \right] \tag{36}$$

Eq. (36) is ultimately achieved by maximizing the sum over the φ_p (φsum). This is because the only variables in Eq. (36) are the elements of the expansion coefficient matrix T [Eq. (31)] for φ_p.

$$\begin{aligned} \varphi sum &= \sum_{j}^{\min basis} \sum_{p}^{val.vir} \left\langle \varphi_p \middle| A_j^* \right\rangle^2 \\ &= \sum_{j}^{\min basis} \sum_{p}^{val.vir} \left(\sum_{v}^{vir} T_{vp} \left\langle \phi_v \middle| A_j^* \right\rangle \right) \left(\sum_{w}^{vir} T_{wp} \left\langle \phi_w \middle| A_j^* \right\rangle \right) \\ &= \sum_p \sum_v \sum_w T_{vp} T_{wp} B_{vw} \end{aligned} \tag{37}$$

T is defined in Eq. (31) and $B_{vw} = \sum_j \left\langle \phi_v \middle| A_j^* \right\rangle \left\langle \phi_w \middle| A_j^* \right\rangle = \sum_j a_{vj}^* a_{wj}^*$

The B matrix is diagonalized, and the T matrix is formed from the p eigenvectors of B with the p largest eigenvalues, i.e. $BT_p = \beta_p T_p$, where β_p is the pth eigenvalue of the matrix B. $\varphi sum = \sum_p \sum_v \beta_p T_{vp} T_{vp} = \sum_p \beta_p$ is maximized. Once the matrix T is determined, the set of P valence virtual orbitals φ_p can be determined using Eq. (31). This effectively is a process of optimizing the valence virtual space in such a way that the QUAMBOs deviate least from the free-atom minimal basis AOs. Subsequently, the normalized expansion coefficients a'_{nj} and a'_{vj} are obtained as in Eq. (35). Using these QUAMBOs as the atomic basis set, one can obtain orbital energies by diagonalizing the corresponding Fock matrix. These orbital energies are then used in the CT energy

expression. The diagonalization also recovers the canonical occupied orbitals and generates the valence virtual orbitals (VVOs) that are then used in the CT calculations.

Numerical Results and Discussion

A. Computational Methodology

The codes for generating VVOs in the preparative *ab initio* runs to generate an EFP, and for using VVOs to calculate the EFP-EFP CT energy and gradient have been implemented in the electronic structure quantum chemistry package GAMESS.[15] Five basis sets [6-31+G(d,p), 6-31++G(d,p), 6-31++G(df,p), 6-311++G(d,p), 6-311++G(3df,2p)] are used here to test the code. The five dimer systems (Fig. 1) chosen as the test systems are water dimer, methanol-water, ammonia-water, ammonium-water and ammonium-nitrate, illustrated in Figure 1. These five test systems represent different types of charge transfer interactions: the CT interactions between polar neutral molecules, between charged molecules and between neutral and charged molecules. In addition, a cluster of four pairs of ammonium-nitrate dimers are used as a larger test system since the contrast in both the CT energy and the computational time is more apparent. The dimer systems were optimized at the RHF/6-31+G(d,p) level of theory and the cluster of $(\text{ammonium-nitrate})_4$ was obtained from a previous study[10] (Fig. 1). The individual molecules in the dimer were used to construct the EFP potentials. The exception is the water EFP potential, in which case the geometry used to construct the potential has an O-H bond length of 0.9468 Å and an H-O-H angle of 106.7°. The RVS analysis[13] was performed at these optimized geometries with the aforementioned basis sets to obtain the benchmark CT energies. The benchmark CT gradients were computed by three-point

numerical differencing the EFP CT energies, using step sizes of 0.001 Bohr for translation and 0.001 radian for rotation. The CT energies and gradients for the dimer systems were computed at both equilibrium and non-equilibrium intermolecular distances. To demonstrate time saving for large systems, 7 $(H_2O)_{64}$ clusters, 10 $(H_2O)_{128}$ clusters and 10 $(H_2O)_{256}$ clusters were chosen as test systems. Single point energy and single point energy+gradient calculations were carried out on a single Dell x86_64 CPU running at 2660 MHz. The aforementioned calculations were carried out using CMOs as well for comparison. All of the calculations were performed using GAMESS.[16]

B. Accuracy

(I) Model systems at equilibrium distances

Table 1 presents the CT energies of the five dimer systems at equilibrium separation and the cluster of four ammonium-nitrates. These energies are calculated in three ways: the RVS analysis to give benchmark CT energies, and EFP calculations using either CMOs or VVOs for the CT interaction. In most cases, the VVO-calculated CT energies are closer to the RVS CT energies than are those obtained from the CMOs. The variation of the VVO-calculated CT energies from basis to basis is small (< 0.5 kcal/mol). In fact, the values hardly change for the three relatively small basis sets [6-31+G(d,p), 6-31++G(d,p) and 6-31++G(df,p)]. In addition, it is interesting to note that the CT energies calculated with VVOs using the largest basis set, 6-311++G(3df,2p), are always smaller than those from smaller basis sets. This is expected since the energy lowering from the CT interaction arises in part from insufficient monomer basis sets.[10,17] Therefore, one expects the CT energy to decrease as one moves toward the complete

basis set limit. Interestingly, this trend is not observed consistently in the RVS calculations. For systems involving charged species, such as the ammonium-nitrate pair, one can encounter convergence problems and may need to adjust the convergence threshold in RVS calculations.

(II) Non-equilibrium distances

It is important to ensure that one can predict the CT energy accurately, not only at the equilibrium distance but also at other, non-equilibrium, distances. It is particularly important to obtain the correct limiting behavior. Taking the equilibrium distance as zero and shorter distances as negative, the CT energies were calculated for the five dimer systems at various distances away from equilibrium, ranging from -0.5 to 1.2 Å. The five dimer systems exhibit similar behavior and therefore only the water dimer system is shown in Figure 2. In most cases, the CT energies predicted using VVOs agree better with the RVS results than do those obtained from CMOs. At ~0.5 Å and longer than the equilibrium distances, CT energies approach zero as they should. As two molecules get closer, the magnitudes of the CT energies increase quickly. Both types of MOs predict the correct limiting behavior. The deviation from RVS CT energies increases for both types of MOs as the intermolecular distances get smaller than the equilibrium distances; but the VVO errors increase less rapidly, creating larger errors only at very small intermolecular distances. In general, VVOs tend to underestimate and CMOs overestimate the CT energies relative to the RVS values.

For water dimer (Fig. 2), the VVO-calculated CT energy error only becomes noticeable at about - 0.2 Å, whereas the CMO-predicted CT energy starts to exhibit a noticeable discrepancy even around the equilibrium distance. The absolute deviation for

VVO-predicted CT energies is generally smaller than that for the CMOs at all distances examined. Other dimer systems behave similarly. In all cases, VVOs underestimate the CT energies at -0.5 Å. However, this distance may not be of much physical significance and distance-dependent screening/scaling might be introduced in the future if necessary. In summary, one can expect VVO-predicted EFP2-EFP2 CT interaction energies to be quite accurate in the region where most physical and chemical situations occur.

(III) Gradients

The analytic EFP CT gradient code has been modified to use VVOs as an alternative option to calculate the EFP-EFP CT gradients. The benchmarking gradient results were computed using the numerical gradient code in GAMESS with a step size of 0.001 bohr for translation and 0.001 radians for rotation. Both analytic and numerical gradients are calculated at both the equilibrium and non-equilibrium distances. For all calculations, the differences between the analytic and numerical gradients using VVOs are within 10^{-7} Hartree/Bohr.

C. Efficiency/Timing

Using valence virtual orbitals in the EFP CT formulation greatly reduces the number of orbitals used in EFP CT calculations, and this causes a significant reduction in the required computer time. Comparative CPU times for one of the $(H_2O)_{256}$ clusters are shown in Table II. The time saving is global: for all of the terms in the CT energy formula [Eqs. (26) and (27)], the computational times drop by at least 50% compared to the times required for the analogous CMO calculations. The total CPU time for an EFP-

EFP energy calculation and single point gradient calculation for the $(NH_4^+ \text{ --- } NO_3^-)_4$ system are presented in Figures 3(a) and 3(b), respectively. For both energy and gradient calculations, the total CPU time increases linearly with the number of basis functions. For CMOs, the CPU time increases much more rapidly. The average total CPU time for the energy and gradient calculations, respectively, for the 7 $(H_2O)_{64}$ clusters, 10 $(H_2O)_{128}$ clusters and 10 $(H_2O)_{256}$ clusters are plotted as a function of the number of water molecules in Figures 4(a) and 4(b). A linear scaling is again observed. The use of VVOs significantly reduces the linear scaling coefficients. As the number of basis functions increases or the system size increases, the time saved by using VVOs is amplified. This is easily understood because the number of canonical virtual orbitals increases steeply while the number of minimal basis orbitals stays the same as the number of basis functions increases. Due to this new implementation, molecular dynamical (MD) simulations of EFP water clusters are able to run with CT included in the water potential[18]. In general, one can expect a 50% or more time saving when using the recommended EFP basis set, 6-311++G(3df,2p).

Conclusion

The occupied + valence virtual orbitals have been implemented as an alternative for calculating the EFP-EFP charge transfer energy and gradient. QUAMBOs furnish a basis that can exactly expand the SCF occupied orbitals, and projection of QUAMBOs onto the virtual space select that part of the virtual space that contains the most important correlating orbitals. The number of QUAMBOs is constant for a particular system. Therefore, the use of QUAMBOs to obtain VVOs improves the efficiency of EFP-EFP

CT calculations markedly while retaining, and in some cases improving the accuracy of the CT energies.

Acknowledgment

This material is based upon work supported by the Air Force Office of Scientific Research under AFOSR Award No. FA9550-11-1-0099. Discussions with Professor Hui Li are gratefully acknowledged.

Appendix

The different combinations of Eqs. (18) – (21) lead to four possible formulae for CT energy of fragment A due to fragment B (Eqs. A1 – A4). Four analogous formulae for the charge transfer energy of B due to A are not shown here.

$$CT^{A(B)} \approx 2\sum_{i}^{occA}\sum_{n}^{virB}\frac{1}{1-\sum_{m}^{allA}\left(S_{nm}\right)^{2}}\frac{V_{in}^{EFB}-\sum_{m}^{allA}S_{nm}V_{im}^{EFB}}{\left(F_{ii}^{A}-T_{nn}\right)} \times\left[V_{in}^{EFB}-\sum_{m}^{allA}S_{nm}V_{im}^{EFB}-\sum_{j}^{occB}S_{ij}\left(V_{nj}^{EFA}-\sum_{m}^{allA}S_{nm}V_{mj}^{EFA}\right)\right] \quad \textbf{(A1)}$$

$$CT^{A(B)} \approx 2\sum_{i}^{occA}\sum_{n}^{virB}\frac{1}{1-\sum_{m}^{allA}\left(S_{nm}\right)^{2}}\frac{V_{in}^{EFB}-\sum_{m}^{allA}S_{nm}V_{im}^{EFB}}{\left(F_{ii}^{A}-T_{nn}\right)} \times\left[-T_{in}+\sum_{m}^{allA}S_{nm}T_{im}+\sum_{j}^{occB}S_{ij}\left(T_{nj}-\sum_{m}^{allA}S_{nm}T_{mj}\right)\right] \quad \textbf{(A2)}$$

$$CT^{A(B)} \approx 2\sum_{i}^{occA}\sum_{n}^{virB}\frac{1}{1-\sum_{m}^{allA}\left(S_{nm}\right)^{2}}\frac{V_{in}^{EFB}-\sum_{m}^{allA}S_{nm}V_{im}^{EFB}}{\left(F_{ii}^{A}-T_{nn}\right)} \times\left[-T_{in}+\sum_{m}^{allA}S_{nm}T_{im}-\sum_{j}^{occB}S_{ij}\left(V_{nj}^{EFA}-\sum_{m}^{allA}S_{nm}V_{mj}^{EFA}\right)\right] \quad \textbf{(A3)}$$

$$CT^{A(B)} \approx 2\sum_{i}^{occA}\sum_{n}^{virB}\frac{1}{1-\sum_{m}^{allA}\left(S_{nm}\right)^{2}}\frac{V_{in}^{EFB}-\sum_{m}^{allA}S_{nm}V_{im}^{EFB}}{\left(F_{ii}^{A}-T_{nn}\right)} \times\left[V_{in}^{EFB}-\sum_{m}^{allA}S_{nm}V_{im}^{EFB}+\sum_{j}^{occB}S_{ij}\left(T_{nj}-\sum_{m}^{allA}S_{nm}T_{mj}\right)\right] \quad \textbf{(A4)}$$

It is difficult to judge the accuracy of the four formulae without numerical results since the various approximations involve all the matrix elements, not just the expectation values of an operator. The accuracies could depend on various factors: basis sets, electronic structures of the molecules, the shape of the orbitals used, that is, canonical or localized.[10] In order to determine which formula is the best when using VVOs, the CT energies for the five dimer systems are presented in Table III.

In all cases tested, Eq. (A2) gives very large positive numbers that are unphysical. Eq (A1) significantly underestimates the magnitude of the CT energies. Eq (A3) shows unpredictable behavior: large positive numbers for water dimer and ammonium-water dimer and underestimated CT energies for the other three systems. Eq. (A4) not only produces negative CT energies in all cases but also closest to the RVS benchmarking numbers.

Reference

1. G. L. Zubay, *Biochemistry* Wm. C. Brown Publishers, 1993

2. W. Saenger, Principles of Nucleic Acid Structure; Springer-Verlag: New York, 1984

3. Q. A. Smith and M. S. Gordon, J. Phys. Chem. A **115**, 11269 (2011)

4. P. N. Day, J. H. Jensen, M. S. Gordon, S. P. Webb, W.J. Stevens, M. Krauss, D. Garmer, H. Basch, D. Cohen, J. Chem. Phys. **105**, 1968 (1996)

5. M. S. Gordon, M. A. Freitag, P. Bandyopadhyay, J. H. Jensen, V. Kairys, W. J. Stevens, J. Phys. Chem. A **105**, 293 (2001)

6. A. J. Stone, Chem. Phys. Lett. **83**, 233 (1981); A. J. Stone and M. Alderton, Mol. Phys. **56**, 1047 (1985)

7. A. D., Becke, Phys. Rev. A **38**, 3098 (1988); C. Lee, W. Yang and R. G. Parr, Phys. Rev. B **37**, 785 (1988)

8. J. H. Jensen and M. S. Gordon, Mol. Phys. **89**, 1313 (1996)

9. I. Adamovic and M. S. Gordon, Mol. Phys. **103**, 379 (2005)

10. H. Li, M. S. Gordon, J. H. Jensen, J. Chem. Phys. **124**, 214108 (2006)

11. M. D. Hands and L.V. Slipchenko, J. Phys. Chem. B **116**, 2775 (2012)

12. W. C. Lu, C. Z. Wang, M. W. Schmidt, L. Bytautas, K. M. Ho, K. Ruedenberg, J. Chem. Phys. **120**, 2629 (2004)

13. W. J. Stevens and W. H. Fink, Chem. Phys. Lett. **139**, 15 (1987)

14. K. Kitaura and K. Morokuma, Int. J. Quantum Chem. **10**, 325 (1976)

15. A. Fröman and P.-O. Löwdin, J. Phys. Chem. Solids, **23**, 75 (1962); B. Jeziorski, M. Bulski, L. Piela, Int. J. Quantum Chem. **10**, 281 (1976)

16. M. W. Schmidt, K. K. Baldridge, J. A. Boatz *et al.*, J. Comput. Chem. **14**, 1347 (1993); M. S. Gordon, M. W. Schmidt. 2005. *Advances in electronic structure theory: GAMESS a decade later*. In *Theory and Applications of Computational Chemistry* ed. CE Dykstra, G Frenking, KS Kim, GE Scuseria, pp. Ch. 41: Elsevier

17. A. J. Stone, *The Theory of Intermolecular Forces*; Oxford University Press: Oxford, 1996

18. C. Resch, in preparation

FIG. 1. The structures of the test systems (from left to right) upper row: water-water, methanol-water, ammonia-water; lower row: ammonium-water, ammonium-nitrate and $(\text{ammonium-nitrate})_4$.

FIG. 2. EFP-EFP charge transfer energies for water-water dimer at various distances with basis sets (a) 6-31+G(d,p), (b) 6-31++G(d,p), (c) 6-31++G(df,p), (d) 6-311++G(d,p) and (e) 6-311++G(3df,2p).

FIG. 3. Total CPU time versus number of basis functions using either CMO or VVO, (a) EFP-EFP energy calculation, (b) Single-point EFP-EFP gradient calculation.

FIG. 4. Total CPU time versus number of water molecules using CMO vs. VVO, (a) EFP-EFP energy calculation, (b) Single-point EFP-EFP gradient calculation.

TABLE I. Charge transfer energies (kcal/mol) obtained from the RVS analysis, EFP (canonical occupied + virtual molecular orbitals) and EFP (occupied +valence virtual orbitals) for the five dimer systems and (ammonium-nitrate)$_4$ system with five basis sets. The dimer geometries were optimized with RHF/6-31+G(d,p).

	Water-water			Methanol-water			Ammonia-water		
Basis sets	RVS	CMO	VVO	RVS	CMO	VVO	RVS	CMO	VVO
6-31+G(d,p)	**-0.55**	-0.85	-0.51	**-0.53**	-0.78	-0.58	**-0.91**	-1.63	-0.86
6-31++G(d,p)	**-0.49**	-0.75	-0.51	**-0.46**	-0.77	-0.58	**-0.93**	-1.25	-0.85
6-31++G(df,p)	**-0.47**	-0.79	-0.51	**-0.44**	-0.81	-0.58	**-0.86**	-1.32	-0.87
6-311++G(d,p)	**-0.53**	-0.82	-0.47	**-0.51**	-0.78	-0.53	**-0.95**	-0.94	-0.75
6-311++G(3df,2p)	**-0.65**	-0.44	-0.35	**-0.63**	-0.31	-0.44	**-1.20**	-0.18	-0.52

	Ammonium-water			Ammonium-nitrate			(ammonium-nitrate)$_4$		
Basis sets	RVS	CMO	VVO	RVS	CMO	VVO	RVS	CMO	VVO
6-31+G(d,p)	**-2.33**	-2.75	-2.05	**-7.88**	-5.00	-5.36	**-15.19**	-10.47	-15.32
6-31++G(d,p)	**-2.19**	-2.64	-2.04	**-7.90**	-5.53	-5.38	**-15.08**	-12.45	-15.32
6-31++G(df,p)	**-2.12**	-2.79	-2.05	**-7.85**	-6.09	-5.30	**-15.10**	-13.41	-15.38
6-311++G(d,p)	**-2.35**	-3.13	-2.03	**-8.27**	-7.12	-5.30	**-15.07**	-14.70	-15.19
6-311++G(3df,2p)	**-2.85**	-1.95	-1.79	**-6.98**	-3.80	-5.28	**-12.76**	-8.14	-15.59

TABLE II. The CPU time spent for various terms in an EFP-EFP charge transfer energy calculation for one $(H_2O)_{256}$ cluster. Other water clusters of the same size give similar results. T_{AA} is the kinetic energy integral of fragment A, S_{AB} and T_{AB} are the overlap and kinetic energy integrals between fragments A and B, V are the one-electron electrostatic potential integrals. For instance, V_{AA}^{EFB} represents the matrix elements of the electrostatic potential due to B. E_{CT} means assembling of all the terms and calculating the charge transfer energy once all of the required integrals are available. Times are in seconds.

	CMO	VVO
T_{AA}	31.66	16.42
S_{AB} and T_{AB}	8.42	0.37
V_{AA}^{EFB}	145.19	15.73
V_{BB}^{EFA}	145.76	15.79
V_{AB}^{EFA}	75.11	12.93
V_{AB}^{EFB}	75.10	13.06
E_{CT}	2.25	0.01

TABLE III. Charge transfer energies (kcal/mol) obtained from Eqs. (A1) – (A4) in the Appendix using valence virtual orbitals together with RVS-calculated charge transfer energies as benchmarks (in bold) for the five dimer systems: water dimer, methanol-water, ammonia-water, ammonium-water and ammonium-nitrate.

Basis set		Water-water	Methanol-water	Ammonia-water	Ammonium-water	Ammonium-nitrate
6-31+G(d,p)	**RVS**	**-0.55**	**-0.53**	**-0.91**	**-2.33**	**-7.88**
	A1	-0.05	-0.05	-0.07	-0.40	-0.92
	A2	1.62	1.71	1.29	7.11	13.94
	A3	2.08	-0.24	-0.32	8.75	-4.82
	A4	-0.50	-0.58	-0.86	-2.05	-5.36
6-31++G(d,p)	**RVS**	**-0.49**	**-0.46**	**-0.93**	**-2.19**	**-7.9**
	A1	-0.05	-0.05	-0.07	-0.40	-0.92
	A2	1.60	1.67	1.28	7.06	13.87
	A3	2.06	-0.25	-0.31	8.70	-4.80
	A4	-0.49	-0.58	-0.85	-2.04	-5.38
6-31++G(df,p)	**RVS**	**-0.47**	**-0.44**	**-0.86**	**-2.12**	**-7.85**
	A1	-0.05	-0.05	-0.07	-0.40	-0.92
	A2	1.62	1.68	1.27	7.08	13.84
	A3	2.08	-0.25	-0.33	8.74	-4.78
	A4	-0.50	-0.58	-0.87	-2.05	-5.38
6-311++G(d,p)	**RVS**	**-0.53**	**-0.51**	**-0.95**	**-2.35**	**-8.27**
	A1	-0.04	-0.04	-0.05	-0.38	-0.87
	A2	1.45	1.51	1.08	6.93	13.54
	A3	1.87	-0.19	-0.26	8.57	-4.40
	A4	-0.45	-0.53	-0.75	-2.03	-5.30
6-311++G(3df,2p)	**RVS**	**-0.65**	**-0.63**	**-1.2**	**-2.85**	**-6.98**
	A1	-0.03	-0.03	-0.03	-0.33	-0.86
	A2	1.18	1.21	0.77	6.46	13.09
	A3	1.47	-0.15	-0.16	7.88	-4.36
	A4	-0.34	-0.44	-0.52	-1.79	-5.28

CHAPTER 3 THE R^{-7} DISPERSION INTERACTION IN THE GENERAL EFFECTIVE FRAGMENT POTENTIAL METHOD

A paper accepted by *The Journal of Chemical Theory and Computation*

Peng Xu, Federico Zahariev, Mark S. Gordon

Abstract

The R^{-7} term (E7) in the dispersion expansion is developed in the framework of the general effective fragment potential (EFP2) method, formulated with the dynamic anisotropic Cartesian polarizability tensors over the imaginary frequency range. The E7 formulation is presented in terms of both the total molecular polarizability and the localized molecular orbital (LMO) contributions. An origin transformation from the center of mass to the LMO centroids is incorporated for the computation of the LMO dipole-quadrupole polarizability. The two forms considered for the damping function for the R^{-7} dispersion interaction, the overlap-based and Tang-Toennies damping functions, are extensions of the existing damping functions for the R^{-6} term in the dispersion expansion. The R^{-7} dispersion interaction is highly orientation-dependent: it can be either attractive or repulsive, and its magnitude can change substantially as the relative orientation of two interacting molecules changes. Although the R^{-7} dispersion energy rotationally averages to zero, it may be significant for systems in which rotational

averaging does not occur, such as rotationally rigid molecular systems as in molecular solids or constrained surface reactions.

Introduction

The dispersion interaction, a non-classical phenomenon, arises from the correlated movement of electrons. In the language of a multipole description of the charge distributions of molecules, it can be thought of as the interaction between induced multipoles. Although weak, the dispersion interaction plays an important role in many phenomena. For example, the dispersion contribution to the water-water hydrogen bond is non-trivial[1], dispersion is a key component in π-stacking interactions[2–5], and provides the essence of the binding of noble gases[6,7].

The dispersion interaction energy is often expressed as an expansion in inverse powers of the interatomic or intermolecular distance,[8]

$$E_{disp} = C_6 R^{-6} + C_7 R^{-7} + C_8 R^{-8} + \ldots \quad (1)$$

The C_n coefficients in Eq. (1) are expansion coefficients that may be derived from first principles or fitted in some manner, and each term corresponds to one or more induced multipole-induced multipole interactions. The dispersion interaction can be formulated in terms of second-order Rayleigh-Schrödinger perturbation theory, where the perturbation operator is expressed as multipole expansions of the two interacting molecules.[9] The R^{-6} dispersion interaction term is accounted for by using the dynamic dipole-dipole polarizability over the imaginary frequency range.[10] The R^{-7} dispersion term arises from the mixing of dipole-dipole interactions with dipole-quadrupole interactions.[11] In this

paper the R^{-7} contribution to the dispersion energy will be called E7 for brevity. E7 is zero for atoms and centrosymmetric molecules. For non-centrosymmetric molecules, E7 does depend on the relative orientation of the molecules[9,11], and that is an important consideration.

The effective fragment potential (EFP) method, developed by Gordon and coworkers,[12] is a discrete method for studying the entire range of intermolecular interactions. The original implementation, EFP1, was designed solely for water and involves a fitted repulsive potential. The second implementation, the general effective fragment potential (EFP2) method contains no fitted parameters and can be generated for any (closed-shell) molecule. In this paper, EFP2 will be called EFP unless a distinction between EFP1 and EFP2 needs to be made. The interaction energy between two molecules/fragments is calculated using properties of the two isolated molecules. The required properties are generated in a prior MAKEFP calculation. The interaction energy is divided into five components, which may be classified in two categories: the Coulomb interaction, polarization/induction and dispersion are long-range interactions ($U \sim R^{-n}$). Exchange repulsion and charge transfer are short-range interactions ($U \sim e^{-\alpha R}$).

The EFP Coulomb interaction is modeled by the Stone distributed multipolar analysis (DMA) method[13,14]. The multipole expansion is truncated at the octopole term, and the expansion centers are the nuclei and bond midpoints.[12] The EFP polarization term arises from the interaction between an induced dipole on one fragment and the electric field due to all of the other fragments.[12] It is modeled with localized molecular orbital (LMO) anisotropic static dipole polarizability tensors. The induced dipole is iterated to self-consistency, thereby introducing many-body effects. The exchange repulsion term is

obtained from a power expansion of the intermolecular LMO overlap integral, truncated at the second order in the current implementation.[15] Charge transfer (CT) is the interaction between the occupied orbitals of one molecule and the virtual orbitals of another molecule. The CT interaction between two EFP fragments is derived from a second-order perturbative approach.[16,17] A power expansion of the intermolecular overlap is used for the CT term as well, but the truncation is at first order. The leading term in the dispersion interaction, which will be discussed in Section II, is described using the dynamic (frequency-dependent) isotropic dipole polarizability of LMOs over the imaginary frequency range.[18] This gives rise to the isotropic R^{-6} dispersion energy. Currently, the higher order dispersion energy is approximated as one third of this isotropic R^{-6} energy. The goal of this paper is to derive an explicit expression for E7 and to evaluate the relative importance of this term.

This paper is organized as follows: Section II presents a detailed derivation of E7, in terms of the Cartesian molecular dynamic polarizability tensors and in terms of LMO dynamic polarizability tensors. Implementation of the polarizability and damping functions is also described. Computational details, including the benchmarking system LiH -- LiH and other dimer systems, are described in Section III. Results are presented and discussed in Section IV. Conclusions and future work are provided in Section V.

Theory

In the framework of Rayleigh-Schrödinger perturbation theory (RSPT), the dispersion interaction energy between two closed-shell nondegenerate ground state molecules is part of the second order interaction energy,[9,19]

$$E^{disp} = -\sum_{\substack{m\neq 0\\ n\neq 0}} \frac{< 0_A 0_B | \hat{V} | mn >< mn | \hat{V} | 0_A 0_B >}{E_m^A + E_n^B - E_0^A - E_0^B} \quad (2)$$

where 0_A and 0_B are the ground states of molecules A and B, respectively, and m and n are the excited states of molecules A and B, respectively. Correspondingly, E_m^A is the energy of the mth excited state of molecule A. The other Es are similarly defined. The unperturbed Hamiltonian is the sum of the Hamiltonians of the isolated molecules A and B.

$$\hat{H}_0 = \hat{H}_0^A + \hat{H}_0^B \quad (3)$$

The perturbation operator $\hat{V}$ is the interaction operator, which contains the electrostatic interaction between the constituent particles. By expressing the charge distributions of the two molecules A and B as two multipole expansions, one can express the interaction operator as:

$$\hat{V} = T^{AB} q^A q^B + \sum_{\alpha}^{x,y,z} T_\alpha^{AB} (q^A \mu_\alpha^B - \mu_\alpha^A q^B) - \sum_{\alpha,\beta}^{x,y,z} T_{\alpha\beta}^{AB} \mu_\alpha^A \mu_\beta^B - \frac{1}{3} \sum_{\alpha\beta\gamma}^{x,y,z} T_{\alpha\beta\gamma}^{AB} (\mu_\alpha^A \theta_{\beta\gamma}^B - \theta_{\alpha\beta}^A \mu_\gamma^B) \ldots (4)$$

where q^A is the total charge on molecule A. μ_α^B is the αth component of the dipole moment of molecule B. $\theta_{\beta\gamma}^B$ is the βγth component of the quadrupole moment of B. The electrostatic T tensors are defined as follows:

$$T^{AB} = \frac{1}{4\pi\varepsilon_0 R} \quad (5a)$$

$$T_\alpha^{AB} = \frac{1}{4\pi\varepsilon_0} \nabla_\alpha \frac{1}{R} = -\frac{R_\alpha}{4\pi\varepsilon_0 R^3} \quad (5b)$$

$$T_{\alpha\beta}^{AB} = \frac{1}{4\pi\varepsilon_0}\nabla_\alpha\nabla_\beta\frac{1}{R} = \frac{3R_\alpha R_\beta - R^2\delta_{\alpha\beta}}{4\pi\varepsilon_0 R^5} \tag{5c}$$

$$T_{\alpha\beta\gamma}^{AB} = \frac{1}{4\pi\varepsilon_0}\nabla_\alpha\nabla_\beta\nabla_\gamma\frac{1}{R} = -\frac{15R_\alpha R_\beta R_\gamma - 3R^2(R_\alpha\delta_{\beta\gamma} + R_\beta\delta_{\alpha\gamma} + R_\gamma\delta_{\alpha\beta})}{4\pi\varepsilon_0 R^7} \tag{5d}$$

where **R** = **B** – **A**. Here **B** and **A** are the expansion center coordinates at which the multipole expansions are obtained. At this stage, only a single-center multipole expansion for each molecule is carried out. There is some arbitrariness in the definition of the multipoles because the choice of the expansion center is arbitrary. The charge is a scalar and is independent of the expansion center. The dipole moment of a neutral molecule is invariant under a change of the expansion center.[9] However, the higher moments, such as quadrupole moments, depend on the location of the expansion center. In the literature, this phenomenon is commonly referred to as "origin dependence"[9,11]; in this work the word "origin" refers to the expansion center. The convention that is used here is discussed in subsequent sections.

Consider the total wave function of a system AB in the long-range approximation, where there is no significant overlap between the two molecular wave functions and hence no exchange effect, then the total wave function is the Hartree product of the individual wave functions:

$$|0_A 0_B\rangle = |0_A\rangle|0_B\rangle \text{ and } |mn\rangle = |m\rangle|n\rangle \tag{6}$$

Truncating the interaction operator (Eq. (4)) at the dipole-quadrupole term and substituting Eqs. (4) and (6) into Eq. (2) gives

$$E^{disp} =$$

$$-\sum_{\substack{m\neq 0\\ n\neq 0}} \frac{\left\{\begin{array}{l} \langle 0_A|\langle 0_B|\sum_{\alpha\beta}^{x,y,z} T_{\alpha\beta}^{AB}\mu_\alpha^A\mu_\beta^B|m\rangle|n\rangle\langle m|\langle n|\sum_{\gamma\sigma}^{x,y,z} T_{\gamma\sigma}^{AB}\mu_\gamma^A\mu_\sigma^B|0_A\rangle|0_B\rangle \\ +\langle 0_A|\langle 0_B|\sum_{\alpha\beta}^{x,y,z} T_{\alpha\beta}^{AB}\mu_\alpha^A\mu_\beta^B|m\rangle|n\rangle\langle m|\langle n|\left(\frac{1}{3}\sum_{\gamma\sigma\kappa}^{x,y,z} T_{\gamma\sigma\kappa}^{AB}(\mu_\gamma^A\theta_{\sigma\kappa}^B-\theta_{\gamma\sigma}^A\mu_\kappa^B)\right)|0_A\rangle|0_B\rangle \\ +\langle 0_A|\langle 0_B|\left(\frac{1}{3}\sum_{\alpha\beta\gamma}^{x,y,z} T_{\alpha\beta\gamma}^{AB}(\mu_\alpha^A\theta_{\beta\gamma}^B-\theta_{\alpha\beta}^A\mu_\gamma^B)\right)|m\rangle|n\rangle\langle m|\langle n|\sum_{\sigma\kappa}^{x,y,z} T_{\sigma\kappa}^{AB}\mu_\sigma^A\mu_\kappa^B|0_A\rangle|0_B\rangle \\ +\langle 0_A|\langle 0_B|\left(\frac{1}{3}\sum_{\alpha\beta\gamma}^{x,y,z} T_{\alpha\beta\gamma}^{AB}(\mu_\alpha^A\theta_{\beta\gamma}^B-\theta_{\alpha\beta}^A\mu_\gamma^B)\right)|m\rangle|n\rangle\langle m|\langle n|\left(\frac{1}{3}\sum_{\lambda\sigma\kappa}^{x,y,z} T_{\lambda\sigma\kappa}^{AB}(\mu_\lambda^A\theta_{\sigma\kappa}^B-\theta_{\lambda\sigma}^A\mu_\kappa^B)\right)|0_A\rangle|0_B\rangle \end{array}\right\}}{(E_m^A-E_0^A)+(E_n^B-E_0^B)}$$

(7)

The integrals that involve the charge q may be expressed in the form $\langle 0_A|q^A|m\rangle = q^A\langle 0_A|m\rangle = 0$ since q is a scalar and the ground and excited states of the same molecule are orthogonal to each other. Hence Eq. (7) starts from the dipole-dipole term. From Eqs. (5c) and (5d), $T_{\alpha\beta}$ and $T_{\gamma\sigma\kappa}$ are of the order R^{-3} and R^{-4}, respectively. Therefore E7 arises from the 2nd and 3rd terms in Eq. (7). The 1st term of Eq. (7) is the familiar R^{-6} dispersion term. The last term in Eq. (7) is part of the R^{-8} dispersion term, which will be discussed in a subsequent paper. Collecting the terms for E7 and simplifying the notation by using $E_{m0} = E_m - E_0$ yields

$$E7 = -\sum_{\substack{m\neq 0\\ n\neq 0}} \frac{\left\{\begin{array}{l}\langle 0_A|\langle 0_B|\sum_{\alpha\beta}^{x,y,z} T^{AB}_{\alpha\beta}\mu^A_\alpha\mu^B_\beta|m\rangle|n\rangle\langle m|\langle n|\left(\frac{1}{3}\sum_{\gamma\sigma\kappa}^{x,y,z} T^{AB}_{\gamma\sigma\kappa}(\mu^A_\gamma\theta^B_{\sigma\kappa}-\theta^A_{\gamma\sigma}\mu^B_\kappa)\right)|0_A\rangle|0_B\rangle \\ +\langle 0_A|\langle 0_B|\left(\frac{1}{3}\sum_{\alpha\beta\gamma}^{x,y,z} T^{AB}_{\alpha\beta\gamma}(\mu^A_\alpha\theta^B_{\beta\gamma}-\theta^A_{\alpha\beta}\mu^B_\gamma)\right)|m\rangle|n\rangle\langle m|\langle n|\sum_{\sigma\kappa}^{x,y,z} T^{AB}_{\sigma\kappa}\mu^A_\sigma\mu^B_\kappa|0_A\rangle|0_B\rangle\end{array}\right\}}{(E^A_m-E^A_0)+(E^B_n-E^B_0)} \qquad (8)$$

$$= -\sum_{\substack{m\neq 0\\ n\neq 0}} \frac{2\left\{\langle 0_A|\langle 0_B|\sum_{\alpha\beta}^{x,y,z} T^{AB}_{\alpha\beta}\mu^A_\alpha\mu^B_\beta|m\rangle|n\rangle\langle m|\langle n|\left(\frac{1}{3}\sum_{\gamma\sigma\kappa}^{x,y,z} T^{AB}_{\gamma\sigma\kappa}(\mu^A_\gamma\theta^B_{\sigma\kappa}-\theta^A_{\gamma\sigma}\mu^B_\kappa)\right)|0_A\rangle|0_B\rangle\right\}}{E^A_{m0}+E^B_{n0}}$$

The indices α,β,γ,σ,κ all run over the Cartesian coordinates x, y and z, hence the first and second terms in the first equality of Eq. (8) are equivalent and may be combined into one term. The T tensors are constant at a fixed configuration. Rearranging the integrand yields,

$$E7 = -2\sum_{\alpha\beta\gamma\sigma\kappa}^{x,y,z} T^{AB}_{\alpha\beta}T^{AB}_{\gamma\sigma\kappa}\sum_{\substack{m\neq 0\\ n\neq 0}}\frac{1}{E^A_{m0}+E^B_{n0}}\times$$

$$\left[\begin{array}{l}<0_A|\mu^A_\alpha|m><m|\mu^A_\gamma|0_A><0_B|\mu^B_\beta|n><n|\frac{1}{3}\theta^B_{\sigma\kappa}|0_B>- \\ <0_A|\mu^A_\alpha|m><m|\frac{1}{3}\theta^A_{\gamma\sigma}|0_A><0_B|\mu^B_\beta|n><n|\mu^B_\kappa|0_B>\end{array}\right] \qquad (9)$$

The denominator of Eq. (9) is transformed by the Casimir-Polder identity[9,20]:

$$\frac{1}{A+B} = \frac{2}{\pi}\int_0^\infty \frac{AB}{(A^2+\omega^2)(B^2+\omega^2)}d\omega \qquad (10)$$

Applying Eq. (10) to the denominator in Eq. (9) yields

$$\frac{1}{E^A_{m0}+E^B_{n0}} = \frac{1}{\hbar}\frac{1}{\omega^A_{m0}+\omega^B_{n0}} = \frac{2}{\pi}\frac{1}{\hbar}\int_0^\infty d\omega \frac{\omega^A_{m0}\omega^B_{n0}}{\left[(\omega^A_{m0})^2+\omega^2\right]\left[(\omega^B_{n0})^2+\omega^2\right]} \qquad (11)$$

Now the integrand can be written as a product of a term involving only A and a term involving only B:

$$E7 = -2\sum_{\alpha\beta\gamma\sigma\kappa}^{x,y,z} T_{\alpha\beta}^{AB} T_{\gamma\sigma\kappa}^{AB} \frac{1}{\hbar}\frac{2}{\pi}\frac{1}{3}\int_0^\infty d\omega \left\{ \begin{array}{l} \sum_{\substack{m\neq 0 \\ n\neq 0}} \left(\frac{\omega_{m0}^A \langle 0_A|\mu_\alpha^A|m\rangle\langle m|\mu_\gamma^A|0_A\rangle}{(\omega_{m0}^A)^2+\omega^2} \right)\left(\frac{\omega_{n0}^B \langle 0_B|\mu_\beta^B|n\rangle\langle n|\theta_{\sigma\kappa}^B|0_B\rangle}{(\omega_{n0}^B)^2+\omega^2} \right) \\ -\sum_{\substack{m\neq 0 \\ n\neq 0}} \left(\frac{\omega_{m0}^A \langle 0_A|\mu_\alpha^A|m\rangle\langle m|\theta_{\gamma\sigma}^A|0_A\rangle}{(\omega_{m0}^A)^2+\omega^2} \right)\left(\frac{\omega_{n0}^B \langle 0_B|\mu_\beta^B|n\rangle\langle n|\mu_\kappa^B|0_B\rangle}{(\omega_{n0}^B)^2+\omega^2} \right) \end{array} \right\} \quad (12)$$

From time-dependent perturbation theory, one can express the dynamic dipole-dipole and dipole-quadrupole polarizabilities as, respectively,

$$\alpha_{\alpha\beta}(\omega) = 2\sum_{m\neq 0} \frac{\omega_{m0}\langle 0|\mu_\alpha|m\rangle\langle m|\mu_\beta|0\rangle}{\hbar(\omega_{m0}^2-\omega^2)} \quad (13)$$

$$A_{\alpha,\beta\gamma}(\omega) = 2\sum_{n\neq 0} \frac{\omega_{n0}\langle 0|\mu_\alpha|n\rangle\langle n|\theta_{\beta\gamma}|0\rangle}{\hbar(\omega_{n0}^2-\omega^2)} \quad (14)$$

Since $\omega^2 = -(i\omega)^2$, one can cast the E7 expression in terms of dynamic dipole-quadrupole polarizability tensors over the imaginary frequency range:

$$\begin{aligned} E7 &= -2\sum_{\alpha\beta\gamma\sigma\kappa}^{x,y,z} T_{\alpha\beta}^{AB} T_{\gamma\sigma\kappa}^{AB} \frac{2\hbar}{\pi}\int_0^\infty d\omega \left\{ \frac{1}{3}\bullet\frac{1}{2}\bullet\frac{1}{2}\alpha_{\alpha\gamma}^A(i\omega)A_{\beta,\sigma\kappa}^B(i\omega) - \frac{1}{3}\bullet\frac{1}{2}\bullet\frac{1}{2}\alpha_{\beta\kappa}^B(i\omega)A_{\alpha,\gamma\sigma}^A(i\omega) \right\} \\ &= -\frac{\hbar}{3\pi}\sum_{\alpha\beta\gamma\sigma\kappa}^{x,y,z} T_{\alpha\beta}^{AB} T_{\gamma\sigma\kappa}^{AB} \int_0^\infty d\omega \left[\alpha_{\alpha\gamma}^A(i\omega)A_{\beta,\sigma\kappa}^B(i\omega) - \alpha_{\beta\kappa}^B(i\omega)A_{\alpha,\gamma\sigma}^A(i\omega) \right] \end{aligned} \quad (15)$$

The integral in Eq. (15) is evaluated numerically using a 12-point Gauss-Legendre quadrature. By a change of variable,

$$\omega = \omega_0\frac{1+t}{1-t} \text{ and } d\omega = \frac{2\omega_0}{(1-t)^2}dt, \quad (16)$$

the integral in Eq. (15) becomes

$$\begin{aligned}
&\int_0^\infty d\omega\left[\alpha^A_{\alpha\gamma}(i\omega)A^B_{\beta,\sigma\kappa}(i\omega)-\alpha^B_{\beta\kappa}(i\omega)A^A_{\alpha,\gamma\sigma}(i\omega)\right]\\
&=\int_{-1}^{1}dt\,\frac{2\omega_0}{(1-t)^2}\left[\alpha^A_{\alpha\gamma}(i\omega(t))A^B_{\beta,\sigma\kappa}(i\omega(t))-\alpha^B_{\beta\kappa}(i\omega(t))A^A_{\alpha,\gamma\sigma}(i\omega(t))\right]\\
&=\sum_{n=1}^{12}W(n)\frac{2\omega_0}{(1-t_n)^2}\left[\alpha^A_{\alpha\gamma}(i\omega_n)A^B_{\beta,\sigma\kappa}(i\omega_n)-\alpha^B_{\beta\kappa}(i\omega_n)A^A_{\alpha,\gamma\sigma}(i\omega_n)\right]
\end{aligned} \tag{17}$$

where W(n) and t_n are the Gauss-Legendre weights and abscissas, which have been determined previously for the R^{-6} term in the dispersion energy.[18,19] The optimal value for ω_0 is found to be 0.3.[21] Now the E7 dispersion energy is

$$E7=-\frac{\hbar}{3\pi}\sum_{\alpha\beta\gamma\sigma\kappa}^{x,y,z}T^{AB}_{\alpha\beta}T^{AB}_{\gamma\sigma\kappa}\sum_{n=1}^{12}W(n)\frac{2\omega_0}{(1-t_n)^2}\left[\alpha^A_{\alpha\gamma}(i\omega_n)A^B_{\beta,\sigma\kappa}(i\omega_n)-\alpha^B_{\beta\kappa}(i\omega_n)A^A_{\alpha,\gamma\sigma}(i\omega_n)\right] \tag{18}$$

A distributed multipole expansion model of the molecule has the advantages that one attains improved convergence properties and a better description of the molecular charge distribution[9,14,22]. In particular for dispersion, a distributed treatment portrays a more realistic picture of the response of the molecule from non-uniform fields due to other molecular systems.

If one divides the molecule into “regions”, each described by its own multipole expansion with its own origin, the interaction operator V has the form[9,23,24]:

$$\hat{V}=\sum_{a\in A}\sum_{b\in B}\left[T^{ab}q^aq^b+T^{ab}_{\alpha}\left(q^a\mu^b_\alpha-\mu^a_\alpha q^b\right)+T^{ab}_{\alpha\beta}\left(\frac{1}{3}q^a\theta^b_{\alpha\beta}-\mu^a_\alpha\mu^b_\beta+\frac{1}{3}\theta^a_{\alpha\beta}q^b\right)+\ldots\right] \tag{19}$$

The double sum runs over the expansion centers **a** of molecule A and **b** of molecule B. The T^{ab} are the electrostatic tensors between two expansion centers **a** and **b**. Note that Einstein convention, the repeated-subscript summation convention, is used here for Cartesian coordinates (suffix) to avoid cumbersome equations. Substituting Eq. (19), truncated at the dipole-quadrupole term, into Eq. (2) and combining with Eq. (6) gives,

$$
\begin{aligned}
E^{disp} &= -\sum_{\substack{m\neq 0\\ n\neq 0}} \sum_{a,c\in A} \sum_{b,d\in B} \frac{\left\{\begin{array}{l}
\langle 0_A|\langle 0_B|T^{ab}_{\alpha\beta}\mu^a_\alpha\mu^b_\beta|m\rangle|n\rangle\langle m|\langle n|T^{cd}_{\gamma\sigma}\mu^c_\gamma\mu^d_\sigma|0_A\rangle|0_B\rangle \\
+\langle 0_A|\langle 0_B|T^{ab}_{\alpha\beta}\mu^a_\alpha\mu^b_\beta|m\rangle|n\rangle\langle m|\langle n|\frac{1}{3}T^{cd}_{\gamma\sigma\kappa}(\mu^c_\gamma\theta^d_{\sigma\kappa}-\theta^c_{\gamma\sigma}\mu^d_\kappa)|0_A\rangle|0_B\rangle \\
+\langle 0_A|\langle 0_B|\frac{1}{3}T^{ab}_{\alpha\beta\gamma}(\mu^a_\alpha\theta^b_{\beta\gamma}-\theta^a_{\alpha\beta}\mu^b_\gamma)|m\rangle|n\rangle\langle m|\langle n|T^{cd}_{\sigma\kappa}\mu^c_\sigma\mu^d_\kappa|0_A\rangle|0_B\rangle \\
+\langle 0_A|\langle 0_B|\frac{1}{3}T^{ab}_{\alpha\beta\gamma}(\mu^a_\alpha\theta^b_{\beta\gamma}-\theta^a_{\alpha\beta}\mu^b_\gamma)|m\rangle|n\rangle\langle m|\langle n|\frac{1}{3}T^{cd}_{\lambda\sigma\kappa}(\mu^c_\lambda\theta^d_{\sigma\kappa}-\theta^c_{\lambda\sigma}\mu^d_\kappa)|0_A\rangle|0_B\rangle
\end{array}\right\}}{E^A_{m0}+E^B_{n0}} \\
&= -\sum_{\substack{m\neq 0\\ n\neq 0}} \sum_{a,c\in A} \sum_{b,d\in B} \frac{\left\{T^{ab}_{\alpha\beta}T^{cd}_{\gamma\sigma}\langle 0_A|\mu^a_\alpha|m\rangle\langle 0_B|\mu^b_\beta|n\rangle\langle m|\mu^c_\gamma|0_A\rangle\langle n|\mu^d_\sigma|0_B\rangle\right\}}{E^A_{m0}+E^B_{n0}} \\
&\quad -\sum_{\substack{m\neq 0\\ n\neq 0}} \sum_{a,c\in A} \sum_{b,d\in B} \frac{1}{3} \frac{\left\{\begin{array}{l}
T^{ab}_{\alpha\beta}T^{cd}_{\gamma\sigma\kappa}\langle 0_A|\mu^a_\alpha|m\rangle\langle 0_B|\mu^b_\beta|n\rangle\langle m|\mu^c_\gamma|0_A\rangle\langle n|\theta^d_{\sigma\kappa}|0_B\rangle \\
-T^{ab}_{\alpha\beta}T^{cd}_{\gamma\sigma\kappa}\langle 0_A|\mu^a_\alpha|m\rangle\langle 0_B|\mu^b_\beta|n\rangle\langle m|\theta^c_{\gamma\sigma}|0_A\rangle\langle n|\mu^d_\kappa|0_B\rangle \\
+T^{ab}_{\alpha\beta\gamma}T^{cd}_{\sigma\kappa}\langle 0_A|\mu^a_\alpha|m\rangle\langle 0_B|\theta^b_{\beta\gamma}|n\rangle\langle m|\mu^c_\sigma|0_A\rangle\langle n|\mu^d_\kappa|0_B\rangle \\
-T^{ab}_{\alpha\beta\gamma}T^{cd}_{\sigma\kappa}\langle 0_A|\theta^a_{\alpha\beta}|m\rangle\langle 0_B|\mu^b_\gamma|n\rangle\langle m|\mu^c_\sigma|0_A\rangle\langle n|\mu^d_\kappa|0_B\rangle
\end{array}\right\}}{E^A_{m0}+E^B_{n0}} \\
&\quad -\sum_{\substack{m\neq 0\\ n\neq 0}} \sum_{a,c\in A} \sum_{b,d\in B} \frac{1}{9} \frac{\left\{T^{ab}_{\alpha\beta\gamma}T^{cd}_{\gamma\sigma\kappa}\left[\begin{array}{l}
\langle 0_A|\mu^a_\alpha|m\rangle\langle 0_B|\theta^b_{\beta\gamma}|n\rangle\langle m|\mu^c_\lambda|0_A\rangle\langle n|\theta^d_{\sigma\kappa}|0_B\rangle \\
-\langle 0_A|\theta^a_{\alpha\beta}|m\rangle\langle 0_B|\mu^b_\gamma|n\rangle\langle m|\mu^c_\lambda|0_A\rangle\langle n|\theta^d_{\sigma\kappa}|0_B\rangle \\
-\langle 0_A|\mu^a_\alpha|m\rangle\langle 0_B|\theta^b_{\beta\gamma}|n\rangle\langle m|\theta^c_{\lambda\sigma}|0_A\rangle\langle n|\mu^d_\kappa|0_B\rangle \\
+\langle 0_A|\theta^a_{\alpha\beta}|m\rangle\langle 0_B|\mu^b_\gamma|n\rangle\langle m|\theta^c_{\lambda\sigma}|0_A\rangle\langle n|\mu^d_\kappa|0_B\rangle
\end{array}\right]\right\}}{E^A_{m0}+E^B_{n0}}
\end{aligned}
\tag{20}
$$

Each term in the second equality of Eq. (20) can be symbolically represented as

$$
\sum_{\substack{m\neq 0\\ n\neq 0}} \sum_{a,c\in A} \sum_{b,d\in B} \frac{T^{ab}T^{cd}Q^aQ^cQ^bQ^d}{E_{m0}+E_{n0}} \tag{21}
$$

In Eq. (21) Q^a symbolizes the integral of a multipole moment expanded about the center **a**. By going through the same derivation as the single-expansion-center model, the dispersion energy calculated using the distributed model can be symbolically represented as

$$E_{disp} = \frac{1}{\hbar}\frac{2}{\pi}\sum_{\substack{m\neq 0\\ n\neq 0}}\sum_{a,c\in A}\sum_{b,d\in B}\int_0^\infty d\omega \frac{\omega_{m0}^A \omega_{n0}^B T^{ab} T^{cd} Q^a Q^c Q^b Q^d}{\left[(\omega_{m0}^A)^2+\omega^2\right]\left[(\omega_{n0}^B)^2+\omega^2\right]}$$
$$= \frac{1}{\hbar}\frac{2}{\pi}\sum_{a,c\in A}\sum_{b,d\in B} T^{ab} T^{cd}\int_0^\infty d\omega \left(\sum_{m\neq 0}\frac{\omega_{m0}^A Q^a Q^c}{\left[(\omega_{m0}^A)^2+\omega^2\right]}\right)\left(\sum_{n\neq 0}\frac{\omega_{n0}^B Q^b Q^d}{\left[(\omega_{n0}^B)^2+\omega^2\right]}\right) \quad (22)$$

Note that the two T tensors in Eq. (22) can now be different from each other. The terms in large brackets in the second equality in Eq. (22) have the form of a multipole-multipole dynamic polarizability tensor P [Eq. (23)]. The two multipole moments in Eq. (23) do not necessarily have the same expansion centers (that is, **a** can be different from **c**).

$$P^{ac} = \sum_{m\neq 0}\frac{\omega_{m0}^A Q^a Q^c}{\left[(\omega_{m0}^A)^2+\omega^2\right]} \quad (23)$$

Stone and Tong[23] termed the polarizability with the same expansion center (a = c) as 'local'. If the expansion centers differ (a ≠ c), the polarizability is termed 'non-local'. The non-local polarizability arises naturally from a distributed formulation in which a field in one region causes a response in another region of the same molecule. Stone and Tong have shown, in spherical tensor formalism, that the non-local multipole-multipole polarizability can be transformed into the local form by a shifting procedure provided that

the centers of the moments are not moved too far. This shifting procedure transforms the dispersion energy expression to a familiar site-site description:

$$E_{disp} = \frac{1}{\hbar}\frac{2}{\pi}\sum_{a\in A}\sum_{b\in B} T^{ab}T^{c\to a,d\to b}\int_0^\infty d\omega \left(\sum_{m\neq 0}\frac{\omega_{m0}^A Q^a Q^{c\to a}}{\left[(\omega_{m0}^A)^2+\omega^2\right]}\right)\left(\sum_{n\neq 0}\frac{\omega_{n0}^B Q^b Q^{d\to b}}{\left[(\omega_{n0}^B)^2+\omega^2\right]}\right) \quad (24)$$
$$= \frac{1}{\hbar}\frac{2}{\pi}\sum_{a\in A}\sum_{b\in B} T^{ab}T^{ab}\int_0^\infty d\omega P^a P^b$$

$Q^{c\to a}$ and $Q^{d\to b}$ symbolize the multipole moments whose centers have been shifted. This shifting treatment is formally exact at sufficiently long range. Stone and Tong have demonstrated that less than 2% error is incurred for small systems using the shifted formula[23].

In the EFP method, each LMO is taken to be a distributed "region" and naturally the LMO centroids are chosen as the expansion centers. Jensen and Gordon[25] introduced and implemented the localized charge distribution (LCD) method[26–32] for Hatree-Fock wave functions, in which the key idea is to partition the nuclear charge and assign part of the nuclear charge to a particular LMO predominantly associated with that nucleus. This "local" nuclear charge and the electrons in the LMO together constitute an electrically neutral LCD. The dipole moments of such neutral localized charge distributions are invariant with respect to the shifting. Consequently the dipole-dipole polarizability is the same before and after the shift. For the dipole-quadrupole polarizability, one can shift the origin of the dipole moment to coincide with the origin of the quadrupole moment, and again this gives an LMO dipole-quadrupole polarizability that is identical to that before the shift. Thus, the polarizabilities that are relevant to E7 are unchanged and a distributed

E7 expression without the non-local polarizabilities can be easily written. The E7 derived from the distributed multipole expansion at the centroids of LMOs is

$$E7(LMO) = -\frac{1}{3}\frac{\hbar}{\pi}\sum_{k\in A}^{LMO}\sum_{j\in B}^{LMO}\sum_{\alpha\beta\gamma\sigma\kappa}^{x,y,z} T_{\alpha\beta}^{kj}T_{\gamma\sigma\kappa}^{kj}\int_0^\infty d\omega\left[\alpha_{\alpha\gamma}^{k}(i\omega)A_{\beta,\sigma\kappa}^{j}(i\omega) - \alpha_{\beta\kappa}^{j}(i\omega)A_{\alpha,\gamma\sigma}^{k}(i\omega)\right] \quad (25)$$

where α^k is the dipole-dipole dynamic polarizability of the kth LMO expanded at its centroid. Similarly, A^j is the dipole-quadrupole dynamic polarizability of the jth LMO expanded at its centroid. This E7 dispersion energy is called E7 (LMO), to distinguish it from E7 calculated using molecular polarizabilities, which are called E7 (molecular).

The molecular dynamic polarizability can be partitioned into LMO contributions:

$$P^A(\omega) = \sum_{l\in A}^{LMO} P_l^A(\omega) \quad (26)$$

The decomposition is always valid for polarizabilities of any rank when the LMO polarizabilities use the same expansion center as the molecular polarizability. For the dipole-dipole polarizability, the dipole moments are invariant with respect to the origins as discussed above. So the LMO dynamic dipole polarizability that is obtained at the center of mass is equal to the LMO polarizability obtained at the centroids of the LMOs. However, the quadrupole moments are origin-dependent, which means the LMO dynamic dipole-quadrupole polarizability expanded at the centroids of the LMOs will be different from those expanded at the center-of-mass. The dipole-quadrupole polarizabilities obtained using different origins are related through the following transformation:

$$A'^{l}_{\alpha,\beta\gamma} = A^{l}_{\alpha,\beta\gamma} - \left(\frac{3}{2} r'_{\beta} \alpha^{l}_{\gamma\alpha} + \frac{3}{2} r'_{\gamma} \alpha^{l}_{\alpha\beta} - \sum_{\kappa} r'_{\kappa} \alpha^{l}_{\kappa\alpha} \delta_{\beta\gamma} \right) \tag{27}$$

where **r'** is the shift of the origin from the center of mass to the centroid of the lth LMO. A^{l} and A'^{l} are the dynamic LMO dipole-quadrupole polarizabilities expanded at the center of mass and the centroid of LMO l, respectively.

Renaming the transformed LMO dipole-quadrupole polarizability as A^{l} (i.e., dropping the superscript prime), substituting the transformed A^{l} into Eq. (25), and applying the same Gauss-Legendre numerical integration procedure, the final distributed E7 expression becomes

$$E7(LMO) = -\frac{1}{3}\frac{\hbar}{\pi} \sum_{k\in A}^{LMO} \sum_{j\in B}^{LMO} \sum_{\alpha\beta\gamma\sigma\kappa}^{x,y,z} T^{kj}_{\alpha\beta} T^{kj}_{\gamma\sigma\kappa} \sum_{n=1}^{12} W(n) \frac{2\omega_0}{(1-t_n)^2} \left[\alpha^{k}_{\alpha\gamma}(i\omega_n) A^{j}_{\beta,\sigma\kappa}(i\omega_n) - \alpha^{j}_{\beta\kappa}(i\omega_n) A^{k}_{\alpha,\gamma\sigma}(i\omega_n) \right] \tag{28}$$

To calculate the LMO dynamic dipole-quadrupole polarizability, the approach described by Champagne et al is followed[33]. The response is calculated in the same way as in the dipole-dipole case.[10,18]

$$\left(H^{(2)} H^{(1)} - (i\nu)^2 \right) Z = -H^{(2)} P \tag{29}$$

$H^{(1)}$ is the real orbital Hessian matrix.

$$H^{(1)}_{aibj} = (\varepsilon_a - \varepsilon_i)\delta_{ab}\delta_{ij} + 4(ai \mid bj) - (ab \mid ij) - (aj \mid bi) \tag{30}$$

where ε_i and ε_a are the occupied and virtual Hartree-Fock orbital energies, respectively. (ai|bj) etc. are the two-electron integrals over the molecular orbital basis. $H^{(2)}$ is used to calculate the magnetizability and is defined as

$$H^{(2)}_{aibj} = (\varepsilon_a - \varepsilon_i)\delta_{ab}\delta_{ij} + (ab \mid ij) - (aj \mid bi) \tag{31}$$

P in Eq. (29) is the perturbation, and in this case, is the dipole moment matrix,

$$P_{ai} = \langle \phi_a \mid \hat{\mu} \mid \phi_i \rangle \tag{32}$$

Once the response matrix Z is obtained, it is combined with the quadrupole moment integrals to form the dipole-quadrupole polarizability.

$$A_{\alpha,\beta\gamma}(i\nu) = \sum_{ai} 2 \langle \phi^a \mid \hat{\theta}_{\beta\gamma} \mid \phi^i \rangle Z^{ai}_{\alpha}(i\nu) \tag{33}$$

where the subscripts run over Cartesian coordinates and the superscripts i and a refer to the occupied and virtual orbital indices, respectively. Eq (33) gives the molecular dipole-quadrupole polarizability at the center of mass. The dipole-quadrupole contribution from the l^{th} LMO is obtained by transforming the canonical occupied orbitals to localized orbitals and summing over only the virtual orbitals.

$$A^{l}_{\alpha,\beta\gamma}(i\nu) = \sum_{a}^{vir} 2 \left(\sum_{i}^{occ} \langle \phi^a \mid \hat{\theta}_{\beta\gamma} \mid \phi^i \rangle T^{il} \right) \left(\sum_{i}^{occ} Z^{ai}_{\alpha}(i\nu) T^{il} \right) \tag{34}$$

Then the origin shift as in Eq. (27) is carried out to yield the LMO dipole-quadrupole polarizability at the respective centroid.

As for the R^{-6} contribution to the dispersion energy, a damping function is necessary for E7 to have the correct asymptotic behavior as R approaches zero. Both Tang-Toennies[34] and overlap-based[35] damping functions have been derived. The Tang-Toennies damping function for E7 has the form

$$f_7^{TT}(R) = 1 - \left(\sum_{k=0}^{7} \frac{(bR)^k}{k!} \right) \exp(-bR) \tag{35}$$

where the parameter b was previously chosen to be 1.5 for the E6 term[18,35]. The overlap-based damping function for E7 is

$$f_7^S = 1 - S^2 \sum_{n=0}^{3} \frac{(-2\ln|S|)^n}{n!} = 1 - S^2 \left(1 + (-2\ln|S|) + \frac{(-2\ln|S|)^2}{2!} + \frac{(-2\ln|S|)^3}{3!} \right) \tag{36}$$

where S is the matrix of the intermolecular overlap integrals over the LMOs.

Codes have been implemented into the GAMESS[36,37] software package to compute the dynamic molecular dipole-dipole and dipole-quadrupole polarizabilities expanded at the center of mass of the molecule, the dynamic LMO dipole-quadrupole polarizability expanded at the center of mass of the molecule, the origin shift from the center of mass to the LMO centroids for the LMO dipole-quadrupole polarizability, E7 using the molecular polarizability (Eq. 15) and using the distributed LMO polarizability (Eq. 25), overlap-based and Tang-Toennies damping functions, and auxiliary subroutines that write and read the dynamic polarizabilities.

The anisotropic R^{-6} dispersion interaction obtained from the molecular and LMO dipole-dipole polarizability, E6 (molecular) and E6 (LMO), respectively, have previously been derived[18,19]:

$$E6(molecular) = -\frac{\hbar}{2\pi}\sum_{\alpha\beta\sigma\lambda}^{x,y,z} T_{\alpha\beta}^{AB} T_{\sigma\lambda}^{AB} \int_0^\infty \alpha_{\alpha\sigma}^{A}(i\omega)\alpha_{\beta\lambda}^{B}(i\omega)\,d\omega \tag{37}$$

$$E6(LMO) = -\frac{\hbar}{2\pi}\sum_{k\in A}^{LMO}\sum_{j\in B}^{LMO}\sum_{\alpha\beta\sigma\lambda}^{x,y,z} T_{\alpha\beta}^{kj} T_{\sigma\lambda}^{kj} \int_0^\infty \alpha_{\alpha\sigma}^{k}(i\omega)\alpha_{\beta\lambda}^{j}(i\omega)\,d\omega \tag{38}$$

These anisotropic E6 expressions have been implemented in GAMESS as well, to illustrate the comparisons of the R^{-6} and R^{-7} dispersion interaction in this study.

Computational details

There are relatively few E7 calculations for molecules of arbitrary geometry in the literature, although explicit orientation dependent E7 expressions have been developed[38] for simple systems such as a pair of linear molecules. Magnasco and coworkers have done a series of studies on the LiH – LiH system in which they calculated full-CI quality, imaginary frequency-dependent dipole-dipole and dipole-quadrupole polarizabilities for ground state LiH and C_6 and C_7 dispersion coefficients for LiH – LiH.[39–42] The angle-dependent C_n dispersion coefficients for two linear molecules is[38–42]

$$\begin{aligned} &C_n(\theta_A,\theta_B,\varphi) = \sum_{L_A L_B M} C_n^{L_A L_B M} P_{L_A}^{M}(\cos\theta_A) P_{L_B}^{M}(\cos\theta_B)\cos M\varphi \\ &n = l_a + l_a^{'} + l_b + l_b^{'} + 2, \quad 0 \le M \le \min(L_A, L_B) \\ &|\, l_a - l_a^{'} \,| \le L_A \le l_a + l_a^{'}, \quad |\, l_b - l_b^{'} \,| \le L_B \le l_b + l_b^{'} \end{aligned} \tag{39}$$

The relative orientation of two LiH molecules is schematically illustrated in Fig. 1 in which θ_A, θ_B and φ are the angles that specify the relative orientation. The angle θ varies from 0 to π, and the angle φ varies from 0 to 2 π. In Figure 1, the increments in φ were taken to be p/4. l specifies the angular momentum quantum numbers of A and B. L_A and L_B are the resultant total angular momentum L of molecule A and molecule B, respectively. The P_L^M in Eq. (39) are the associated Legendre polynomials. The coefficient, $C_n^{L_A L_B M}$, is best expressed in terms of irreducible dispersion constants, which are linear combinations of elementary dispersion constants $C_{ab} = \left(1/2\pi\right)\int_0^\infty du\alpha_a(iu)\alpha_b(iu)$ where $a = l_a l_a' m$, $b = l_b l_b' m$ are labels specifying polarizabilities in spherical tensor form. Given the $C_7^{L_A L_B M}$,[40,42] an in-house Python program was written to generate LiH – LiH dimers of various relative orientations and to calculate $C_7(\theta_A, \theta_B, \varphi)$ and consequently E7 = C_7/R^7. R is the distance between the centers of mass of the two LiH molecules and is kept at 10 Bohr to ensure negligible overlap. The E7 values obtained in this manner are taken as the reference (benchmark) values against which the EFP E7 values will be compared. The E7 (benchmark) values can be directly compared with the EFP E7 (molecular) values since the center of mass is the EFP molecular polarizability expansion center and defines the EFP T tensors.

The molecular dynamic polarizabilities over the imaginary frequency range are computed in a preparatory time-dependent Hartree-Fock calculation in GAMESS with the 6-311++G(3df,2p) basis set. In the next section, E7 (molecular) is compared directly to the E7 (benchmark). The distributed LMO polarizabilities over the same imaginary frequency range are generated with the same 6-311++G(3df,2p) basis set, and the

expansion centers are shifted to the LMO centroids. The distributed E7, E7 (LMO), is calculated according to Eq. (25).

E6 (molecular), E7 (molecular), E6 (LMO), E7 (LMO), as well as the isotropic E6 (molecular) and E6 (LMO) have also been calculated for the following dimer systems: Ar, H_2, HF, water, ammonia, methane, methanol, and dicholoromethane. The equilibrium geometries of these dimer systems are taken from the previous study of the EFP-ab initio dispersion interaction.[19] All of the monomer EFP potentials are generated with the 6-311++G(3df,2p) basis set except methanol (6-311++G(2d,2p)) and dicholoromethane (6-31+G(d)). The SAPT calculations for these two systems were carried out using the smaller basis sets due to computational cost. The EFP potential energy curves, both E7 (LMO) alone and E6 (LMO)+E7 (LMO), have been generated for $(H_2O)_2$ and $(CH_4)_2$ by varying the intermolecular (center of mass to center of mass) distance from -0.8 Å to 0.8 Å, in increments of 0.2 Å, with respect to the equilibrium distance. Two damped potential energy curves, using the Tang-Toennies and overlap-based damping functions have also been generated. The E6 (LMO)+E7 (LMO) curves are compared to symmetry adapted perturbation theory (SAPT)[43] dispersion energies, which are available from previous studies[19]. All of the calculations described above were performed with the GAMESS software package[36,37].

Results and Discussion

By systematically varying θ_A, θ_B and φ as described in Section III, a total of 200 different configurations of LiH – LiH dimers were generated. The E7 (molecular) values for these configurations, calculated using the molecular dipole-dipole and dipole-

quadrupole polarizabilities expanded about the center of mass of the individual LiH molecules are compared in Table S1 (supporting information) to the E7 (benchmark) results by calculating the ratio E7 (molecular)/ E7 (benchmark). The agreement is excellent, with an average ratio of ~93% and a standard deviation of ~4%. The deviation is most likely attributable to the fact that EFP polarizabilities are generated using time dependent Hartree-Fock in which only CIS excited states are included. In contrast, the polarizabilities in references 29 and 30 are based on full configuration interaction (FCI). For configurations with parallel LiH ($\theta_A = \theta_B$), both E7 (benchmark) and E7 (molecular) are numerically tiny and are considered to be zero with an undefined ratio.

To better illustrate the E7 (molecular) trends Figures 2 and 3 are plotted using selected data from Table S1. LiH – LiH E7 (molecular) depends on the three angles, $\theta_A, \theta_B, \varphi$. To examine the φ-dependence, E7 (molecular) values for fixed θ_A and θ_B are plotted in Fig 2 as a function of φ. In Fig. 2, $\theta_A = \pi / 4$ is chosen as a representative example, and each line represents E7 (molecular) for a particular value of θ_B. As φ varies, E7 is almost constant for a particular θ_A and θ_B combination. Other θ_A and θ_B combinations behave similarly. It is also interesting to note that E7, unlike E6, can be either attractive or repulsive. From Fig 2 it can also be seen that E7 is quite sensitive to changes in θ_B. This observation is much more apparent in Fig. 3. Knowing that E7 is rather insensitive to variations of φ, Fig. 3 presents E7 with respect to changes of θ_A for fixed $\varphi = 0$. Each curve represents a different θ_B angle. As θ_A varies, the order of magnitude of E7 changes substantially and in some cases, the sign also changes. Similar curves are obtained for varying θ_B with fixed θ_A.

By examining the numbers in Fig. 3 and Table 1, some interesting observations may be made: The configurations that are symmetric about the lower left to upper right diagonal line, $(\theta_A, \theta_B, \varphi)$ and $(\pi - \theta_B, \pi - \theta_A, \varphi)$, have identical E7. This is expected since they are merely the mirror image of each other. The configurations that are symmetric about the upper left to lower right diagonal line have E7s that are ~equal in magnitude (difference < 1%) and opposite in sign. Such a relationship is expected from Eq. (39) and is verified by EFP calculations. These symmetry relationships are maintained for other values of φ and give rise to a rotationally averaged E7 (molecular) of zero.

A direct comparison for E7 (LMO) is difficult. Most distributed models use atomic polarizabilities that will (incorrectly) give a zero distributed E7. The centroid of the valence LMO of LiH does not coincide with its center of mass and therefore an E7 calculated using LMOs does not necessarily equal the E7 based on the molecular polarizability. However, it can be proved [see Appendix] that if the origins of the two interacting molecules are shifted uniformly, that is, in same direction and magnitude, E7 is invariant. This provides a way to check the origin shift implementation and the implementation for calculating E7 (LMO): Instead of shifting the expansion centers of the LMO polarizability from the center of mass to the LMO centroids, one can shift the expansion centers to an arbitrary point such that the shifting vectors are the same for the two interacting molecules. Then the E7 calculated from the molecular polarizability and the E7 calculated from this “arbitrarily” distributed polarizability should match. This indeed is the case for all of the configurations of LiH—LiH dimers assessed in this study.

Table 2 presents E7 (molecular) and E7 (LMO) computed for various dimer systems at their equilibrium configurations. Note that for Ar, the molecular dipole-quadrupole polarizability is the atomic dipole-quadrupole polarizability. Since an atom is centrosymmetric, its dipole-quadrupole polarizability is zero and consequently its E7 (molecular) is also zero. However, atomic LMOs do not necessarily possess an inversion center. Hence the LMO dipole-quadrupole polarizability of Ar atom is not zero, nor is E7 (LMO). The molecule H_2 contains an inversion center that also coincides with the H_2 LMO inversion center. It is expected that both molecular and LMO dipole-quadrupole polarizability tensors are zero, which give zero E7 (molecular) and E7 (LMO). In some cases, E7 (molecular) and E7 (LMO) can have different signs, reflecting the fact that different multipole expansions give different descriptions of the potential at a truncated finite order. E6 (molecular) and E6 (LMO), as well as their isotropic counterparts for these dimer systems are also computed and shown in Table 2. The isotropic E6 (molecular) deviate very little from the anisotropic E6 (molecular). For the distributed model, the deviations between isotropic and anisotropic E6 (LMO) are comparatively larger, although the absolute deviation is still less than 0.5 kcal/mol. This validates the isotropic approximation. At the equilibrium configurations of these dimer systems, E7 values (both the molecular and the distributed) are typically only a small fraction of the E6 values, although their signs can be different. For $(H_2O)_2$ and $(NH_3)_2$, E7 values are ~ 50% of E6 values and opposite in sign. When the sums E6+E7 are compared to the SAPT values, the errors are still relatively large, indicating that the series in Eq. (1) is not converged at the R^{-7} term and at least the R^{-8} dispersion term is necessary.

One interesting observation is that the dispersion contributions calculated from molecular and LMO polarizabilities can be strikingly different. For example, E6 (LMO) for H_2O and NH_3 dimers are more than double the corresponding E6 (molecular) values. E7 (LMO) and E7 (molecular) can also be rather different. In some cases, E7 (molecular) and E7 (LMO) have different signs, not surprising since the E7 sign is not always negative. To illustrate how these differences arise, consider the simplest case, isotropic E6 (LMO) and E6 (molecular)[18,19]:

$$\begin{aligned} isotropic\ E6\ (molecular) &= \frac{C_6^{AB}}{R_{AB}^6} = \frac{\alpha^A \alpha^B}{R_{AB}^6} = \frac{\left(\sum_{k\in A} \alpha^k\right)\left(\sum_{l\in B} \alpha^l\right)}{R_{AB}^6} \\ &= \sum_{kl}^{LMO} \frac{\alpha^k \alpha^l}{R_{AB}^6} = \sum_{kl}^{LMO} \frac{C_6^{kl}}{R_{AB}^6} \end{aligned} \tag{40}$$

$$isotropic\ E6\ (LMO) = \sum_{kl}^{LMO} \frac{C_6^{kl}}{R_{kl}^6} = \sum_{kl}^{LMO} \frac{\alpha^k \alpha^l}{R_{kl}^6} \tag{41}$$

where $\alpha = \frac{1}{3}\left(\alpha_{xx} + \alpha_{yy} + \alpha_{zz}\right)$ is the isotropic dynamic dipole-dipole polarizability. Since the dipole-dipole polarizability is invariant with respect to the origin shift, the molecular dipole-dipole polarizability can be partitioned into LMO contributions exactly (See Eq. 26). Consequently, the dispersion coefficient C_6^{AB} can be partitioned into C_6^{kl} contributions. The difference between the two E6 expressions in Eqs. 40 and 41 comes from the difference between R_{AB} and R_{kl}. R_{AB} is the distance between the centers of mass of A and B. R_{kl} is the distance between the centroids of LMOs k and l, respectively. By an extension of this argument, anisotropic molecular and distributed LMO formulations use different T tensors [See Eqs. (37, 38)] and consequently yield different dispersion

energies. Moreover, for E7 (LMO), the LMO dipole-quadrupole polarizability is also being transformed by the origin-shift formula (Eq. 27). In essence, the different definitions of the electrostatic T tensors and the origin shifting transformation are the causes of the discrepancy between the dispersion energies calculated with molecular and LMO formulations. Fundamentally, the two formulations express the interaction operator as two different expansions. The total dispersion energies calculated by the two expansions theoretically converge to the same value, just as the oscillator strengths based on the dipole length and the dipole velocity converge to the exact result in the limit of a full configuration interaction wave function. Conceptually the distributed formulation is expected to converge faster by the following argument. A molecular dipole can be regarded as two separated point charges, a molecular quadrupole can be considered as arising from the separation of two dipoles. In other words, the distributed multipoles of lower rank may resemble molecular multipoles of higher rank.[44] Consequently, E6 (LMO) captures higher order dispersion terms such as E7 (molecular) and even higher order contributions. So, agreement between the two formulations will be achieved for the total dispersion energy when the molecular and distributed multipole expansions are carried out to complete order, although there is no one-to-one correspondence between the individual terms of the different expansions.

Figure 4 plots the E7 (LMO) values of two dimer systems, $(H_2O)_2$ and $(CH_4)_2$, at various intermolecular distances, from -0.8 Å to 0.8 Å with respect to the equilibrium distance. Both un-damped values and damped E7 (LMO) using the two different damping functions are plotted. As mentioned in Section II, the purpose of the damping function is to ensure the correct asymptotic behavior as R approaches zero. From Figure 4, the Tang-

Toennies function appears to over-damp E7 (LMO), i.e. Tang-Toennies damped E7 (LMO) tends to be too weak at shorter intermolecular distances. Hence the overlap-based damping function is chosen to be the default damping option for EFP-EFP E7 (LMO) calculations.

Figure 5 compares the E6 (LMO)+E7 (LMO) dispersion energies for $(H_2O)_2$ and $(CH_4)_2$, with or without damping, to the SAPT values. Overall, the overlap-damped dispersion curve resembles the SAPT curve better. At short intermolecular distances, the overlap-damped $(H_2O)_2$ dispersion energy appears to be more negative than the non-damped value although it is closer to the SAPT value. This is because the non-damped E7 (LMO) is positive and much larger than the overlap-damped E7 (LMO), which makes the sum of E6 and E7 less negative. The Tang-Toennies damping function shows the same over-damping problem noted above.

Conclusion and Future work

A general expression for the R^{-7} contribution to the dispersion energy between two molecular systems in the EFP framework has been derived and implemented in the GAMESS software package. The R^{-7} dispersion interaction can be computed using either molecular (E7 (molecular)) or LMO (E7 (LMO)) dynamic dipole-quadrupole polarizability tensors over the imaginary frequency range. The molecular dynamic dipole-quadrupole polarizability is computed from the dipole response and the quadrupole moments. For E7 (LMO), the proper LMO dynamic dipole-quadrupole polarizabilities are obtained after an origin shift transformation from the center of mass to the centroids of the LMOs. Two types of damping functions, overlap-based and Tang-

Toennies damping functions, have been implemented for the calculation of E7 (LMO). Both E7 (molecular) and E7 (LMO) magnitudes can change substantially and their signs can also change as the relative orientations of the molecules change. In other words, E7 is highly orientation-dependent. For systems with constrained configurations, e.g. molecular solids or crystal structures or reactions occurring on a surface, E7 could be a significant contribution to the total dispersion interaction. E7 is probably is not critical for room temperature gas phase or liquid phase structures where molecules are free to rotate and the E7 interactions are averaged out. The difference between the dispersion energies calculated with molecular and LMO polarizabilities is a manifestation of different expansions of the interaction operator truncated at a finite order. The comparison between SAPT with E6+E7 values suggests that the dispersion series is not converged at E7 and at least R^{-8} dispersion term should be added. The distributed formulation is expected to converge faster. Although this work has been presented in the context of the effective fragment potential method, the conclusions that are drawn here are very likely applicable to fully quantum calculations as well.

In order to perform geometry optimizations and molecular dynamics simulations, gradients of the R^{-7} dispersion energy will be the focus of future studies.

Acknowledgement

This work was supported by a grant from Air Force Office of Scientific Research. The authors are grateful for very helpful discussions with Mr. Stephen Berg, Dr. Roger D. Amos, Professor Lyudmila Slipchenko and Professor Piotr Piecuch.

Appendix

Since the dipole-quadrupole polarizability is origin-dependent, the question to ask naturally is, is E7 also origin-dependent?

Suppose the shift of the expansion centers is $r^{A'}$ and $r^{B'}$ for molecule A and B, respectively. Accordingly, the dipole-quadrupole polarizabilities of A and B become,

$$A^{A'}_{\alpha,\gamma\sigma} = A^{A}_{\alpha,\gamma\sigma} - \left(\frac{3}{2} r^{A'}_{\gamma} \alpha^{A}_{\sigma\alpha} + \frac{3}{2} r^{A'}_{\sigma} \alpha^{A}_{\alpha\gamma} - r^{A'}_{\mu} \alpha^{A}_{\mu\alpha} \delta_{\gamma\sigma} \right) \tag{A1}$$

$$A^{B'}_{\beta,\sigma\kappa} = A^{B}_{\beta,\sigma\kappa} - \left(\frac{3}{2} r^{B'}_{\sigma} \alpha^{B}_{\kappa\beta} + \frac{3}{2} r^{B'}_{\kappa} \alpha^{B}_{\beta\sigma} - r^{B'}_{\mu} \alpha^{B}_{\mu\beta} \delta_{\sigma\kappa} \right) \tag{A2}$$

The superscripts A and B denote the original expansion centers for molecules A and B, respectively. And A' and B' denote the new expansion centers. The subscripts denote the Cartesian coordinates x, y and z. δ is the Kronecker delta function. Note that due to the origin-shift, the T tensors are also altered. Therefore now the E7 expression becomes

$$E7 = -\frac{\hbar}{3\pi} T^{A'B'}_{\alpha\beta} T^{A'B'}_{\gamma\sigma\kappa} \int_0^\infty d\omega \left[\alpha^{A'}_{\alpha\gamma}(i\omega) A^{B'}_{\beta,\sigma\kappa}(i\omega) - \alpha^{B'}_{\beta\kappa}(i\omega) A^{A'}_{\alpha,\gamma\sigma}(i\omega) \right]$$

$$= -\frac{\hbar}{3\pi} T^{A'B'}_{\alpha\beta} T^{A'B'}_{\gamma\sigma\kappa} \int_0^\infty d\omega \left[\begin{array}{l} \alpha^{A}_{\alpha\gamma}(i\omega) \left(A^{B}_{\beta,\sigma\kappa}(i\omega) - \left(\frac{3}{2} r^{B'}_{\sigma} \alpha^{B}_{\kappa\beta}(i\omega) + \frac{3}{2} r^{B'}_{\kappa} \alpha^{B}_{\beta\sigma}(i\omega) - r^{B'}_{\mu} \alpha^{B}_{\mu\beta}(i\omega) \delta_{\sigma\kappa} \right) \right) \\ -\alpha^{B}_{\beta\kappa}(i\omega) \left(A^{A}_{\alpha,\gamma\sigma}(i\omega) - \left(\frac{3}{2} r^{A'}_{\gamma} \alpha^{A}_{\sigma\alpha}(i\omega) + \frac{3}{2} r^{A'}_{\sigma} \alpha^{A}_{\alpha\gamma}(i\omega) - r^{A'}_{\mu} \alpha^{A}_{\mu\alpha}(i\omega) \delta_{\gamma\sigma} \right) \right) \end{array} \right] \tag{A3}$$

From Eq. (A3), E7 calculated from these new polarizabilities, in general, do not necessarily equal to the E7 calculated previously.

However, if $r^{A'} = r^{B'} = r'$, i.e. uniform translation of the origins, the T tensors are unchanged because the intermolecular distance R that defines the T tensors remains the same. Now Eq (A3) becomes

$$E7 = -\frac{\hbar}{3\pi} T^{AB}_{\alpha\beta} T^{AB}_{\gamma\sigma\kappa} \int_0^\infty d\omega \begin{bmatrix} \alpha^A_{\alpha\gamma}(i\omega)\left(A^B_{\beta,\sigma\kappa}(i\omega) - \left(\frac{3}{2} r'_\sigma \alpha^B_{\kappa\beta}(i\omega) + \frac{3}{2} r'_\kappa \alpha^B_{\beta\sigma}(i\omega) - r'_\mu \alpha^B_{\mu\beta}(i\omega)\delta_{\sigma\kappa} \right) \right) \\ -\alpha^B_{\beta\kappa}(i\omega)\left(A^A_{\alpha,\gamma\sigma}(i\omega) - \left(\frac{3}{2} r'_\gamma \alpha^A_{\sigma\alpha}(i\omega) + \frac{3}{2} r'_\sigma \alpha^A_{\alpha\gamma}(i\omega) - r'_\mu \alpha^A_{\mu\alpha}(i\omega)\delta_{\gamma\sigma} \right) \right) \end{bmatrix} \quad \text{(A4)}$$

The change in E7 is

$$E7 = -\frac{\hbar}{3\pi} T^{AB}_{\alpha\beta} T^{AB}_{\gamma\sigma\kappa} \int_0^\infty d\omega \begin{bmatrix} -\alpha^A_{\alpha\gamma}(i\omega)\left(\frac{3}{2} r'_\sigma \alpha^B_{\kappa\beta}(i\omega) + \frac{3}{2} r'_\kappa \alpha^B_{\beta\sigma}(i\omega) - r'_\mu \alpha^B_{\mu\beta}(i\omega)\delta_{\sigma\kappa} \right) \\ +\alpha^B_{\beta\kappa}(i\omega)\left(\frac{3}{2} r'_\gamma \alpha^A_{\sigma\alpha}(i\omega) + \frac{3}{2} r'_\sigma \alpha^A_{\alpha\gamma}(i\omega) - r'_\mu \alpha^A_{\mu\alpha}(i\omega)\delta_{\gamma\sigma} \right) \end{bmatrix}$$

$$= -\frac{\hbar}{3\pi} \int_0^\infty d\omega \begin{bmatrix} -\frac{3}{2} T^{AB}_{\alpha\beta} T^{AB}_{\gamma\sigma\kappa} r'_\sigma \alpha^A_{\alpha\gamma}(i\omega)\alpha^B_{\kappa\beta}(i\omega) - \frac{3}{2} T^{AB}_{\alpha\beta} T^{AB}_{\gamma\sigma\kappa} r'_\kappa \alpha^A_{\alpha\gamma}(i\omega)\alpha^B_{\beta\sigma}(i\omega) + T^{AB}_{\alpha\beta} T^{AB}_{\gamma\sigma\kappa} \alpha^A_{\alpha\gamma}(i\omega) r'_\mu \alpha^B_{\mu\beta}(i\omega)\delta_{\sigma\kappa} \\ +\frac{3}{2} T^{AB}_{\alpha\beta} T^{AB}_{\gamma\sigma\kappa} r'_\gamma \alpha^B_{\beta\kappa}(i\omega)\alpha^A_{\sigma\alpha}(i\omega) + \frac{3}{2} T^{AB}_{\alpha\beta} T^{AB}_{\gamma\sigma\kappa} r'_\sigma \alpha^B_{\beta\kappa}(i\omega)\alpha^A_{\alpha\gamma}(i\omega) - T^{AB}_{\alpha\beta} T^{AB}_{\gamma\sigma\kappa} \alpha^B_{\beta\kappa}(i\omega) r'_\mu \alpha^A_{\mu\alpha}(i\omega)\delta_{\gamma\sigma} \end{bmatrix} \quad \text{(A5)}$$

Since the dipole-dipole polarizability is symmetric with respect to interchange of the two suffixes, the 1st and the second last terms in Eq. (A5) cancel each other. By the definition of the T tensors, the T tensors with two or more suffixes are invariant with respect to interchange of suffixes. The 2nd and 4th terms can be rewritten as

$$\begin{aligned} &-\frac{3}{2} T^{AB}_{\beta\alpha} \alpha^A_{\alpha\gamma}(i\omega) T^{AB}_{\gamma\sigma\kappa} r'_\kappa \alpha^B_{\sigma\beta}(i\omega) \\ &+\frac{3}{2} T^{AB}_{\beta\alpha} \alpha^A_{\alpha\sigma}(i\omega) T^{AB}_{\sigma\kappa\gamma} r'_\gamma \alpha^B_{\kappa\beta}(i\omega) \end{aligned} \quad \text{(A6)}$$

Recall that Einstein summation convention is used here: a repeated subscript implies summation over that subscript. Therefore one can see that the two terms in (A6) are equal in magnitude and opposite in sign, and hence cancel each other. The 3rd term in Eq. (A5) is

$$T_{\alpha\beta}^{AB} T_{\gamma\sigma\kappa}^{AB} \alpha_{\alpha\gamma}^{A}(i\omega) r_{\mu}^{'} \alpha_{\mu\beta}^{B}(i\omega) \delta_{\sigma\kappa} = (T_{\gamma\sigma\kappa}^{AB} \delta_{\sigma\kappa}) \alpha_{\gamma\alpha}^{A}(i\omega) T_{\alpha\beta}^{AB} \alpha_{\beta\mu}^{B}(i\omega) r_{\mu}^{'} \tag{A7}$$

The term in the parenthesis

$$\begin{aligned} T_{\gamma\sigma\kappa}^{AB} \delta_{\sigma\kappa} &= T_{\gamma\sigma\sigma}^{AB} \\ &= \frac{15 R_\gamma R_\sigma R_\sigma - 3R^2 \left(R_\gamma \delta_{\sigma\sigma} + R_\sigma \delta_{\gamma\sigma} + R_\sigma \delta_{\gamma\sigma} \right)}{R^7} \\ &= \frac{15 R_\gamma R^2 - 3R^2 \left(3R_\gamma + 2R_\sigma \delta_{\gamma\sigma} \right)}{R^7} \\ &= \frac{15 R_\gamma R^2 - 3R^2 \left(3R_\gamma + 2R_\gamma \right)}{R^7} \\ &= \frac{15 R_\gamma R^2 - 15 R^2 R_\gamma}{R^7} \\ &= 0 \end{aligned} \tag{A8}$$

Again, the Einstein summation convention is implied here. Hence the 3rd term, and similarly the last term, in Eq. (A5) are both zero. So, overall E7 is unchanged when the origin-shifts are the same for both molecules.

References

(1) Pruitt, S. R.; Leang, S. S.; Xu, P.; Fedorov, D. G.; Gordon, M. S. Hexamers and Witchamers: Which Hex Do You Choose?. *Comput. Theor. Chem.* **2013**, *1021*, 70–83.

(2) Burley, S. K.; Petsko, G. A. Aromatic-Aromatic Interaction: A Mechanism of Protein Structure Stabilization. *Sci. (Washington, DC, United States)* **1985**, *229*, 23–28.

(3) Saenger, W. *Principles of Nucleic Acid Structure.*; Springer-Verlag, 1984; p. 556 pp.

(4) Lerman, L. S. Structural Considerations in the Interaction of Deoxyribonucleic Acid and Acridines. *mol. biol.* **1961**, *3*, 18–30.

(5) Brana, M. F.; Cacho, M.; Gradillas, A.; De B., P.-T.; Ramos, A. Intercalators as Anticancer Drugs. *Curr. Pharm. Des.* **2001**, *7*, 1745–1780.

(6) Eisenschitz, R.; London, F. The Relation between the van Der Weals Forces and the Homeopolar Valence Forces. *Zeitschrift fuer Phys.* **1930**, *60*, 491–527.

(7) London, F. Theory and Systematics of Molecular Forces. *Zeitschrift fuer Phys.* **1930**, *63*, 245–279.

(8) London, F. The General Theory of Molecular Forces. *Trans. Faraday Soc.* **1937**, *33*, 8–26.

(9) Stone, A. J.; Editor. *The Theory of Intermolecular Forces.*; Oxford Univ Press, 1996.

(10) Amos, R. D.; Handy, N. C.; Knowles, P. J.; Rice, J. E.; Stone, A. J. AB-Initio Prediction of Properties of Carbon Dioxide, Ammonia, and Carbon Dioxide...ammonia. *J. Phys. Chem.* **1985**, *89*, 2186–2192.

(11) Buckingham, A. D. Theory of Long-Range Dispersion Forces. *Discuss. Faraday Soc.* **1965**, *No. 40*, 232–238.

(12) Day, P. N.; Jensen, J. H.; Gordon, M. S.; Webb, S. P.; Stevens, W. J.; Krauss, M.; Garmer, D.; Basch, H.; Cohen, D. An Effective Fragment Method for Modeling Solvent Effects in Quantum Mechanical Calculations. *J. Chem. Phys.* **1996**, *105*, 1968–1986.

(13) Stone, A. J. Distributed Multipole Analysis, or How to Describe a Molecular Charge Distribution. *Chem. Phys. Lett.* **1981**, *83*, 233–239.

(14) Stone, A. J.; Alderton, M. Distributed Multipole Analysis Methods and Applications. *Mol. Phys.* **1985**, *56*, 1047–1064.

(15) Jensen, J. H.; Gordon, M. S. An Approximate Formula for the Intermolecular Pauli Repulsion between Closed Shell Molecules. *Mol. Phys.* **1996**, *89*, 1313–1325.

(16) Li, H.; Gordon, M. S.; Jensen, J. H. Charge Transfer Interaction in the Effective Fragment Potential Method. *J. Chem. Phys.* **2006**, *124*, 214108/1–214108/16.

(17) Xu, P.; Gordon, M. S. Charge Transfer Interaction Using Quasiatomic Minimal-Basis Orbitals in the Effective Fragment Potential Method. *J. Chem. Phys.* **2013**, *139*, 194104/1–194104/11.

(18) Adamovic, I.; Gordon, M. S. Dynamic Polarizability, Dispersion Coefficient C6 and Dispersion Energy in the Effective Fragment Potential Method. *Mol. Phys.* **2005**, *103*, 379–387.

(19) Smith, Q. A.; Ruedenberg, K.; Gordon, M. S.; Slipchenko, L. V. The Dispersion Interaction between Quantum Mechanics and Effective Fragment Potential Molecules. *J. Chem. Phys.* **2012**, *136*, 244107/1–244107/12.

(20) Casimir, H. B. G.; Polder, D. The Influence of Retardation on the London-van Der Waals Forces. *Phys. Rev.* **1948**, *73*, 360–372.

(21) Gross, E. K. U.; Ullrich, C. A.; Gossmann, U. J. Density Functional Theory of Time-Dependent Systems. *NATO ASI Ser. Ser. B Phys.* **1995**, *337*, 149–171.

(22) Stone, A. J. Distributed Polarizabilities. *Mol. Phys.* **1985**, *56*, 1065–1082.

(23) Stone, A. J.; Tong, C. S. Local and Nonlocal Dispersion Models. *Chem. Phys.* **1989**, *137*, 121–135.

(24) Williams, G. J.; Stone, A. J. Distributed Dispersion: A New Approach. *J. Chem. Phys.* **2003**, *119*, 4620–4628.

(25) Jensen, J. H.; Gordon, M. S. Ab Initio Localized Charge Distributions: Theory and a Detailed Analysis of the Water Dimer-Hydrogen Bond. *J. Phys. Chem.* **1995**, *99*, 8091–8107.

(26) England, W.; Gordon, M. S. Localized Charge Distributions. I. General Theory, Energy Partitioning, and the Internal Rotation Barrier in Ethane. *J. Am. Chem. Soc.* **1971**, *93*, 4649–4657.

(27) England, W.; Gordon, M. S. Localized Charge Distributions. II. Interpretation of the Barriers to Internal Rotation in Hydrogen Peroxide. *J. Am. Chem. Soc.* **1972**, *94*, 4818–4823.

(28) Gordon, M. S.; England, W. Localized Charge Distributions. III. Transferability and Trends of Carbon-Hydrogen Moments and Energies in Acyclic Hydrocarbons. *J. Am. Chem. Soc.* **1972**, *94*, 5168–5178.

(29) Gordon, M. S.; England, W. Localized Charge Distributions. Internal Rotation Barrier in Borazane. *Chem. Phys. Lett.* **1972**, *15*, 59–64.

(30) Gordon, M. S.; England, W. Localized Charge Distributions. V. Internal Rotation Barriers in Methylamine, Methyl Alcohol, Propene, and Acetaldehyde. *J. Am. Chem. Soc.* **1973**, *95*, 1753–1760.

(31) Gordon, M. S. Localized Charge Distributions. VI. Internal Rotation in Formaldoxime and Formic Acid. *J. Mol. Struct.* **1974**, *23*, 399–410.

(32) England, W.; Gordon, M. S.; Ruedenberg, K. Localized Charge Distributions. VII. Transferable Localized Molecular Orbitals for Acyclic Hydrocarbons. *Theor. Chim. Acta* **1975**, *37*, 177–216.

(33) Quinet, O.; Liegeois, V.; Champagne, B. TDHF Evaluation of the Dipole-Quadrupole Polarizability and Its Geometrical Derivatives. *J. Chem. Theory Comput.* **2005**, *1*, 444–452.

(34) Tang, K. T.; Toennies, J. P. An Improved Simple Model for the van Der Waals Potential Based on Universal Damping Functions for the Dispersion Coefficients. *J. Chem. Phys.* **1984**, *80*, 3726–3741.

(35) Slipchenko, L. V; Gordon, M. S. Damping Functions in the Effective Fragment Potential Method. *Mol. Phys.* **2009**, *107*, 999–1016.

(36) Schmidt, M. W.; Baldridge, K. K.; Boatz, J. A.; Elbert, S. T.; Gordon, M. S.; Jensen, J. H.; Koseki, S.; Matsunaga, N.; Nguyen, K. A.; et, al. General Atomic and Molecular Electronic Structure System. *J. Comput. Chem.* **1993**, *14*, 1347–1363.

(37) Gordon, M. S.; Schmidt, M. W. Advances in Electronic Structure Theory: GAMESS a Decade Later. In *Theory Appl. Comput. Chem.: First Forty Years*; Elsevier B.V., 2005; pp. 1167–1189.

(38) Meyer, W. Dynamic Multipole Polarizabilities of Hydrogen and Helium and Long-Range Interaction Coefficients for Hydrogen-Hydrogen, Hydrogen-Helium and Helium-Helium. *Chem. Phys.* **1976**, *17*, 27–33.

(39) Bendazzoli, G. L.; Magnasco, V.; Figari, G.; Rui, M. Full-CI Calculation of Imaginary Frequency-Dependent Dipole Polarizabilities of Ground State LiH and the C6 Dispersion Coefficients of LiH-LiH. *Chem. Phys. Lett.* **2000**, *330*, 146–151.

(40) Luigi Gian, B.; Magnasco, V.; Figari, G.; Rui, M. Full-CI Calculation of Imaginary Frequency-Dependent Dipole-Quadrupole Polarizabilities of Ground State LiH and the C7 Dispersion Coefficients of LiH-LiH. *Chem. Phys. Lett.* **2002**, *363*, 540–543.

(41) Bendazzoli, G. L.; Monari, A.; Magnasco, V.; Figari, G.; Rui, M. An Enlarged Basis Full-CI Calculation of C7 Dispersion Coefficients for the LiH-LiH Homodimer. *Chem. Phys. Lett.* **2003**, *382*, 393–398.

(42) Luigi Gian, B.; Magnasco, V.; Figari, G.; Rui, M. Full-CI Calculation of Imaginary Frequency-Dependent Dipole-Quadrupole Polarizabilities of Ground State LiH and the C7 Dispersion Coefficients of LiH-LiH. [Erratum to Document Cited in CA137:358415]. *Chem. Phys. Lett.* **2003**, *381*, 526–527.

(43) Jeziorski, B.; Moszynski, R.; Szalewicz, K. Perturbation Theory Approach to Intermolecular Potential Energy Surfaces of van Der Waals Complexes. *Chem. Rev. (Washington, DC, United States)* **1994**, *94*, 1887–1930.

(44) Buckingham, A. D. Molecular Quadrupole Moments. *Q. Rev.* **1959**, *8*, 183–214.

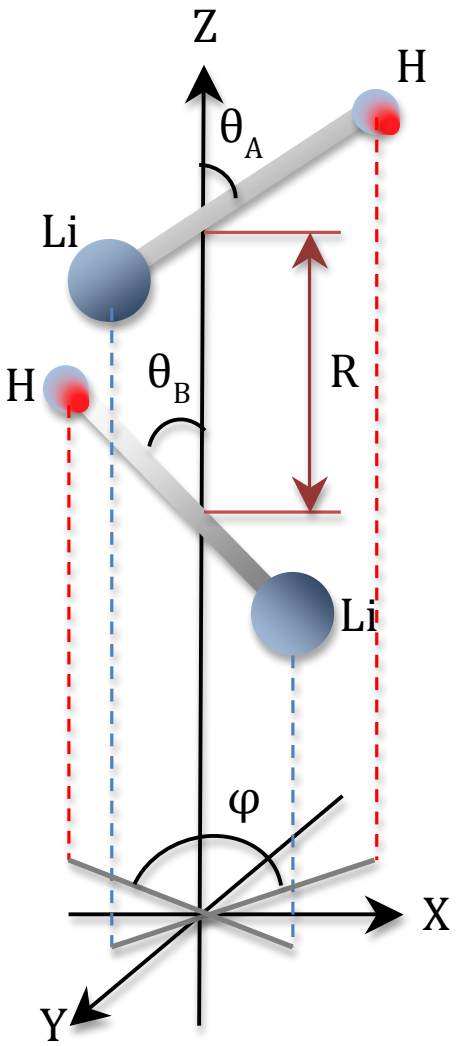

Figure 1 a schematic representation of LiH – LiH dimer. The LiH molecules intersect with Z-axis at their centers of mass. R is the distance between the two centers of mass, which is set to 10 Bohr in this study.

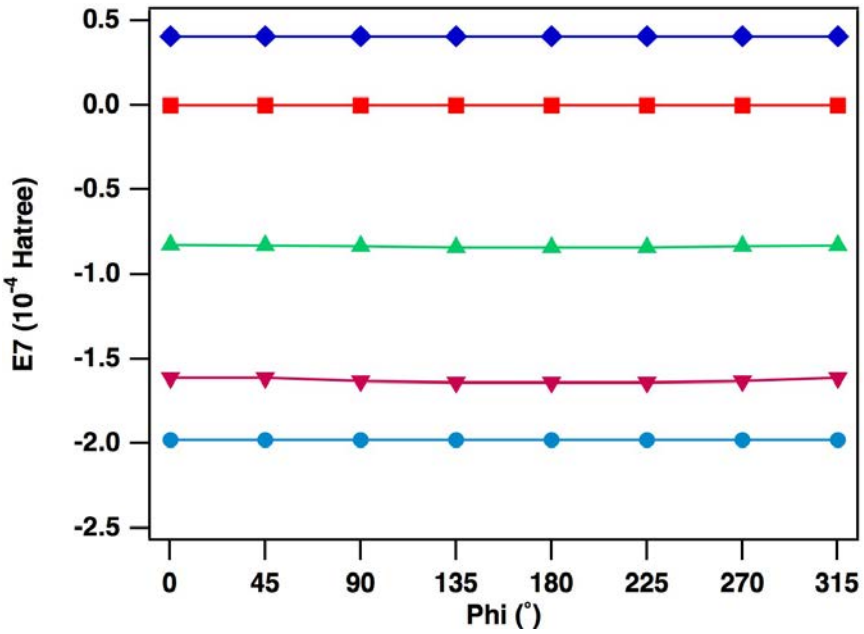

Figure 2 E7 (in 10^{-4} Hartree) as a function of the angle φ, calculated from dynamic molecular polarizabilities over the imaginary frequency range for LiH – LiH dimer with $\theta_A = \pi/4$, θ_B varying from 0 to π and φ from 0 to 2π, in increments of $\pi/4$, from the top line to the bottom line.

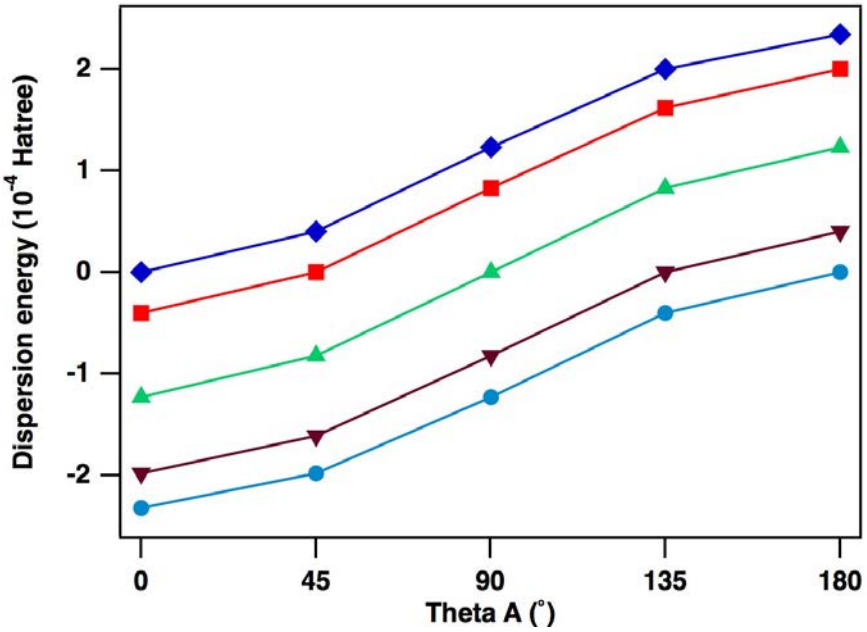

Figure 3 E7 (in 10^{-4} Hartree) as a function of the angle θ_A, calculated from dynamic molecular polarizabilities over the imaginary frequency range for LiH – LiH dimer with $\varphi = 0$, θ_B varying from 0 to π in increments of $\pi/4$, from the top line to the bottom line.

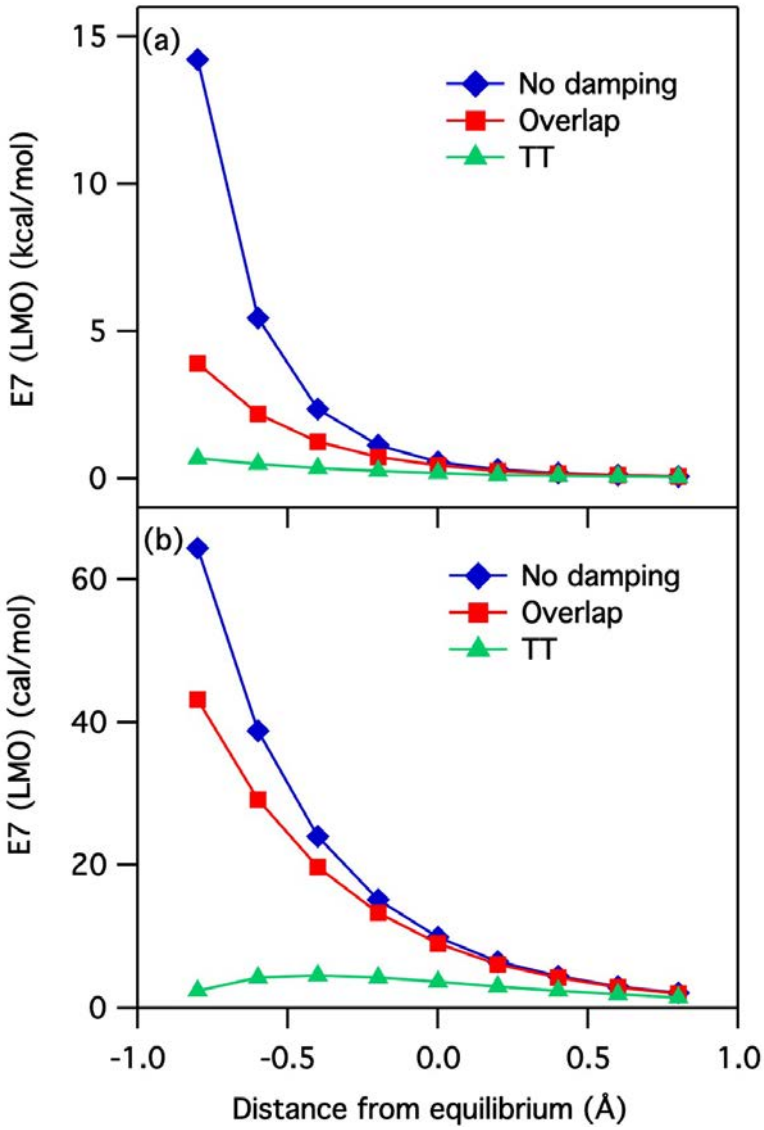

Figure 4 (a) water dimer (b) methane dimer: E7 (LMO) calculated at various intermolecular distances ranging from -0.8 to +0.8 Å away from the equilibrium distance. The effect of two types of damping function are also shown in the figure: the red squares represent the damped E7 (LMO) by an overlap-based damping function and the green triangles represent the damped E7 (LMO) by the Tang-Toennies damping function.

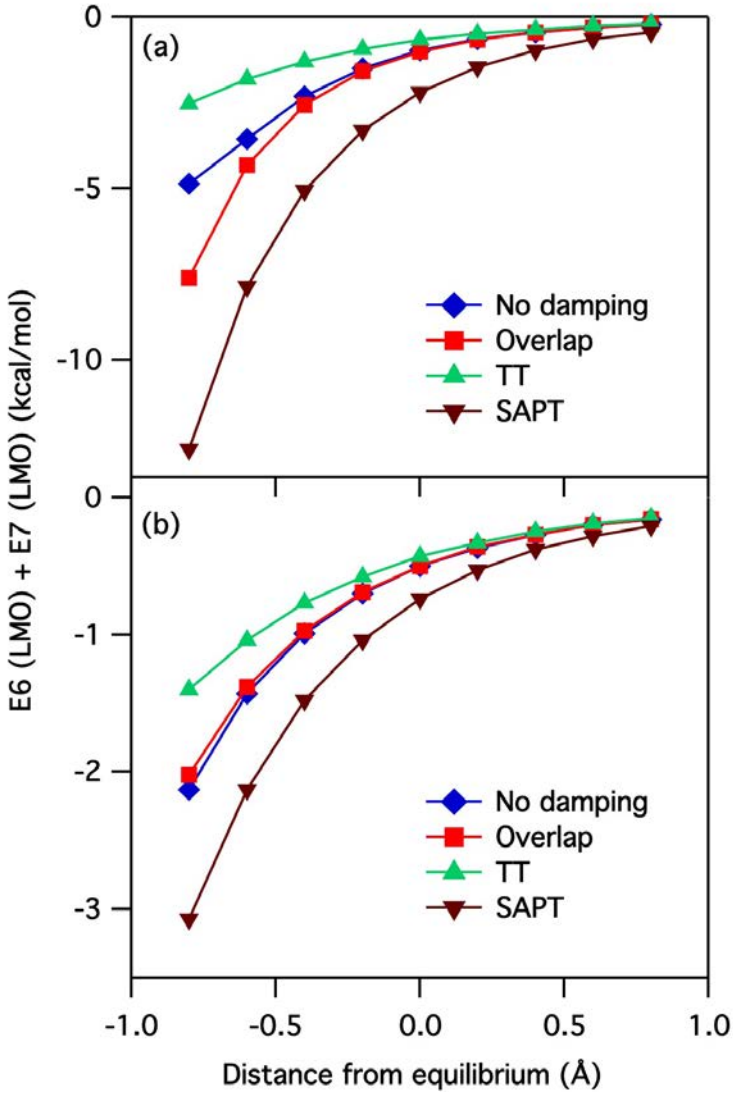

Figure 5 (a) water dimer (b) methane dimer: E6 (LMO)+E7 (LMO) dispersion energy calculated at various intermolecular distances ranging from -0.8 to 0.8 Å away from the equilibrium distance. The effect of the two types of damping function are also shown in the figure: the red squares represent the damped dispersion energy by an overlap-based damping function and the green triangles represent the damped dispersion by the Tang-Tonnies damping function. The SAPT numbers are shown as brown triangles.

Table 1 E7 (molecular) (in Hartree) calculated from dynamic molecular polarizabilities over the imaginary frequency range for LiH – LiH dimer for $\varphi = 0$, θ_A (the x-axis) and θ_B (the y-axis) varying from 0 to π, in increments of π/4.

θ_B \ θ_A	0	π/4	π/2	3π/4	π
0	1.09E-56	4.04E-05	1.23E-04	2.00E-04	2.34E-04
π/4	-4.04E-05	1.18E-15	8.28E-05	1.62E-04	2.00E-04
π/2	-1.23E-04	-8.25E-05	-8.66E-21	8.28E-05	1.23E-04
3π/4	-1.98E-04	-1.61E-04	-8.25E-05	5.38E-16	4.04E-05
π	-2.32E-04	-1.98E-04	-1.23E-04	-4.04E-05	-3.88E-55

Table 2 E6 (molecular), E7 (molecular), E6 (LMO) and E7 (LMO) for various dimer systems at their equilibrium distances, in kcal/mol. Isotropic E6 (molecular) and isotropic E6 (LMO) values calculated from LMO dipole polarizabilities are also presented. The SAPT dispersion+exchange dispersion values are listed here as well.

	SAPT	E6 molecular	E6 molecular isotropic	E7 molecular	E6 LMO	E6 LMO isotropic	E7 LMO
2Ar	-0.390	-0.265	-0.265	0.000	-0.285	-0.295	0.002
$2H_2$	-0.087	-0.058	-0.057	0.000	-0.058	-0.057	0.000
2HF	-1.661	-0.527	-0.499	-0.138	-0.777	-0.661	-0.059
$2H_2O$	-2.191	-0.787	-0.788	-0.107	-1.554	-1.095	0.573
$2NH_3$	-1.909	-0.736	-0.739	-0.046	-1.526	-1.111	0.718
$2CH_4$	-0.736	-0.415	-0.415	0.002	-0.509	-0.570	0.010
2MeOH	-2.253	-0.960	-0.944	0.641	-1.476	-1.252	0.373
$2CH_2Cl_2$	-2.074	-1.197	-1.314	-0.022	-1.802	-1.913	0.421

Supporting information

Table S1 E7 (benchmark) and E7 (molecular), in Hartree, computed for different combination of $(\theta_A, \theta_B, \varphi)$, with θ ranging from 0 to π and φ from 0 to $7\pi/4$ radians. The energies are in scientific notation to make the change of E7 more apparent. The ratio of E7 (molecular)/E7 (benchmark) is in the last column as a percentage.

Θ_A	Θ_B	φ	E7 (benchmark)	E7 (molecular)	E7 (molecular)/ E7 (benchmark) %
0	0	0	-1.69E-21	1.09E-56	/
0	0	π/4	-1.69E-21	4.59E-21	/
0	0	2π/4	-1.69E-21	-3.34E-44	/
0	0	3π/4	-1.69E-21	4.59E-21	/
0	0	π	-1.69E-21	-3.05E-44	/
0	0	5π/4	-1.69E-21	4.59E-21	/
0	0	6π/4	-1.69E-21	-3.34E-44	/
0	0	7π/4	-1.69E-21	4.59E-21	/
0	π/4	0	-4.70E-05	-4.04E-05	85.89%
0	π/4	π/4	-4.70E-05	-4.04E-05	85.89%
0	π/4	2π/4	-4.70E-05	-4.04E-05	85.89%
0	π/4	3π/4	-4.70E-05	-4.04E-05	85.89%
0	π/4	π	-4.70E-05	-4.04E-05	85.89%
0	π/4	5π/4	-4.70E-05	-4.04E-05	85.89%
0	π/4	6π/4	-4.70E-05	-4.04E-05	85.89%
0	π/4	7π/4	-4.70E-05	-4.04E-05	85.89%
0	2π/4	0	-1.33E-04	-1.23E-04	92.52%
0	2π/4	π/4	-1.33E-04	-1.23E-04	92.52%
0	2π/4	2π/4	-1.33E-04	-1.23E-04	92.52%
0	2π/4	3π/4	-1.33E-04	-1.23E-04	92.52%
0	2π/4	π	-1.33E-04	-1.23E-04	92.52%
0	2π/4	5π/4	-1.33E-04	-1.23E-04	92.52%
0	2π/4	6π/4	-1.33E-04	-1.23E-04	92.52%
0	2π/4	7π/4	-1.33E-04	-1.23E-04	92.52%
0	3π/4	0	-2.10E-04	-1.98E-04	94.38%
0	3π/4	π/4	-2.10E-04	-1.98E-04	94.38%
0	3π/4	2π/4	-2.10E-04	-1.98E-04	94.38%
0	3π/4	3π/4	-2.10E-04	-1.98E-04	94.38%
0	3π/4	π	-2.10E-04	-1.98E-04	94.38%
0	3π/4	5π/4	-2.10E-04	-1.98E-04	94.38%
0	3π/4	6π/4	-2.10E-04	-1.98E-04	94.38%
0	3π/4	7π/4	-2.10E-04	-1.98E-04	94.38%

Table S1 continued

0	π	0	-2.49E-04	-2.32E-04	93.15%
0	π	π/4	-2.49E-04	-2.32E-04	93.15%
0	π	2π/4	-2.49E-04	-2.32E-04	93.15%
0	π	3π/4	-2.49E-04	-2.32E-04	93.15%
0	π	π	-2.49E-04	-2.32E-04	93.15%
0	π	5π/4	-2.49E-04	-2.32E-04	93.15%
0	π	6π/4	-2.49E-04	-2.32E-04	93.15%
0	π	7π/4	-2.49E-04	-2.32E-04	93.15%
π/4	0	0	4.70E-05	4.04E-05	85.91%
π/4	0	π/4	4.70E-05	4.04E-05	85.91%
π/4	0	2π/4	4.70E-05	4.04E-05	85.91%
π/4	0	3π/4	4.70E-05	4.04E-05	85.91%
π/4	0	π	4.70E-05	4.04E-05	85.91%
π/4	0	5π/4	4.70E-05	4.04E-05	85.91%
π/4	0	6π/4	4.70E-05	4.04E-05	85.91%
π/4	0	7π/4	4.70E-05	4.04E-05	85.91%
π/4	π/4	0	-7.34E-21	1.18E-15	/
π/4	π/4	π/4	-8.43E-21	-1.37E-08	/
π/4	π/4	2π/4	-3.10E-21	-4.71E-08	/
π/4	π/4	3π/4	4.28E-21	-8.05E-08	/
π/4	π/4	π	5.47E-21	-9.43E-08	/
π/4	π/4	5π/4	4.52E-21	-8.05E-08	/
π/4	π/4	6π/4	-2.83E-21	-4.71E-08	/
π/4	π/4	7π/4	-8.23E-21	-1.37E-08	/
π/4	2π/4	0	-8.58E-05	-8.25E-05	96.21%
π/4	2π/4	π/4	-8.62E-05	-8.29E-05	96.15%
π/4	2π/4	2π/4	-8.70E-05	-8.36E-05	96.01%
π/4	2π/4	3π/4	-8.77E-05	-8.41E-05	95.86%
π/4	2π/4	π	-8.80E-05	-8.43E-05	95.79%
π/4	2π/4	5π/4	-8.77E-05	-8.41E-05	95.86%
π/4	2π/4	6π/4	-8.70E-05	-8.36E-05	96.01%
π/4	2π/4	7π/4	-8.62E-05	-8.29E-05	96.15%
π/4	3π/4	0	-1.66E-04	-1.61E-04	96.56%
π/4	3π/4	π/4	-1.67E-04	-1.61E-04	96.51%
π/4	3π/4	2π/4	-1.69E-04	-1.63E-04	96.38%
π/4	3π/4	3π/4	-1.70E-04	-1.64E-04	96.26%
π/4	3π/4	π	-1.71E-04	-1.64E-04	96.21%
π/4	3π/4	5π/4	-1.70E-04	-1.64E-04	96.26%
π/4	3π/4	6π/4	-1.69E-04	-1.63E-04	96.38%
π/4	3π/4	7π/4	-1.67E-04	-1.61E-04	96.51%
π/4	π	0	-2.10E-04	-1.98E-04	94.38%
π/4	π	π/4	-2.10E-04	-1.98E-04	94.38%
π/4	π	2π/4	-2.10E-04	-1.98E-04	94.38%
π/4	π	3π/4	-2.10E-04	-1.98E-04	94.38%
π/4	π	π	-2.10E-04	-1.98E-04	94.38%
π/4	π	5π/4	-2.10E-04	-1.98E-04	94.38%
π/4	π	6π/4	-2.10E-04	-1.98E-04	94.38%
π/4	π	7π/4	-2.10E-04	-1.98E-04	94.38%

Table S1 continued

2π/4	0	0	1.33E-04	1.23E-04	92.93%
2π/4	0	π/4	1.33E-04	1.23E-04	92.93%
2π/4	0	2π/4	1.33E-04	1.23E-04	92.93%
2π/4	0	3π/4	1.33E-04	1.23E-04	92.93%
2π/4	0	π	1.33E-04	1.23E-04	92.93%
2π/4	0	5π/4	1.33E-04	1.23E-04	92.93%
2π/4	0	6π/4	1.33E-04	1.23E-04	92.93%
2π/4	0	7π/4	1.33E-04	1.23E-04	92.93%
2π/4	π/4	0	8.58E-05	8.28E-05	96.55%
2π/4	π/4	π/4	8.62E-05	8.31E-05	96.45%
2π/4	π/4	2π/4	8.70E-05	8.37E-05	96.21%
2π/4	π/4	3π/4	8.77E-05	8.42E-05	95.96%
2π/4	π/4	π	8.80E-05	8.43E-05	95.85%
2π/4	π/4	5π/4	8.77E-05	8.42E-05	95.96%
2π/4	π/4	6π/4	8.70E-05	8.37E-05	96.21%
2π/4	π/4	7π/4	8.62E-05	8.31E-05	96.45%
2π/4	2π/4	0	5.35E-37	-8.66E-21	/
2π/4	2π/4	π/4	6.74E-37	-2.37E-08	/
2π/4	2π/4	2π/4	7.64E-37	-8.19E-08	/
2π/4	2π/4	3π/4	6.92E-37	-1.41E-07	/
2π/4	2π/4	π	6.90E-37	-1.65E-07	/
2π/4	2π/4	5π/4	7.34E-37	-1.41E-07	/
2π/4	2π/4	6π/4	7.94E-37	-8.19E-08	/
2π/4	2π/4	7π/4	7.01E-37	-2.37E-08	/
2π/4	3π/4	0	-8.58E-05	-8.25E-05	96.21%
2π/4	3π/4	π/4	-8.62E-05	-8.29E-05	96.15%
2π/4	3π/4	2π/4	-8.70E-05	-8.36E-05	96.01%
2π/4	3π/4	3π/4	-8.77E-05	-8.41E-05	95.86%
2π/4	3π/4	π	-8.80E-05	-8.43E-05	95.79%
2π/4	3π/4	5π/4	-8.77E-05	-8.41E-05	95.86%
2π/4	3π/4	6π/4	-8.70E-05	-8.36E-05	96.01%
2π/4	3π/4	7π/4	-8.62E-05	-8.29E-05	96.15%
2π/4	π	0	-1.33E-04	-1.23E-04	92.52%
2π/4	π	π/4	-1.33E-04	-1.23E-04	92.52%
2π/4	π	2π/4	-1.33E-04	-1.23E-04	92.52%
2π/4	π	3π/4	-1.33E-04	-1.23E-04	92.52%
2π/4	π	π	-1.33E-04	-1.23E-04	92.52%
2π/4	π	5π/4	-1.33E-04	-1.23E-04	92.52%
2π/4	π	6π/4	-1.33E-04	-1.23E-04	92.52%
2π/4	π	7π/4	-1.33E-04	-1.23E-04	92.52%
3π/4	0	0	2.10E-04	2.00E-04	95.18%
3π/4	0	π/4	2.10E-04	2.00E-04	95.18%
3π/4	0	2π/4	2.10E-04	2.00E-04	95.18%
3π/4	0	3π/4	2.10E-04	2.00E-04	95.18%
3π/4	0	π	2.10E-04	2.00E-04	95.18%
3π/4	0	5π/4	2.10E-04	2.00E-04	95.18%
3π/4	0	6π/4	2.10E-04	2.00E-04	95.18%
3π/4	0	7π/4	2.10E-04	2.00E-04	95.18%

Table S1 continued

3π/4	π/4	0	1.66E-04	1.62E-04	97.25%
3π/4	π/4	π/4	1.67E-04	1.62E-04	97.18%
3π/4	π/4	2π/4	1.69E-04	1.64E-04	97.03%
3π/4	π/4	3π/4	1.70E-04	1.65E-04	96.87%
3π/4	π/4	π	1.71E-04	1.65E-04	96.80%
3π/4	π/4	5π/4	1.70E-04	1.65E-04	96.87%
3π/4	π/4	6π/4	1.69E-04	1.64E-04	97.03%
3π/4	π/4	7π/4	1.67E-04	1.62E-04	97.18%
3π/4	2π/4	0	8.58E-05	8.28E-05	96.55%
3π/4	2π/4	π/4	8.62E-05	8.31E-05	96.45%
3π/4	2π/4	2π/4	8.70E-05	8.37E-05	96.21%
3π/4	2π/4	3π/4	8.77E-05	8.42E-05	95.96%
3π/4	2π/4	π	8.80E-05	8.43E-05	95.85%
3π/4	2π/4	5π/4	8.77E-05	8.42E-05	95.96%
3π/4	2π/4	6π/4	8.70E-05	8.37E-05	96.21%
3π/4	2π/4	7π/4	8.62E-05	8.31E-05	96.45%
3π/4	3π/4	0	-3.69E-21	5.38E-16	/
3π/4	3π/4	π/4	-2.60E-21	-1.37E-08	/
3π/4	3π/4	2π/4	-8.07E-21	-4.71E-08	/
3π/4	3π/4	3π/4	-1.60E-20	-8.05E-08	/
3π/4	3π/4	π	-1.73E-20	-9.43E-08	/
3π/4	3π/4	5π/4	-1.63E-20	-8.05E-08	/
3π/4	3π/4	6π/4	-8.34E-21	-4.71E-08	/
3π/4	3π/4	7π/4	-2.89E-21	-1.37E-08	/
3π/4	π	0	-4.70E-05	-4.04E-05	85.89%
3π/4	π	π/4	-4.70E-05	-4.04E-05	85.89%
3π/4	π	2π/4	-4.70E-05	-4.04E-05	85.89%
3π/4	π	3π/4	-4.70E-05	-4.04E-05	85.89%
3π/4	π	π	-4.70E-05	-4.04E-05	85.89%
3π/4	π	5π/4	-4.70E-05	-4.04E-05	85.89%
3π/4	π	6π/4	-4.70E-05	-4.04E-05	85.89%
3π/4	π	7π/4	-4.70E-05	-4.04E-05	85.89%
π	0	0	2.49E-04	2.34E-04	94.10%
π	0	π/4	2.49E-04	2.34E-04	94.10%
π	0	2π/4	2.49E-04	2.34E-04	94.10%
π	0	3π/4	2.49E-04	2.34E-04	94.10%
π	0	π	2.49E-04	2.34E-04	94.10%
π	0	5π/4	2.49E-04	2.34E-04	94.10%
π	0	6π/4	2.49E-04	2.34E-04	94.10%
π	0	7π/4	2.49E-04	2.34E-04	94.10%
π	π/4	0	2.10E-04	2.00E-04	95.18%
π	π/4	π/4	2.10E-04	2.00E-04	95.18%
π	π/4	2π/4	2.10E-04	2.00E-04	95.18%
π	π/4	3π/4	2.10E-04	2.00E-04	95.18%
π	π/4	π	2.10E-04	2.00E-04	95.18%
π	π/4	5π/4	2.10E-04	2.00E-04	95.18%
π	π/4	6π/4	2.10E-04	2.00E-04	95.18%
π	π/4	7π/4	2.10E-04	2.00E-04	95.18%

Table S1 continued

π	2π/4	0	1.33E-04	1.23E-04	92.93%
π	2π/4	π/4	1.33E-04	1.23E-04	92.93%
π	2π/4	2π/4	1.33E-04	1.23E-04	92.93%
π	2π/4	3π/4	1.33E-04	1.23E-04	92.93%
π	2π/4	π	1.33E-04	1.23E-04	92.93%
π	2π/4	5π/4	1.33E-04	1.23E-04	92.93%
π	2π/4	6π/4	1.33E-04	1.23E-04	92.93%
π	2π/4	7π/4	1.33E-04	1.23E-04	92.93%
π	3π/4	0	4.70E-05	4.04E-05	85.91%
π	3π/4	π/4	4.70E-05	4.04E-05	85.91%
π	3π/4	2π/4	4.70E-05	4.04E-05	85.91%
π	3π/4	3π/4	4.70E-05	4.04E-05	85.91%
π	3π/4	π	4.70E-05	4.04E-05	85.91%
π	3π/4	5π/4	4.70E-05	4.04E-05	85.91%
π	3π/4	6π/4	4.70E-05	4.04E-05	85.91%
π	3π/4	7π/4	4.70E-05	4.04E-05	85.91%
π	π	0	1.69E-21	-3.88E-55	/
π	π	π/4	1.69E-21	-2.44E-21	/
π	π	2π/4	1.69E-21	-3.30E-43	/
π	π	3π/4	1.69E-21	-2.44E-21	/
π	π	π	1.69E-21	-3.70E-43	/
π	π	5π/4	1.69E-21	-2.44E-21	/
π	π	6π/4	1.69E-21	-3.30E-43	/
π	π	7π/4	1.69E-21	-2.44E-21	/

CHAPTER 4 EXCHANGE REPULSION INTERACTION BETWEEN *AB INITIO* SYSTEM AND EFFECTIVE FRAGMENT POTENTIAL FRAGMENTS

Peng Xu and Mark S. Gordon

Abstract

Extensive formulation and code modification has been made to the previous implementation of exchange repulsion Fock operator (V^{XR}) and energy (E^{XR}) between the *ab initio* (RHF) system and effective fragment potential (EFP) fragments (abbreviated as QM-EFP) to allow the presence of multiple EFP fragments. The fully analytic gradient of the QM-EFP E^{XR} has been derived and implemented.

Introduction

The effective fragment potential method (EFP)[1] has been developed as a quantum-mechanics-based model potential to yield accurate (MP2 quality and CCSD(T) quality in some cases [ref]) intermolecular interaction energies at very low computational cost. The EFP method decomposes the intermolecular interaction into five components: Coulomb, polarization, dispersion, exchange repulsion and charge transfer. Depending on how these interaction terms are described, namely, the last three terms, there are two versions of EFP, EFP1 and EFP2. EFP1 is specifically designed for water by having a repulsive term fitted to either the RHF or DFT water dimer potential to account for some

of the effect of the last three interactions mentioned above. The RHF-fitted and DFT-fitted repulsive potentials can account for none and some dynamic correlation, respectively. The fitted repulsive potential severely limits the application of EFP because an expensive fitting process has to be performed for every new molecular species. EFP2 is therefore developed with the motivation of having explicit expressions for all of the interaction terms without any fitted parameters. Then, an EFP2 potential can be generated for any (closed-shell) molecular species. Hence EFP2 is also referred to as the general effective fragment potential method. Currently only EFP1 has been fully interfaced with *ab initio* methods so that one can have the chemically important region (e.g., a chemical reaction site) described by *ab initio* methods and the spectator region by rigid EFP fragments. The QM-EFP interaction terms are formulated differently from that between EFP potentials (EFP-EFP). For EFP2, QM-EFP Coulomb, polarization and dispersion interactions and their corresponding gradients have been developed and implemented into the *ab initio* quantum chemistry package GAMESS[23].

The Pauli exclusion principle gives rise to the exchange repulsion interaction between electrons of like spin at short range. Exchange repulsion is a purely quantum-mechanical effect that does not have a simple classical analogue. It accounts for part of the rapid increase in interaction energy at short-range. Two approaches for deriving the exchange repulsion interaction have been developed over the years. One is to regard the exchange repulsion as the exchange part of the first-order energy correction in the short-range intermolecular perturbation theory through a density matrix formalism.[4] The other LCAO-MO type approach due to Fröman and Löwdin does not rely on perturbation theory. The interaction energy is the difference between the expectation value of the total

Hamiltonian and the energy of the non-interaction constituting molecules. Jensen and Gordon developed a formula for E^{XR}, initially using density matrix formalism.[5] The other approach leads to the same exchange repulsion formula.[6] A fully analytic EFP-EFP exchange repulsion gradient was subsequently.[7,8] QM-EFP E^{XR} is developed together with the exchange repulsion Fock operator V^{XR}.[6] QM-EFP E^{XR} and V^{XR} have been implemented in GAMESS.[9]

In a previous work, the QM-EFP E^{XR} implementation was limited to one EFP fragment. In the present work, extensive code modifications were accomplished to enable the use of multiple EFP fragments. The fully analytic QM-EFP E^{XR} gradients are presented in Section II. The code modification and testing results are briefly discussed in Section III. Section IV describes the implementation of the QM-EFP E^{XR} gradient. Section V concludes.

Theory

(A) Fock Operator and Energy Expressions

The QM-EFP exchange repulsion energy E^{XR} is[5],

$$\begin{aligned} E^{XR} = & -2\sum_{i\in A}\sum_{j\in B}(ij\,|\,ij)^{SGO} \\ & -2\sum_{i\in A}\sum_{j\in B}S_{ij}\left[2\left(V_{ij}^{A}+G_{ij}^{A}\right)+\sum_{l\in B}F_{jl}^{B}S_{il}\right] \\ & +2\sum_{i\in A}\sum_{j\in B}S_{ij}\left[\sum_{k\in A}S_{kj}\left(F_{ik}^{A}+V_{ik}^{EFP,B}-V_{ik}^{j}\right)+S_{ij}\left(\sum_{I\in A}^{Atom}\frac{-Z_I}{R_{jI}}+2\sum_{k\in A}V_{kk}^{j}\right)\right] \end{aligned} \qquad (1)$$

In Eq. (1) i and k refer to the MOs of the *ab initio* molecule A; j and l refer to the MOs of EFP fragment B. (ij|ij) is an electron repulsion integral, SGO refers to the spherical

Gaussian approximation[10]. S_{ij} is the QM-EFP overlap integral. F_{ik}^{A} and F_{jl}^{B} are the Fock matrices of the *ab initio* and the EFP molecules, respectively. V_{ij}^{A} is the one-electron nuclear attraction term from the molecule A. V_{ik}^{j} is the one-electron potential due to the EFP MO j. The attraction between the electrons of the EFP fragments and nuclei of the *ab initio* molecules is modeled classically as $\sum_{I\in A}^{Atom}\frac{-Z_I}{R_{jI}}$. The two-electron integrals involving EFP MOs is defined as: $G_{ij}^{A}=2J_{ij}^{A}-K_{ij}^{A}=\sum_{k\in A}\left[2(ij\mid kk)-(ik\mid jk)\right]$.

The exchange repulsion Fock operator V^{XR} is obtained by taking the variational derivative with respect to the *ab initio* orbitals[6,9].

$$
\begin{aligned}
V_{mi}^{XR} = & -\sum_{j\in B}(mj\mid ij)^{SGO} \\
& -\frac{1}{2}\sum_{j\in B}S_{mj}\left[2\left(V_{ij}^{A}+G_{ij}^{A}\right)+\sum_{l\in B}F_{jl}^{B}S_{il}\right]-\frac{1}{2}\sum_{j\in B}S_{ij}\left[2\left(V_{mj}^{A}+G_{mj}^{A}\right)+\sum_{l\in B}F_{jl}^{B}S_{ml}\right] \\
& -\sum_{k\in A}\sum_{j\in B}S_{kj}\left[4(kj\mid mi)-(km\mid ji)-(ki\mid jm)\right] \\
& +\sum_{j\in B}S_{mj}\left[\sum_{k\in A}S_{kj}\left(F_{ik}^{A}+V_{ik}^{EFP,B}-V_{ik}^{j}\right)+S_{ij}\left(\sum_{I}^{A}\frac{-Z_I}{R_{jI}}+2\sum_{k}^{A}V_{kk}^{j}\right)\right] \\
& +\sum_{j\in B}S_{ij}\left[\sum_{k\in A}S_{kj}\left(F_{mk}^{A}+V_{mk}^{EFP,B}-V_{mk}^{j}\right)\right]+2\sum_{k\in A}\sum_{j\in B}S_{kj}^{2}V_{mi}^{j} \\
& +\frac{1}{2}\sum_{n\in A}\sum_{k\in A}\sum_{j\in B}S_{kj}S_{nj}\left[4(nk\mid im)-(nm\mid ik)-(ni\mid mk)\right]
\end{aligned}
\qquad (2)
$$

V^{XR} can be separated into one-electron and two-electron terms, h^{XR} and G^{XR}, respectively, so that $E^{XR}=\sum_{i\in A}[2h_{ii}^{XR}+G_{ii}^{XR}]$. The one- and two-electron terms explicitly refer to the *ab initio* orbitals. Now consider the h^{XR} part of V^{XR},

$$
\begin{aligned}
h_{mi}^{XR} &= -\sum_{j\in B}(mj\,|\,ij)^{SGO} \\
&-\frac{1}{2}\sum_{j\in B}S_{mj}\left[2\left(V_{ij}^{A}\right)+\sum_{l\in B}F_{jl}^{B}S_{il}\right]-\frac{1}{2}\sum_{j\in B}S_{ij}\left[2\left(V_{mj}^{A}\right)+\sum_{l\in B}F_{jl}^{B}S_{ml}\right] \qquad (3)\\
&+\sum_{j\in B}S_{mj}\left[S_{ij}\left(\sum_{I}^{A}\frac{-Z_I}{R_{jI}}\right)\right]
\end{aligned}
$$

So, the sum over the diagonal terms gives

$$
\begin{aligned}
\sum_{i\in A}2h_{ii}^{XR} &= -2\sum_{i\in A}\sum_{j\in B}(ij\,|\,ij)^{SGO} \\
&-2\cdot\frac{1}{2}\sum_{i\in A}\sum_{j\in B}S_{ij}\left[2V_{ij}^{A}+\sum_{l\in B}F_{jl}^{B}S_{il}\right]-2\cdot\frac{1}{2}\sum_{i\in A}\sum_{j\in B}S_{ij}\left[2V_{ij}^{A}+\sum_{l\in B}F_{jl}^{B}S_{il}\right] \\
&+2\sum_{i\in A}\sum_{j\in B}S_{ij}\left[S_{ij}\left(\sum_{I}^{A}\frac{-Z_I}{R_{jI}}\right)\right] \\
&= -2\sum_{i\in A}\sum_{j\in B}(ij\,|\,ij)^{SGO}-2\sum_{i\in A}\sum_{j\in B}S_{ij}\left[2V_{ij}^{A}+\sum_{l\in B}F_{jl}^{B}S_{il}\right]+2\sum_{i\in A}\sum_{j\in B}S_{ij}\left[S_{ij}\left(\sum_{I}^{A}\frac{-Z_I}{R_{jI}}\right)\right]
\end{aligned}
$$

(4)

Now, consider the two-electron part, G_{mi}^{XR}, of V^{XR}:

$$
\begin{aligned}
G_{mi}^{XR} &= -\frac{1}{2}\sum_{j\in B}S_{mj}\left(2G_{ij}^{A}\right)-\frac{1}{2}\sum_{j\in B}S_{ij}\left(2G_{mj}^{A}\right)-\sum_{k\in A}\sum_{j\in B}S_{kj}\left[4(kj\,|\,mi)-(km\,|\,ji)-(ki\,|\,jm)\right] \\
&+\sum_{j\in B}S_{mj}\left[\sum_{k\in A}S_{kj}\left(F_{ik}^{A}+V_{ik}^{EFP,B}-V_{ik}^{j}\right)\right]+\sum_{j\in B}S_{ij}\left[\sum_{k\in A}S_{kj}\left(F_{mk}^{A}+V_{mk}^{EFP,B}-V_{mk}^{j}\right)\right] \\
&+\sum_{j\in B}S_{mj}S_{ij}\left(2\sum_{k}^{A}V_{kk}^{j}\right)+2\sum_{k\in A}\sum_{j\in B}S_{kj}^{2}V_{mi}^{j} \\
&+\frac{1}{2}\sum_{n\in A}\sum_{k\in A}\sum_{j\in B}S_{kj}S_{nj}\left[4(nk\,|\,im)-(nm\,|\,ik)-(ni\,|\,mk)\right]
\end{aligned}
\qquad (5)
$$

Summing over the diagonal terms gives:

$$
\begin{aligned}
\sum_{i\in A} G_{ii}^{XR} &= -\frac{1}{2}\sum_{i\in A}\sum_{j\in B} S_{ij}\left(2\sum_{k\in A}\left[2(ij\,|\,kk)-(ik\,|\,jk)\right]\right)-\frac{1}{2}\sum_{i\in A}\sum_{j\in B} S_{ij}\left(2\sum_{k\in A}\left[2(ij\,|\,kk)-(ik\,|\,jk)\right]\right)\\
&-\sum_{i\in A}\sum_{k\in A}\sum_{j\in B} S_{kj}\left[4(kj\,|\,ii)-(ki\,|\,ji)-(ki\,|\,ji)\right]\\
&+\sum_{i\in A}\sum_{j\in B} S_{ij}\left[\sum_{k\in A} S_{kj}\left(F_{ik}^{A}+V_{ik}^{EFP,B}-V_{ik}^{j}\right)+S_{ij}\left(2\sum_{k\in A} V_{kk}^{j}\right)\right]\\
&+\sum_{i\in A}\sum_{j\in B} S_{ij}\left[\sum_{k\in A} S_{kj}\left(F_{ik}^{A}+V_{ik}^{EFP,B}-V_{ik}^{j}\right)\right]+2\sum_{i\in A}\sum_{k\in A}\sum_{j\in B} S_{kj}^{2}V_{ii}^{j}\\
&+\frac{1}{2}\sum_{i\in A}\sum_{n\in A}\sum_{k\in A}\sum_{j\in B} S_{kj}S_{nj}\left[4(nk\,|\,ii)-(ni\,|\,ik)-(ni\,|\,ik)\right]\\
&=-\sum_{i\in A}\sum_{j\in B} S_{ij}\left(2\sum_{k\in A}\left[2(ij\,|\,kk)-(ik\,|\,jk)\right]\right)-\sum_{i\in A}\sum_{k\in A}\sum_{j\in B} S_{kj}2\left[2(kj\,|\,ii)-(ki\,|\,ji)\right]\\
&+2\sum_{i\in A}\sum_{j\in B} S_{ij}\left[\sum_{k\in A} S_{kj}\left(F_{ik}^{A}+V_{ik}^{EFP,B}-V_{ik}^{j}\right)\right]+\sum_{i\in A}\sum_{j\in B} S_{ij}^{2}\left(2\sum_{k\in A} V_{kk}^{j}\right)+2\sum_{i\in A}\sum_{k\in A}\sum_{j\in B} S_{kj}^{2}V_{ii}^{j}\\
&+\sum_{i\in A}\sum_{n\in A}\sum_{k\in A}\sum_{j\in B} S_{kj}S_{nj}\left[2(nk\,|\,ii)-(ni\,|\,ik)\right]\\
&=-2\sum_{i\in A}\sum_{j\in B} S_{ij}\left(2G_{ij}^{A}\right)+2\sum_{i\in A}\sum_{j\in B} S_{ij}\left[\sum_{k\in A} S_{kj}\left(F_{ik}^{A}+V_{ik}^{EFP,B}-V_{ik}^{j}\right)\right]\\
&+\sum_{i\in A}\sum_{j\in B} S_{ij}^{2}\left(2\sum_{k\in A} V_{kk}^{j}\right)+2\sum_{i\in A}\sum_{k\in A}\sum_{j\in B} S_{kj}^{2}V_{ii}^{j}\\
&+\sum_{i\in A}\sum_{n\in A}\sum_{k\in A}\sum_{j\in B} S_{kj}S_{ij}\left[2(ik\,|\,nn)-(in\,|\,nk)\right]
\end{aligned}
\qquad (6)
$$

(B) Exchange Repulsion Gradients

In the derivation below, j and l denote EFP MOs, i, k, m and n denote *ab initio* MOs. Atomic orbitals are denoted by Greek letters. The atoms of the *ab initio* molecule and the EFP fragments are denoted by a and b, respectively.

Derivatives with respect to *ab initio* atom centers

The derivative of Eq. (1) with respect to an *ab initio* atom center, $\mathbf{q}_{\mathbf{a}}$, is

$$\begin{aligned}
\frac{\partial E^{XR}}{\partial q_a} &= -2\sum_i^A\sum_j^B \frac{\partial (ij\,|\,ij)^{SGO}}{\partial q_a} \\
&-2\sum_i^A\sum_j^B\left(\frac{\partial S_{ij}}{\partial q_a}\right)\left[2\left(V_{ij}^A+G_{ij}^A\right)+\sum_l^B F_{jl}^B S_{il}\right]-2\sum_i^A\sum_j^B S_{ij}\left[2\left(\frac{\partial V_{ij}^A}{\partial q_a}+\frac{\partial G_{ij}^A}{\partial q_a}\right)+\sum_l^B F_{jl}^B\left(\frac{\partial S_{il}}{\partial q_a}\right)\right] \\
&+2\sum_i^A\sum_j^B\left(\frac{\partial S_{ij}}{\partial q_a}\right)\left[\sum_k^A S_{kj}\left(F_{ik}^A+V_{ik}^{EFP,B}-V_{ik}^j\right)+S_{ij}\left(\sum_I^A\frac{-Z_I}{R_{jI}}+2\sum_k^A V_{kk}^j\right)\right] \\
&+2\sum_i^A\sum_j^B S_{ij}\left[\begin{array}{l}\sum_k^A\left(\frac{\partial S_{kj}}{\partial q_a}\right)\left(F_{ik}^A+V_{ik}^{EFP,B}-V_{ik}^j\right)+\left(\frac{\partial S_{ij}}{\partial q_a}\right)\left(\sum_I^A\frac{-Z_I}{R_{jI}}+2\sum_k^A V_{kk}^j\right) \\ +\sum_k^A S_{kj}\left(\frac{\partial F_{ik}^A}{\partial q_a}+\frac{\partial V_{ik}^{EFP,B}}{\partial q_a}-\frac{\partial V_{ik}^j}{\partial q_a}\right)+S_{ij}\left(\sum_I^A\frac{\partial}{\partial q_a}\frac{-Z_I}{R_{jI}}+2\sum_k^A\frac{\partial V_{kk}^j}{\partial q_a}\right)\end{array}\right]
\end{aligned} \tag{7}$$

where q_a is the Cartesian coordinate of atom a of the *ab initio* molecule A. The following derivatives are required to evaluate Eq. (7):

$$\frac{\partial (ij\,|\,ij)^{SGO}}{\partial q_a},\quad \frac{\partial S_{ij}}{\partial q_a},\quad \frac{\partial V_{ij}^A}{\partial q_a},\quad \frac{\partial G_{ij}^A}{\partial q_a},\quad \frac{\partial F_{ik}^A}{\partial q_a},\quad \frac{\partial V_{ik}^{EFP,B}}{\partial q_a},\quad \frac{\partial V_{ik}^j}{\partial q_a},\quad \sum_I^A\frac{\partial}{\partial q_a}\frac{-Z_I}{R_{jI}}$$

The derivation of the derivative of the overlap integral is shown here as an example to illustrate the key steps. The details of the full derivation can be found in the Appendix.

$$\begin{aligned}
\frac{\partial S_{ij}}{\partial q_a} &= \frac{\partial}{\partial q_a}\sum_\mu^A\sum_\nu^B C_{\mu i}C_{\nu j}\left(\mu\,|\,\nu\right) \\
&= \sum_\mu^A C_{\mu i}^a\left(\mu\,|\,j\right)+\sum_\mu^A C_{\mu i}\left(\mu^a\,|\,j\right)+\sum_\nu^B C_{\nu j}^a\left(i\,|\,\nu\right)+\sum_\nu^B C_{\nu j}\left(i\,|\,\nu^a\right) \\
&= \sum_\mu^A C_{\mu i}^a\left(\mu\,|\,j\right)+\sum_\mu^A C_{\mu i}\left(\mu^a\,|\,j\right) \\
&= \sum_\mu^A C_{\mu i}^a\left(\mu\,|\,j\right)+S_{ij}^a
\end{aligned} \tag{8}$$

The last two terms in the second equality of Eq. (8) equal zero because EFP MOs are frozen and the EFP AOs are not functions of the *ab initio* coordinates. Note that S_{ij}^{a} is not a shorthand notation for $\partial S_{ij}/\partial q_a$, rather $S_{ij}^{a} = \sum_{\mu}^{A} C_{\mu i}\left(\mu^{a} \mid j\right)$. To avoid solving the time-consuming coupled perturbed Hartree-Fock equations for C^{a}, Eq. (8) is rewritten in terms of orbital response terms

$$\begin{aligned}\frac{\partial S_{ij}}{\partial q_a} &= \sum_{\mu}^{A} C_{\mu i}^{a}\left(\mu \mid j\right) + S_{ij}^{a} = \sum_{\mu}^{A}\sum_{m}^{A} C_{\mu m} U_{mi}^{a}\left(\mu \mid j\right) + S_{ij}^{a} \\ &= \frac{1}{2}\sum_{m}^{A}\sum_{j}^{B}\left(U_{mi}^{a} + U_{im}^{a}\right)S_{mj} + \sum_{i}^{A}\sum_{j}^{B} S_{ij}^{a} \\ &= \sum_{m}^{A}\sum_{j}^{B}\left(-\frac{1}{2}S_{mi}^{a}S_{mj} + S_{ij}^{a}\right)\end{aligned} \tag{9}$$

The last step of Eq. (9) uses the fact that $U_{mi}^{a} + U_{im}^{a} = -S_{mi}^{a}$ [11]

Carrying out the same procedures as above for all the derivative terms, the derivative of E^{XR} with respect to the *ab initio* atom center becomes

$$\frac{\partial E^{XR}}{\partial q_a} = -2\sum_{i}^{A}\sum_{j}^{B}\frac{\partial (ij\,|\,ij)^{SGO}}{\partial q_a}$$
$$+2\sum_{i,m}^{A}\sum_{j}^{B}S^a_{mi}S_{mj}\left(2V^A_{ij}+2G^A_{ij}\right)+2\sum_{i,m}^{A}\sum_{j,l}^{B}S^a_{mi}S_{mj}F^B_{jl}S_{il}$$
$$-2\sum_{i}^{A}\sum_{j}^{B}S^a_{ij}\left(2V^A_{ij}+2G^A_{ij}\right)-2\sum_{i}^{A}\sum_{j}^{B}S_{ij}\left(2V^{A^a}_{ij}+2G^{A^a}_{ij}\right)-4\sum_{i}^{A}\sum_{j,l}^{B}S^a_{ij}F^B_{jl}S_{il}$$
$$-4\sum_{i,k,m}^{A}\sum_{j}^{B}S^a_{mi}S_{mj}S_{kj}\left(F^A_{ik}+V^{EFP,B}_{ik}-V^j_{ik}\right)-2\sum_{i,m}^{A}\sum_{j}^{B}S^a_{mi}S_{mj}S_{ij}\left(\sum_{I}^{A}\frac{-Z_I}{R_{jI}}+2\sum_{k}^{A}V^j_{kk}\right)$$
$$+4\sum_{i,k}^{A}\sum_{j}^{B}S^a_{ij}S_{kj}\left(F^A_{ik}+V^{EFP,B}_{ik}-V^j_{ik}\right)+4\sum_{i}^{A}\sum_{j}^{B}S^a_{ij}S_{ij}\left(\sum_{I}^{A}\frac{-Z_I}{R_{jI}}+2\sum_{k}^{A}V^j_{kk}\right) \qquad (10)$$
$$+2\sum_{i,k}^{A}\sum_{j}^{B}S_{ij}S_{kj}\left(F^a_{ik}+V^{EFP,B^a}_{ik}-V^{j^a}_{ik}\right)+2\sum_{i}^{A}\sum_{j}^{B}S^2_{ij}\left[\frac{(-Z_a)(q_j-q_a)}{R^3_{ja}}-2\sum_{k,m}^{A}S^a_{mk}V^j_{mk}+2\sum_{k}^{A}V^{j^a}_{kk}\right]$$
$$+2\sum_{i,k,m}^{A}\sum_{j}^{B}S_{ij}S^a_{mk}\left[4(ij\,|\,mk)-(im\,|\,jk)-(ik\,|\,mj)\right]$$
$$-\sum_{i,k,m,n}^{A}\sum_{j}^{B}S_{ij}S_{kj}S^a_{mn}\left[4(ik\,|\,mn)-(im\,|\,kn)-(in\,|\,km)\right]$$

Derivatives with respect to EFP centers

The derivative with respect to an EFP center, that is, center of mass of an EFP fragment, is first expressed as,

$$\begin{aligned}\frac{\partial E^{XR}}{\partial q_B} &= -2\sum_i^A\sum_j^B \frac{\partial (ij\,|\,ij)^{SGO}}{\partial q_B} \\ &-2\sum_i^A\sum_j^B\left(\frac{\partial S_{ij}}{\partial q_B}\right)\left[2\left(V_{ij}^A+G_{ij}^A\right)+\sum_l^B F_{jl}^B S_{il}\right] \\ &-2\sum_i^A\sum_j^B S_{ij}\left[2\left(\frac{\partial V_{ij}^A}{\partial q_B}+\frac{\partial G_{ij}^A}{\partial q_B}\right)+\sum_l^B F_{jl}^B\left(\frac{\partial S_{il}}{\partial q_B}\right)+\sum_l^B\left(\frac{\partial F_{jl}^B}{\partial q_B}\right)S_{il}\right] \\ &+2\sum_i^A\sum_j^B\left(\frac{\partial S_{ij}}{\partial q_B}\right)\left[\sum_k^A S_{kj}\left(F_{ik}^A+V_{ik}^{EFP,B}-V_{ik}^j\right)+S_{ij}\left(\sum_I^A\frac{-Z_I}{R_{jI}}+2\sum_k^A V_{kk}^j\right)\right] \\ &+2\sum_i^A\sum_j^B S_{ij}\left[\begin{array}{l}\sum_k^A\left(\frac{\partial S_{kj}}{\partial q_B}\right)\left(F_{ik}^A+V_{ik}^{EFP,B}-V_{ik}^j\right)+\left(\frac{\partial S_{ij}}{\partial q_B}\right)\left(\sum_I^A\frac{-Z_I}{R_{jI}}+2\sum_k^A V_{kk}^j\right) \\ +\sum_k^A S_{kj}\left(\frac{\partial F_{ik}^A}{\partial q_B}+\frac{\partial V_{ik}^{EFP,B}}{\partial q_B}-\frac{\partial V_{ik}^j}{\partial q_B}\right)+S_{ij}\left(\sum_I^A\frac{\partial}{\partial q_B}\frac{-Z_I}{R_{jI}}+2\sum_k^A\frac{\partial V_{kk}^j}{\partial q_B}\right)\end{array}\right]\end{aligned} \tag{11}$$

When an EFP fragment translates, all of its AO centers and MOs translate in the same way. Because EFP fragments are rigid the MO coefficients are constant. Hence the translational derivatives of MO coefficients are zero. The overall translation of an EFP fragment can be decomposed into the individual atomic translation in A.[8,12]

The derivative of the overlap integral yields

$$\begin{aligned}\frac{\partial S_{ij}}{\partial q_B} &= \sum_\mu^A\sum_\nu^B\sum_b^B C_{\mu i}^b C_{\nu j} S_{\mu\nu}+C_{\mu i}C_{\nu j}^b S_{\mu\nu}+C_{\mu i}C_{\nu j}\left(\mu^b\,|\,\nu\right)+C_{\mu i}C_{\nu j}\left(\mu\,|\,\nu^b\right) \\ &= \sum_\mu^A\sum_\nu^B\sum_b^B C_{\mu i}^b C_{\nu j} S_{\mu\nu}+C_{\mu i}C_{\nu j}\left(\mu\,|\,\nu^b\right)\end{aligned} \tag{12}$$

The second term in the first equality vanishes because EFP MOs are frozen and the third term disappears because an AO of an *ab initio* molecule is not a function of the coordinates of fragment B. The derivative of the *ab initio* MO coefficient can be rewritten in terms of the orbital response terms:

$$\frac{\partial S_{ij}}{\partial q_B} = \sum_m^A\sum_b^B U_{mi}^b S_{mj}+\sum_b^B\left(i\,|\,j^b\right) = \sum_m^A\sum_b^B -\frac{1}{2}S_{mi}^b S_{mj}+\sum_b^B\left(i\,|\,j^b\right) = \sum_b^B S_{ij}^b \tag{13}$$

where $S_{ij}^{b} = \left(i \mid j^{b}\right)$ and S_{mi}^{b} is zero because the AOs of the *ab initio* molecule do not depend on the EFP coordinates.

The derivative of E^{XR} with respect to the EFP centers becomes:

$$\begin{aligned}\frac{\partial E^{XR}}{\partial q_B} = & -2\sum_{i}^{A}\sum_{j}^{B}\frac{\partial (ij \mid ij)^{SGO}}{\partial q_B} \\ & -2\sum_{i}^{A}\sum_{j}^{B}\left(\sum_{b}^{B} S_{ij}^{b}\right)\left(2V_{ij}^{A} + 2G_{ij}^{A}\right) - 2\sum_{i}^{A}\sum_{j}^{B} S_{ij}\sum_{b}^{B}\left(2V_{ij}^{A^b} + 2G_{ij}^{A^b}\right) - 4\sum_{i}^{A}\sum_{j,l}^{B}\left(\sum_{b}^{B} S_{ij}^{b}\right) F_{jl}^{B} S_{il} \\ & +4\sum_{i,k}^{A}\sum_{j}^{B}\left(\sum_{b}^{B} S_{ij}^{b}\right) S_{kj}\left(F_{ik}^{A} + V_{ik}^{EFP,B} - V_{ik}^{j}\right) + 4\sum_{i}^{A}\sum_{j}^{B}\left(\sum_{b}^{B} S_{ij}^{b}\right) S_{ij}\left(\sum_{I}^{A}\frac{-Z_I}{R_{jI}} + 2\sum_{k}^{A} V_{kk}^{j}\right) \\ & +2\sum_{i,k}^{A}\sum_{j}^{B} S_{ij} S_{kj}\left(\left\langle i\right|\frac{\partial V^{EFP,B}}{\partial q_B}\left|k\right\rangle + \left\langle i\right|\frac{\partial V^{j}}{\partial q_j}\left|k\right\rangle\right) + 2\sum_{i}^{A}\sum_{j}^{B} S_{ij} S_{ij}\left(\sum_{I}^{A}\frac{Z_I\left(q_j - q_I\right)}{R_{jI}^{3}} + 2\sum_{k}^{A}\left\langle k\right|\frac{\partial V^{j}}{\partial q_j}\left|k\right\rangle\right)\end{aligned}$$

(14)

Code Modification and Testing

The previous implementation of QM-EFP E^{XR} was unable to deal with multiple EFP fragments. As an example, water trimer is shown in Table 1. The notation H_2O-1-23 means that the first water molecule in the input file is treated by the RHF method and the second and third water molecules are treated as EFP fragments. One can see that when two EFP fragments are reversed in the input file, exactly the same E^{XR} are expected but distinctly different E^{XR}s are obtained. In addition, the E^{XR}s obtained by choosing different water molecules as *ab initio* are expected to be very close to each other but very different results are observed.

The basis functions used for EFP fragments are also Gaussian functions, not different from the *ab initio* counterpart and therefore the underlying algorithms for computing the various matrix elements between an *ab initio* molecule and an EFP

fragment are the same as in the usual *ab initio* code. However, due to the fragmentation nature of EFP, the EFP basis functions are organized differently. As a concrete example, the exponents for the Gaussian basis functions for the *ab initio* system are stored as a one-dimensional array, while its EFP counterpart is a two-dimensional array with the second dimension being the maximum number of different EFP potentials.

Sufficient memory allocation and correct indexing for EFP fragments are the two key considerations in the code modification. An EFP-related matrix typically has one index related to counting EFP fragments. To store the EFP-related matrices, one can choose between generating and storing all fragment matrices at once or a single fragment at a time. For example, the overlap matrix between the *ab initio* molecule and EFP fragments, S_{ij}, with i and j being *ab initio* and EFP MO indices, respectively, can be generated and stored once for all the fragments or for one fragment at a time. The key difference between the two approaches is the memory requirement. The former approach requires a memory allocation of (# MOs of *ab initio* molecule × # MOs of all EFP fragments) whereas the latter only needs (# MOs of *ab initio* molecule × # MOs of the largest EFP fragment). Since the S matrix is only an intermediate quantity for computing the V^{XR} and E^{XR}, it is more efficient to use the latter approach. To use the latter approach, the computation and utilization of the S matrix must be in the same loop over the EFP fragments. There are, however, cases for which one must use the former approach. For example, the coefficient matrix that transforms all EFP AOs to MOs, PROVEC, is stored in a dictionary file and retrieved once at the beginning of the calculation. It is necessary to allocate enough memory for it and also very important to be able to 'jump' to the right fragment. Figure 1 is a pictorial representation of PROVEC matrix, where MXBF is the

maximum number of basis functions/AOs of EFP and NTMO is the total number of MOs of all the fragments. The way to 'jump' to the right fragment block is illustrated in Figure 2. The counter JMO is initialized before looping over the EFP fragments and is incremented by the number of MOs of the previous fragment at the end of each iteration. This way, JMO will be the right number for the next fragment.

After extensive code modification (see Appendix) the same water trimer systems were redone and the expected results were observed (Table 1): changes in the order in the input file do not alter the E^{XR} and very similar E^{XR}s are obtained when different water molecules are treated by the *ab initio* method.

Various trimer systems and water clusters $(H_2O)_n$, n = 3-6,16 were tested and compared to benchmarking exchange repulsion energies calculated by the reduced variational space (RVS) method. The 16-water cluster benchmarking result was generated by an all-EFP calculation. All of the structures were optimized with RHF/6-31+G(d,p). The EFP potentials were generated with the 6-311++G(3df,2p) basis set. Each molecule in the clusters was in turn treated as an *ab initio* region with the RHF/6-311++G(3df,2p) basis set. For example, a 3-water cluster has three combinations: H_2O-1-23, H_2O-2-13 and H_2O-3-12. The maximum and minimum errors compared to the RVS E^{XR} are reported in Table 2. Note that the E^{XR} of the system is the sum of all the pair-wise QM-EFP and EFP-EFP E^{XR}. For small clusters (trimer, tetramer and pentamer), even the largest errors are within ~ 4.0 kcal/mol. The medium-sized water clusters showed larger values for the maximum errors but the minimum errors remain comparable with the small clusters. The different approximations used for deriving QM-EFP and

EFP-EFP exchange repulsion lead to different expressions and consequently different E^{XR}.

Implementation of Gradient

The general outline of the QM-EFP exchange repulsion gradient code is to have one driver subroutine (QMEFGXRDR) to allocate the dynamic memory for relevant quantities and to call a subroutine called QMEFGXR that calculates the gradient contributions. All of the quantities required for the gradient are computed in QMEFGXR by calling various subroutines and all of the terms are then assembled according to Eqs (10) and (14).

For the quantities for which both indices are for the *ab initio* region, the derivative codes are available. Only a small modification is done to make the relevant derivative matrices available in QMEFGXR subroutine. For the quantities that involve EFP indices, new subroutines were written.

Conclusion and Future work

The QM-EFP exchange repulsion Fock operator and energy codes were extensively modified. The current implementation allows multiple EFP fragments. For hetero-dimer systems, a modified Fock operator generates much improved exchange repulsion energies. The results from the QM-EFP exchange repulsion and RVS calculations are in good agreement, with minimal errors typically less than 5 kcal/mol. The derivatives of QM-EFP exchange repulsion energy with respect to *ab initio* atom centers and with respect to EFP centers have been implemented. Testing is in progress.

Acknowledgments

The authors have benefited greatly from useful discussions with Dr. Mike Schmidt, Prof. Lyudmila V. Slipchenko and Prof. Hui Li. This material is based upon work supported by the Air Force Office of Scientific Research under AFOSR Award No. FA9550-11-1-0099.

References

(1) Day, P. N.; Jensen, J. H.; Gordon, M. S.; Webb, S. P.; Stevens, W. J.; Krauss, M.; Garmer, D.; Basch, H.; Cohen, D. An Effective Fragment Method for Modeling Solvent Effects in Quantum Mechanical Calculations. *J. Chem. Phys.* **1996**, *105*, 1968–1986.

(2) Schmidt, M. W.; Baldridge, K. K.; Boatz, J. A.; Elbert, S. T.; Gordon, M. S.; Jensen, J. H.; Koseki, S.; Matsunaga, N.; Nguyen, K. A.; et, al. General Atomic and Molecular Electronic Structure System. *J. Comput. Chem.* **1993**, *14*, 1347–1363.

(3) Gordon, M. S.; Schmidt, M. W. Advances in Electronic Structure Theory: GAMESS a Decade Later. In *Theory Appl. Comput. Chem.: First Forty Years*; Elsevier B.V., 2005; pp. 1167–1189.

(4) Jeziorski, B.; Bulski, M.; Piela, L. First-Order Perturbation Treatment of the Short-Range Repulsion in a System of Many Closed-Shell Atoms or Molecules. *Int. J. Quantum Chem.* **1976**, *10*, 281–297.

(5) Jensen, J. H.; Gordon, M. S. An Approximate Formula for the Intermolecular Pauli Repulsion between Closed Shell Molecules. *Mol. Phys.* **1996**, *89*, 1313–1325.

(6) Jensen, J. H. Intermolecular Exchange-Induction and Charge Transfer: Derivation of Approximate Formulas Using Nonorthogonal Localized Molecular Orbitals. *J. Chem. Phys.* **2001**, *114*, 8775–8783.

(7) Jensen, J. H.; Gordon, M. S. An Approximate Formula for the Intermolecular Pauli Repulsion between Closed Shell Molecules. II. Application to the Effective Fragment Potential Method. *J. Chem. Phys.* **1998**, *108*, 4772–4782.

(8) Li, H.; Gordon, M. S. Gradients of the Exchange-Repulsion Energy in the General Effective Fragment Potential Method. *Theor. Chem. Acc.* **2006**, *115*, 385–390.

(9) Kemp, D. D.; Rintelman, J. M.; Gordon, M. S.; Jensen, J. H. Exchange Repulsion between Effective Fragment Potentials and Ab Initio Molecules. *Theor. Chem. Acc.* **2010**, *125*, 481–491.

(10) Jensen, J. H. Modeling Intermolecular Exchange Integrals between Nonorthogonal Molecular Orbitals. *J. Chem. Phys.* **1996**, *104*, 7795–7796.

(11) Yamaguchi, Y.; Goddard, J. D.; Osamura, Y.; Schaefer III., H. F. *A New Dimension to Quantum Chemistry: Analytic Derivative Methods in Ab Initio Molecular Electronic Structure Theory.*; Oxford Univ. Press, 1994; p. 471 pp.

(12) Li, H.; Gordon, M. S.; Jensen, J. H. Charge Transfer Interaction in the Effective Fragment Potential Method. *J. Chem. Phys.* **2006**, *124*, 214108/1–214108/16.

(13) Szabo, A.; Ostlund, N. S. *Modern Quantum Chemistry: Introduction to Advanced Electronic Structure Theory. 1st Ed. Revised.*; McGraw-Hill Publishing Co., 1989; p. 466 pp.

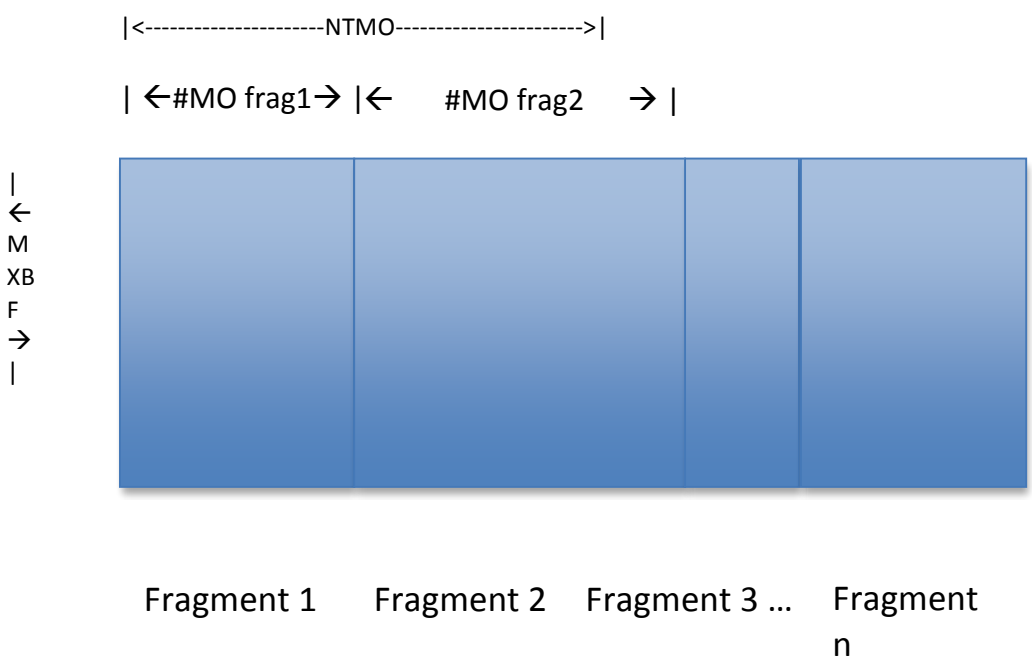

Figure 1. A pictorial representation of PROVEC matrix. Each block represents one EFP fragment.

```
JMO=1
DO MJ = 1,NFRG
 Call STINT
 Call DGEMM
            (…PROVEC(1,JMO)…)
            ……
JMO = JMO+NORB(MJ)
 ENDDO
```

Figure 2. An illustration of the key steps in the code to 'jump' to the correct EFP index.

Table 1 The QM-EFP E^{XR} (in Hartree) of water trimer calculated before and after code modification. H_2O-1-23 means that the 1st water is treated *ab initio* and the 2nd and 3rd water molecules are EFP fragments in that order in the input file.

Water trimer	QM-EFP E^{XR} (before)	QM-EFP E^{XR} (after)
H_2O-1-23	0.237570729	0.018545921
H_2O-1-32	0.023720728	0.018545921
H_2O-2-13	0.060030457	0.020656253
H_2O-2-31	0.052989663	0.020656253
H_2O-3-12	0.103773878	0.018469143
H_2O-3-21	1.120385809	0.018469143

Table 2. Exchange repulsion energies (kcal/mol) obtained from benchmark calculations and smallest and largest errors for QM-EFP calculations. The second and the third columns show the smallest and the largest deviations from the RVS interaction energies when different molecules are treated ab initio. For all systems except $(H_2O)_{16}$, the benchmark results were obtained from the RVS analysis. The $(H_2O)_{16}$ benchmark value is obtained from an all-EFP2 calculation. All of the cluster structures were optimized with RHF/6-31+G(d,p) and the EFP potentials were generated with the 6-311++G(3df,2p) basis set.

Exchange Repulsion (kcal/mol)	Benchmark	QM-EFP error (min)	QM-EFP error (max)
$(H_2O)_3$	15.0	1.6	2.0
$(MeOH)_3$	13.5	0.0	2.7
$((CH_3)_2CO)_3$	5.6	-1.2	-1.4
$(CH_3CN)_3$	5.1	-0.8	-1.2
$(CH_2Cl_2)_3$	1.1	-0.1	1.3
3DMSO	10.1	-2.0	Not converged
$(H_2O)_4$	29.3	-0.9	-1.9
$(H_2O)_5$	39.1	2.4	3.8
$(H_2O)_6$-bag	42.5	1.1	-7.2
$(H_2O)_6$-boat	43.3	-2.4	-6.8
$(H_2O)_6$-book	43.8	0.0	-4.0
$(H_2O)_6$-cage	40.9	0.8	-2.3
$(H_2O)_6$-cyclic	45.0	-3.2	-8.8
$(H_2O)_6$-prism	39.8	0.3	1.5
$(H_2O)_{16}$	118.3	0.3	5.2

Appendix

(A) Derivation of gradients of QM-EFP E^{XR}

The QM-EFP exchange repulsion energy expression is

$$
\begin{aligned}
E^{XR} = & -2\sum_{i}^{A}\sum_{j}^{B}(ij\,|\,ij)^{SGO} \\
& -2\sum_{i}^{A}\sum_{j}^{B}S_{ij}\left[2\left(V_{ij}^{A}+G_{ij}^{A}\right)+\sum_{l}^{B}F_{jl}^{B}S_{il}\right] \\
& +2\sum_{i}^{A}\sum_{j}^{B}S_{ij}\left[\sum_{k}^{A}S_{kj}\left(F_{ik}^{A}+V_{ik}^{EFP,B}-V_{ik}^{j}\right)+S_{ij}\left(\sum_{I}^{A}\frac{-Z_I}{R_{jI}}+2\sum_{k}^{A}V_{kk}^{j}\right)\right]
\end{aligned}
\tag{A1}
$$

The derivative of Eq. (A1) with respect to an *ab initio* atom center, $\mathbf{q_a}$, is

$$
\begin{aligned}
\frac{\partial E^{XR}}{\partial q_a} = & -2\sum_{i}^{A}\sum_{j}^{B}\frac{\partial(ij\,|\,ij)^{SGO}}{\partial q_a} \\
& -2\sum_{i}^{A}\sum_{j}^{B}\left(\frac{\partial S_{ij}}{\partial q_a}\right)\left[2\left(V_{ij}^{A}+G_{ij}^{A}\right)+\sum_{l}^{B}F_{jl}^{B}S_{il}\right]-2\sum_{i}^{A}\sum_{j}^{B}S_{ij}\left[2\left(\frac{\partial V_{ij}^{A}}{\partial q_a}+\frac{\partial G_{ij}^{A}}{\partial q_a}\right)+\sum_{l}^{B}F_{jl}^{B}\left(\frac{\partial S_{il}}{\partial q_a}\right)\right] \\
& +2\sum_{i}^{A}\sum_{j}^{B}\left(\frac{\partial S_{ij}}{\partial q_a}\right)\left[\sum_{k}^{A}S_{kj}\left(F_{ik}^{A}+V_{ik}^{EFP,B}-V_{ik}^{j}\right)+S_{ij}\left(\sum_{I}^{A}\frac{-Z_I}{R_{jI}}+2\sum_{k}^{A}V_{kk}^{j}\right)\right] \\
& +2\sum_{i}^{A}\sum_{j}^{B}S_{ij}\left[\begin{array}{l}\sum_{k}^{A}\left(\frac{\partial S_{kj}}{\partial q_a}\right)\left(F_{ik}^{A}+V_{ik}^{EFP,B}-V_{ik}^{j}\right)+\left(\frac{\partial S_{ij}}{\partial q_a}\right)\left(\sum_{I}^{A}\frac{-Z_I}{R_{jI}}+2\sum_{k}^{A}V_{kk}^{j}\right) \\ +\sum_{k}^{A}S_{kj}\left(\frac{\partial F_{ik}^{A}}{\partial q_a}+\frac{\partial V_{ik}^{EFP,B}}{\partial q_a}-\frac{\partial V_{ik}^{j}}{\partial q_a}\right)+S_{ij}\left(\sum_{I}^{A}\frac{\partial}{\partial q_a}\frac{-Z_I}{R_{jI}}+2\sum_{k}^{A}\frac{\partial V_{kk}^{j}}{\partial q_a}\right)\end{array}\right]
\end{aligned}
\tag{A2}
$$

where q_a is the Cartesian coordinate of atom a of the *ab initio* molecule A. The following derivatives are required to evaluate Eq. (A2):

$$
\frac{\partial(ij\,|\,ij)^{SGO}}{\partial q_a},\quad \frac{\partial S_{ij}}{\partial q_a},\quad \frac{\partial V_{ij}^{A}}{\partial q_a},\quad \frac{\partial G_{ij}^{A}}{\partial q_a},\quad \frac{\partial F_{ik}^{A}}{\partial q_a},\quad \frac{\partial V_{ik}^{EFP,B}}{\partial q_a},\quad \frac{\partial V_{ik}^{j}}{\partial q_a},\quad \sum_{I}^{A}\frac{\partial}{\partial q_a}\frac{-Z_I}{R_{jI}}
$$

The derivative of $-Z_I/R_{jI}$ is trivial, use the x-coordinate of $\mathbf{q}_a$ as an example

$$\begin{aligned}\sum_I^A \frac{\partial}{\partial x_a}\frac{-Z_I}{R_{jI}} &= -Z_a\frac{\partial R_{ja}^{-1}}{\partial x_a} = \left(-Z_a\right)\frac{\partial\left[\left(x_j-x_a\right)^2+\left(y_j-y_a\right)^2+\left(z_j-z_a\right)^2\right]^{-1/2}}{\partial x_a}\\ &= \left(-Z_a\right)\left(-\frac{1}{2}\right)\left[\left(x_j-x_a\right)^2+\left(y_j-y_a\right)^2+\left(z_j-z_a\right)^2\right]^{-3/2}2\left(x_j-x_a\right)(-1)\\ &= \frac{\left(-Z_a\right)\left(x_j-x_a\right)}{R_{ja}^3}\end{aligned} \tag{A3}$$

Where I is the nucleus of the molecule A and only the terms with I=a survive.

$$\begin{aligned}\frac{\partial S_{ij}}{\partial q_a} &= \frac{\partial}{\partial q_a}\sum_\mu^A\sum_\nu^B C_{\mu i}C_{\nu j}\left(\mu\,|\,\nu\right)\\ &= \sum_\mu^A C_{\mu i}^a\left(\mu\,|\,j\right)+\sum_\mu^A C_{\mu i}\left(\mu^a\,|\,j\right)+\sum_\nu^B C_{\nu j}^a\left(i\,|\,\nu\right)+\sum_\nu^B C_{\nu j}\left(i\,|\,\nu^a\right)\\ &= \sum_\mu^A C_{\mu i}^a\left(\mu\,|\,j\right)+\sum_\mu^A C_{\mu i}\left(\mu^a\,|\,j\right)\\ &= \sum_\mu^A C_{\mu i}^a\left(\mu\,|\,j\right)+S_{ij}^a\end{aligned} \tag{A4}$$

The last two terms in the second equality are equal to zero because EFP MOs are frozen and the EFP AOs are not a function of the *ab initio* coordinates. Note that S_{ij}^a is not a shorthand notation for $\partial S_{ij}/\partial q_a$, rather $S_{ij}^a = \sum_\mu^A C_{\mu i}\left(\mu^a\,|\,j\right)$. To avoid solving the time-consuming coupled perturbed Hartree-Fock equations for C^a, Eq. (A4) is rewritten in terms of orbital response terms

$$\begin{aligned}\sum_i^A\sum_j^B \frac{\partial S_{ij}}{\partial q_a} &= \sum_i^A\sum_j^B\left(\sum_\mu^A\sum_m^A C_{\mu m}U_{mi}^a(\mu\,|\,j)+S_{ij}^a\right)\\ &= \frac{1}{2}\left[\sum_{i,m}^A\sum_j^B U_{mi}^a(m\,|\,j)+U_{im}^a(m\,|\,j)\right]+\sum_i^A\sum_j^B S_{ij}^a\\ &= \frac{1}{2}\sum_{i,m}^A\sum_j^B\left(U_{mi}^a+U_{im}^a\right)S_{mj}+\sum_i^A\sum_j^B S_{ij}^a\\ &= \sum_{i,m}^A\sum_j^B\left(-\frac{1}{2}S_{mi}^aS_{mj}+S_{ij}^a\right)\end{aligned} \tag{A5}$$

The last step of Eq. (A5) uses the fact that $U_{mi}^a+U_{im}^a=-S_{mi}^a$ [11]

The derivative of the nuclear-electron attraction term, $\frac{\partial V_{ij}^A}{\partial q_a}$, involves the derivative of the ab initio MO and the derivative of the operator.

$$\begin{aligned}\sum_i^A\sum_j^B \frac{\partial V_{ij}^A}{\partial q_a} &= \frac{\partial}{\partial q_a}\sum_i^A\sum_j^B\sum_\mu^A\sum_\nu^B C_{\mu i}C_{\nu j}\langle\mu|V^A|\nu\rangle\\ &= \sum_i^A\sum_j^B\sum_\mu^A\sum_\nu^B C_{\mu i}^aC_{\nu j}\langle\mu|V^A|\nu\rangle+C_{\mu i}C_{\nu j}\langle\mu^a|V^A|\nu\rangle+C_{\mu i}C_{\nu j}\langle\mu|V^{A^a}|\nu\rangle\\ &= \sum_{i,m}^A\sum_j^B -\frac{1}{2}S_{mi}^aV_{mj}^A+\sum_i^A\sum_j^B\left(\langle i^a|V^A|j\rangle+\langle i|V^{A^a}|j\rangle\right)\\ &= \sum_{i,m}^A\sum_j^B -\frac{1}{2}S_{mi}^aV_{mj}^A+\sum_i^A\sum_j^B V_{ij}^{A^a}\end{aligned} \tag{A6}$$

where $V_{ij}^{A^a}=\langle i^a|V^A|j\rangle+\langle i|V^{A^a}|j\rangle$

The derivative of the two-electron matrix element involving an EFP MO looks like

$$
\begin{aligned}
\sum_i^A \sum_j^B \frac{\partial G_{ij}^A}{\partial q_a} &= \frac{\partial}{\partial q_a} \sum_i^A \sum_j^B \sum_k^A \left[2(ij \mid kk) - (ik \mid jk) \right] \\
&= \frac{\partial}{\partial q_a} \sum_i^A \sum_j^B \sum_k^A \sum_{\mu\nu\lambda}^A C_{\mu i} C_{\nu k} C_{\lambda k} \left[2(\mu j \mid \nu\lambda) - \frac{1}{2}(\mu\nu \mid j\lambda) - \frac{1}{2}(\mu\lambda \mid \nu j) \right] \\
&= \sum_i^A \sum_j^B \sum_k^A \sum_{\mu\nu\lambda}^A \left\{ \begin{array}{l}
C_{\mu i}^a C_{\nu k} C_{\lambda k} \left[2(\mu j \mid \nu\lambda) - \frac{1}{2}(\mu\nu \mid j\lambda) - \frac{1}{2}(\mu\lambda \mid \nu j) \right] \\
+ C_{\mu i} C_{\nu k}^a C_{\lambda k} \left[2(\mu j \mid \nu\lambda) - \frac{1}{2}(\mu\nu \mid j\lambda) - \frac{1}{2}(\mu\lambda \mid \nu j) \right] \\
+ C_{\mu i} C_{\nu k} C_{\lambda k}^a \left[2(\mu j \mid \nu\lambda) - \frac{1}{2}(\mu\nu \mid j\lambda) - \frac{1}{2}(\mu\lambda \mid \nu j) \right] \\
+ C_{\mu i} C_{\nu k} C_{\lambda k} \left[\begin{array}{l}
2(\mu^a j \mid \nu\lambda) + 2(\mu j \mid \nu^a \lambda) + 2(\mu j \mid \nu\lambda^a) \\
-\frac{1}{2}(\mu^a \nu \mid j\lambda) - \frac{1}{2}(\mu\nu^a \mid j\lambda) - \frac{1}{2}(\mu\nu \mid j\lambda^a) \\
-\frac{1}{2}(\mu^a \lambda \mid \nu j) - \frac{1}{2}(\mu\lambda \mid \nu^a j) - \frac{1}{2}(\mu\lambda^a \mid \nu j)
\end{array} \right]
\end{array} \right\} \\
&= \sum_i^A \sum_j^B \sum_k^A \left\{ \begin{array}{l}
\sum_m^A U_{mi}^a \left[2(mj \mid kk) - \frac{1}{2}(mk \mid jk) - \frac{1}{2}(mk \mid kj) \right] \\
+ \sum_m^A U_{mk}^a \left[2(ij \mid mk) - \frac{1}{2}(im \mid jk) - \frac{1}{2}(ik \mid mj) \right] \\
+ \sum_m^A U_{mk}^a \left[2(ij \mid km) - \frac{1}{2}(ik \mid jm) - \frac{1}{2}(im \mid kj) \right] \\
+ \left[\begin{array}{l}
2(i^a j \mid kk) + 2(ij \mid k^a k) + 2(ij \mid kk^a) \\
-\frac{1}{2}(i^a k \mid jk) - \frac{1}{2}(ik^a \mid jk) - \frac{1}{2}(ik \mid jk^a) \\
-\frac{1}{2}(i^a k \mid kj) - \frac{1}{2}(ik \mid k^a j) - \frac{1}{2}(ik^a \mid kj)
\end{array} \right]
\end{array} \right\} \\
&= \sum_j^B \sum_{i,k,m}^A -\frac{1}{2} S_{mi}^a \left[2(mj \mid kk) - (mk \mid jk) \right] \\
&+ \sum_j^B \sum_{i,k,m}^A -\frac{1}{2} S_{mk}^a \left[4(ij \mid mk) - (im \mid jk) - (ik \mid mj) \right] \\
&+ \sum_i^A \sum_j^B \sum_k^A \left[2(i^a j \mid kk) - (i^a k \mid jk) + 4(ij \mid k^a k) - (ik^a \mid jk) - (ik \mid jk^a) \right] \\
&= -\sum_j^B \sum_{i,m}^A \frac{1}{2} S_{mi}^a G_{mj}^A - \sum_j^B \sum_{i,k,m}^A \frac{1}{2} S_{mk}^a \left[4(ij \mid mk) - (im \mid jk) - (ik \mid mj) \right] + \sum_i^A \sum_j^B G_{ij}^{A^a}
\end{aligned}
\tag{A7}
$$

Where $\sum_{i}^{A}\sum_{j}^{B} G_{ij}^{A^a} = \sum_{i}^{A}\sum_{j}^{B}\sum_{k}^{A}\left[2\left(i^a j \mid kk\right) - \left(i^a k \mid jk\right) + 4\left(ij \mid k^a k\right) - \left(ik^a \mid jk\right) - \left(ik \mid jk^a\right)\right]$

The derivative of the Fock matrix of molecule A can be broken down to one- and two-electron contributions.

$$\sum_{i,k}^{A} \frac{\partial F_{ik}^{A}}{\partial q_a} = \sum_{i,k}^{A}\left(\frac{\partial h_{ik}}{\partial q_a} + \frac{\partial G_{ik}^{A}}{\partial q_a}\right) \tag{A8}$$

$$\begin{aligned}
\sum_{i,k}^{A} \frac{\partial h_{ik}}{\partial q_a} &= \frac{\partial}{\partial q_a}\sum_{i,k}^{A}\sum_{\mu,\nu}^{A} C_{\mu i} C_{\nu k} h_{\mu\nu} \\
&= \sum_{i,k}^{A}\sum_{\mu,\nu}^{A} C_{\mu i}^{a} C_{\nu k} h_{\mu\nu} + C_{\mu i} C_{\nu k}^{a} h_{\mu\nu} + C_{\mu i} C_{\nu k} h_{\mu\nu}^{a} \\
&= \sum_{i,k}^{A}\sum_{\mu,\nu}^{A}\sum_{m}^{A}\left(C_{\mu m} U_{mi}^{a} C_{\nu k} h_{\mu\nu} + C_{\mu i} C_{\nu m} U_{mk}^{a} h_{\mu\nu}\right) + \sum_{i,k}^{A} h_{ik}^{a} \\
&= \sum_{i,k,m}^{A} -\frac{1}{2} S_{mi}^{a} h_{mk} - \frac{1}{2} S_{mk}^{a} h_{mi} + \sum_{i,k}^{A} h_{ik}^{a} \\
&= \sum_{i,k,m}^{A} -S_{mi}^{a} h_{mk} + \sum_{i,k}^{A} h_{ik}^{a}
\end{aligned} \tag{A9}$$

Both i and k run over the occupied orbitals of the *ab initio* molecule and the first two terms in the second last equality are equivalent.

$$
\begin{aligned}
&\sum_{i,k}^{A}\frac{\partial G_{ik}^{A}}{\partial q_a}\\
&=\frac{\partial}{\partial q_a}\sum_{i,k,n}^{A}\sum_{\mu\nu\lambda\sigma}^{A}C_{\mu i}C_{\nu k}C_{\lambda n}C_{\sigma n}\left[2(\mu\nu\,|\,\lambda\sigma)-\frac{1}{2}(\mu\lambda\,|\,\nu\sigma)-\frac{1}{2}(\mu\sigma\,|\,\nu\lambda)\right]\\
&=\sum_{i,k,n}^{A}\sum_{\mu\nu\lambda\sigma}^{A}\begin{pmatrix}C_{\mu i}^{a}C_{\nu k}C_{\lambda n}C_{\sigma n}+C_{\mu i}C_{\nu k}^{a}C_{\lambda n}C_{\sigma n}\\+C_{\mu i}C_{\nu k}C_{\lambda n}^{a}C_{\sigma n}+C_{\mu i}C_{\nu k}C_{\lambda n}C_{\sigma n}^{a}\end{pmatrix}\left[2(\mu\nu\,|\,\lambda\sigma)-\frac{1}{2}(\mu\lambda\,|\,\nu\sigma)-\frac{1}{2}(\mu\sigma\,|\,\nu\lambda)\right]\\
&+\sum_{i,k,n}^{A}\sum_{\mu\nu\lambda\sigma}^{A}C_{\mu i}C_{\nu k}C_{\lambda n}C_{\sigma n}\begin{bmatrix}2(\mu^{a}\nu\,|\,\lambda\sigma)-\frac{1}{2}(\mu^{a}\lambda\,|\,\nu\sigma)-\frac{1}{2}(\mu^{a}\sigma\,|\,\nu\lambda)\\+2(\mu\nu^{a}\,|\,\lambda\sigma)-\frac{1}{2}(\mu\lambda\,|\,\nu^{a}\sigma)-\frac{1}{2}(\mu\sigma\,|\,\nu^{a}\lambda)\\+2(\mu\nu\,|\,\lambda^{a}\sigma)-\frac{1}{2}(\mu\lambda^{a}\,|\,\nu\sigma)-\frac{1}{2}(\mu\sigma\,|\,\nu\lambda^{a})\\+2(\mu\nu\,|\,\lambda\sigma^{a})-\frac{1}{2}(\mu\lambda\,|\,\nu\sigma^{a})-\frac{1}{2}(\mu\sigma^{a}\,|\,\nu\lambda)\end{bmatrix}\\
&=\sum_{i,k,n}^{A}\sum_{m}^{A}U_{mi}^{a}\left[2(mk\,|\,nn)-\frac{1}{2}(mn\,|\,kn)-\frac{1}{2}(mn\,|\,kn)\right]\\
&+\sum_{i,k,n}^{A}\sum_{m}^{A}U_{mk}^{a}\left[2(im\,|\,nn)-\frac{1}{2}(in\,|\,mn)-\frac{1}{2}(in\,|\,mn)\right]\\
&+\sum_{i,k,n}^{A}\sum_{m}^{A}U_{mn}^{a}\left[2(ik\,|\,mn)-\frac{1}{2}(im\,|\,kn)-\frac{1}{2}(in\,|\,km)\right]\\
&+\sum_{i,k,n}^{A}\sum_{m}^{A}U_{mn}^{a}\left[2(ik\,|\,nm)-\frac{1}{2}(in\,|\,km)-\frac{1}{2}(im\,|\,kn)\right]\\
&+\sum_{i,k,f}^{A}\begin{bmatrix}2(i^{a}k\,|\,nn)-(i^{a}n\,|\,kn)+2(ik^{a}\,|\,nn)-(in\,|\,k^{a}n)\\+4(ik\,|\,n^{a}n)-(in^{a}\,|\,kn)-(in\,|\,kn^{a})\end{bmatrix}\\
&=\sum_{i,k,n}^{A}\sum_{m}^{A}\left[U_{mi}^{a}\left[2(mk\,|\,nn)-(mn\,|\,kn)\right]+U_{mk}^{a}\left[2(im\,|\,nn)-(in\,|\,mn)\right]\right]\\
&+\sum_{i,k,n}^{A}\sum_{m}^{A}U_{mn}^{a}\left[4(ik\,|\,mn)-(im\,|\,kn)-(in\,|\,km)\right]\\
&+\sum_{i,k,n}^{A}\begin{bmatrix}2(i^{a}k\,|\,nn)-(i^{a}n\,|\,kn)+2(ik^{a}\,|\,nn)-(in\,|\,k^{a}n)\\+4(ik\,|\,n^{a}n)-(in^{a}\,|\,kn)-(in\,|\,kn^{a})\end{bmatrix}\\
&=\sum_{i,k,m,n}^{A}\left\{-\frac{1}{2}S_{mi}^{a}G_{mk}^{A}-\frac{1}{2}S_{mk}^{a}G_{mi}^{A}-\frac{1}{2}S_{mn}^{a}\left[4(ik\,|\,mn)-(im\,|\,kn)-(in\,|\,km)\right]\right\}+\sum_{i,k}^{A}G_{ik}^{A^{a}}\\
&=-\sum_{i,k,m}^{A}S_{mi}^{a}G_{mk}^{A}-\sum_{i,k,m,n}^{A}\left[\frac{1}{2}S_{mn}^{a}\left[4(ik\,|\,mn)-(im\,|\,kn)-(in\,|\,km)\right]\right]+\sum_{i,k}^{A}G_{ik}^{A^{a}}
\end{aligned}
\tag{A10}
$$

where $\sum_{i,k}^{A} G_{ik}^{A^a} = \sum_{i,k,n}^{A} \begin{bmatrix} 2\left(i^a k \mid nn\right) - \left(i^a n \mid kn\right) + 2\left(ik^a \mid nn\right) - \left(in \mid k^a n\right) \\ +4\left(ik \mid n^a n\right) - \left(in^a \mid kn\right) - \left(in \mid kn^a\right) \end{bmatrix}$

Now combine Eq. (A9) and (A10)

$$\begin{aligned} \sum_{i,k}^{A} \frac{\partial F_{ik}^{A}}{\partial q_a} &= \sum_{i,k,m}^{A} -S_{mi}^{a} h_{mk} + \sum_{i,k}^{A} h_{ik}^{a} - \sum_{i,k,m}^{A} S_{mi}^{a} G_{mk}^{A} - \sum_{i,k,m,n}^{A} \left[\frac{1}{2} S_{mn}^{a} \left[4\left(ik \mid mn\right) - \left(im \mid kn\right) - \left(in \mid km\right) \right] \right] + \sum_{i,k}^{A} G_{ik}^{A^a} \\ &= \sum_{i,k,m}^{A} -S_{mi}^{a} F_{mk}^{A} + \sum_{i,k}^{A} F_{ik}^{A^a} - \sum_{i,k,m,n}^{A} \left[\frac{1}{2} S_{mn}^{a} \left[4\left(ik \mid mn\right) - \left(im \mid kn\right) - \left(in \mid km\right) \right] \right] \end{aligned} \tag{A11}$$

The operators of both $\frac{\partial V_{ik}^{EFP,B}}{\partial q_a}$ and $\frac{\partial V_{ik}^{j}}{\partial q_a}$ are functions of EFP fragment B hence the derivatives come from the contributions of derivatives of MOs. These two terms are derived similarly. Here only the derivation for $\frac{\partial V_{ik}^{EFP,B}}{\partial q_a}$ is given.

$$\begin{aligned} \sum_{i,k}^{A} \frac{\partial V_{ik}^{EFP,B}}{\partial q_a} &= \frac{\partial}{\partial q_a} \sum_{i,k}^{A} \sum_{\mu,\nu}^{A} C_{\mu i} C_{\nu k} \left(\mu \mid V^{EFP,B} \mid \nu \right) \\ &= \sum_{i,k}^{A} \sum_{\mu,\nu}^{A} \left[C_{\mu i}^{a} C_{\nu k} \left(\mu \mid V^{EFP,B} \mid \nu \right) + C_{\mu i} C_{\nu k}^{a} \left(\mu \mid V^{EFP,B} \mid \nu \right) \right] \\ &+ \sum_{i,k}^{A} \sum_{\mu,\nu}^{A} \left[C_{\mu i} C_{\nu k} \left(\mu^a \mid V^{EFP,B} \mid \nu \right) + C_{\mu i} C_{\nu k} \left(\mu \mid V^{EFP,B} \mid \nu^a \right) \right] \\ &= \sum_{i,k,m}^{A} \left(U_{mi}^{a} V_{mk}^{EFP,B} + U_{mk}^{a} V_{im}^{EFP,B} \right) + \sum_{i,k}^{A} \left(i^a \mid V^{EFP,B} \mid k \right) + \left(i \mid V^{EFP,B} \mid k^a \right) \\ &= \sum_{i,k,m}^{A} -\frac{1}{2} \left(S_{mi}^{a} V_{mk}^{EFP,B} + S_{mk}^{a} V_{im}^{EFP,B} \right) + \sum_{i,k}^{A} V_{ik}^{EFP,B^a} \\ &= -\sum_{i,k,m}^{A} S_{mi}^{a} V_{mk}^{EFP,B} + \sum_{i,k}^{A} V_{ik}^{EFP,B^a} \end{aligned} \tag{A12}$$

And similarly,

$$\sum_{i,k}^{A} \frac{\partial V_{ik}^{j}}{\partial q_a} = -\sum_{i,k,m}^{A} S_{mi}^{a} V_{mk}^{j} + \sum_{i,k}^{A} V_{ik}^{j^a} \tag{A13}$$

Now substitute Eqs. (A3), (A5-7) and (A11-13) back into Eq. (A2) and look at them term by term,

$$
\begin{aligned}
&-2\sum_{i}^{A}\sum_{j}^{B}\left(\frac{\partial S_{ij}}{\partial q_a}\right)\left[2\left(V_{ij}^{A}+G_{ij}^{A}\right)+\sum_{l}^{B}F_{jl}^{B}S_{il}\right] \\
&=-2\sum_{i}^{A}\sum_{j}^{B}\sum_{m}^{A}\left(-\frac{1}{2}S_{mi}^{a}S_{mj}+S_{ij}^{a}\right)\left[2\left(V_{ij}^{A}+G_{ij}^{A}\right)+\sum_{l}^{B}F_{jl}^{B}S_{il}\right] \\
&=\sum_{i,m}^{A}\sum_{j}^{B}S_{mi}^{a}S_{mj}\left(2V_{ij}^{A}+2G_{ij}^{A}\right)+\sum_{i,m}^{A}\sum_{j,l}^{B}S_{mi}^{a}S_{mj}F_{jl}^{B}S_{il} \\
&-2\sum_{i}^{A}\sum_{j}^{B}S_{ij}^{a}\left(2V_{ij}^{A}+2G_{ij}^{A}\right)-2\sum_{i}^{A}\sum_{j,l}^{B}S_{ij}^{a}F_{jl}^{B}S_{il}
\end{aligned}
\tag{A14}
$$

$$
\begin{aligned}
&-2\sum_{i}^{A}\sum_{j}^{B}S_{ij}\left[2\left(\frac{\partial V_{ij}^{A}}{\partial q_a}+\frac{\partial G_{ij}^{A}}{\partial q_a}\right)+\sum_{l}^{B}F_{jl}^{B}\left(\frac{\partial S_{il}}{\partial q_a}\right)\right] \\
&=-2\sum_{i}^{A}\sum_{j}^{B}S_{ij}\left[\begin{array}{l}2\left(\begin{array}{l}\left(\sum_{m}^{A}\left(-\frac{1}{2}S_{mi}^{a}V_{mj}^{A}+V_{ij}^{A^a}\right)\right)+\\ \left(-\sum_{m}^{A}\frac{1}{2}S_{mi}^{a}G_{mj}^{A}-\sum_{k,m}^{A}\frac{1}{2}S_{mk}^{a}\left[4\left(ij\mid mk\right)-\left(im\mid jk\right)-\left(ik\mid mj\right)\right]+G_{ij}^{A^a}\right)\end{array}\right)\\ +\sum_{l}^{B}F_{jl}^{B}\sum_{m}^{A}\left(-\frac{1}{2}S_{mi}^{a}S_{ml}+S_{il}^{a}\right)\end{array}\right] \\
&=\sum_{i}^{A}\sum_{j}^{B}\left[\left(\begin{array}{l}\sum_{m}^{A}2S_{ij}S_{mi}^{a}\left(V_{mj}^{A}+G_{mj}^{A}\right)-2S_{ij}\left(2V_{ij}^{A^a}+2G_{ij}^{A^a}\right)\\ +2\sum_{k,m}^{A}S_{ij}S_{mk}^{a}\left[4\left(ij\mid mk\right)-\left(im\mid jk\right)-\left(ik\mid mj\right)\right]\end{array}\right)+\sum_{l}^{B}\sum_{m}^{A}S_{ij}\left(F_{jl}^{B}S_{mi}^{a}S_{ml}-2F_{jl}^{B}S_{il}^{a}\right)\right] \\
&=\sum_{i,m}^{A}\sum_{j}^{B}S_{ij}S_{mi}^{a}\left(2V_{mj}^{A}+2G_{mj}^{A}\right)+\sum_{i,m}^{A}\sum_{j,l}^{B}S_{ij}S_{mi}^{a}S_{ml}F_{jl}^{B} \\
&-\sum_{i}^{A}\sum_{j}^{B}2S_{ij}\left(2V_{ij}^{A^a}+2G_{ij}^{A^a}\right)-\sum_{i}^{A}\sum_{j,l}^{B}2S_{ij}S_{il}^{a}F_{jl}^{B} \\
&+2\sum_{i,k,m}^{A}\sum_{j}^{B}S_{ij}S_{mk}^{a}\left[4\left(ij\mid mk\right)-\left(im\mid jk\right)-\left(ik\mid mj\right)\right]
\end{aligned}
$$

(A15)

$$2\sum_{i}^{A}\sum_{j}^{B}\frac{\partial S_{ij}}{\partial q_a}\left[\sum_{k}^{A}S_{kj}\left(F_{ik}^{A}+V_{ik}^{EFP,B}-V_{ik}^{j}\right)+S_{ij}\left(\sum_{I}^{A}\frac{-Z_I}{R_{jI}}+2\sum_{k}^{A}V_{kk}^{j}\right)\right]$$

$$=2\sum_{i}^{A}\sum_{j}^{B}\sum_{m}^{A}\left(-\frac{1}{2}S_{mi}^{a}S_{mj}+S_{ij}^{a}\right)\left[\sum_{k}^{A}S_{kj}\left(F_{ik}^{A}+V_{ik}^{EFP,B}-V_{ik}^{j}\right)+S_{ij}\left(\sum_{I}^{A}\frac{-Z_I}{R_{jI}}+2\sum_{k}^{A}V_{kk}^{j}\right)\right] \quad \text{(A16)}$$

$$=-\sum_{i,k,m}^{A}\sum_{j}^{B}S_{mi}^{a}S_{mj}S_{kj}\left(F_{ik}^{A}+V_{ik}^{EFP,B}-V_{ik}^{j}\right)-\sum_{i,m}^{A}\sum_{j}^{B}S_{mi}^{a}S_{mj}S_{ij}\left(\sum_{I}^{A}\frac{-Z_I}{R_{jI}}+2\sum_{k}^{A}V_{kk}^{j}\right)$$

$$+2\sum_{i,k}^{A}\sum_{j}^{B}S_{ij}^{a}S_{kj}\left(F_{ik}^{A}+V_{ik}^{EFP,B}-V_{ik}^{j}\right)+2\sum_{i}^{A}\sum_{j}^{B}S_{ij}^{a}S_{ij}\left(\sum_{I}^{A}\frac{-Z_I}{R_{jI}}+2\sum_{k}^{A}V_{kk}^{j}\right)$$

$$2\sum_{i}^{A}\sum_{j}^{B}S_{ij}\left[\sum_{k}^{A}\frac{\partial S_{kj}}{\partial q_a}\left(F_{ik}^{A}+V_{ik}^{EFP,B}-V_{ik}^{j}\right)+\frac{\partial S_{ij}}{\partial q_a}\left(\sum_{I}^{A}\frac{-Z_I}{R_{jI}}+2\sum_{k}^{A}V_{kk}^{j}\right)\right]$$

$$=2\sum_{i}^{A}\sum_{j}^{B}S_{ij}\left[\begin{array}{l}\sum_{k}^{A}\sum_{m}^{A}\left(-\frac{1}{2}S_{mk}^{a}S_{mj}+S_{kj}^{a}\right)\left(F_{ik}^{A}+V_{ik}^{EFP,B}-V_{ik}^{j}\right)\\+\sum_{m}^{A}\left(-\frac{1}{2}S_{mi}^{a}S_{mj}+S_{ij}^{a}\right)\left(\sum_{I}^{A}\frac{-Z_I}{R_{jI}}+2\sum_{k}^{A}V_{kk}^{j}\right)\end{array}\right] \quad \text{(A17)}$$

$$=-\sum_{i,k,m}^{A}\sum_{j}^{B}S_{ij}S_{mk}^{a}S_{mj}\left(F_{ik}^{A}+V_{ik}^{EFP,B}-V_{ik}^{j}\right)-\sum_{i,m}^{A}\sum_{j}^{B}S_{ij}S_{mi}^{a}S_{mj}\left(\sum_{I}^{A}\frac{-Z_I}{R_{jI}}+2\sum_{k}^{A}V_{kk}^{j}\right)$$

$$+2\sum_{i,k}^{A}\sum_{j}^{B}S_{ij}S_{kj}^{a}\left(F_{ik}^{A}+V_{ik}^{EFP,B}-V_{ik}^{j}\right)+2\sum_{i}^{A}\sum_{j}^{B}S_{ij}S_{ij}^{a}\left(\sum_{I}^{A}\frac{-Z_I}{R_{jI}}+2\sum_{k}^{A}V_{kk}^{j}\right)$$

$$2\sum_{i}^{A}\sum_{j}^{B}S_{ij}\left[\sum_{k}^{A}S_{kj}\left(\frac{\partial F_{ik}^{A}}{\partial q_a}+\frac{\partial V_{ik}^{EFP,B}}{\partial q_a}-\frac{\partial V_{ik}^{j}}{\partial q_a}\right)+S_{ij}\left(\sum_{I}^{A}\frac{\partial}{\partial q_a}\frac{-Z_I}{R_{jI}}+2\sum_{k}^{A}\frac{\partial V_{kk}^{j}}{\partial q_a}\right)\right]$$

$$=2\sum_{i}^{A}\sum_{j}^{B}S_{ij}\left\{\begin{array}{l}\displaystyle\sum_{k}^{A}S_{kj}\left[\begin{array}{l}\displaystyle\sum_{m}^{A}-S_{mi}^{a}F_{mk}^{A}+F_{ik}^{a}-\sum_{m,n}^{A}\left[\frac{1}{2}S_{mn}^{a}\left[4(ik\,|\,mn)-(im\,|\,kn)-(in\,|\,km)\right]\right]\\ \displaystyle-\sum_{m}^{A}S_{mi}^{a}V_{mk}^{EFP,B}+V_{ik}^{EFP,B^a}-\left(-\sum_{m}^{A}S_{mi}^{a}V_{mk}^{j}+V_{ik}^{j^a}\right)\end{array}\right]\\ \displaystyle+S_{ij}\left[\frac{(-Z_a)(q_j-q_a)}{R_{ja}^{3}}+2\left(-\sum_{k,m}^{A}S_{mk}^{a}V_{mk}^{j}+\sum_{k}^{A}V_{kk}^{j^a}\right)\right]\end{array}\right\}$$

$$=-2\sum_{i,k,m}^{A}\sum_{j}^{B}S_{ij}S_{kj}S_{mi}^{a}\left(F_{mk}^{A}+V_{mk}^{EFP,B}-V_{mk}^{j}\right)+2\sum_{i,k}^{A}\sum_{j}^{B}S_{ij}S_{kj}\left(F_{ik}^{a}+V_{ik}^{EFP,B^a}-V_{ik}^{j^a}\right)$$

$$-\sum_{i,k,m,n}^{A}\sum_{j}^{B}S_{ij}S_{kj}S_{mn}^{a}\left[4(ik\,|\,mn)-(im\,|\,kn)-(in\,|\,km)\right]$$

$$+2\sum_{i}^{A}\sum_{j}^{B}S_{ij}^{2}\frac{(-Z_a)(q_j-q_a)}{R_{ja}^{3}}-4\sum_{i,k,m}^{A}\sum_{j}^{B}S_{ij}^{2}S_{mk}^{a}V_{mk}^{j}+4\sum_{i,k}^{A}\sum_{j}^{B}S_{ij}^{2}V_{kk}^{j^a}$$

(A18)

Now adding up Eqs. (A14-18)

$$\frac{\partial E^{XR}}{\partial q_a} = -2\sum_{i}^{A}\sum_{j}^{B}\frac{\partial (ij\,|\,ij)^{SGO}}{\partial q_a}$$
$$+\sum_{i,m}^{A}\sum_{j}^{B} S^a_{mi}S_{mj}\left(2V^A_{ij}+2G^A_{ij}\right)+\sum_{i,m}^{A}\sum_{j,l}^{B} S^a_{mi}S_{mj}F^B_{jl}S_{il}$$
$$-2\sum_{i}^{A}\sum_{j}^{B} S^a_{ij}\left(2V^A_{ij}+2G^A_{ij}\right)-2\sum_{i}^{A}\sum_{j,l}^{B} S^a_{ij}F^B_{jl}S_{il}$$
$$\sum_{i,m}^{A}\sum_{j}^{B} S_{ij}S^a_{mi}\left(2V^A_{mj}+2G^A_{mj}\right)+\sum_{i,m}^{A}\sum_{j,l}^{B} S_{ij}S^a_{mi}S_{ml}F^B_{jl}$$
$$-\sum_{i}^{A}\sum_{j}^{B} 2S_{ij}\left(2V^{A^a}_{ij}+2G^{A^a}_{ij}\right)-2\sum_{i}^{A}\sum_{j,l}^{B} S_{ij}S^a_{il}F^B_{jl}$$
$$+2\sum_{i,k,m}^{A}\sum_{j}^{B} S_{ij}S^a_{mk}\left[4(ij\,|\,mk)-(im\,|\,jk)-(ik\,|\,mj)\right]$$
$$-\sum_{i,k,m}^{A}\sum_{j}^{B} S^a_{mi}S_{mj}S_{kj}\left(F^A_{ik}+V^{EFP,B}_{ik}-V^j_{ik}\right)-\sum_{i,m}^{A}\sum_{j}^{B} S^a_{mi}S_{mj}S_{ij}\left(\sum_{I}^{A}\frac{-Z_I}{R_{jI}}+2\sum_{k}^{A}V^j_{kk}\right)$$
$$+2\sum_{i,k}^{A}\sum_{j}^{B} S^a_{ij}S_{kj}\left(F^A_{ik}+V^{EFP,B}_{ik}-V^j_{ik}\right)+2\sum_{i}^{A}\sum_{j}^{B} S^a_{ij}S_{ij}\left(\sum_{I}^{A}\frac{-Z_I}{R_{jI}}+2\sum_{k}^{A}V^j_{kk}\right)$$
$$-\sum_{i,k,m}^{A}\sum_{j}^{B} S_{ij}S^a_{mk}S_{mj}\left(F^A_{ik}+V^{EFP,B}_{ik}-V^j_{ik}\right)-\sum_{i,m}^{A}\sum_{j}^{B} S_{ij}S^a_{mi}S_{mj}\left(\sum_{I}^{A}\frac{-Z_I}{R_{jI}}+2\sum_{k}^{A}V^j_{kk}\right)$$
$$+2\sum_{i,k}^{A}\sum_{j}^{B} S_{ij}S^a_{kj}\left(F^A_{ik}+V^{EFP,B}_{ik}-V^j_{ik}\right)+2\sum_{i}^{A}\sum_{j}^{B} S_{ij}S^a_{ij}\left(\sum_{I}^{A}\frac{-Z_I}{R_{jI}}+2\sum_{k}^{A}V^j_{kk}\right)$$
$$-2\sum_{i,k,m}^{A}\sum_{j}^{B} S_{ij}S_{kj}S^a_{mi}\left(F^A_{mk}+V^{EFP,B}_{mk}-V^j_{mk}\right)+2\sum_{i,k}^{A}\sum_{j}^{B} S_{ij}S_{kj}\left(F^a_{ik}+V^{EFP,B^a}_{ik}-V^{j^a}_{ik}\right)$$
$$-\sum_{i,k,m,n}^{A}\sum_{j}^{B} S_{ij}S_{kj}S^a_{mn}\left[4(ik\,|\,mn)-(im\,|\,kn)-(in\,|\,km)\right]$$
$$+2\sum_{i}^{A}\sum_{j}^{B} S^2_{ij}\frac{(-Z_a)(q_j-q_a)}{R^3_{ja}}-4\sum_{i,k,m}^{A}\sum_{j}^{B} S^2_{ij}S^a_{mk}V^j_{mk}+4\sum_{i,k}^{A}\sum_{j}^{B} S^2_{ij}V^{j^a}_{kk}$$

(A19)

Rearrange the terms and combine the terms of the same color that are equivalent or identical.

$$\frac{\partial E^{XR}}{\partial q_a} = -2\sum_{i}^{A}\sum_{j}^{B}\frac{\partial (ij\,|\,ij)^{SGO}}{\partial q_a}$$

$$+2\sum_{i,m}^{A}\sum_{j}^{B}S_{mi}^{a}S_{mj}\left(2V_{ij}^{A}+2G_{ij}^{A}\right)+2\sum_{i,m}^{A}\sum_{j,l}^{B}S_{mi}^{a}S_{mj}F_{jl}^{B}S_{il}$$

$$-2\sum_{i}^{A}\sum_{j}^{B}S_{ij}^{a}\left(2V_{ij}^{A}+2G_{ij}^{A}\right)-2\sum_{i}^{A}\sum_{j}^{B}S_{ij}\left(2V_{ij}^{A^a}+2G_{ij}^{A^a}\right)-4\sum_{i}^{A}\sum_{j,l}^{B}S_{ij}^{a}F_{jl}^{B}S_{il}$$

$$-4\sum_{i,k,m}^{A}\sum_{j}^{B}S_{mi}^{a}S_{mj}S_{kj}\left(F_{ik}^{A}+V_{ik}^{EFP,B}-V_{ik}^{j}\right)-2\sum_{i,m}^{A}\sum_{j}^{B}S_{mi}^{a}S_{mj}S_{ij}\left(\sum_{I}^{A}\frac{-Z_I}{R_{jI}}+2\sum_{k}^{A}V_{kk}^{j}\right)$$

$$+4\sum_{i,k}^{A}\sum_{j}^{B}S_{ij}^{a}S_{kj}\left(F_{ik}^{A}+V_{ik}^{EFP,B}-V_{ik}^{j}\right)+4\sum_{i}^{A}\sum_{j}^{B}S_{ij}^{a}S_{ij}\left(\sum_{I}^{A}\frac{-Z_I}{R_{jI}}+2\sum_{k}^{A}V_{kk}^{j}\right) \qquad \text{(A20)}$$

Now, $\frac{\partial (ij\,|\,ij)^{SGO}}{\partial q_a}$ is dealt with.

$$+2\sum_{i,k}^{A}\sum_{j}^{B}S_{ij}S_{kj}\left(F_{ik}^{a}+V_{ik}^{EFP,B^a}-V_{ik}^{j^a}\right)+2\sum_{i}^{A}\sum_{j}^{B}S_{ij}^{2}\left[\frac{(-Z_a)(q_j-q_a)}{R_{ja}^{3}}-2\sum_{k,m}^{A}S_{mk}^{a}V_{mk}^{j}+2\sum_{k}^{A}V_{kk}^{j^a}\right]$$

$$+2\sum_{i,k,m}^{A}\sum_{j}^{B}S_{ij}S_{mk}^{a}\left[4(ij\,|\,mk)-(im\,|\,jk)-(ik\,|\,mj)\right]$$

$$-\sum_{i,k,m,n}^{A}\sum_{j}^{B}S_{ij}S_{kj}S_{mn}^{a}\left[4(ik\,|\,mn)-(im\,|\,kn)-(in\,|\,km)\right]$$

$$
\begin{aligned}
&-2\sum_{i}^{A}\sum_{j}^{B}\frac{\partial(ij\,|\,ij)^{SGO}}{\partial q_a} \\
&=-2\sum_{i}^{A}\sum_{j}^{B}\sum_{\mu\nu}^{AO\in A}\frac{\partial}{\partial q_a}\left[C_{\mu i}C_{\nu i}(\mu j\,|\,\nu j)^{SGO}\right] \\
&=-2\sum_{i}^{A}\sum_{j}^{B}\sum_{\mu\nu}^{AO\in A}\frac{\partial}{\partial q_a}\left\{C_{\mu i}C_{\nu i}\frac{2}{\sqrt{\pi}}\sqrt{\frac{2\alpha_{\mu j}\alpha_{\nu j}}{\alpha_{\mu j}+\alpha_{\nu j}}}S_{\mu j}S_{\nu j}F_0\left[\frac{1}{4}\left(\frac{2\alpha_{\mu j}\alpha_{\nu j}}{\alpha_{\mu j}+\alpha_{\nu j}}R_{\mu\nu}^2\right)\right]\right\} \\
&=-2\sum_{i}^{A}\sum_{j}^{B}\sum_{\mu\nu}^{AO\in A}\left\{\begin{aligned}
&C_{\mu i}^{a}C_{\nu i}\frac{2}{\sqrt{\pi}}\sqrt{\frac{2\alpha_{\mu j}\alpha_{\nu j}}{\alpha_{\mu j}+\alpha_{\nu j}}}S_{\mu j}S_{\nu j}F_0\left[\frac{1}{4}\left(\frac{2\alpha_{\mu j}\alpha_{\nu j}}{\alpha_{\mu j}+\alpha_{\nu j}}R_{\mu\nu}^2\right)\right] \\
&+C_{\mu i}C_{\nu i}^{a}\frac{2}{\sqrt{\pi}}\sqrt{\frac{2\alpha_{\mu j}\alpha_{\nu j}}{\alpha_{\mu j}+\alpha_{\nu j}}}S_{\mu j}S_{\nu j}F_0\left[\frac{1}{4}\left(\frac{2\alpha_{\mu j}\alpha_{\nu j}}{\alpha_{\mu j}+\alpha_{\nu j}}R_{\mu\nu}^2\right)\right] \\
&+C_{\mu i}C_{\nu i}\frac{\partial}{\partial q_a}\left[\frac{2}{\sqrt{\pi}}\sqrt{\frac{2\alpha_{\mu j}\alpha_{\nu j}}{\alpha_{\mu j}+\alpha_{\nu j}}}S_{\mu j}S_{\nu j}F_0\left[\frac{1}{4}\left(\frac{2\alpha_{\mu j}\alpha_{\nu j}}{\alpha_{\mu j}+\alpha_{\nu j}}R_{\mu\nu}^2\right)\right]\right]
\end{aligned}\right\}
\end{aligned}
\tag{A21}
$$

In the last equality of Eq. (A21), the first two terms just involve the derivative of the MO coefficients and can be easily obtained using the response coefficient matrix U.

$$
\begin{aligned}
&-2\sum_{i}^{A}\sum_{j}^{B}\sum_{\mu\nu}^{AO\in A}C_{\mu i}^{a}C_{\nu i}\frac{2}{\sqrt{\pi}}\sqrt{\frac{2\alpha_{\mu j}\alpha_{\nu j}}{\alpha_{\mu j}+\alpha_{\nu j}}}S_{\mu j}S_{\nu j}F_0\left[\frac{1}{4}\left(\frac{2\alpha_{\mu j}\alpha_{\nu j}}{\alpha_{\mu j}+\alpha_{\nu j}}R_{\mu\nu}^2\right)\right] \\
&=-2\sum_{i}^{A}\sum_{j}^{B}\sum_{\mu\nu}^{AO\in A}\sum_{m}^{A}C_{\mu m}U_{mi}^{a}C_{\nu i}\frac{2}{\sqrt{\pi}}\sqrt{\frac{2\alpha_{\mu j}\alpha_{\nu j}}{\alpha_{\mu j}+\alpha_{\nu j}}}S_{\mu j}S_{\nu j}F_0\left[\frac{1}{4}\left(\frac{2\alpha_{\mu j}\alpha_{\nu j}}{\alpha_{\mu j}+\alpha_{\nu j}}R_{\mu\nu}^2\right)\right] \\
&=\sum_{i}^{A}\sum_{j}^{B}\sum_{\mu\nu}^{AO\in A}\sum_{m}^{A}C_{\mu m}S_{mi}^{a}C_{\nu i}\frac{2}{\sqrt{\pi}}\sqrt{\frac{2\alpha_{\mu j}\alpha_{\nu j}}{\alpha_{\mu j}+\alpha_{\nu j}}}S_{\mu j}S_{\nu j}F_0\left[\frac{1}{4}\left(\frac{2\alpha_{\mu j}\alpha_{\nu j}}{\alpha_{\mu j}+\alpha_{\nu j}}R_{\mu\nu}^2\right)\right]
\end{aligned}
\tag{A22}
$$

And similarly

$$
\begin{aligned}
&-2\sum_{i}^{A}\sum_{j}^{B}\sum_{\mu\nu}^{AO\in A}C_{\mu i}C_{\nu i}^{a}\frac{2}{\sqrt{\pi}}\sqrt{\frac{2\alpha_{\mu j}\alpha_{\nu j}}{\alpha_{\mu j}+\alpha_{\nu j}}}S_{\mu j}S_{\nu j}F_0\left[\frac{1}{4}\left(\frac{2\alpha_{\mu j}\alpha_{\nu j}}{\alpha_{\mu j}+\alpha_{\nu j}}R_{\mu\nu}^2\right)\right] \\
&=\sum_{i}^{A}\sum_{j}^{B}\sum_{\mu\nu}^{AO\in A}\sum_{m}^{A}C_{\mu i}C_{\nu m}S_{mi}^{a}\frac{2}{\sqrt{\pi}}\sqrt{\frac{2\alpha_{\mu j}\alpha_{\nu j}}{\alpha_{\mu j}+\alpha_{\nu j}}}S_{\mu j}S_{\nu j}F_0\left[\frac{1}{4}\left(\frac{2\alpha_{\mu j}\alpha_{\nu j}}{\alpha_{\mu j}+\alpha_{\nu j}}R_{\mu\nu}^2\right)\right]
\end{aligned}
\tag{A23}
$$

Since m and i both run over the occupied orbitals of the *ab initio* molecule A, and μ and ν both run over the AO basis of molecule A. Eqs (A22) and (A23) are equivalent and can be combined.

The last term of Eq. (A21) is much more involved algebraically with repeated use of the chain rule and product rule.

$$
\begin{aligned}
&-2\sum_{i}^{A}\sum_{j}^{B}\sum_{\mu\nu}^{AO\in A} C_{\mu i}C_{\nu i}\frac{\partial}{\partial q_a}\left[\frac{2}{\sqrt{\pi}}\sqrt{\frac{2\alpha_{\mu j}\alpha_{\nu j}}{\alpha_{\mu j}+\alpha_{\nu j}}}S_{\mu j}S_{\nu j}F_0\left[\frac{1}{4}\left(\frac{2\alpha_{\mu j}\alpha_{\nu j}}{\alpha_{\mu j}+\alpha_{\nu j}}R_{\mu\nu}^2\right)\right]\right] \\
&=-2\sum_{i}^{A}\sum_{j}^{B}\sum_{\mu\nu}^{AO\in A}\frac{2}{\sqrt{\pi}}C_{\mu i}C_{\nu i}\left[\begin{aligned}&\frac{\partial}{\partial q_a}\left(\sqrt{\frac{2\alpha_{\mu j}\alpha_{\nu j}}{\alpha_{\mu j}+\alpha_{\nu j}}}S_{\mu j}S_{\nu j}\right)F_0\left[\frac{1}{4}\left(\frac{2\alpha_{\mu j}\alpha_{\nu j}}{\alpha_{\mu j}+\alpha_{\nu j}}R_{\mu\nu}^2\right)\right] \\ &+\left(\sqrt{\frac{2\alpha_{\mu j}\alpha_{\nu j}}{\alpha_{\mu j}+\alpha_{\nu j}}}S_{\mu j}S_{\nu j}\right)\frac{\partial}{\partial q_a}\left(F_0\left[\frac{1}{4}\left(\frac{2\alpha_{\mu j}\alpha_{\nu j}}{\alpha_{\mu j}+\alpha_{\nu j}}R_{\mu\nu}^2\right)\right]\right)\end{aligned}\right]
\end{aligned}
\tag{A24}
$$

Now,

$$\frac{\partial}{\partial q_a}\left(\sqrt{\frac{2\alpha_{\mu j}\alpha_{\nu j}}{\alpha_{\mu j}+\alpha_{\nu j}}}S_{\mu j}S_{\nu j}\right)$$

$$=\left(\frac{\partial}{\partial q_a}\left(\frac{2\alpha_{\mu j}\alpha_{\nu j}}{\alpha_{\mu j}+\alpha_{\nu j}}\right)^{1/2}\right)S_{\mu j}S_{\nu j}+\left(\frac{2\alpha_{\mu j}\alpha_{\nu j}}{\alpha_{\mu j}+\alpha_{\nu j}}\right)^{1/2}\left[\left(\frac{\partial S_{\mu j}}{\partial q_a}\right)S_{\nu j}+S_{\mu j}\left(\frac{\partial S_{\nu j}}{\partial q_a}\right)\right]$$

$$=\frac{1}{2}\left(\frac{2\alpha_{\mu j}\alpha_{\nu j}}{\alpha_{\mu j}+\alpha_{\nu j}}\right)^{-1/2}\left[\frac{\partial}{\partial q_a}\left(\frac{2\alpha_{\mu j}\alpha_{\nu j}}{\alpha_{\mu j}+\alpha_{\nu j}}\right)\right]S_{\mu j}S_{\nu j}+\left(\frac{2\alpha_{\mu j}\alpha_{\nu j}}{\alpha_{\mu j}+\alpha_{\nu j}}\right)^{1/2}\left[\left\langle\mu^a\middle|j\right\rangle S_{\nu j}+S_{\mu j}\left\langle\nu^a\middle|j\right\rangle\right]$$

$$=\frac{1}{2}\left(\frac{2\alpha_{\mu j}\alpha_{\nu j}}{\alpha_{\mu j}+\alpha_{\nu j}}\right)^{-1/2}\left[\frac{\left(\alpha_{\mu j}+\alpha_{\nu j}\right)\frac{\partial\left(2\alpha_{\mu j}\alpha_{\nu j}\right)}{\partial q_a}-\left(2\alpha_{\mu j}\alpha_{\nu j}\right)\frac{\partial\left(\alpha_{\mu j}+\alpha_{\nu j}\right)}{\partial q_a}}{\left(\alpha_{\mu j}+\alpha_{\nu j}\right)^2}\right]S_{\mu j}S_{\nu j} \qquad \text{(A25)}$$

The expression in blue will be used later.

$$+\left(\frac{2\alpha_{\mu j}\alpha_{\nu j}}{\alpha_{\mu j}+\alpha_{\nu j}}\right)^{1/2}\left[S^a_{\mu j}S_{\nu j}+S_{\mu j}S^a_{\nu j}\right]$$

Recall that $\alpha_{\mu j}=-\frac{2}{R^2_{\mu j}}\ln\left|S_{\mu j}\right|$, both R and S have functional dependence on the coordinates of nuclear a of the *ab initio* molecule A.

$$=\frac{1}{2}\left(\frac{2\alpha_{\mu j}\alpha_{\nu j}}{\alpha_{\mu j}+\alpha_{\nu j}}\right)^{-1/2}\left[\frac{\left(\alpha_{\mu j}+\alpha_{\nu j}\right)\left(2\frac{\partial\alpha_{\mu j}}{\partial q_a}\alpha_{\nu j}+2\alpha_{\mu j}\frac{\partial\alpha_{\nu j}}{\partial q_a}\right)-\left(2\alpha_{\mu j}\alpha_{\nu j}\right)\left(\frac{\partial\alpha_{\mu j}}{\partial q_a}+\frac{\partial\alpha_{\nu j}}{\partial q_a}\right)}{\left(\alpha_{\mu j}+\alpha_{\nu j}\right)^2}\right]S_{\mu j}S_{\nu j}$$

$$\frac{\partial\alpha_{\mu j}}{\partial q^a}=-\frac{\partial}{\partial q^a}\frac{2\ln\left|S_{\mu j}\right|}{R^2_{\mu j}}$$

$$+\left(\frac{2\alpha_{\mu j}\alpha_{\nu j}}{\alpha_{\mu j}+\alpha_{\nu j}}\right)^{1/2}\left[S^a_{\mu j}S_{\nu j}+S_{\mu j}S^a_{\nu j}\right]$$

$$=-\frac{R^2_{\mu j}\frac{\partial\left(2\ln\left|S_{\mu j}\right|\right)}{\partial q^a}-2\ln\left|S_{\mu j}\right|\frac{\partial\left[\left(x_\mu-x_j\right)^2+\left(y_\mu-y_j\right)^2+\left(z_\mu-z_j\right)^2\right]}{\partial q^a}}{R^4_{\mu j}} \qquad \text{(A26)}$$

Take $q^a=x^a$ for concreteness,

$$\frac{\partial \alpha_{\mu j}}{\partial x^a} = -\frac{R_{\mu j}^2\left(\frac{2S_{\mu j}^a}{S_{\mu j}}\right) - 2\ln\left|S_{\mu j}\right|\left[2\left(x_\mu - x_j\right)\delta_{\mu a}\right]}{R_{\mu j}^4} \tag{A27}$$

where the delta function equals 1 if the basis function μ is centered at atom a in the molecule A and equals 0 otherwise. Eq. (A27) can then be substituted back into Eq. (A25).

The F_0 function is defined as[13]

$$F_0(t) = t^{-1/2}\int_0^{t^{1/2}} e^{-y^2}\,dy \tag{A28}$$

It is related to the error function by[13]

$$F_0(t) = \frac{1}{2}\left(\frac{\pi}{t}\right)^{1/2} erf\left(t^{1/2}\right) \tag{A29}$$

The derivative of the error function is

$$\frac{d}{dz}erf(z) = \frac{2}{\sqrt{\pi}}e^{-z^2} \tag{A30}$$

Let $z = t^{1/2}$, then $dz/dt = \frac{1}{2}t^{-1/2}$

$$\begin{aligned}
\frac{d}{dt}F_0(t) &= \frac{1}{2}\left[\frac{d}{dt}\left(\frac{\pi}{t}\right)^{1/2}\right]erf\left(t^{1/2}\right) + \frac{1}{2}\left(\frac{\pi}{t}\right)^{1/2}\left[\frac{d}{dt}erf\left(t^{1/2}\right)\right] \\
&= \frac{1}{2}\left(-\frac{1}{2}\right)\pi^{1/2}t^{-3/2}erf\left(t^{1/2}\right) + \frac{1}{2}\left(\frac{\pi}{t}\right)^{1/2}\left[\frac{d}{dz}erf(z)\frac{dz}{dt}\right] \\
&= -\frac{1}{2}\frac{1}{t}\left[\frac{1}{2}\left(\frac{\pi}{t}\right)^{1/2}erf\left(t^{1/2}\right)\right] + \frac{1}{2}\left(\frac{\pi}{t}\right)^{1/2}\frac{2}{\sqrt{\pi}}e^{-t}\frac{1}{2}t^{-1/2} \\
&= -\frac{1}{2t}F_0(t) + \frac{1}{2t}e^{-t}
\end{aligned} \tag{A31}$$

Now let $t = \frac{1}{4}\left(\frac{2\alpha_{\mu j}\alpha_{\nu j}}{\alpha_{\mu j}+\alpha_{\nu j}} R_{\mu\nu}^2 \right) = t\left(q_a\right)$, which is a function of the nuclear coordinates itself.

$$\begin{aligned} \frac{\partial}{\partial q_a} F_0\left(t\left(q_a\right)\right) &= \frac{dF_0}{dt}\frac{\partial t}{\partial q_a} \\ &= \frac{dF_0}{dt} \times \frac{\partial}{\partial q_a}\frac{1}{4}\left(\frac{2\alpha_{\mu j}\alpha_{\nu j}}{\alpha_{\mu j}+\alpha_{\nu j}} R_{\mu\nu}^2 \right) \\ &= \frac{1}{4}\frac{dF_0}{dt}\left[R_{\mu\nu}^2 \frac{\partial}{\partial q_a}\left(\frac{2\alpha_{\mu j}\alpha_{\nu j}}{\alpha_{\mu j}+\alpha_{\nu j}} \right) + \frac{2\alpha_{\mu j}\alpha_{\nu j}}{\alpha_{\mu j}+\alpha_{\nu j}} \frac{\partial R_{\mu\nu}^2}{\partial q_a} \right] \end{aligned} \tag{A32}$$

$\frac{\partial}{\partial q_a}\left(\frac{2\alpha_{\mu j}\alpha_{\nu j}}{\alpha_{\mu j}+\alpha_{\nu j}} \right)$ has been derived in Eq. (25) (shown in blue).

$$\begin{aligned} \frac{\partial R_{\mu\nu}^2}{\partial x_a} &= \frac{\partial}{\partial x_a}\left[\left(x_\mu - x_\nu\right)^2 + \left(y_\mu - y_\nu\right)^2 + \left(z_\mu - z_\nu\right)^2 \right] \\ &= 2\left(x_\mu - x_\nu\right)\delta_{ac} \end{aligned} \tag{A33}$$

where δ_{ac} =1 if the atom c, where the basis function μ resides, coincides with the atom a. All the terms that are needed for evaluating Eq. (24) are derived.

(B) Analytic QM-EFP exchange repulsion gradient with respect to EFP centers

The derivative with respect to an EFP center, that is, the center of mass of an EFP fragment.

$$
\begin{aligned}
\frac{\partial E^{XR}}{\partial q_B} &= -2\sum_i^A\sum_j^B \frac{\partial (ij\,|\,ij)^{SGO}}{\partial q_B} \\
&-2\sum_i^A\sum_j^B\left(\frac{\partial S_{ij}}{\partial q_B}\right)\left[2\left(V_{ij}^A+G_{ij}^A\right)+\sum_l^B F_{jl}^B S_{il}\right] \\
&-2\sum_i^A\sum_j^B S_{ij}\left[2\left(\frac{\partial V_{ij}^A}{\partial q_B}+\frac{\partial G_{ij}^A}{\partial q_B}\right)+\sum_l^B F_{jl}^B\left(\frac{\partial S_{il}}{\partial q_B}\right)+\sum_l^B\left(\frac{\partial F_{jl}^B}{\partial q_B}\right)S_{il}\right] \\
&+2\sum_i^A\sum_j^B\left(\frac{\partial S_{ij}}{\partial q_B}\right)\left[\sum_k^A S_{kj}\left(F_{ik}^A+V_{ik}^{EFP,B}-V_{ik}^j\right)+S_{ij}\left(\sum_I^A\frac{-Z_I}{R_{jI}}+2\sum_k^A V_{kk}^j\right)\right] \\
&+2\sum_i^A\sum_j^B S_{ij}\left[\begin{array}{l}\sum_k^A\left(\frac{\partial S_{kj}}{\partial q_B}\right)\left(F_{ik}^A+V_{ik}^{EFP,B}-V_{ik}^j\right)+\left(\frac{\partial S_{ij}}{\partial q_B}\right)\left(\sum_I^A\frac{-Z_I}{R_{jI}}+2\sum_k^A V_{kk}^j\right) \\ +\sum_k^A S_{kj}\left(\frac{\partial F_{ik}^A}{\partial q_B}+\frac{\partial V_{ik}^{EFP,B}}{\partial q_B}-\frac{\partial V_{ik}^j}{\partial q_B}\right)+S_{ij}\left(\sum_I^A\frac{\partial}{\partial q_B}\frac{-Z_I}{R_{jI}}+2\sum_k^A\frac{\partial V_{kk}^j}{\partial q_B}\right)\end{array}\right]
\end{aligned}
\tag{A34}
$$

Forces

When an EFP fragment translates, all of its AO centers and MOs translate in the same way. Because EFP fragments are rigid the MO coefficients are constant. Hence the translational derivatives of MO coefficients are zero. The overall translation of an EFP fragment can be decomposed into the individual atomic translations in A.[8,12]

The derivative of the overlap integral yields

$$
\begin{aligned}
\frac{\partial S_{ij}}{\partial q_B} &= \sum_\mu^A\sum_\nu^B\sum_b^B C_{\mu i}^b C_{\nu j} S_{\mu\nu} + C_{\mu i} C_{\nu j}^b S_{\mu\nu} + C_{\mu i} C_{\nu j}\left(\mu^b\,|\,\nu\right) + C_{\mu i} C_{\nu j}\left(\mu\,|\,\nu^b\right) \\
&= \sum_\mu^A\sum_\nu^B\sum_b^B C_{\mu i}^b C_{\nu j} S_{\mu\nu} + C_{\mu i} C_{\nu j}\left(\mu\,|\,\nu^b\right)
\end{aligned}
\tag{A35}
$$

where b stands for the atoms of fragment B. The second term in the first equality vanishes because EFP MOs are frozen, and the third term disappears because the AO of *ab initio* molecule is not a function of coordinates of fragment B. The derivative of the *ab initio* MO coefficient can be rewritten in terms of the orbital response terms:

$$\frac{\partial S_{ij}}{\partial q_B} = \sum_m^A \sum_b^B U_{mi}^b S_{mj} + \sum_b^B \left(i \mid j^b\right) = \sum_m^A \sum_b^B -\frac{1}{2} S_{mi}^b S_{mj} + \sum_b^B \left(i \mid j^b\right) = \sum_b^B S_{ij}^b \tag{A36}$$

where $S_{ij}^b = \left(i \mid j^b\right)$ and S_{mi}^b equals to zero because AOs of the *ab initio* molecule do not depend on EFP coordinates.

The operator of V_{ij}^A is the potential due to the *ab initio* molecule hence do not contribute to the derivative with respect to EFP coordinates,

$$\frac{\partial V_{ij}^A}{\partial q_B} = \sum_b^B \left(i \mid V^A \mid j^b\right) = \sum_b^B V_{ij}^{A^b} \tag{A37}$$

And

$$\frac{\partial G_{ij}^A}{\partial q_B} = \sum_b^B \sum_k^A \left[2\left(ij^b \mid kk\right) - (ik \mid j^b k)\right] = \sum_b^B G_{ij}^{A^b} \tag{A38}$$

When the EFP fragment B translates or rotates about its center of mass, the Fock matrix F_{jl}^B is not changing.

$$\frac{\partial F_{jl}^B}{\partial q_B} = \sum_b^B \frac{\partial F_{jl}^B}{\partial q_b} = 0 \tag{A39}$$

The Fock matrix of *ab initio* molecule A has no dependence on B. Hence

$$\frac{\partial F_{ik}^A}{\partial q_B} = \sum_b^B \frac{\partial F_{ik}^A}{\partial q_b} = 0 \tag{A40}$$

R_{jI} is the distance between EFP jth LMO centroid and Ith nuclear coordinate of molecule A. Since an EFP fragment is rigid, the translational movements of the centroids and the center of mass are the same, i.e. $\partial q_j / \partial q_B = 1$. Use the x-coordinate as a concrete example,

$$\sum_I^A \frac{\partial}{\partial x_B}\frac{-Z_I}{R_{jI}} = \sum_I^A -Z_I\left(\frac{\partial x_j}{\partial x_B}\right)\left(\frac{\partial}{\partial x_j}\left[\left(x_j-x_I\right)^2+\left(y_j-y_I\right)^2+\left(z_j-z_I\right)^2\right]^{-1/2}\right)$$
$$= \sum_I^A -Z_I\left(-\frac{1}{2}\right)2\left(x_j-x_I\right)\left[\left(x_j-x_I\right)^2+\left(y_j-y_I\right)^2+\left(z_j-z_I\right)^2\right]^{-3/2} \qquad \text{(A41)}$$
$$= \sum_I^A \frac{Z_I\left(x_j-x_I\right)}{R_{jI}^3}$$

Similarly the operator $V^j = -1/r_j$ has implicit dependence on the center of mass of the EFP fragment.

$$\frac{\partial V_{ik}^j}{\partial x_B} = \langle i|\frac{\partial V^j}{\partial x_B}|k\rangle = -\left(\frac{\partial x_j}{\partial x_B}\right)\langle i|\frac{\partial V^j}{\partial x_j}|k\rangle = \langle i|\frac{\partial V^j}{\partial x_j}|k\rangle \qquad \text{(A42)}$$

For operator $V^{EFP,B}$, which is the electrostatic potential expressed as a multipole expansion, there is a functional dependence on the nuclear coordinates of B.

$$\frac{\partial V_{ik}^{EFP,B}}{\partial q_B} = \langle i|\frac{\partial V^{EFP,B}}{\partial q_B}|k\rangle = \sum_{b\in B}\langle i|\frac{\partial V^{EFP,B}}{\partial q_b}|k\rangle \qquad \text{(A43)}$$

Now substituting various terms back into Eq. (A34) yields

$$
\begin{aligned}
\frac{\partial E^{XR}}{\partial q_B} &= -2\sum_i^A\sum_j^B \frac{\partial (ij\,|\,ij)^{SGO}}{\partial q_B} \\
&\quad -2\sum_i^A\sum_j^B\left(\sum_b^B S_{ij}^b\right)\left[2\left(V_{ij}^A+G_{ij}^A\right)+\sum_l^B F_{jl}^B S_{il}\right] \\
&\quad -2\sum_i^A\sum_j^B S_{ij}\left[2\left(\sum_b^B V_{ij}^{A^b}+\sum_b^B G_{ij}^{A^b}\right)+\sum_l^B F_{jl}^B\left(\sum_b^B S_{il}^b\right)\right] \\
&\quad +2\sum_i^A\sum_j^B\left(\sum_b^B S_{ij}^b\right)\left[\sum_k^A S_{kj}\left(F_{ik}^A+V_{ik}^{EFP,B}-V_{ik}^j\right)+S_{ij}\left(\sum_I^A\frac{-Z_I}{R_{jI}}+2\sum_k^A V_{kk}^j\right)\right] \\
&\quad +2\sum_i^A\sum_j^B S_{ij}\left[\begin{array}{l}\sum_k^A\left(\sum_b^B S_{kj}^b\right)\left(F_{ik}^A+V_{ik}^{EFP,B}-V_{ik}^j\right)+\left(\sum_b^B S_{ij}^b\right)\left(\sum_I^A\frac{-Z_I}{R_{jI}}+2\sum_k^A V_{kk}^j\right) \\ +\sum_k^A S_{kj}\left(\langle i|\frac{\partial V^{EFP,B}}{\partial q_B}|k\rangle+\langle i|\frac{\partial V^j}{\partial x_B}|k\rangle\right)+S_{ij}\left(\sum_I^A\frac{Z_I\left(q_j-q_I\right)}{R_{jI}^3}+2\sum_k^A\langle k|\frac{\partial V^j}{\partial x_B}|k\rangle\right)\end{array}\right] \\
&= -2\sum_i^A\sum_j^B \frac{\partial (ij\,|\,ij)^{SGO}}{\partial q_B} \\
&\quad -2\sum_i^A\sum_j^B\sum_b^B S_{ij}^b\left(2V_{ij}^A+2G_{ij}^A\right)-2\sum_i^A\sum_{j,l}^B\sum_b^B S_{ij}^b F_{jl}^B S_{il} \\
&\quad -2\sum_i^A\sum_j^B\sum_b^B S_{ij}\left(2V_{ij}^{A^b}+2G_{ij}^{A^b}\right)-2\sum_i^A\sum_{j,l}^B\sum_b^B S_{ij}F_{jl}^B S_{il}^b \\
&\quad +2\sum_{i,k}^A\sum_j^B\sum_b^B S_{ij}^b S_{kj}\left(F_{ik}^A+V_{ik}^{EFP,B}-V_{ik}^j\right)+2\sum_i^A\sum_j^B\sum_b^B S_{ij}^b S_{ij}\left(\sum_I^A\frac{-Z_I}{R_{jI}}+2\sum_k^A V_{kk}^j\right) \\
&\quad +2\sum_{i,k}^A\sum_j^B\sum_b^B S_{ij}S_{kj}^b\left(F_{ik}^A+V_{ik}^{EFP,B}-V_{ik}^j\right)+2\sum_i^A\sum_j^B\sum_b^B S_{ij}S_{ij}^b\left(\sum_I^A\frac{-Z_I}{R_{jI}}+2\sum_k^A V_{kk}^j\right) \\
&\quad +2\sum_{i,k}^A\sum_j^B S_{ij}S_{kj}\left(\langle i|\frac{\partial V^{EFP,B}}{\partial q_B}|k\rangle+\langle i|\frac{\partial V^j}{\partial x_B}|k\rangle\right)+2\sum_i^A\sum_j^B S_{ij}S_{ij}\left(\sum_I^A\frac{Z_I\left(q_j-q_I\right)}{R_{jI}^3}+2\sum_k^A\langle k|\frac{\partial V^j}{\partial x_B}|k\rangle\right) \\
&= -2\sum_i^A\sum_j^B \frac{\partial (ij\,|\,ij)^{SGO}}{\partial q_B} \\
&\quad -2\sum_i^A\sum_j^B\left(\sum_b^B S_{ij}^b\right)\left(2V_{ij}^A+2G_{ij}^A\right)-2\sum_i^A\sum_j^B S_{ij}\sum_b^B\left(2V_{ij}^{A^b}+2G_{ij}^{A^b}\right)-4\sum_i^A\sum_{j,l}^B\left(\sum_b^B S_{ij}^b\right)F_{jl}^B S_{il} \\
&\quad +4\sum_{i,k}^A\sum_j^B\left(\sum_b^B S_{ij}^b\right)S_{kj}\left(F_{ik}^A+V_{ik}^{EFP,B}-V_{ik}^j\right)+4\sum_i^A\sum_j^B\left(\sum_b^B S_{ij}^b\right)S_{ij}\left(\sum_I^A\frac{-Z_I}{R_{jI}}+2\sum_k^A V_{kk}^j\right) \\
&\quad +2\sum_{i,k}^A\sum_j^B S_{ij}S_{kj}\left(\langle i|\frac{\partial V^{EFP,B}}{\partial q_B}|k\rangle+\langle i|\frac{\partial V^j}{\partial x_B}|k\rangle\right)+2\sum_i^A\sum_j^B S_{ij}S_{ij}\left(\sum_I^A\frac{Z_I\left(q_j-q_I\right)}{R_{jI}^3}+2\sum_k^A\langle k|\frac{\partial V^j}{\partial x_B}|k\rangle\right)
\end{aligned}
\tag{A44}
$$

where the terms of the same color are equivalent and combined.

$$
\begin{aligned}
&-2\sum_{i}^{A}\sum_{j}^{B}\frac{\partial(ij\,|\,ij)^{SGO}}{\partial q_B}\\
&=-2\sum_{i}^{A}\sum_{j}^{B}\sum_{\mu\nu}^{AO\in A}\frac{\partial}{\partial q_B}\left[C_{\mu i}C_{\nu i}(\mu j\,|\,\nu j)\right]\\
&=-2\sum_{i}^{A}\sum_{j}^{B}\sum_{\mu\nu}^{AO\in A}\frac{\partial}{\partial q_B}\left\{C_{\mu i}C_{\nu i}\frac{2}{\sqrt{\pi}}\sqrt{\frac{2\alpha_{\mu j}\alpha_{\nu j}}{\alpha_{\mu j}+\alpha_{\nu j}}}S_{\mu j}S_{\nu j}F_0\left[\frac{1}{4}\left(\frac{2\alpha_{\mu j}\alpha_{\nu j}}{\alpha_{\mu j}+\alpha_{\nu j}}R_{\mu\nu}^2\right)\right]\right\}\\
&=-2\sum_{i}^{A}\sum_{j}^{B}\sum_{\mu\nu}^{AO\in A}\left\{\begin{array}{l}
C_{\mu i}^{B}C_{\nu i}\frac{2}{\sqrt{\pi}}\sqrt{\frac{2\alpha_{\mu j}\alpha_{\nu j}}{\alpha_{\mu j}+\alpha_{\nu j}}}S_{\mu j}S_{\nu j}F_0\left[\frac{1}{4}\left(\frac{2\alpha_{\mu j}\alpha_{\nu j}}{\alpha_{\mu j}+\alpha_{\nu j}}R_{\mu\nu}^2\right)\right]\\
+C_{\mu i}C_{\nu i}^{B}\frac{2}{\sqrt{\pi}}\sqrt{\frac{2\alpha_{\mu j}\alpha_{\nu j}}{\alpha_{\mu j}+\alpha_{\nu j}}}S_{\mu j}S_{\nu j}F_0\left[\frac{1}{4}\left(\frac{2\alpha_{\mu j}\alpha_{\nu j}}{\alpha_{\mu j}+\alpha_{\nu j}}R_{\mu\nu}^2\right)\right]\\
+C_{\mu i}C_{\nu i}\frac{\partial}{\partial q_B}\left[\frac{2}{\sqrt{\pi}}\sqrt{\frac{2\alpha_{\mu j}\alpha_{\nu j}}{\alpha_{\mu j}+\alpha_{\nu j}}}S_{\mu j}S_{\nu j}F_0\left[\frac{1}{4}\left(\frac{2\alpha_{\mu j}\alpha_{\nu j}}{\alpha_{\mu j}+\alpha_{\nu j}}R_{\mu\nu}^2\right)\right]\right]
\end{array}\right\} \qquad \text{(A45)}\\
&=-2\sum_{i}^{A}\sum_{j}^{B}\sum_{\mu\nu}^{AO\in A}\left\{C_{\mu i}C_{\nu i}\frac{\partial}{\partial q_B}\left[\frac{2}{\sqrt{\pi}}\sqrt{\frac{2\alpha_{\mu j}\alpha_{\nu j}}{\alpha_{\mu j}+\alpha_{\nu j}}}S_{\mu j}S_{\nu j}F_0\left[\frac{1}{4}\left(\frac{2\alpha_{\mu j}\alpha_{\nu j}}{\alpha_{\mu j}+\alpha_{\nu j}}R_{\mu\nu}^2\right)\right]\right]\right\}\\
&=-2\sum_{i}^{A}\sum_{j}^{B}\sum_{\mu\nu}^{AO\in A}C_{\mu i}C_{\nu i}\left[\begin{array}{l}
\frac{\partial}{\partial q_B}\left(\frac{2}{\sqrt{\pi}}\sqrt{\frac{2\alpha_{\mu j}\alpha_{\nu j}}{\alpha_{\mu j}+\alpha_{\nu j}}}S_{\mu j}S_{\nu j}\right)F_0\left[\frac{1}{4}\left(\frac{2\alpha_{\mu j}\alpha_{\nu j}}{\alpha_{\mu j}+\alpha_{\nu j}}R_{\mu\nu}^2\right)\right]\\
+\left(\frac{2}{\sqrt{\pi}}\sqrt{\frac{2\alpha_{\mu j}\alpha_{\nu j}}{\alpha_{\mu j}+\alpha_{\nu j}}}S_{\mu j}S_{\nu j}\right)\frac{\partial}{\partial q_B}\left(F_0\left[\frac{1}{4}\left(\frac{2\alpha_{\mu j}\alpha_{\nu j}}{\alpha_{\mu j}+\alpha_{\nu j}}R_{\mu\nu}^2\right)\right]\right)
\end{array}\right]
\end{aligned}
$$

Firstly,

$$
\begin{aligned}
&\frac{\partial}{\partial q_B}\left(\sqrt{\frac{2\alpha_{\mu j}\alpha_{\nu j}}{\alpha_{\mu j}+\alpha_{\nu j}}}S_{\mu j}S_{\nu j}\right)\\
&=\frac{1}{2}\left(\frac{2\alpha_{\mu j}\alpha_{\nu j}}{\alpha_{\mu j}+\alpha_{\nu j}}\right)^{-1/2}\left[\frac{(\alpha_{\mu j}+\alpha_{\nu j})\left(2\frac{\partial\alpha_{\mu j}}{\partial q_B}\alpha_{\nu j}+2\alpha_{\mu j}\frac{\partial\alpha_{\nu j}}{\partial q_B}\right)-(2\alpha_{\mu j}\alpha_{\nu j})\left(\frac{\partial\alpha_{\mu j}}{\partial q_B}+\frac{\partial\alpha_{\nu j}}{\partial q_B}\right)}{(\alpha_{\mu j}+\alpha_{\nu j})^2}\right]S_{\mu j}S_{\nu j} \qquad \text{(A46)}\\
&+\left(\frac{2\alpha_{\mu j}\alpha_{\nu j}}{\alpha_{\mu j}+\alpha_{\nu j}}\right)^{1/2}\sum_{b}^{B}\left[S_{\mu j}^{b}S_{\nu j}+S_{\mu j}S_{\nu j}^{b}\right]
\end{aligned}
$$

To evaluate Eq. (A46) the derivative of α needs to be calculated.

$$\begin{aligned}\frac{\partial \alpha_{\mu j}}{\partial q^B} &= -\frac{\partial}{\partial q^B}\frac{2\ln\left|S_{\mu j}\right|}{R_{\mu j}^2} \\ &= -\frac{R_{\mu j}^2\dfrac{\partial\left(2\ln\left|S_{\mu j}\right|\right)}{\partial q^B} - 2\ln\left|S_{\mu j}\right|\dfrac{\partial\left[\left(x_\mu - x_j\right)^2 + \left(y_\mu - y_j\right)^2 + \left(z_\mu - z_j\right)^2\right]}{\partial q^B}}{R_{\mu j}^4}\end{aligned} \tag{A47}$$

Take $q^B=x^B$, the x-coordinate of the center of mass of EFP fragment B for concreteness,

$$\begin{aligned}\frac{\partial \alpha_{\mu j}}{\partial x^B} &= -\frac{R_{\mu j}^2\left(\dfrac{2S_{\mu j}^B}{S_{\mu j}}\right) - 2\ln\left|S_{\mu j}\right|\left(\dfrac{\partial x_j}{\partial x_B}\right)\dfrac{\partial\left[\left(x_\mu - x_j\right)^2 + \left(y_\mu - y_j\right)^2 + \left(z_\mu - z_j\right)^2\right]}{\partial x^j}}{R_{\mu j}^4} \\ &= -\frac{R_{\mu j}^2\left(\sum_b^B \dfrac{2S_{\mu j}^b}{S_{\mu j}}\right) + 2\ln\left|S_{\mu j}\right|\left[2\left(x_\mu - x_j\right)\right]}{R_{\mu j}^4}\end{aligned} \tag{A48}$$

Note that $\frac{\partial x_j}{\partial x_B} = 1$ because EFP fragments are rigid. Next,

$$\frac{\partial}{\partial q_B}\left(F_0\left[\frac{1}{4}\left(\frac{2\alpha_{\mu j}\alpha_{\nu j}}{\alpha_{\mu j}+\alpha_{\nu j}}R_{\mu\nu}^2\right)\right]\right) = \frac{dF_0(t)}{dt}\frac{\partial t}{\partial q_B} \tag{A49}$$

where $t = \frac{1}{4}\left(\frac{2\alpha_{\mu j}\alpha_{\nu j}}{\alpha_{\mu j}+\alpha_{\nu j}}R_{\mu\nu}^2\right)$

$$\frac{\partial t}{\partial q_B} = \frac{1}{4}\frac{\partial}{\partial q_B}\left(\frac{2\alpha_{\mu j}\alpha_{\nu j}}{\alpha_{\mu j}+\alpha_{\nu j}}R_{\mu\nu}^2\right) = \frac{1}{4}\left[\frac{\partial}{\partial q_B}\left(\frac{2\alpha_{\mu j}\alpha_{\nu j}}{\alpha_{\mu j}+\alpha_{\nu j}}\right)R_{\mu\nu}^2 + \left(\frac{2\alpha_{\mu j}\alpha_{\nu j}}{\alpha_{\mu j}+\alpha_{\nu j}}\right)\frac{\partial R_{\mu\nu}^2}{\partial q_B}\right] \tag{A50}$$

$\frac{\partial R_{\mu\nu}^2}{\partial x_B} = 0$ since $R_{\mu\nu}$ is only a function of the nuclear coordinates of the ab initio molecule.

So

$$\frac{\partial}{\partial q_B}F_0\left(t\left(q_a\right)\right)=\frac{1}{4}\frac{dF_0}{dt}\left[R_{\mu\nu}^2\frac{\partial}{\partial q_B}\left(\frac{2\alpha_{\mu j}\alpha_{\nu j}}{\alpha_{\mu j}+\alpha_{\nu j}}\right)\right] \tag{A51}$$

$$-2\sum_i^A\sum_j^B\frac{\partial\left(ij\,|\,ij\right)^{SGO}}{\partial q_B}$$

$$=-2\sum_i^A\sum_j^B\sum_{\mu\nu}^{AO\in A}C_{\mu i}C_{\nu i}\left\{\begin{array}{l}\left[\begin{array}{l}\frac{1}{2}\left(\frac{2\alpha_{\mu j}\alpha_{\nu j}}{\alpha_{\mu j}+\alpha_{\nu j}}\right)^{-1/2}S_{\mu j}S_{\nu j}\times\\ \left[\begin{array}{l}\left(\alpha_{\mu j}+\alpha_{\nu j}\right)^{-1}\left(2\frac{\partial\alpha_{\mu j}}{\partial q_B}\alpha_{\nu j}+2\alpha_{\mu j}\frac{\partial\alpha_{\nu j}}{\partial q_B}\right)\\ -\frac{\left(2\alpha_{\mu j}\alpha_{\nu j}\right)}{\left(\alpha_{\mu j}+\alpha_{\nu j}\right)^2}\left(\frac{\partial\alpha_{\mu j}}{\partial q_B}+\frac{\partial\alpha_{\nu j}}{\partial q_B}\right)\end{array}\right]\\ +\left(\frac{2\alpha_{\mu j}\alpha_{\nu j}}{\alpha_{\mu j}+\alpha_{\nu j}}\right)^{1/2}\sum_b^B\left[S_{\mu j}^bS_{\nu j}+S_{\mu j}S_{\nu j}^b\right]\end{array}\right]\times F_0\left[\frac{1}{4}\left(\frac{2\alpha_{\mu j}\alpha_{\nu j}}{\alpha_{\mu j}+\alpha_{\nu j}}R_{\mu\nu}^2\right)\right]\\ +\left(\frac{2}{\sqrt{\pi}}\sqrt{\frac{2\alpha_{\mu j}\alpha_{\nu j}}{\alpha_{\mu j}+\alpha_{\nu j}}}S_{\mu j}S_{\nu j}\right)\frac{1}{4}\frac{dF_0}{dt}\left[R_{\mu\nu}^2\frac{\partial}{\partial q_B}\left(\frac{2\alpha_{\mu j}\alpha_{\nu j}}{\alpha_{\mu j}+\alpha_{\nu j}}\right)\right]\end{array}\right\} \tag{A52}$$

(B) Code Modification of QM-EFP exchange repulsion interaction

Two-electron integrals

Currently, the computation of two-electron integrals (TEI) involved in QM-EFP exchange repulsion is done conventionally, i.e. stored on disk and retrieved later when needed. The storage of TEI is accomplished by two subroutines: QOUTEFP and FINAL_EFP. The TEI are sequentially stored onto the records (storage unit), each of which holds NINTMX integrals. This is handled by the subroutine QOUTEFP. For each fragment, the last record may be only partially filled and is handled by the subroutine

FINAL_EFP. In the current implementation, after filling the partial record, the record index NREC and the integral index ICOUNT is reset by the subroutine FINAL_EFP so that the QM-EFP TEI of the next fragment will be stored at the beginning of a new record. (Fig A1) The previous implementation did not separate the storage of TEI of different fragments by resetting the counters, which caused confusion when retrieving those TEI.

Besides the exchange integral (mj|ij) or (ij|ij) that are approximated by SGO approximations, two types of TEIs appear in the QM-EFP exchange repulsion Fock operator. Type I has all four MOs belonging to the *ab initio* molecule A, e.g. (nk|im); type II has one EFP MO and three *ab initio* MOs, e.g. (kj|mi) with j being the EFP MO.

Compare the usual *ab initio* 2-electron integrals with type I term. Denote capital letters for AO indices and small letters for MO indices.

ab initio 2-electron integrals in AO basis:

$$G_{IJ} = \sum_{K}^{AO}\sum_{L}^{AO} D_{KL}\left[(IJ\,|\,KL) - \frac{1}{4}(IK\,|\,JL) - \frac{1}{4}(IL\,|\,JK)\right] \tag{A53}$$

Type I term:

$$\begin{aligned}
&\frac{1}{2}\sum_{n}^{A}\sum_{j}^{B}\sum_{k}^{A} S_{nj}S_{kj}\left[4(nk\,|\,mi) - (in\,|\,km) - (nm\,|\,ki)\right] \\
&= 2\sum_{n}^{A}\sum_{k}^{A}\sum_{I}^{AO\in A}\sum_{J}^{AO\in A}\sum_{K}^{AO\in A}\sum_{L}^{AO\in A}\left(\sum_{j}^{B} S_{nj}S_{kj}\right) C_n^I C_k^J C_m^K C_i^L \left[(IJ\,|KL) - \frac{1}{4}(LI\,|\,JK) - \frac{1}{4}(IK\,|\,JL)\right] \\
&= 2\sum_{I}^{AO\in A}\sum_{J}^{AO\in A}\sum_{K}^{AO\in A}\sum_{L}^{AO\in A}\left(\sum_{n}^{A}\sum_{k}^{A} C_n^I C_k^J \left(S^2\right)_{nk}\right) C_m^K C_i^L \left[(IJ\,|KL) - \frac{1}{4}(LI\,|\,JK) - \frac{1}{4}(IK\,|\,JL)\right] \\
&= 2\sum_{K}^{AO\in A}\sum_{L}^{AO\in A} C_m^K C_i^L \left\{\sum_{I}^{AO\in A}\sum_{J}^{AO\in A}\left(S^{2'}\right)^{IJ}\left[(IJ\,|KL) - \frac{1}{4}(LI\,|\,JK) - \frac{1}{4}(IK\,|\,JL)\right]\right\}
\end{aligned} \tag{A54}$$

One can see that the term in the curly parentheses resembles the *ab initio* 2-electron integrals with a density-like $S^{2'}$ matrix. Thus the code can be simply modified by taking the conventional code and replacing the density matrix with the $S^{2'}$ matrix. It is important to realize that although both indices of the $S^{2'}$ matrix (I and J) is on molecule A, it is derived from a product of two overlap matrices by summing over the index j, which counts MOs on the EFP fragment. Therefore the $S^{2'}$ matrix is different for different fragments. The type I term is then obtained by the appropriate transformation and multiplied by a factor two.

Type II terms:

$$
\begin{aligned}
&-\sum_{j}^{B} S_{mj} G_{ij}^{A} = -\sum_{j}^{B} S_{mj} \sum_{k}^{A} \left[2(ij \mid kk) - (ik \mid jk) \right] \\
&= -\sum_{j}^{B} S_{mj} \sum_{k}^{A} \sum_{I}^{AO\in A} \sum_{J}^{AO\in B} \sum_{K}^{AO\in A} \sum_{L}^{AO\in A} C_i^I C_j^J C_k^K C_k^L \left[2(IJ \mid KL) - \frac{1}{2}(IK \mid JL) - \frac{1}{2}(IL \mid JK) \right] \\
&= -\sum_{I}^{AO\in A} \sum_{J}^{AO\in B} C_i^I \left(\sum_{j}^{B} S_{mj} C_j^J \right) \left\{ \sum_{K}^{AO\in A} \sum_{L}^{AO\in A} \left(\sum_{k}^{A} C_k^K C_k^L \right) \left[2(IJ \mid KL) - \frac{1}{2}(IK \mid JL) - \frac{1}{2}(IL \mid JK) \right] \right\} \\
&= -\sum_{I}^{AO\in A} \sum_{J}^{AO\in B} 2C_i^I \left(S'_{mJ} \right) \left\{ \sum_{K}^{AO\in A} \sum_{L}^{AO\in A} \left(D^{KL} \right) \left[(IJ \mid KL) - \frac{1}{4}(IK \mid JL) - \frac{1}{4}(IL \mid JK) \right] \right\}
\end{aligned}
\tag{A55}
$$

In Eq. (55), the term in the curly parentheses is essentially the same as in the *ab initio* case except that J is an AO on the EFP fragments.

$$
\begin{aligned}
&-\sum_{k}^{A} \sum_{j}^{B} S_{kj} \left[4(kj \mid mi) - (km \mid ji) - (ki \mid jm) \right] \\
&= -4\sum_{k}^{A} \sum_{j}^{B} S_{kj} \sum_{I}^{AO\in A} \sum_{J}^{AO\in B} \sum_{K}^{AO\in A} \sum_{L}^{AO\in A} C_k^I C_j^J C_m^K C_i^L \left[(IJ \mid KL) - \frac{1}{4}(IK \mid JL) - \frac{1}{4}(IL \mid JK) \right] \\
&= -\sum_{I}^{AO\in A} \sum_{J}^{AO\in B} \sum_{K}^{AO\in A} \sum_{L}^{AO\in A} C_m^K C_i^L \left(\sum_{k}^{A} \sum_{j}^{B} C_k^I C_j^J S_{kj} \right) \left[4(IJ \mid KL) - (IK \mid JL) - (IL \mid JK) \right] \\
&= -\sum_{K}^{AO\in A} \sum_{L}^{AO\in A} C_m^K C_i^L \left\{ \sum_{I}^{AO\in A} \sum_{J}^{AO\in B} S'_{IJ} \left[4(IJ \mid KL) - (IK \mid JL) - (IL \mid JK) \right] \right\}
\end{aligned}
\tag{A56}
$$

In Eq. (56) the transformed overlap matrix acts as the density matrix. The TEI involving one EFP index only has permutation symmetry between two *ab initio* indices in the ket, i.e. (IJ|KL)=(IJ|LK). This permutation symmetry was not taken advantage of in the previous implementation. The new implementation makes use of the permutation symmetry to give a more efficient and cleaner code. It should be mentioned that in the above equation, S'_{IJ} is not simply the overlap matrix between AOs. Rather, it is the matrix transformed from the MO overlap matrix. To see this more clearly,

$$S_{ik} = \langle \varphi_i | \varphi_k \rangle = \delta_{ik} = \left\langle \sum_{\mu}^{AO} \chi_\mu C_{\mu i} \middle| \sum_{\nu}^{AO} \chi_\nu C_{\nu k} \right\rangle, \text{ i.e. } S^{MO} = C^\dagger S^{AO} C = I$$

Therefore $\left(C^\dagger\right)^{-1} = S^{AO}C$ and $C^{-1} = C^\dagger S^{AO}$. Hence the AO overlap matrix can be back-transformed from the MO overlap matrix by $S^{AO} = \left(C^\dagger\right)^{-1} S^{MO} C^{-1} = \left(S^{AO}C\right) S^{MO} \left(C^\dagger S^{AO}\right)$. By comparison, the transformed S' matrix is simply $S'^{,AO} = C^\dagger S^{MO} C$.

Schwarz inequality screening

The computation and processing of TEI are time-consuming. Besides taking advantage of the permutation symmetry, using Schwarz inequality to skip the computation of TEI that contribute little to the final energy saves time, especially for the conventional approach where I/O may add significant time cost. The Schwarz inequality implies that a TEI such as (ij|kl) obeys the following relationship:

$(ij \mid kl) \leq \left(K_{ij}\right)^{1/2} \left(K_{kl}\right)^{1/2}$ where $K_{ij} = (ij \mid ij)$ and $K_{kl} = (kl \mid kl)$. In the context of QM-EFP TEI, j is EFP AO index and the other three indices are the *ab initio* AO indices. The exchange integrals involving EFP are computed using the SGO approximation. Both the

EFP and *ab initio* basis functions are ordered in shells and consequently the integrals are arranged in shell blocks. The largest exchange integral in each block is picked out and the quantity $\left(K_{ij}\right)^{1/2}\left(K_{kl}\right)^{1/2}$ is formed and compared to a threshold value. If $\left(K_{ij}\right)^{1/2}\left(K_{kl}\right)^{1/2}$ is smaller than this threshold value the corresponding block of TEI (ij|kl) can be skipped. The time saving due to the Schwarz inequality screening is demonstrated in Fig. A2. Fig. A2 plots the total CPU time saving, which is the difference in total CPU time with and without Schwarz inequality screening, as a function of the number of EFP fragments for acetone clusters and dichloromethane clusters. The cluster sizes range from 2 up to 5 molecules, one of which is treated as *ab initio* molecule. The time saving grows linearly as the number of EFP fragments increases. The exchange repulsion energies with and without screening are the same.

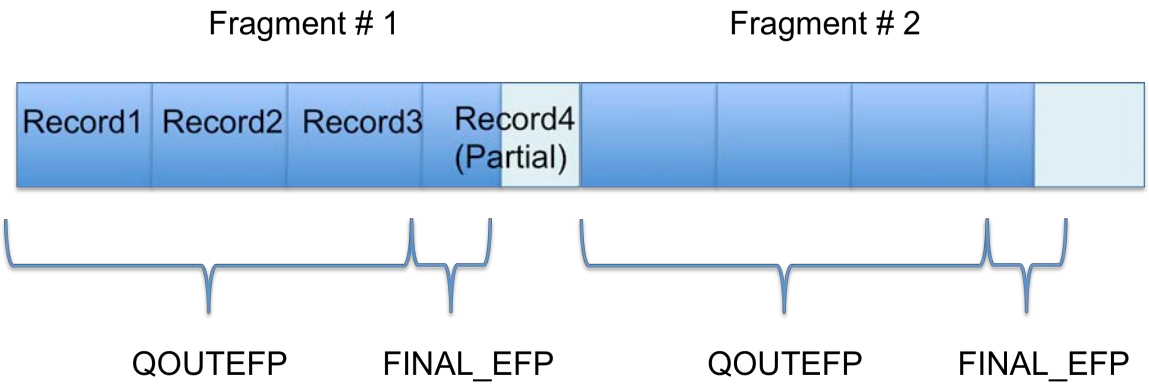

Figure A1. a pictorial representation of the storage of QM-EFP two-electron integrals.

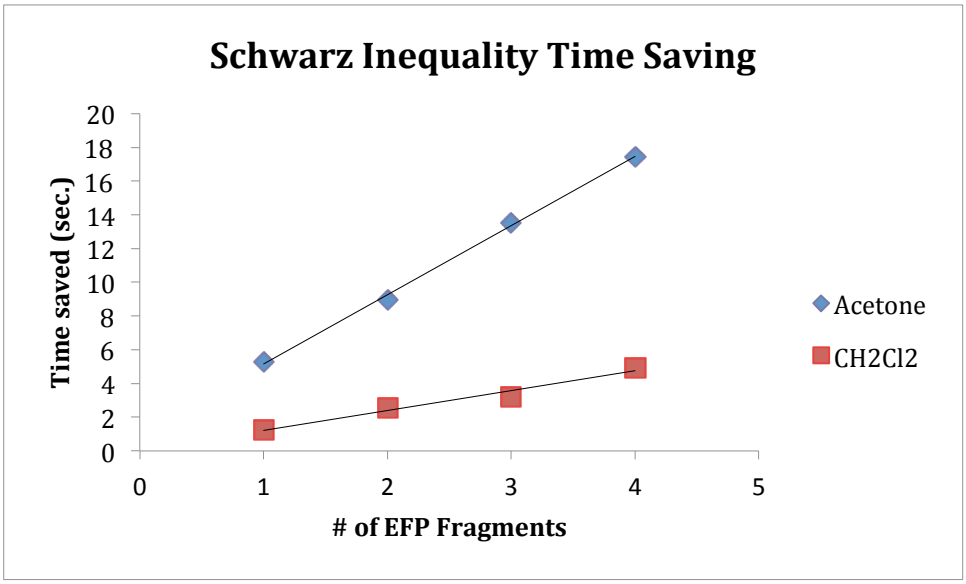

Figure A2 the total CPU time saving for acetone and dichloromethane clusters ranging from 2 to 5 molecules.

CHAPTER 5 RENORMALIZED COUPLED CLUSTER APPROACHES IN THE CLUSTER-IN-MOLECULE FRAMEWORK: PREDICTING VERTICAL ELECTRON BINDING ENERGIES OF THE ANIONIC WATER CLUSTERS $(H_2O)_n^-$

A paper submitted to *The Journal of Physical Chemistry*

Peng Xu and Mark S. Gordon

Abstract

Anionic water clusters are generally considered to be extremely challenging to model using fragmentation approaches due to the diffuse nature of the excess electron distribution. The local correlation coupled cluster (CC) framework cluster-in-molecule (CIM) approach combined with the completely renormalized CR-CC(2,3) method (abbreviated CIM/CR-CC(2,3)) is shown to be a viable alternative for computing the vertical electron binding energies (VEBE). CIM/CR-CC(2,3) with the threshold parameter ζ set to 0.001, as a trade-off between accuracy and computational cost, demonstrates the reliability of predicting the VEBE, with an average percentage error of ~ 15%. The errors are predominantly from the electron correlation energy. The CIM/CR-CC(2,3) approach provides the ease of a black-box type calculation with few threshold parameters to manipulate. The cluster sizes that can be studied by high-level *ab initio* methods are significantly increased in comparison with full CC calculations.

Introduction

The hydrated electron, the simplest reducing agent, still captures intense interest in the scientific community, even after its first experimental detection half a century ago.[1] The hydrated electron plays a key role as an important intermediate in many physical, chemical and biological processes such as in radiation chemistry and atmospheric chemistry.[2] Despite persistent efforts to understand this seemingly simple species, the very nature of the hydrated electron is still under debate. This is partly because of the ubiquitous presence of the hydrated electron in diverse environments, in particular, in bulk (e_{aq}^-) and in finite-sized water clusters [$\left(H_2O\right)_n^-$]. Finite-sized anionic water clusters, especially small water clusters (n=2-6), provide an appealing starting point for understanding the hydrated electron because one can study them with sophisticated electronic structure theory methods. Experiments under well-controlled conditions can also be carried out for small anionic water clusters.[3–9] However, the binding characteristics of the excess electron in bulk and in smaller water clusters are generally different.[10] The smaller water clusters tend to bind the excess electron weakly, and often the excess electron density exceeds the size of the cluster. As the cluster size gets larger, the binding becomes stronger and is expected to converge to the bulk behavior.

Theoretical studies play an important role in unveiling both a dynamic and a microscopically revealing picture of the hydrated electron, especially with regard to the transition from finite-size water clusters to the bulk. Two approaches have primarily been used to study the hydrated electron, static and statistical. The statistical approach employs Monte Carlo (MC) or molecular dynamics (MD) simulation techniques to study the statistically averaged properties. A recent review by Turi and Rossky[11] presents a nice

discussion of statistical methods. The inherent quantum nature of the excess electron means that at least this excess electron must be treated with quantum mechanics. The static approach focuses primarily on minima on the hydrated electron potential energy surface (PES) with methods of varying complexity; for example, treating only one electron quantum mechanically, such as the quantum Drude model developed by Jordan and coworkers[12–14] or a many-electron treatment using correlated *ab initio* methods. Density functional theory (DFT) is also a popular approach although its success depends heavily on the choice of the functional. Considering the rapidly increasing complexity of the $(H_2O)_n^-$ PES with increasing n, it is not clear that one functional will work equally well for all sizes and motifs of $(H_2O)_n^-$. The present work focuses on the static approach.

It has been recognized that electron correlation is important in the binding of the excess electron[15–18] and that correlated methods such as second order perturbation theory (MP2) or coupled cluster theory with singe, double, and perturbative triple excitations, CCSD(T), should be used. Moreover the $(H_2O)_n^-$ systems are sensitive to the choice of basis set. In particular, diffuse functions have been demonstrated to be necessary to describe the flexible and diffuse excess electron density.[15,16,18] Taken together, these realizations severely limit the size of the systems that can be studied by well correlated *ab initio* methods, given that MP2 and CCSD(T) formally scale as N^5 and N^7, respectively, with N being the number of basis functions. $(H_2O)_{33}^-$ and $(H_2O)_7^-$ are the largest clusters that have been studied to date by MP2 and CCSD(T), respectively, with the 6-31(+,3+)G* basis set. In this basis set each H atom has two additional s-type diffuse functions.[15] In the current study, MP2 and the completely renormalized coupled cluster

method, CR-CC(2,3), aka CR-CCSD(T)$_L$, are employed, since the CR-CC(2,3) approach is at least as accurate as CCSD(T) and often provides CCSDT quality results at a computational cost that is similar to that of CCSD(T).[19]

"Locality" is a relative concept. Although it is relatively diffuse, the excess electron density is not completely delocalized (such as the electron 'sea' in metals), especially viewed in the context of bulk water. It is possible to find water cluster motifs in which the excess electron density is localized and to treat such a motif as one open-shell fragment and rest of the system as closed-shell fragments. The natural parallelism of fragmentation approaches reduces memory and CPU time costs, both of which are bottlenecks in correlated electronic structure calculations. Furthermore, a multi-layer construction, i.e., different levels of theory for different layers (regions) of the system, has been implemented for many fragmentation methods. In principle, the fragmentation approach should allow much larger anionic water clusters to be examined by *ab initio* methods. In the present work, one particular fragmentation approach, the cluster-in-molecule (CIM)[20–22] method, will be assessed in terms of the accuracy of vertical electron binding energies (VEBE).

The remainder of the paper is arranged as follows. The main idea of the single-environment (SE) CIM is described briefly in Section II. Section III presents the computational details. The results are reported and discussed in Section IV. Conclusions are drawn in Section V.

Methods

The central premise of fragmentation approaches is that chemical processes are local phenomena. For fragmentation methods, it is crucial to have a sensible and reliable

method for fragmenting the system so that the locality is maintained. It is also desirable to have the fragment definitions as controlled and automated as possible. For the solvated electron the excess electron density is relatively diffuse and spread over several water molecules and may also extend beyond the atoms in a small cluster, rendering fragmentation difficult. The CIM method provides a possible solution to this problem.

CIM is a linear scaling local correlation approach. The CIM method is based on the premise that the total correlation energy of a system can be obtained as the sum of the contributions from the occupied orthonormal LMOs (central LMOs) and their respective occupied (environmental) and unoccupied localized orbital domains, since the correlation contributions from spatially distant LMO pairs are expected to be negligible.[20,23–28]

In this work, the single-environment (SE) CIM method is used. The SE CIM coupled cluster (CC) approach has been demonstrated to work well for weakly bound molecular clusters, with subsystems that apparently do not vary with the nuclear geometry.[22] The construction of SE CIM subsystems is detailed in reference 22. Unlike most other fragmentation methods whose fragmentation schemes are entirely atom-based, often with distance cutoffs, the CIM method is LMO-based and the Fock matrix elements are used as a key threshold parameter. This local correlation approach is 'black box' in the sense that one does not require detailed prior knowledge of the system to know how to fragment it. This feature is particularly useful for the diverse motifs of $\left(H_2O\right)_n^-$. However, the threshold parameters do need to be adjusted from their default values for the $\left(H_2O\right)_n^-$ systems.

Computational details

The water clusters examined in this work range from 2 to 20 water molecules denoted as nw.* where n is the number of water molecules in the system and * is an index for the particular isomer, either numerical or alphabetical. The structures of $(H_2O)_n^-$, n = 2-7, 14, 20, indicated by an alphabetical index, are obtained from the studies by Herbert et. al.[15–17]. The water clusters *6w.1* to *6w.5* were obtained from a study by Jordan and coworkers.[14] The 8-water clusters and the cluster *12w.1* were obtained from Monte Carlo simulated annealing simulations conducted by the authors, followed by MP2/aug-cc-pVTZ [29,30] geometry optimization and verified to be minima by Hessian calculations.

Single point energy calculations were carried out for the clusters $(H_2O)_n^-$ obtained from studies by Herbert et. al.[15–17] at the MP2 level of theory using three basis sets: 6-31++G(d,p), 6-31++G(df,p) and 6-311++G(d,p). The energies of the neutral clusters with the same geometries as the corresponding anions were also computed with these three basis sets. In this study, the VEBE is defined as VEBE = E (anion cluster) – E (neutral cluster at anionic structure). A negative VEBE indicates that the anion is at least metastable with respect to the autodetachment of the excess electron. Since a finite basis set is used, a positive VEBE is less conclusive, suggesting the anion is unstable relative to the neutral cluster but the excess electron may be confined by an inadequate basis set. The clusters with positive VEBE are not further investigated with CIM. By comparing VEBEs calculated using the aforementioned three basis sets, 6-31++G(d,p) was chosen for the CR-CC(2,3) and CIM calculations as a compromise between accuracy and

computational cost. Due to the high computational cost, the full CR-CC(2,3) calculations were only done for those $(H_2O)_n^-$ clusters with n ≤ 7 that have a negative VEBE. For all clusters with negative VEBEs (Fig 1), the VEBEs were also calculated using CIM/CR-CC(2,3)/6-31++G(d,p) with default threshold settings.

There are three key threshold parameters in CIM that can alter the size of the subsystems and consequently affect the binding energy and the computational efficiency. Each occupied LMO φ_i is taken to be a "central" LMO. An occupied LMO φ_j is considered to be an "environmental" LMO for a specific central LMO φ_i if the magnitude of the Fock matrix element, $\left|\langle\varphi_i|f|\varphi_j\rangle\right|$, is greater than the threshold ζ. So, the smaller the value of ζ, the more environmental LMOs are included and the larger the subsystem is. The default value of ζ is 0.003. The central LMO φ_i and the associated environmental LMOs $\{\varphi_j\}$ form an occupied LMO domain {I}. It is possible that all of the occupied LMOs in one domain are included in another larger domain. In that case the two domains {I} and {J} are combined to form a composite domain {IJ}. The central LMOs of the larger domain {IJ} now contain two central LMOs, φ_i and φ_j. The second threshold parameter is a Mulliken population cutoff (ATMMLK). For each LMO φ_i all of the atoms in the entire system are ranked in the order of decreasing Mulliken orbital populations in φ_i. A given LMO φ_i is assigned to an atom if the Mulliken population on the atom in LMO φ_i exceeds ATMMLK. The smaller ATMMLK is, the more atoms would be included in a subsystem. The default value of ATMMLK is 0.15.[22] Considering the diffuse nature of the solvated electron system, reducing the Mulliken

charge cutoff may diminish the cost benefit of CIM. So ATMMLK=0.15 is used in this study. Lastly, η is the threshold for selecting the unoccupied LMOs that are associated with a subsystem. The subsystem unoccupied LMOs are selected from the set of unoccupied LMOs of the extended subsystem. The larger the value of η, the more unoccupied orbitals will be retained. The definition and construction of the extended subsystem and the unoccupied LMOs is discussed in detail in Ref. 22. The default value of η is set to 0.2. The values of ζ and η were chosen by predicting the VEBE for several small clusters that have a broad range of VEBEs. ζ is chosen to be 0.001 while η remains at its default value. CIM/CR-CC(2,3) calculations were then performed with the chosen set of parameters (ζ = 0.001, ATMMLK = 0.15, η = 0.2) for all clusters that have negative VEBEs.

To quantify the charge distributions of the anionic and neutral clusters, atomic charges were computed by fitting to the electrostatic potential at points that are selected according to an algorithm due to Spackman.[31] The differences in the atomic charges between anionic and neutral clusters were computed. All of the calculations were performed with the GAMESS electronic structure code.[32,33]

Results and Discussion

The MP2 VEBEs of water clusters $\left(H_2O\right)_n^-$, n = 2-7,14 and 20, were examined using the three basis sets discussed in Section 3 (See Table 1) and compared with the previously calculated MP2/6-31(1+,3+)G*[15–17] VEBEs by Herbert et. al.. The 6-31(1+,3+)G* basis set, compared to the 6-31++G* basis, has two additional diffuse s

functions on H atoms with their exponents decreased by a successive factor of 3.32.[15] The diffuse functions on H atoms have been shown to be crucial for the binding of the excess electron.[15] However the 6-31(1+,3+)G* basis is not employed in the present study, because the CIM method may have difficulties constructing the unoccupied LMOs of subsystems,[20] or the very large subsystems that are created may require more memory than is available on one processor (CR-CC(2,3) only runs in serial).

Table 1 tabulates the MP2 VEBE results with all four basis sets. The addition of a set of f polarization functions hardly changes the binding energies in comparison with the 6-31++G(d,p) VEBEs. The VEBEs predicted by the triple zeta basis set are reasonably close to the 6-31++G(d,p) VEBEs. For all of the clusters listed in Table 1, MP2/6-31(1+,3+)G* predicts negative VEBEs. For the smallest clusters (n = 2-4) MP2/6-31++G(d,p) predicts mostly positive VEBEs. However, for n>4, the two sets of VEBE are in qualitative agreement, with the MP2/6-31++G(d,p) predicting VEBEs that are generally ~3-6 kcal/mol smaller in magnitude than the MP2/6-31(1+,3+)G* VEBE values, but with the same sign. The small clusters with positive VEBE still do not bind the excess electron even after MP2/6-31++G(d,p) geometry optimization. MP2 with the smaller 6-31+G(d,p) basis set (results not shown in Table 1) predicts that most of the clusters in Table 1 have positive VEBE. The Dunning correlation consistent aug-cc-pvTZ basis set does not produce negative VEBEs for the very small clusters and already becomes computationally demanding for 6-water clusters. Consequently, the 6-31++G(d,p) basis is chosen as a good compromise for the present work.

Herbert and Head-Gordon[15] noted that the magnitudes of the MP2 electron detachment energies are consistently ~30 meV (0.69 kcal/mol) smaller than the

corresponding CCSD(T) values using the same basis set. The MP2 error is essentially independent of the magnitude of the binding energy or the structure motif. A similar conclusion can be drawn from the results in Table 2 for MP2 and CR-CC(2,3): the magnitudes of MP2 VEBEs are on average ~0.67 kcal/mol lower than the CR-CC(2,3) values. This observation is important for the present study, since MP2 VEBEs for larger clusters can provide good benchmarks for CIM/CR-CC(2,3) and can therefore be used to obtain estimated CR-CC(2,3) VEBE values when CR-CC(2,3) is too challenging for the entire system.

The MP2 and CR-CC(2,3) VEBEs calculated with the 6-31++G(d,p) basis set are compared in Table 3. The CR-CC(2,3) VEBE values of the clusters with $n \geq 8$ are estimated by adding -0.67 kcal/mol to the corresponding MP2 values. These estimated CR-CC(2,3) VEBEs are in *italics* to emphasize that they are only used as a guideline. The clusters that have positive VEBE in Table 1 do not appear in Table 3. The VEBE calculated using CIM/CR-CC(2,3) are also tabulated in Table 3. The percent error (% error) is used to assess the quality of the results rather than the absolute errors. The % errors are calculated as (CIM/CR-CC(2,3) VEBE – CR-CC(2,3) VEBE)/CR-CC(2,3) VEBE. Using the CIM default ζ =0.003, the predicted VEBEs are in poor agreement with the benchmark VEBEs, with an average % error of 76%. Relative to CR-CC(2,3) VEBEs, the RMS error of CIM/CR-CC(2,3) (ζ =0.003) is 23.65 kcal/mol, two orders of magnitude larger compared to that of MP2 (0.68 kcal/mol). Moreover there seems to be no pattern as to whether the error over- or under-estimates the VEBE. The default CIM threshold parameters were originally benchmarked[22] mainly using neutral systems

(alkanes, water clusters), and they appear to be inadequate for delocalized anionic systems like $(H_2O)_n^-$.

As mentioned in the computational details section, some threshold parameters may influence the construction of subsystems and consequently the CIM correlation energy. To find the optimal values of these parameters, small clusters with large VEBE errors are examined by varying ζ and η. Table 4 presents the VEBEs for the *4w.a*, *5w.d* and *5w.e* clusters calculated at different ζ values. At ζ = 0.003, CIM/CR-CC(2,3) produces VEBEs that deviate significantly from the CR-CC(2,3) results. For ζ = 0.002, some improvement can be seen although the results are still far from satisfactory. ζ = 0.001 yields much improved VEBEs. The RMS errors for the three clusters in Table 4 are reduced from 4.99 kcal/mol for ζ = 0.003 to 0.58 kcal/mol for ζ = 0.001. For ζ = 0.003 or 0.002, CIM generates 4 subsystems for both the anionic and neutral *5w.e* cluster, while for ζ = 0.001, CIM generates only one subsystem for both anionic and neutral *5w.e* clusters. Therefore, the computed CIM/CR-CC(2,3) VEBE is identical to the CR-CC(2,3) VEBE. The anionic *5w.d* cluster is also not fragmented. This lack of fragmentation means that CIM recognizes that this cluster is too delocalized to fragment. Table 5 illustrates that there is little dependence of the predicted VEBE for the 6w.5 cluster on changes in the parameter η.

The CIM/CR-CC(2,3) calculations reported in Table 3 were also performed with ζ = 0.001 and other parameters kept as their default values. Two observations can be made immediately. First, the average percent error decreases from 76% to 15%. Second, the CIM/CR-CC(2,3) method with ζ = 0.001 almost always underestimates the VEBE.

The RMS error of CIM/CR-CC(2,3) with ζ = 0.001 is 2.34 kcal/mol, about 10 times smaller than that with ζ = 0.003.

The MP2/6-31++G(d,p) and CR-CC(2,3)/6-31++G(d,p) electron correlation contributions to the VEBE are shown in Table 6. The MP2/6-31++G(d,p) VEBE electron correlation contribution is ~ 0.67 kcal/mol smaller in magnitude than that obtained with CR-CC(2,3)/6-31++G(d,p) for n ≤ 7. This is expected since MP2 and CR-CC(2,3) use the same HF reference wave function. The CR-CC(2,3) VEBE correlation contributions for n > 7 are therefore estimated by adding -0.67 kcal/mol to MP2 correlation energies and are listed *in italics*. By comparing to the VEBEs listed in Table 3, one can see that the correlation energy is crucial for the binding of the excess electron. For small clusters (n = 2-5), the excess electron will not bind at the Hartree-Fock level. For most of the 6- and 7-water clusters the VEBEs come almost entirely from electron correlation. As the cluster size increases, the percentage contribution of electron correlation to the VEBE decreases. However, the correlation effect is still a significant portion of the VEBE, with the smallest contribution among the clusters examined here being ~20% for the 12w.1 cluster. The variation of the correlation energy contributions with the size of the system is much smaller than the variation of VEBEs with the size of the cluster and different configurations of the same size.

The CIM/CR-CC(2,3) errors for the total VEBE and the correlation contributions compared to the corresponding CR-CC(2,3) values [CIM/CR-CC(2,3) – CR-CC(2,3)] are also tabulated in Table 6. The errors in the VEBE come entirely from the correlation energy errors. This is because CIM splits the electron correlation energies into

contributions from subsystems, but the reference HF energy is calculated for the entire system.

Unfortunately, examination of the entries in Table 6 does not reveal a clear relationship between the cluster size and the correlation energy errors of $\left(H_2O\right)_n^-$ and $\left(H_2O\right)_n$. The signs of the errors are almost always positive (CIM correlation energies are less negative) which means (not surprisingly) that CIM tends to under-estimate the correlation energies. The error in the calculated VEBE depends, of course on the relative errors in the anion and in the corresponding neutral cluster. If both anionic and neutral clusters have similar errors with the same sign (both large errors or both small errors), the resulting VEBE error is small, for example, *6w.1* and *6w.2*. An interesting example is the cluster *6w.e*: Upon decreasing ζ from 0.003 to 0.001, the correlation energy errors for both the anionic and neutral clusters decrease. However, the improvement of the anion correlation energy is much less than that of the neutral cluster, so the ζ =0.001 VEBE error is larger than that for 0.003. In most cases, the errors of the neutral clusters are smaller since the electron distributions in the neutral clusters are more localized. The majority of the clusters have the same number of subsystems generated by CIM for the anion and its neutral counterpart. Of course, the LMO composition of the anion and neutral subsystems do not necessarily match. Hence, the difference between the anionic and neutral correlation errors is a manifestation of the difference in the degree of localization (or delocalization). In the present work, the biggest difference in the number of subsystems between an anion and the corresponding neutral is three for *5w.4* and *8w.2*.

The excess electron charge distribution can be studied by taking the difference between the atomic charges of the anionic and neutral clusters that are computed by fitting to their electrostatic potentials.[31] Of course, there is no unique way to define atomic charges. So, these atomic charges should be viewed as qualitative indicators for understanding the CIM subsystems. Consider, for example, *6w.5*. The atomic charge difference is shown in Figure 2(a). The excess electron, indicated by negative charge differences on atom centers, is essentially evenly distributed over the hydrogen atoms that point into the cavity, while the other hydrogen atoms that form the hydrogen network are hardly changed, behaving like 'spectators'. This particular 'internally solvated' anionic cluster would naturally be considered to be one open-shell system and requires no further fragmentation. In fact, such delocalized systems would be extremely difficult, if not impossible, to deal with for any fragmentation scheme, because fragmentation approaches are based on the locality of the chemistry. The excess electron distribution polarizes the OH bonds pointing towards the cavity. The anion oxygen atoms become slightly more positively charged compared to their neutral counterparts. A sensible fragmentation should include both the hydrogen atoms pointing into the cavity and all of the polarized oxygen atoms. Figures 2(b) and 2(c) show the CIM fragmented subsystems of the anion using $\zeta = 0.003$ and $\zeta = 0.001$, respectively. Each of the subsystems in Figure 2(b) encompasses three water molecules on one side and the three mostly negatively charged hydrogen atoms on the other side, while the subsystems in Figure 2(c) also include the three oxygen atoms on the other side, leaving out three 'spectator' hydrogen atoms on the other side. Larger subsystems should improve the results in general. In this case, all six OH bonds equally polarized by the excess electron are

included in each subsystem in Figure 2(c). The number of subsystems is also reduced in Figure 2(c) relative to Figure 2(b).

In terms of the computational cost, the effect of changing ζ from 0.003 to 0.001 is manifested in two ways. The sizes of most of the subsystems increase, and the number of subsystems may change. The magnitude of the increase in the computational demand varies from system to system. Using *14w.a* and *14w.b* as examples, the replicated memory requirement for each subsystem is reported in Table 7 in units of 1 megaword where a word is defined as 64 bits. One can see that almost all of the subsystems of *14w.a* and *14w.b* increase in size when ζ decreases, but the change of ζ impacts *14w.b* subsystems much more than in *14w.a*. *14w_n* indicates the neutral counterparts of the anions. The fact that the increase in computational demand for the neutral cluster *14w_n.b* is much less compared to that of 14w.b is again a demonstration of the difference in the degree of localization between the anion and the neutral.

The CIM method significantly reduces the memory requirement compared to an *ab initio* calculation of the whole system. For example, a CR-CC(2,3)/6-31++G(d,p) calculation of 7-water clusters requires ~ 1378 megawords while the largest subsystem of 7 water clusters require ~ 480 megawords, and many other subsystems need less than 100 megawords. For 20-water clusters, MP2/6-31++G(d,p) requires ~ 4776 megawords (serial calculation), while a CIM/CR-CC(2,3) using the same basis set requires 447 megawords for the largest subsystem and ~ 97 megawords on average. So, even though empirically corrected MP2 calculations do very well for the VEBE, the reduced CIM/CR-

CC(2,3) memory requirements will allow calculations on much larger clusters. In addition, such empirical corrections may not be available for all properties of interest.

Conclusions

The excess electron in finite anionic water clusters is diffuse, and electron correlation plays an important role in the binding of the excess electron to the water clusters, especially smaller clusters (2-5 water molecules). The cluster-in-molecule (CIM) method in combination with CR-CC(2,3) is assessed in this study in terms of the accuracy of VEBE for anionic water clusters in the range of 4 – 20 water molecules. The use of LMO domains for dividing the whole system provides the ease of a 'black-box' type calculation, with just three threshold parameters. Setting the threshold parameter ζ to 0.001 provides reasonably accurate VEBEs at an affordable computational expense. At present, the CIM method in GAMESS is a sequential code. However, the implementation of a distributed parallel code is in progress. Such a parallel code will considerably reduce the computational cost of CIM calculations. The CIM/CR-CC(2,3) method may be a viable alternative approach for obtaining benchmarking numbers for water clusters when traditional coupled-cluster theory calculations for the entire system are difficult or impossible.

Acknowledgement

The authors gratefully thank Professor John Herbert and Dr. Albert DeFusco who kindly provided the geometries of many $(H_2O)_n^-$ clusters that are considered in this work.

Discussions with Dr. DeFusco and Professor Piotr Piecuch are greatly appreciated. This material is based upon work supported by the Air Force Office of Scientific Research under AFOSR Award No. FA9550-11-1-0099.

Reference

(1) Hart, E. J.; Boag, J. W. Absorption Spectrum of the Hydrated Electron in Water and in Aqueous Solutions. *J. Am. Chem. Soc.* **1962**, *84*, 4090–4095.

(2) Garrett, B. C.; Dixon, D. A.; Camaioni, D. M.; Chipman, D. M.; Johnson, M. A.; Jonah, C. D.; Kimmel, G. A.; Miller, J. H.; Rescigno, T. N.; Rossky, P. J.; et al. Role of Water in Electron-Initiated Processes and Radical Chemistry: Issues and Scientific Advances. *Chem. Rev. (Washington, DC, United States)* **2005**, *105*, 355–389.

(3) Haberland, H.; Ludewigt, C.; Schindler, H. G.; Worsnop, D. R. Experimental Observation of the Negatively Charged Water Dimer and Other Small (H2O)n- Clusters. *J. Chem. Phys.* **1984**, *81*, 3742–3744.

(4) Haberland, H.; Schindler, H. G.; Worsnop, D. R. Mass Spectra of Negatively Charged Water and Ammonia Clusters. *Berichte der Bunsen-Gesellschaft* **1984**, *88*, 270–272.

(5) Coe, J. V; Lee, G. H.; Eaton, J. G.; Arnold, S. T.; Sarkas, H. W.; Bowen, K. H.; Ludewigt, C.; Haberland, H.; Worsnop, D. R. Photoelectron Spectroscopy of Hydrated Electron Cluster Anions, (H2O)n=2-69-. *J. Chem. Phys.* **1990**, *92*, 3980–3982.

(6) Sanov, A.; Lineberger, W. C. Dynamics of Cluster Anions: A Detailed Look at Condensed-Phase Interactions. *PhysChemComm [online Comput. file]* **2002**, 165–177.

(7) Verlet, J. R. R.; Bragg, A. E.; Kammrath, A.; Cheshnovsky, O.; Neumark, D. M. Observation of Large Water-Cluster Anions with Surface-Bound Excess Electrons. *Sci. (Washington, DC, United States)* **2005**, *307*, 93–96.

(8) Lee, G. H.; Arnold, S. T.; Eaton, J. G.; Bowen, K. H. Electronic Properties of Dipole-Bound (H2O)2-, (D2O)2-, (H2O)2-Arn=1,2,3, and (D2O)2-Arn=1,2,3 Using Negative Ion Photoelectron Spectroscopy. *Chem. Phys. Lett.* **2000**, *321*, 333–337.

(9) Knapp, M.; Echt, O.; Kreisle, D.; Recknagel, E. Trapping of Low Energy Electrons at Preexisting, Cold Water Clusters. *J. Chem. Phys.* **1986**, *85*, 636–637.

(10) Neumark, D. M. Spectroscopy and Dynamics of Excess Electrons in Clusters. *Mol. Phys.* **2008**, *106*, 2183–2197.

(11) Turi, L.; Rossky, P. J. Theoretical Studies of Spectroscopy and Dynamics of Hydrated Electrons. *Chem. Rev. (Washington, DC, United States)* **2012**, *112*, 5641–5674.

(12) Sommerfeld, T.; Jordan, K. D. Quantum Drude Oscillator Model for Describing the Interaction of Excess Electrons with Water Clusters: An Application to (H2O)13-. *J. Phys. Chem. A* **2005**, *109*, 11531–11538.

(13) Sommerfeld, T.; Jordan, K. D. Electron Binding Motifs of (H2O)n- Clusters. *J. Am. Chem. Soc.* **2006**, *128*, 5828–5833.

(14) Sommerfeld, T.; DeFusco, A.; Jordan, K. D. Model Potential Approaches for Describing the Interaction of Excess Electrons with Water Clusters: Incorporation of Long-Range Correlation Effects. *J. Phys. Chem. A* **2008**, *112*, 11021–11035.

(15) Herbert, J. M.; Head-Gordon, M. Calculation of Electron Detachment Energies for Water Cluster Anions: An Appraisal of Electronic Structure Methods, with Application to (H2O)20- and (H2O)24-. *J. Phys. Chem. A* **2005**, *109*, 5217–5229.

(16) Herbert, J. M.; Head-Gordon, M. Accuracy and Limitations of Second-Order Many-Body Perturbation Theory for Predicting Vertical Detachment Energies of Solvated-Electron Clusters. *Phys. Chem. Chem. Phys.* **2006**, *8*, 68–78.

(17) Williams, C. F.; Herbert, J. M. Influence of Structure on Electron Correlation Effects and Electron-Water Dispersion Interactions in Anionic Water Clusters. *J. Phys. Chem. A* **2008**, *112*, 6171–6178.

(18) Jordan, K. D.; Wang, F. Theory of Dipole-Bound Anions. *Annu. Rev. Phys. Chem.* **2003**, *54*, 367–396.

(19) Wloch, M.; Lodriguito, M. D.; Piecuch, P.; Gour, J. R. Two New Classes of Non-Iterative Coupled-Cluster Methods Derived from the Method of Moments of Coupled-Cluster Equations. *Mol. Phys.* **2006**, *104*, 2149–2172.

(20) Li, S.; Shen, J.; Li, W.; Jiang, Y. An Efficient Implementation of the “Cluster-in-Molecule” Approach for Local Electron Correlation Calculations. *J. Chem. Phys.* **2006**, *125*, 074109/1–074109/10.

(21) Li, W.; Piecuch, P.; Gour, J. R.; Li, S. Local Correlation Calculations Using Standard and Renormalized Coupled-Cluster Approaches. *J. Chem. Phys.* **2009**, *131*, 114109/1–114109/30.

(22) Li, W.; Piecuch, P. Improved Design of Orbital Domains within the Cluster-in-Molecule Local Correlation Framework: Single-Environment Cluster-in-Molecule Ansatz and Its Application to Local Coupled-Cluster Approach with Singles and Doubles. *J. Phys. Chem. A* **2010**, *114*, 8644–8657.

(23) Pulay, P. Localizability of Dynamic Electron Correlation. *Chem. Phys. Lett.* **1983**, *100*, 151–154.

(24) Hampel, C.; Werner, H.-J. Local Treatment of Electron Correlation in Coupled Cluster Theory. *J. Chem. Phys.* **1996**, *104*, 6286–6297.

(25) Schutz, M.; Werner, H.-J. Low-Order Scaling Local Electron Correlation Methods. IV. Linear Scaling Local Coupled-Cluster (LCCSD). *J. Chem. Phys.* **2001**, *114*, 661–681.

(26) Scuseria, G. E.; Ayala, P. Y. Linear Scaling Coupled Cluster and Perturbation Theories in the Atomic Orbital Basis. *J. Chem. Phys.* **1999**, *111*, 8330–8343.

(27) Foerner, W.; Ladik, J.; Otto, P.; Cizek, J. Coupled-Cluster Studies. II. The Role of Localization in Correlation Calculations on Extended Systems. *Chem. Phys.* **1985**, *97*, 251–262.

(28) Li, S.; Ma, J.; Jiang, Y. Linear Scaling Local Correlation Approach for Solving the Coupled Cluster Equations of Large Systems. *J. Comput. Chem.* **2002**, *23*, 237–244.

(29) Dunning Jr., T. H. Gaussian Basis Sets for Use in Correlated Molecular Calculations. I. The Atoms Boron through Neon and Hydrogen. *J. Chem. Phys.* **1989**, *90*, 1007–1023.

(30) Kendall, R. A.; Dunning Jr., T. H.; Harrison, R. J. Electron Affinities of the First-Row Atoms Revisited. Systematic Basis Sets and Wave Functions. *J. Chem. Phys.* **1992**, *96*, 6796–6806.

(31) Spackman, M. A. Potential Derived Charges Using a Geodesic Point Selection Scheme. *J. Comput. Chem.* **1996**, *17*, 1–18.

(32) Schmidt, M. W.; Baldridge, K. K.; Boatz, J. A.; Elbert, S. T.; Gordon, M. S.; Jensen, J. H.; Koseki, S.; Matsunaga, N.; Nguyen, K. A.; et, al. General Atomic and Molecular Electronic Structure System. *J. Comput. Chem.* **1993**, *14*, 1347–1363.

(33) Gordon, M. S.; Schmidt, M. W. Advances in Electronic Structure Theory: GAMESS a Decade Later. In *Theory Appl. Comput. Chem.: First Forty Years*; Elsevier B.V., 2005; pp. 1167–1189.

Figure 1. The geometries of the $(H_2O)_n^-$, n = 4-20, studied by CIM in this work.

Figure 2 (a) The atomic charge difference between the anionic and the neutral clusters of 6w.5; (b) The six subsystems constructed by CIM/CR-CC(2,3) with ζ = 0.003; (c) the two subsystems constructed by CIM/CR-CC(2,3) with ζ = 0.001

Table 1 MP2 VEBE (kcal/mol) for anionic water clusters $(H_2O)_n^-$, n = 2-7, 14, 20.

	MP2[a] 6-31(1+,3+)G*	MP2 6-31++G(d,p)	MP2 6-31++G(df,p)	MP2 6-311++G(d,p)
2w	-0.61	12.47	12.43	13.27
3w.a	-0.16	13.35	13.30	14.00
3w.b	-3.26	6.19	6.14	7.05
4w.a	-8.02	-1.94	-2.01	-0.85
4w.b	-4.57	3.17	3.10	4.05
4w.c	-0.95	11.15	11.09	11.86
4w.d	-5.69	1.73	1.66	2.66
4w.e	-4.42	3.66	3.61	4.63
4w.f	-6.05	1.53	1.47	2.43
5w.a	-9.38	-3.48	-3.54	-2.44
5w.b	-1.76	9.36	9.29	10.13
5w.c	-10.28	-5.09	-5.16	-4.03
5w.d	-6.52	-0.61	-0.69	-0.40
5w.e	-8.50	-2.56	-2.63	-1.62
5w.f	-8.25	-1.83	-1.90	-0.91
6w.a	-0.20	12.11	12.08	12.78
6w.b	-16.26	-13.24	-13.35	-11.96
6w.c	-0.46	11.16	11.13	11.76
6w.d	-2.30	8.20	8.13	8.96
6w.e	-10.78	-5.63	-5.71	-4.59
6w.f	-11.65	-6.95	-7.03	-5.75
6w.g	-10.20	-5.11	-5.19	-4.18
7w.a	-14.66	-10.74	-10.83	-9.62
7w.b	-13.17	-8.65	-8.72	-7.70
7w.c	-10.44	-4.17	-4.24	-3.23
14w.a	-19.36	-14.81	-14.90	-13.83
14w.b	-21.65	-20.87	-21.07	-19.94
20w.a	-25.32	-21.77	-21.87	-20.65
20w.b	-20.35	-16.48	-16.57	-15.48
20w.c	-14.84	-10.44	-10.52	-9.59

[a] The MP2/6-31(1+,3+)G* VEBEs are taken from references 7-9[*].

[*] The structures and the electron detachment energies are available in the supporting information for these three references at http://chemistry.osu.edu/~herbert/reprints/JPCA_112_6171_suppinfo.txt

Table 2 VEBE (kcal/mol) computed using MP2 and CR-CC(2,3) at 6-31++G(d,p) basis set for $\left(H_2O\right)_n^-$, n = 4 - 7

	MP2 6-31++G(d,p)	CR-CC(2,3) 6-31++G(d,p)
4w.a	-1.94	-2.59
5w.a	-3.48	-4.26
5w.c	-5.09	-5.70
5w.d	-0.61	-1.49
5w.e	-2.56	-3.22
5w.f	-1.83	-2.34
6w.1	-3.09	-4.11
6w.2	-6.83	-7.51
6w.3	-13.22	-13.67
6w.4	-5.31	-6.08
6w.5	-13.89	-14.46
6w.b	-13.24	-13.80
6w.e	-5.63	-6.34
6w.f	-6.95	-7.84
6w.g	-5.11	-5.68
7w.a	-10.74	-11.48
7w.b	-8.65	-9.18
7w.c	-4.17	-4.68

Table 3 VEBEs (kcal/mol) for $(H_2O)_n$, n = 4 – 20, calculated using MP2, CR-CC(2,3), and CIM-CR-CC(2,3) with the 6-31++G(d,p) basis set. The CR-CC(2,3) VEBEs for clusters larger than 7 water molecules are estimated from MP2 values (in *italics*). The % errors relative to those estimated values are also in *italics*. The MP2 and CIM RMS errors are given in kcal/mol

	MP2	CR-CC(2,3)	CIM/ CR-CC(2,3) ζ =0.003	% Error	CIM/ CR-CC(2,3) ζ =0.001	% Error
4w.a	-1.94	-2.59	-0.80	-69%	-1.95	-25%
5w.a	-3.48	-4.26	-3.65	-14%	-4.15	-3%
5w.c	-5.09	-5.70	-5.82	2%	-5.11	-10%
5w.d	-0.61	-1.49	-9.74	556%	-2.26	52%
5w.e	-2.56	-3.22	-1.40	-57%	-3.21	0%
5w.f	-1.83	-2.34	-8.07	245%	-1.40	-40%
6w.1	-3.09	-4.11	-3.29	-20%	-3.88	-6%
6w.2	-6.83	-7.51	-6.77	-10%	-6.53	-13%
6w.3	-13.22	-13.67	-7.94	-42%	-8.15	-40%
6w.4	-5.31	-6.08	-10.40	71%	-5.11	-16%
6w.5	-13.89	-14.46	-39.46	173%	-13.13	-9%
6w.b	-13.24	-13.80	-17.28	25%	-12.26	-11%
6w.e	-5.63	-6.34	-5.44	-14%	-2.81	-56%
6w.f	-6.95	-7.84	-13.61	74%	-6.20	-21%
6w.g	-5.11	-5.68	-10.81	90%	-5.00	-12%
7w.a	-10.74	-11.48	-14.40	26%	-10.83	-6%
7w.b	-8.65	-9.18	-8.26	-10%	-8.26	-10%
7w.c	-4.17	-4.68	-3.94	-16%	-4.30	-8%
8w.2	21.42	*-22.09*	-22.98	*4%*	-21.06	*-5%*
8w.4	-25.39	*-26.07*	-19.16	*-26%*	-23.25	*-11%*
8w.5	-19.30	*-19.98*	-24.60	*23%*	-18.23	*-9%*
8w.6	-23.37	*-24.04*	-25.28	*5%*	-21.48	*-11%*
8w.7	-22.63	*-23.31*	-22.80	*-2%*	-21.50	*-8%*
8w.8	-24.61	*-25.28*	-32.26	*28%*	-24.88	*-2%*
8w.9	-18.64	*-19.31*	-31.99	*66%*	-17.65	*-9%*
8w.10	-27.01	*-27.69*	-23.78	*-14%*	-26.51	*-4%*
8w.11	-24.29	*-24.96*	-30.79	*23%*	-24.79	*-1%*
8w.12	-15.08	*-15.76*	-20.70	*31%*	-15.02	*-5%*
12w.1	-48.79	*-49.46*	-42.28	*-15%*	-44.71	*-10%*
12w.a	-16.23	*-16.90*	-15.03	*-11%*	-15.68	*-7%*
14w.a	-14.81	*-15.48*	-12.45	*-20%*	-12.66	*-18%*
14w.b	-20.87	*-21.54*	-10.47	*-51%*	-21.93	*2%*
20w.a	-21.77	*-22.44*	-14.89	*-34%*	-15.45	*-31%*
20w.b	-16.48	*-17.15*	-151.70	*785%*	-12.20	*-29%*

Table 3 continued

20w.c	-10.44	*-11.11*	-8.77	*-21%*	-9.27	*-17%*
RMS error	0.68		23.65		2.34	

Table 4 VEBEs (kcal/mol) of three clusters computed using CR-CC(2,3), and CIM/CR-CC(2,3) with three ζ values and the 6-31++G(d,p) basis set. The RMS errors are in kcal/mol.

	4w.a	5w.d	5w.e	RMS error
CR-CC(2,3)	-2.59	-1.49	-3.22	
CIM/CR-CC(2,3) ζ = 0.003 (default)	-0.80	-9.74	-1.40	4.99
CIM/CR-CC(2,3) ζ = 0.002	-0.85	-2.60	-1.79	1.45
CIM/CR-CC(2,3) ζ = 0.001	-1.95	-2.26	-3.21	0.58

Table 5 VEBEs (in kcal/mol) of three clusters computed using CR-CC(2,3) and CIM/CR-CC(2,3) with three values of η and the 6-31++G(d,p) basis set.

	6w.5
CR-CC(2,3)	-14.46
CIM/CR-CC(2,3) η = 0.2 (default)	-39.46
CIM/CR-CC(2,3) η = 0.3	-39.08
CIM/CR-CC(2,3) η = 0.4	-37.50

Table 6 MP2, CR-CC(2,3) and CIM/CR-CC(2,3) correlation energy contributions [anionic correlation energy – neutral correlation energy] to the VEBE (kcal/mol).

	MP2 Corr. E.	CR-CC(2,3) Corr. E.	CIM/CR-CC(2,3) Total VEBE Error	CIM/CR-CC(2,3) Corr. E. Error	CIM/CR-CC(2,3) Anionic Corr. E. Error	CIM/CR-CC(2,3) Neutral Corr. E. Error
4w.a	-5.59	-6.24	0.64	0.64	0.79	0.15
5w.a	-5.81	-6.60	0.11	0.11	0.44	0.33
5w.c	-5.82	-6.43	0.59	0.59	1.21	0.63
5w.d	-5.47	-6.35	-0.78	-0.78	0.01	0.79
5w.e	-5.89	-6.55	0.00	0.00	0.00	0.00
5w.f	-5.51	-6.02	0.94	0.94	0.84	-0.09
6w.1	-5.64	-6.66	0.24	0.24	4.05	3.82
6w.2	-5.90	-6.58	0.98	0.98	4.27	3.28
6w.3	-6.39	-6.85	5.53	5.53	7.06	1.53
6w.4	-5.65	-6.43	0.97	0.97	0.78	-0.19
6w.5	-5.43	-6.01	1.33	1.33	1.06	-0.27
6w.b	-6.57	-7.13	1.54	1.54	3.33	1.79
6w.e	-6.03	-6.74	3.53	3.53	5.12	1.59
6w.f	-5.79	-6.68	1.64	1.64	2.53	0.89
6w.g	-5.78	-6.34	0.68	0.68	0.85	0.17
7w.a	-6.29	-7.03	0.65	0.65	2.91	2.26
7w.b	-6.07	-6.60	0.91	0.91	1.97	1.06
7w.c	-5.64	-6.15	0.37	0.37	0.16	-0.21
8w.2	-6.47	*-7.14*	1.03	1.03		
8w.4	-7.45	*-8.12*	2.82	2.82		
8w.5	-7.01	*-7.68*	1.74	1.74		
8w.6	-6.56	*-7.23*	2.56	2.56		
8w.7	-6.84	*-7.51*	1.80	1.80		
8w.8	-7.22	*-7.89*	0.40	0.40		
8w.9	-6.85	*-7.52*	1.66	1.66		
8w.10	-7.24	*-7.91*	1.17	1.17		
8w.11	-6.83	*-7.50*	0.17	0.17		
8w.12	-6.46	*-7.13*	0.74	0.74		
12w.1	-9.90	*-10.57*	4.75	4.75		
12w.a	-7.63	*-8.30*	1.22	1.22		
14w.a	-6.35	*-7.02*	2.82	2.82		
14w.b	-11.05	*-11.72*	-0.39	-0.39		
20w.a	-6.61	*-7.28*	6.99	6.99		
20w.b	-6.34	*-7.01*	4.95	4.95		
20w.c	-6.34	*-7.01*	1.84	1.84		

Table 7. Memory requirement (in mwords) for the CIM subsystems of the clusters 14w.a and 14w.b and their neutral counterparts with different ζ values. 14w_n designates the neutral counterparts.

	14w.a		14w_n.a		14w.b		14w_n.b	
ζ subsystem	0.003	0.001	0.003	0.001	0.003	0.001	0.003	0.001
1	62	119	62	119	42	292	43	135
2	45	89	45	94	50	135	50	64
3	80	371	42	57	52	96	52	96
4	35	122	35	122	290	3780	73	448
5	62	122	62	122	44	122	61	122
6	45	91	45	94	42	706	44	304
7	42	81	32	84	59	149	59	149
8	57	57	57	57	29	2216	29	1066
9	45	125	45	125	50	135	52	113
10	61	61	61	61	218	3256	20	144
11	44	127	44	61	132	1633	19	55
12	36	62	36	62	68	250	68	164
13	111	295	61	61	412	4743	79	701
14	104	194	61	113	40	91	32	94

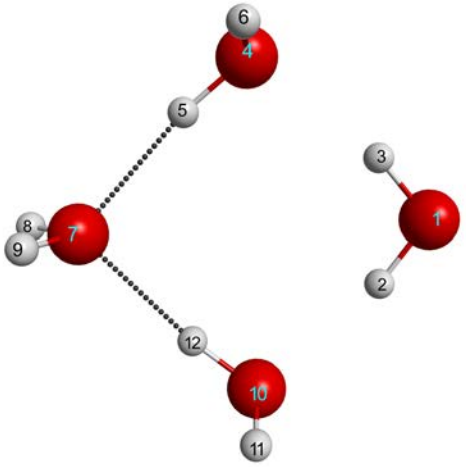

4w.1

Figure 1 continued

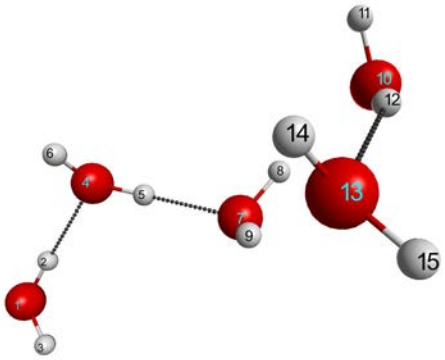

5w.1

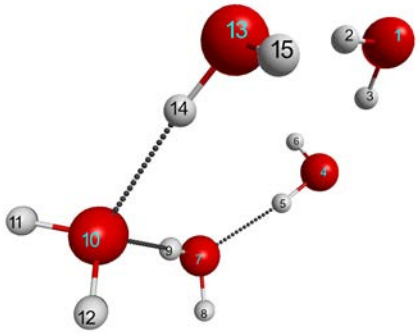

5w.3

Figure 1 continued

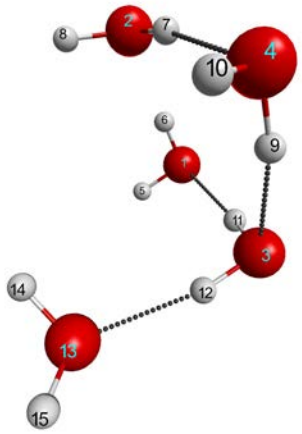

5w.4

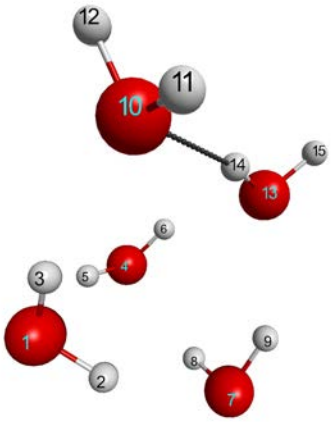

5w.5

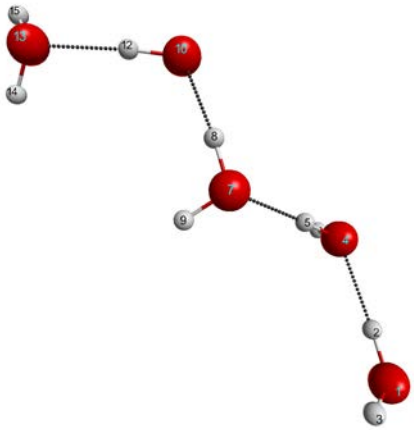

5w.6

Figure 1 continued

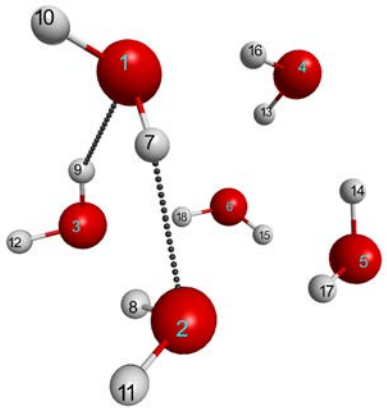

6w.1

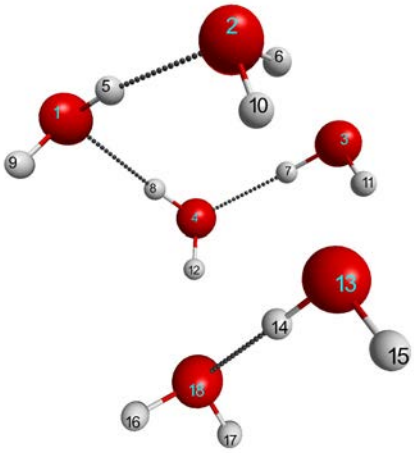

6w.2

Figure 1 continued

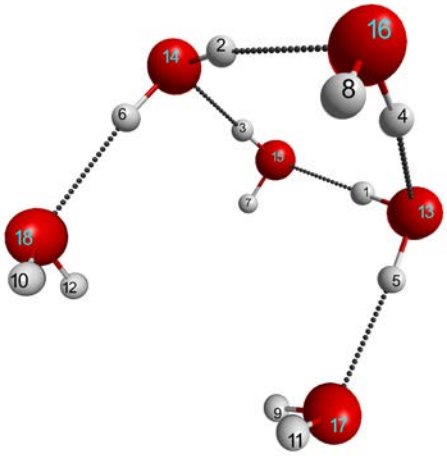

6w.3

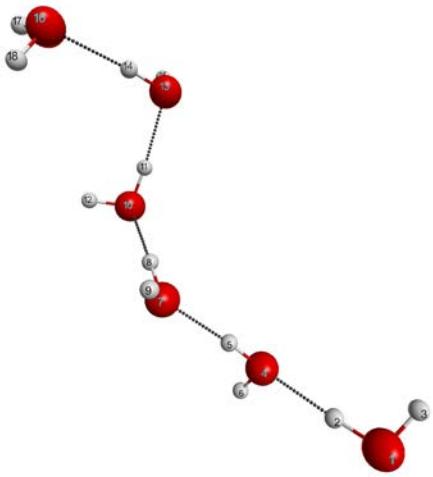

6w.4

Figure 1 continued

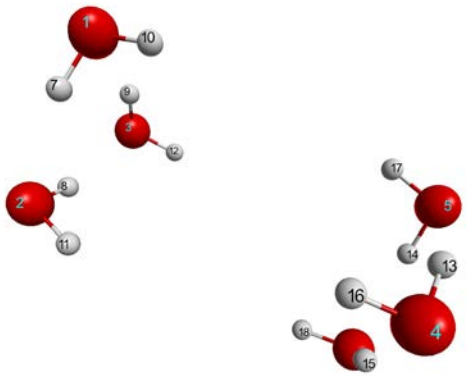

6w.5

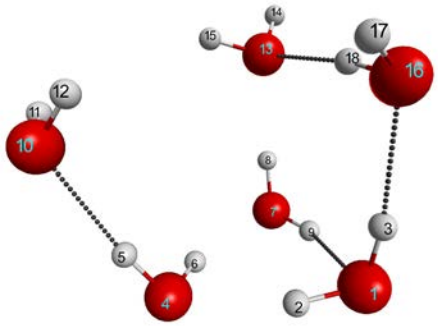

6w.b

Figure 1 continued

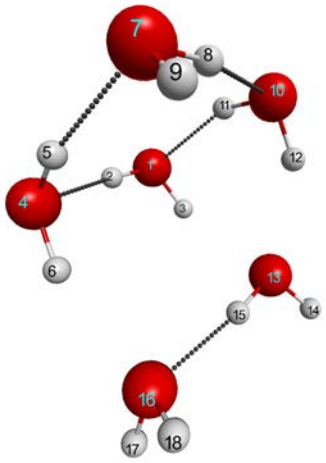

6w.e

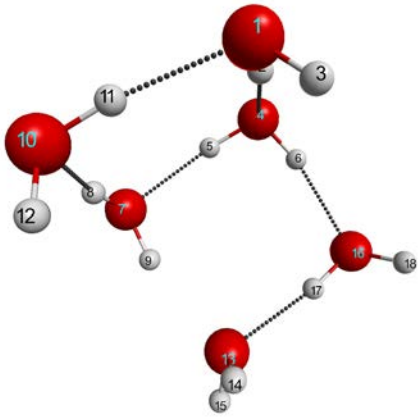

6w.f

Figure 1 continued

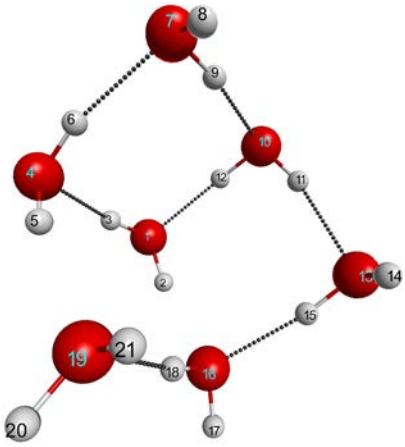

7w.a

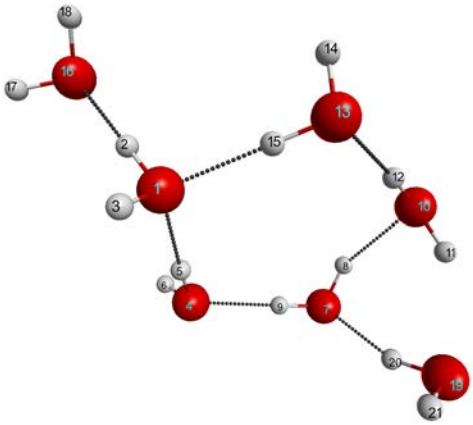

7w.b

Figure 1 continued

7w.c

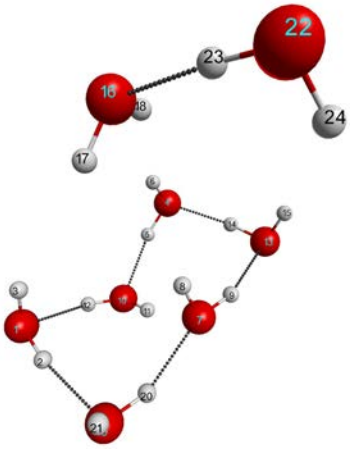

8w.2

Figure 1 continued

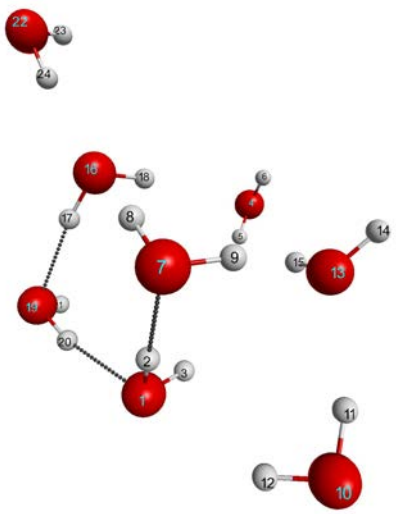

8w.4

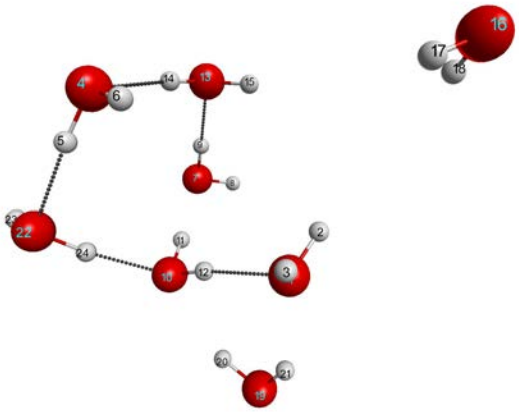

8w.5

Figure 1 continued

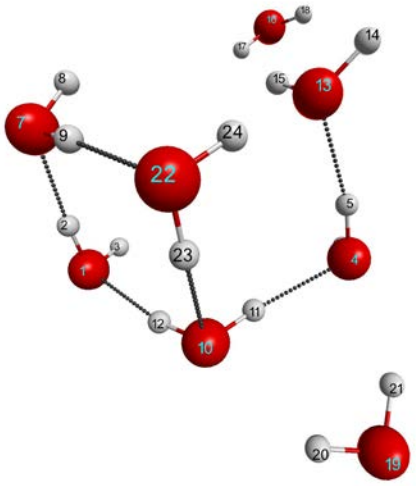

8w.6

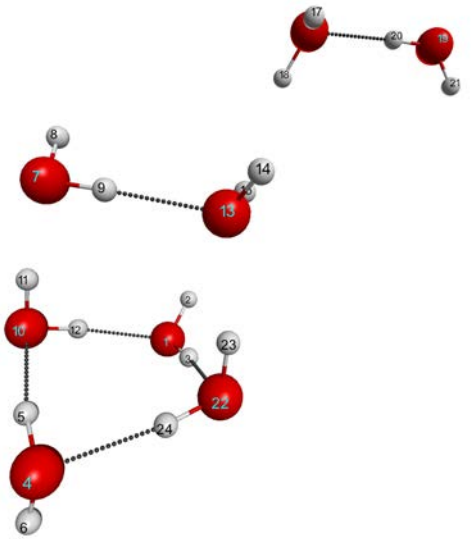

8w.7

Figure 1 continued

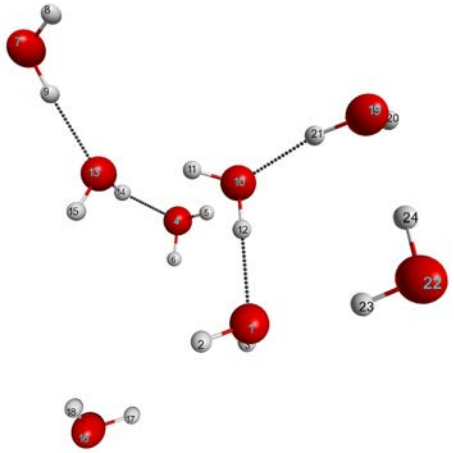

8w.8

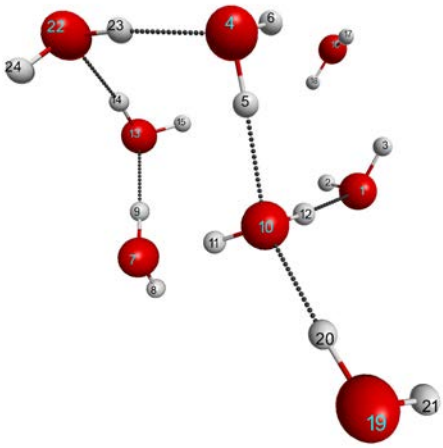

8w.9

Figure 1 continued

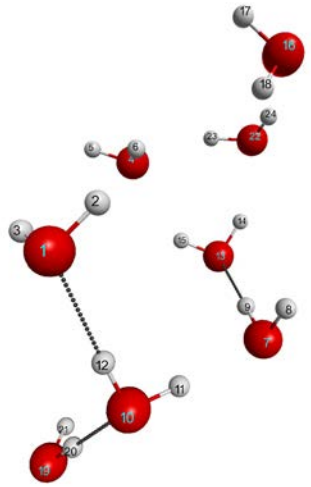

8w.10

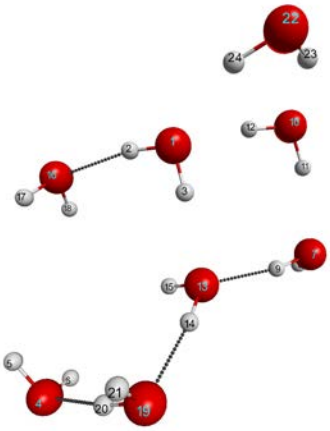

8w.11

Figure 1 continued

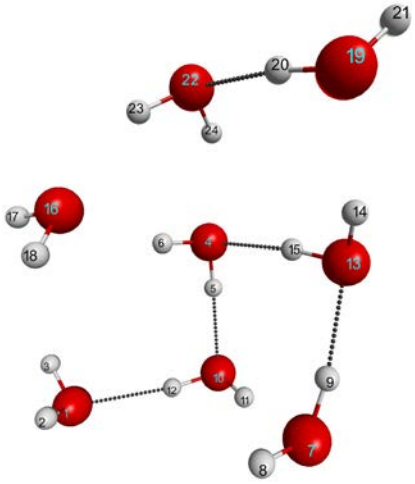

8w.12

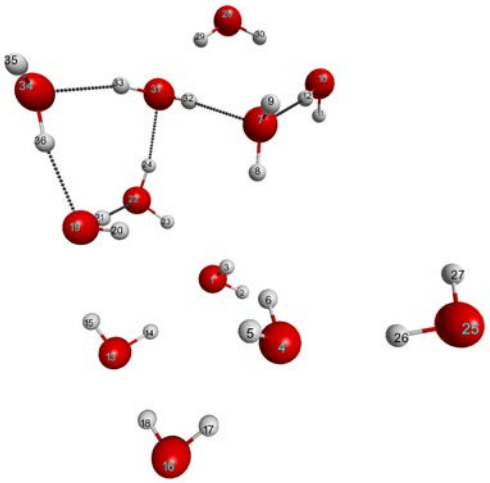

12w.1

Figure 1 continued

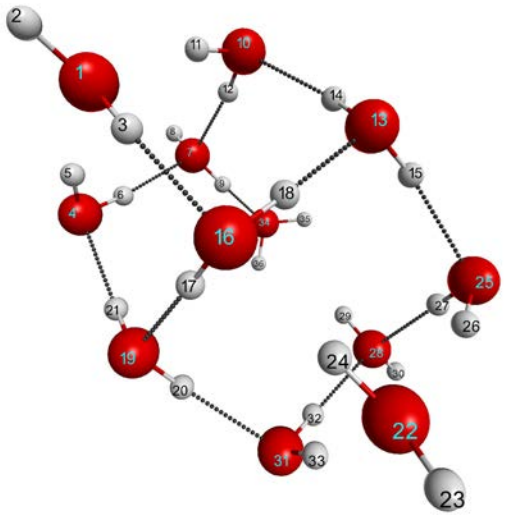

12w.a

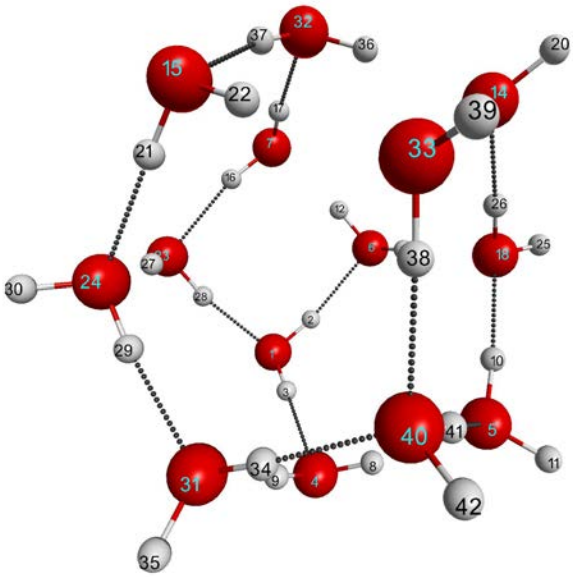

14w.a

Figure 1 continued

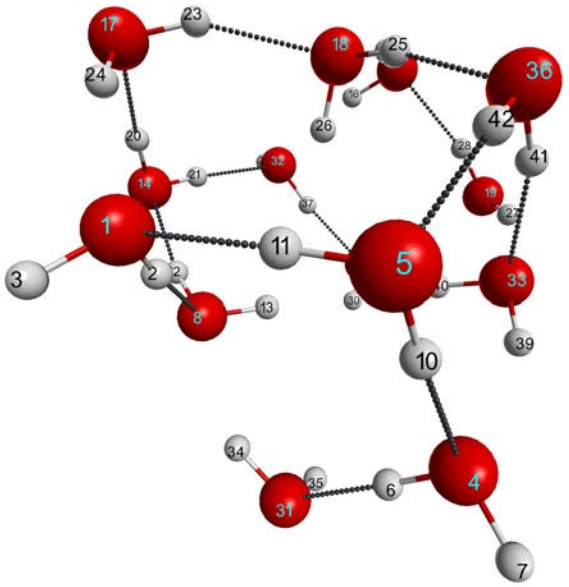

14w.b

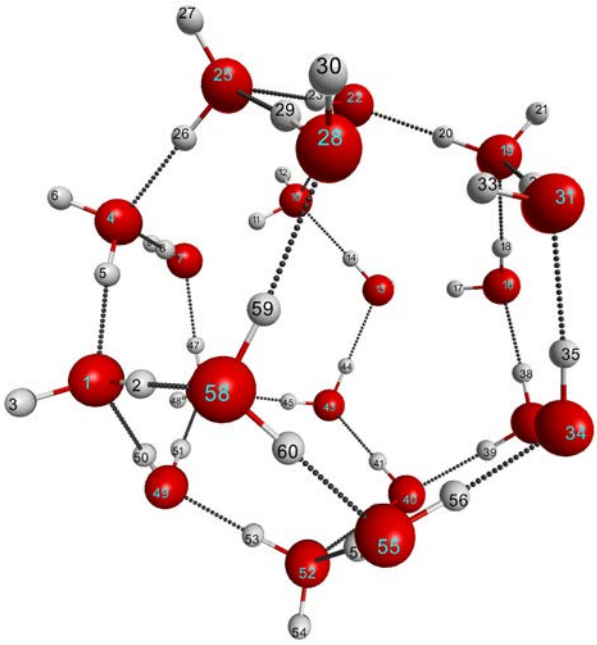

20w.a

Figure 1 continued

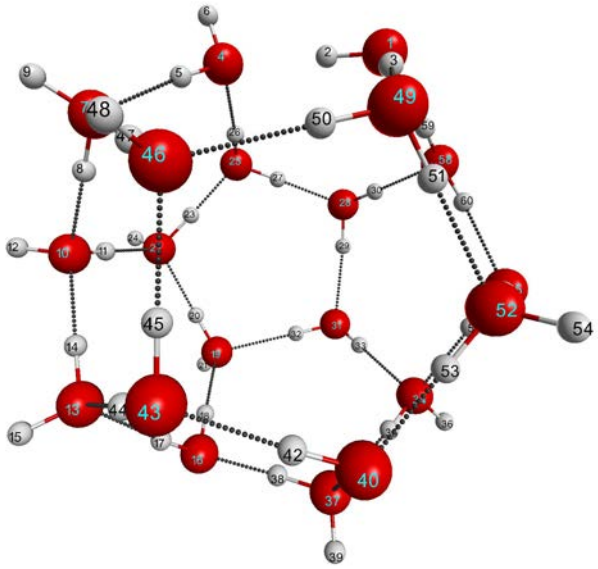

20w.b

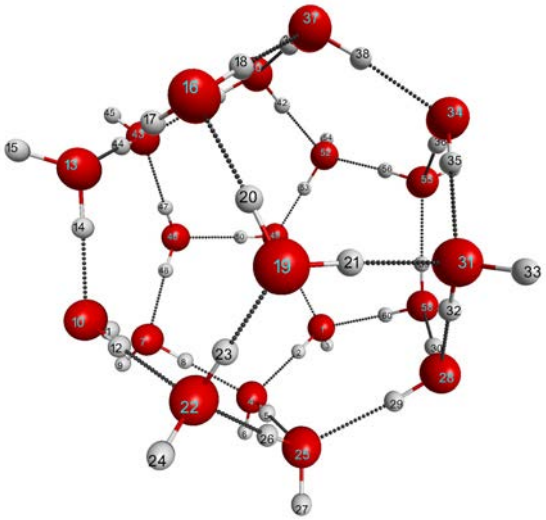

20w.c

Figure 1

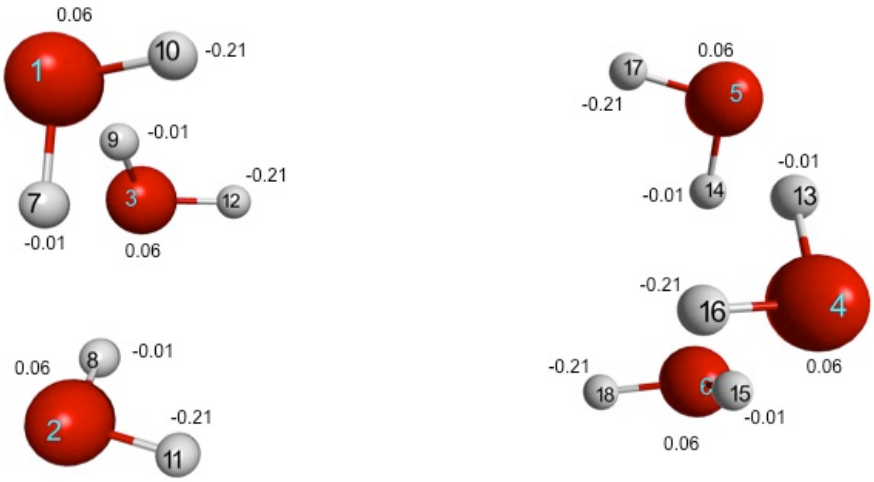

Figure 2(a)

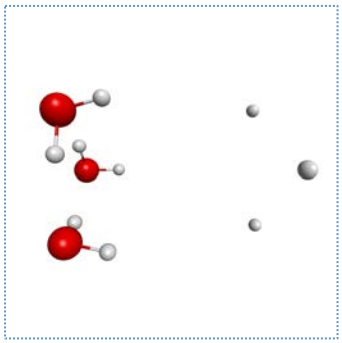

6w.5 subsystem 1

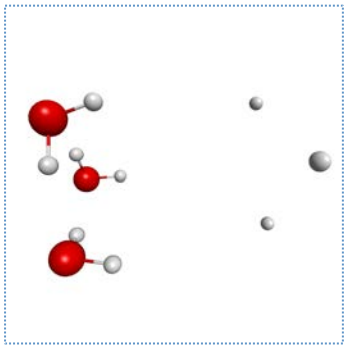

6w.5 subsystem 2

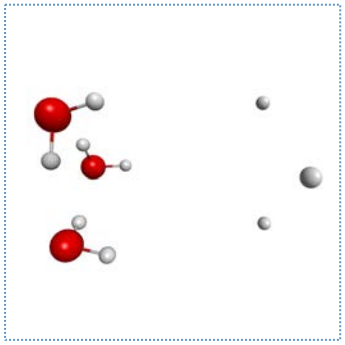

6w.5 subsystem 3

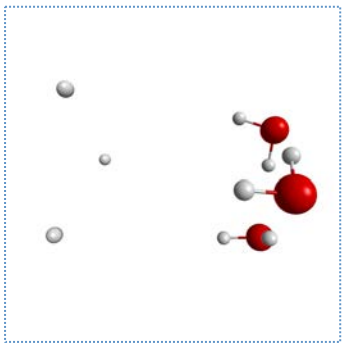

6w.5 subsystem 4

Figure 2(b)

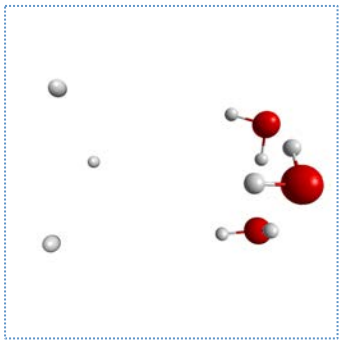

6w.5 subsystem 5

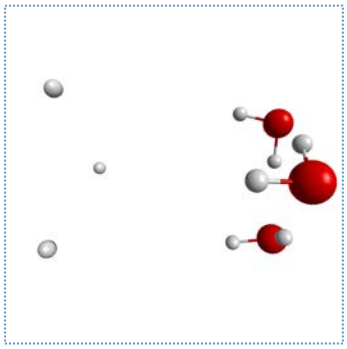

6w.5 subsystem 6

Figure 2(b) continued

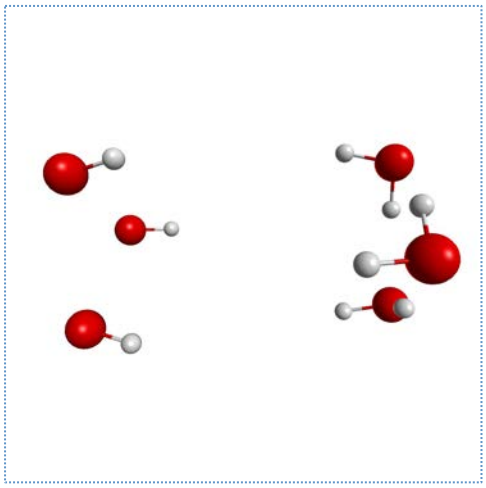

6w.5 subsystem 1

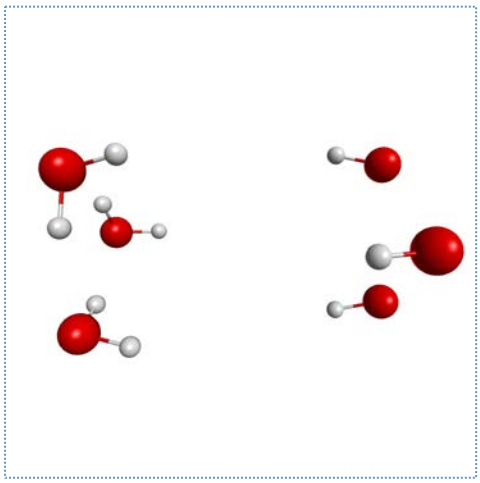

6w.5 subsystem 2

Figure 2(c)

CHAPTER 6 THEORETICAL STUDY OF THE BINDING OF SILANE (SiH_4) WITH BORANE (BH_3), DIBORANE (B_2H_6) AND BORON TRICHOLORIDE (BCl_3): THE ROLE OF CORE-ELECTRON CORRELATION

A paper published in

The Journal of Physical Chemistry A **2012**, *116*, 11668

Peng Xu, Mark S. Gordon, Binh Nguyen

Abstract

Equilibrium structures and energies of gas-phase molecular complexes SiH_4---BH_3, SiH_4---B_2H_6 and SiH_4---BCl_3 were determined using second-order Møller-Plesset perturbation theory (MP2) and the aug-cc-pVTZ basis set, with and without explicit core electron correlation. Single-point energies are calculated for the MP2-optimized structures using MP2 with the aug-cc-pVQZ basis set and using coupled-cluster theory (CCSD(T)) with both the aug-cc-pVTZ and the aug-cc-pVQZ basis sets to extrapolate to the complete basis set (CBS). Partition functions were calculated using the harmonic oscillator/rigid-rotor approximation at the MP2/aug-cc-pVTZ level of theory. The explicit core electron correlation is demonstrated to have significant impact on the structures and binding energies and binding enthalpies of these complexes. The binding enthalpies were obtained at various temperatures ranging from 0K to the dissociation temperatures of the complexes. The potential energy surfaces of the three complexes were explored, and no transition states were found along the pathways from separated species to the complexes.

Introduction

The chemical vapor deposition (CVD) technique is a process widely used in the semiconductor industry to produce thin films, in which source gas/precursor molecules are transformed into a solid on the surface of a substrate[1]. Silane (SiH_4) is a common precursor used in the CVD process due to its high volatility. Several boron compounds, borane (BH_3), diborane (B_2H_6) and boron tricholoride (BCl_3), are commonly used as precursors for the fabrication of boron doped thin films. At the initial stage of the CVD process, silane and boron-containing source gases interact through thermal initiation. Various chemical processes could occur, producing radical or charged species depending on the surrounding conditions. However, in this study, the processes of interest are the formation of the addition complexes:

$$SiH_4 + BH_3 \rightarrow SiH_4\text{---}BH_3 \qquad (1a)$$

$$SiH_4 + B_2H_6 \rightarrow SiH_4\text{---}B_2H_6 \qquad (1b)$$

$$SiH_4 + BCl_3 \rightarrow SiH_4\text{---}BCl_3 \qquad (1c)$$

In these processes, temperature can potentially influence the stability of both the reactants and the products, which in turn will affect the subsequent steps in the CVD process. Therefore it is crucial to understand the temperature effects on these binding processes.

The goals of this study are twofold: (1) To predict accurate structures and binding energies and binding enthalpies for the SiH_4---BH_3, SiH_4---B_2H_6 and SiH_4---BCl_3 complexes with high level *ab initio* methods and to determine how increasing the temperature affects the binding energies; (2) To explore the potential energy surfaces of these complexes along the formation pathway, in particular, to search for possible transition states. The binding energies ΔE_b are defined as the energy changes associated

with reactions (1). For example, for reaction (1a) $\Delta E_b = E(SiH_4\text{---}BH_3) - E(SiH_4) - E(BH_3)$, where E_x refers to the total electronic energy of species x. The binding enthalpies at 0K are obtained from $\Delta E_b + \Delta(ZPE)$ where ZPE_x is the zero point vibrational energy for species x, obtained using the harmonic oscillator approximation. Further temperature corrections, using standard methods, yield the corresponding binding enthalpies at the higher temperatures. For clarity, the absolute (positive) binding energies and enthalpies are quoted in this work.

The paper is organized as follows: the computational methods employed in this study are presented in Section II. In Section III, results and discussion are arranged to elucidate the results of the study. Conclusions are drawn in Section IV.

Computational Methods

The geometries of SiH_4, BH_3, B_2H_6 and BCl_3 were optimized using second-order Møller-Plesset perturbation theory (MP2) with the augmented correlation-consistent triple-zeta basis set (aug-cc-pVTZ). The geometries of the complexes $SiH_4\text{---}BH_3$, $SiH_4\text{---}B_2H_6$ and $SiH_4\text{---}BCl_3$ were optimized with the same level of theory and basis set. Harmonic vibrational frequencies for all the optimized species were evaluated to confirm that each molecular species is a genuine minimum on their respective potential energy surfaces. Single point energies were computed for these optimized geometries using coupled cluster theory with single, double and perturbative (non-iterative) triple excitations (CCSD(T)) using the same aug-cc-pVTZ basis set. The aforementioned calculations by default used the frozen core approximation that assumes the core electrons are inert during the electron correlation calculations.

To determine the importance of core electron correlation for the systems of interest, an identical set of calculations was carried out with all core electrons treated explicitly. Explicit core electron correlation generally adds a significant computational cost. The lowest-lying molecular orbitals (MOs) are expected to contribute very little to the relative energies and geometries of the molecular species in this study. Hence, in an attempt to reduce the computational cost while retaining accuracy, all of the calculations mentioned above were repeated with the Si 1s orbitals frozen. For BCl_3 and the SiH_4---BCl_3 complex the three Cl 1s orbitals were also frozen. Freezing more of the core electrons (the outer core) results in significant changes in the predicted geometries and relative energies. In addition, as a less computationally demanding alternative approach to describe the core electrons, Huzinaga's model core potential (MCP)[2] with the equivalent TZ quality basis was employed to optimize the geometries of all of the clusters and their components. In the MCP method, the core electrons are replaced by the MCP, which incorporates scalar relativistic effects. The valence electrons are described with the associated triple zeta basis set.

The binding energies and binding enthalpies obtained with outer core electrons included in the correlation part of the calculations are extrapolated to the complete basis set (CBS) limit at both the MP2 and CCSD(T) levels of theory. Both the HF reference energies and the correlation energies are extrapolated using two basis sets (two-point extrapolation), aug-cc-pVTZ and aug-ccpVQZ. Single point energies are computed with the aug-cc-pVQZ basis set at the TZ-optimized geometries. The two-point extrapolation formula of Karton and Martin[3] is used for the HF energies:

$$E(X) = E(CBS) + \frac{A}{X^{\alpha}}$$

α = 5.34 for the aug-cc-pVTZ/QZ pair.

The correlation energy extrapolation is accomplished using [4]

$$E_{corr}(X) = E_{corr}(CBS) + aX^{-3}$$

Using the vibrational frequency information to calculate the appropriate harmonic oscillator/rigid rotor partition functions, the binding enthalpies were calculated at different temperatures. To determine if barriers exist during the formation process, re-optimization of the geometries was started from separated components of the complexes (~ 5Å apart). The re-optimized complexes were compared to the original optimized structures. All calculations were carried out using GAMESS program[5].

Results and Discussion

The minimum energy structures optimized at the MP2/aug-cc-pVTZ level of theory with full explicit core electron correlation for all of the molecular species involved in this study are shown in Figure 1. It has been suggested that electron correlation is important in describing the binding of these complexes and that the Hartree-Fock (HF) method fails to predict the correct structure for the SiH_4---BH_3 complex[6].

Usually, core electrons are excluded from the electron correlation calculations, since most chemical phenomena involve only the valence electrons. Excluding the core electrons, i.e. frozen core approximation (FC), can save significant computational cost. However, in the present study, the core electron correlation is shown to play a key role in the prediction of both the Si--B distances and the binding energies and enthalpies of the three complexes. The geometries (Table 1) and binding energies (Table 2) of the SiH_4---BH_3, SiH_4---B_2H_6 and SiH_4---BCl_3 complexes exhibit significant differences, depending on whether or not core correlation is included in the calculations. For the SiH_4---BH_3

complex, including the core correlation causes a decrease in the Si---B distance by ~0.04 Å. This in turn results in an ~4 kcal/mol increase in the binding energy. Similarly for SiH_4---BCl_3, the shortening of the Si--B distance caused by the inclusion of core correlation, enhances the binding energy by nearly a factor of two. The effect of core electron correlation is most dramatic for the SiH_4---B_2H_6 complex. For this species, it was not possible to locate a minimum energy structure unless core correlation was included in the calculation. Indeed, the SiH_4---B_2H_6 complex is unbound at the CCSD(T)/aug-cc-pVTZ level of theory without the inclusion of core electron correlation.

In heavier elements like Si, it is likely that the "outer core" (i.e., 2s, 2p) electrons are more important for predicting properties than the "inner core" 1s electrons. This is referred to as the partial frozen core approximation (PFC) in this paper. Close inspection of MOs reveals that lowest MOs of SiH4 and BCl3 are essentially the Si 1s atomic orbital and Cl 1s atomic orbital with the orbital energies -68.77 and -104.86 Hartree, respectively. On the other hand, the lowest-lying MOs of BH_3 and B_2H_6 are largely boron in character and all higher than -10.00 Hartree. Therefore, one can consider freezing the electrons in the Si 1s orbital and Cl 1s orbitals during the electron correlation part of the calculation. The structures and binding energies that are obtained when the Si 1s core electrons and, in the case of SiH4 --- BCl3, also Cl 1s core electrons are not correlated are also listed in Tables 1 and 2. The resulting structures and binding energies demonstrate that the 1s electrons of Si and Cl play little role in the binding.

The MCP predicted Si--B distances in the three complexes lie in between those with and without the inclusion of core correlation, but more closely resemble the frozen-

core-approximation results. The same is true for the binding energies. Thus, the use of MCPs is not a viable alternative to including core correlation in the calculations.

Of the three complexes considered here, SiH_4---BH_3 is overwhelmingly the most strongly bound, with one silane hydrogen shared with the boron atom, forming a bridged structure. In fact, the B—H distance for this hydrogen (1.271Å) is shorter than the corresponding Si—H distance (1.636Å). The Si—H distance is ~1.472Å in isolated SiH_4 and the B—H distance is ~1.181Å in isolated BH_3. In the complex, one of the SiH_4 hydrogens is pulled and therefore elongated by the boron upon forming the bridged structure. The BH_3 is planar before binding and adopts a pseudo-tetrahedral geometry after binding to the SiH_4. After binding, the distances between silicon and the other three hydrogens in SiH_4 are hardly affected (the changes are less than 0.01 Å). The only noticeable change in the BH_3 bond lengths is that the distance between the boron and one of its hydrogens (#9 in Figure 1(e)) stretches from 1.1811 Å to 1.217 Å. This exceptionally strong interaction between SiH_4 and BH_3 may be due to the electron-deficient nature of boron, which frequently leads to bridging structures[7]. In contrast, in SiH_4---BCl_3, the electronegative chlorine atoms mitigate this tendency, thereby making the interaction between silane and boron tricholoride much weaker. The SiH_4---B_2H_6 complex exhibits the weakest binding, possibly due to the relative stability of the three-center two-electron bonds formed among the two boron atoms and two bridging hydrogens[8].

Extrapolation of the binding energies to the complete basis set

The binding energies of the three complexes are extrapolated to the complete basis set limit (CBS) at the MP2 and CCSD(T) level of theories. The results are presented

in Table 3. The 0K binding enthalpies at the CBS limit are computed using the MP2/aug-cc-pVTZ ZPE, assuming the ZPE changes little from aug-cc-pVTZ to the CBS limit. At the CBS limit, the SiH4 --- BH3 complex is still quite strongly bound with over 10 kcal/mol binding energy. The other two complexes exhibit similar binding strength differing by ~ 0.4 kcal/mol at the MP2 level of theory and 0.1 kcal/mol with CCSD(T).

Temperature effect on the binding energies

The binding enthalpies computed at MP2/aug-cc-pVTZ at various temperatures for the three complexes are plotted in Figure 2. The three curves show similar trends: a slight increase to a maximum binding enthalpy, followed by a monotonic decrease. The SiH_4---BH_3 complex binds most strongly at ~ 400K and remains bound until ~ 4000K. SiH_4---B_2H_6 and SiH_4---BCl_3 reach their maximum binding enthalpies between 50 K and approach dissociation at ~ 500K and ~1100 K, respectively.

Potential Energy Surfaces (PES)

To explore the potential energy surfaces of these complexes, MP2/aug-cc-pVTZ (including Si and Cl outer core correlation) optimizations were performed starting from the separated components of the three complexes (~5Å apart). In all three cases, the separated complexes fall back to the original minima found in this study with no barriers. It is interesting that SiH_4---BH_3 and SiH_4---B_2H_6 required tighter gradient convergence tolerance, which suggests that these two complexes have a relatively flat region near the minima on the PES. The fact that no transition states were found indicates that, at 0K, the kinetics of the binding processes between silane and the boron compounds studied in this project are diffusion-limited.

Conclusions

The equilibrium structures of SiH_4---BH_3, SiH_4---B_2H_6 and SiH_4---BCl_3 complexes were determined at the MP2/aug-cc-pVTZ level of theory. Explicit core correlation, in particular, the outer core, is shown to play a crucial role in predicting both the structures and binding energies and binding enthalpies for all three complexes. The binding energies and 0K binding enthalpies at aug-cc-pVTZ basis set agree very well with the single point CCSD(T)/aug-cc-pVTZ results, the most accurate method employed in this study. The binding energies and 0K binding enthalpies including explicit outer core electron correlation are extrapolated to the complete basis set at both the MP2 and CCSD(T) levels of theory. Using model core potentials provides only a small improvement over the frozen core results. The binding enthalpies of the three complexes were evaluated from 0K to the dissociation temperature of each complex. All three complexes exhibit a similar trend, in which there is a slight increase in the binding enthalpy followed by a monotonic decrease as the temperature rises. At 0K, there are no barriers for the formation of the complexes.

Acknowledgement

This work was supported by the Dow Corning Corporation. The authors sincerely thank Dr. S. Hu for providing some of the cluster structures as our starting point and greatly appreciate useful discussions with Drs. Laimis Bytautas and Federico Zahariev.

References

1. *Chemical Vapor Deposition*: *Principles and Applications*; Hitchman, M. L., Jensen, K. F., Eds.; Academic Press: London, 1993.

2. *Computational Chemistry, vol. 3,* Klobukowski, M., Huzinaga, S. and Sakai, Y., pp. 49-74 in J. Leszczynski, (1999)

3. A. Karton and J. M.L. Martin (2006) “Comment on: ‘Estimating the Hartree-Fock limit from finite basis set calculations’ [Jensen F(2005) Theor. Chem. Acc. 113:267]” Theoretical Chemistry Accounts **115**: 330-333

4. L. Bytautas and K. Ruedenberg (2005) “Correlation energy extrapolation by intrinsic scaling. IV. Accurate binding energies of the homonuclear diatomic molecules carbon, nitrogen, oxygen and fluorine” The Journal of Chemical Physics **122**,154110

5. M. W. Schmidt, K. K. Baldridge, J. A. Boatz, S. T. Elbert, M. S. Gordon, J. J. Jensen, S. Koseki, N. Matsunaga, K. A. Nguyen, S. Su, T. L. Windus, M. Dupuis, and J. A. Montgomery, J. Comput. Chem. **14**, 1347 (1993); M. S. Gordon and M. W. Schmidt, in *Theory and Applications of Computational Chemistry, the First Forty Years*, edited by C. E. Dykstra, G. Frenking, K. S. Kim, and G. E. Scuseria (Elsevier, Amsterdam, 2005), pp. 1167.

6. Hu, S. W., J. Kim, et al. (2002). "Insights into the nature of SiH4-BH3 complex: Theoretical investigation of new mechanistic pathways involving SiH3• and BH4• radicals." Journal of Physical Chemistry A **106**(29): 6817-6822.

7. Hu, S. W., Y. Wang, et al. (2003). "Gas phase reactions between SiH4 and B2H6: A theoretical study." Journal of Physical Chemistry A **107**(10): 1635-1640.

8. Longuet-Higgins, H. C., Bell, R. P. (1943). “The structure of the Boron Hydrides” J. Chem. Soc. 250-255

Figure 1. Equilibrium structures of (a) SiH4, (b) BH_3, (c) B_2H_6, (d) BCl_3, (e) SiH_4---BH_3, (f) SiH_4---B_2H_6 and (g) SiH_4---BCl_3 at MP2/Aug-cc-pVTZ with all the core electrons explicitly included in the electron correlation calculation.

Figure 2. Binding enthalpies of (a) SiH_4---BH_3 (b) SiH_4---B_2H_6 (c) SiH_4---BCl_3 at different temperatures with all the core electrons treated explicitly.

Figure1

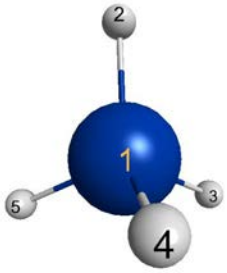

(a) SiH_4

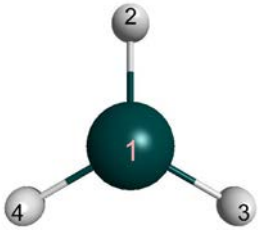

(b) BH_3

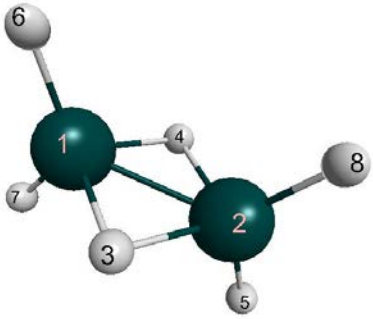

(c) B_2H_6

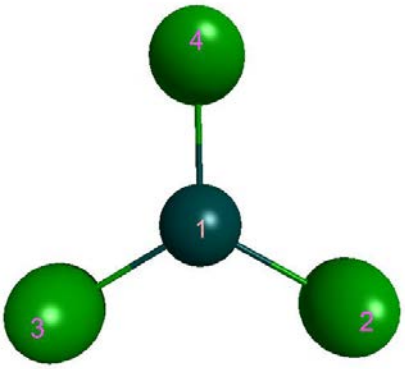

(d) BCl_3

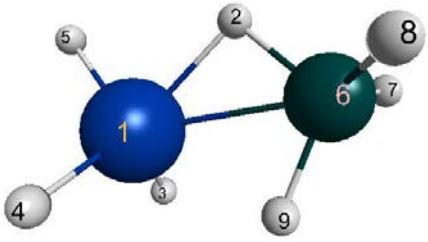

(e) SiH_4---BH_3

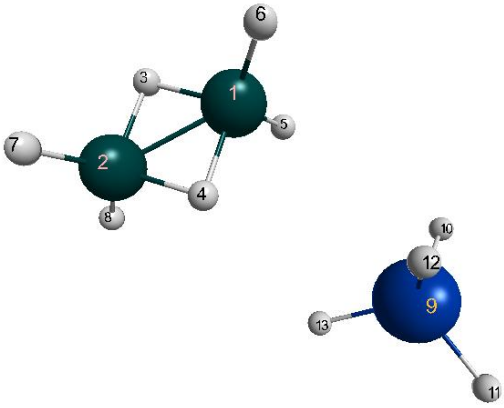

(f) SiH_4---B_2H_6

Figure 1 continued

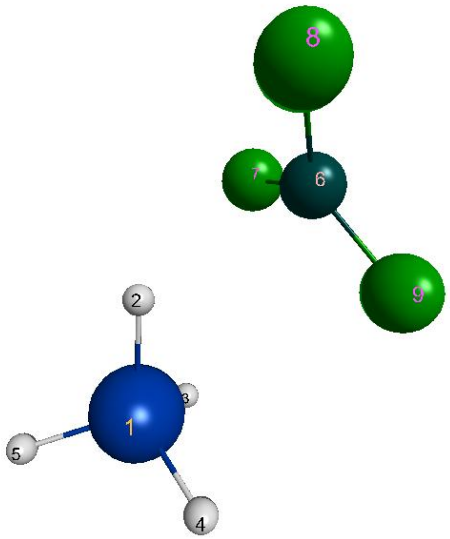

(g) SiH_4---BCl_3

Figure 2

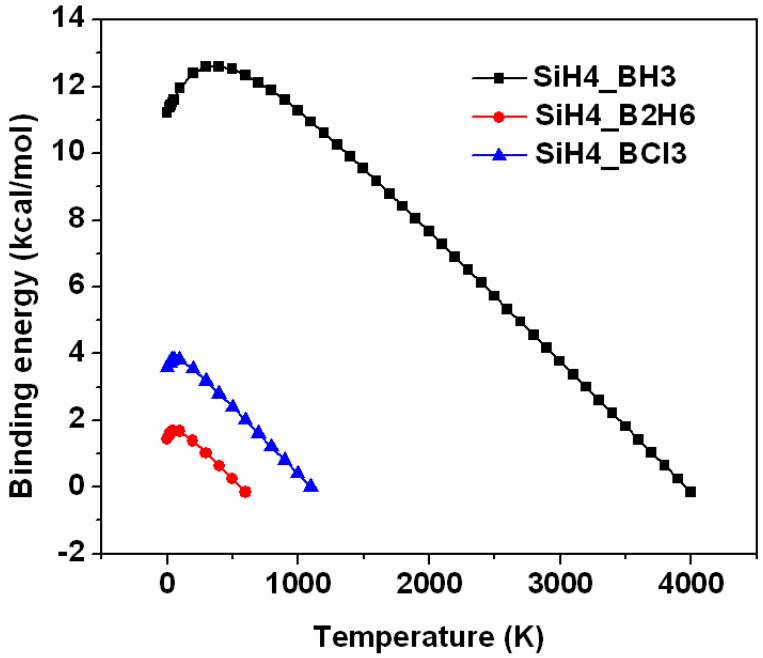

Figure 2 continued

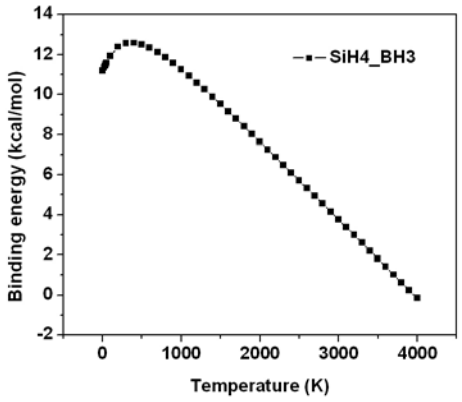

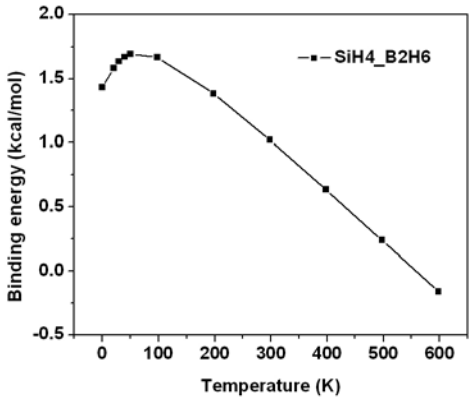

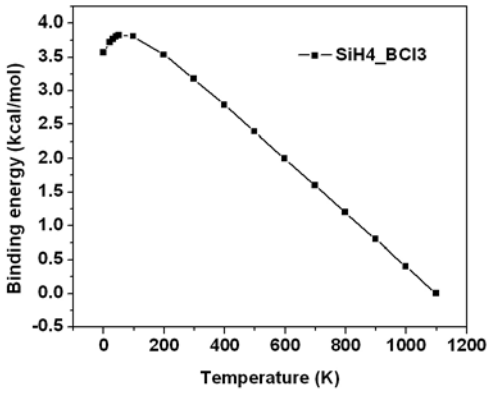

Table 1 Si---B distances for the optimized complexes. The columns from left to right are in the order: all electrons (including all core electrons) are treated explicitly; the lowest-lying core electrons (partial frozen core approximation) are frozen; all core electrons are frozen (frozen core approximation) and core electrons replaced by model core potential. For SiH_4---B_2H_6, both Si---B distances are shown. All the distances are in Å.

Si---B distance	Full core correlation	Partial frozen core approximation	Frozen core approximation	Model Core Potential
SiH_4---BH_3	2.138	2.139	2.179	2.159
SiH_4---B_2H_6	3.624, 4.434	3.624, 4.440	3.908, 4.377	3.738, 4.568
SiH_4---BCl_3	3.601	3.605	3.782	3.713

Table 2 The binding energies (kcal/mol) and 0K binding enthalpies (in parentheses) for SiH_4---BH_3, SiH_4---B_2H_6 and SiH_4---BCl_3 complexes calculated at MP2/aug-cc-pVTZ. The fourth and fifth columns show the binding energies and 0K enthalpies obtained if the partial frozen core or frozen core approximations are invoked, respectively. The binding energies obtained using MCPs are in the last column.

Binding Energy (kcal/mol)	MP2 aug-cc-pVTZ (full core correlation)	CCSD(T) aug-cc-pVTZ (full core correlation)	MP2 aug-cc-pVTZ (partial frozen core)	MP2 aug-cc-pVTZ (frozen core)	Model Core Potential
SiH4 – BH3	15.9 (11.2)	14.8	15.8(11.1)	11.9 (7.3)	11.0
SiH4 – B2H6	2.2 (1.4)	2.2	2.1(1.4)	Fails to locate a minimum	1.3
SiH4 – BCl3	4.4 (3.6)	4.1	4.3(3.5)	2.4 (1.7)	3.2

Table 3 The binding energies (excluding ZP corrections) extrapolated to the CBS limit for both MP2 and CCSD(T) levels of theory. In both cases, the partially frozen core results are used for the extrapolation. The 0K binding enthalpies are in parentheses.

	MP2 Partial Frozen Core	CCSD(T) Partial Frozen Core
SiH4 --- BH3	13.1 (8.5)	11.9 (7.3)
SiH4 --- B2H6	1.7 (1.0)	1.7 (1.0)
SiH4 --- BCl3	2.1 (1.3)	1.6 (0.8)

CHAPTER 7 CONCLUSION

The body of this dissertation is dedicated to the study of various types of intermolecular interactions in the framework of the effective fragment potential method (EFP). Localized molecular orbital (LMO) plays a central role in EFP, as well as the other fragmentation methods, cluster-in-molecules (CIM), employed in Chapter 5 of this dissertation.

The projection of the quasiatomic minimal-basis-set orbitals (QUAMBOs) onto the SCF virtual space selects a 'chemically important' subset of the full virtual space called valence virtual space. Diagonalization of the Fock matrix in this much smaller valence virtual space gives rise to the valence virtual orbitals (VVOs). Accuracy-wise, the EFP charge transfer (CT) energies obtained by using the occupied MOs + VVOs are generally as accurate as those obtained with full virtual space. The 'quasiatomic' attribute of QUAMBOs makes the CT energies much less dependent on the choice of basis set. Because the number of QUAMBOs is identical to the number of minimal-basis MOs of a molecule, the computational cost for CT energy and gradient are dramatically reduced.

The R^{-7} term in the dispersion expansion is developed in the framework of EFP formulated with Cartesian polarizability tensors over imaginary frequencies. The formulation is developed both in terms of molecular and LMO polarizabilities. The contrast between the R^{-7} dispersion term (E7) and R^{-6} dispersion term (E6) is very great: E7 is highly anisotropic while isotropic approximation for E6 is fairly good. E6 is always attractive while E7 can be either attractive or repulsive. Although E7 has a rotational average of zero, its importance should not be underestimated for solid-phase structures

and constrained reactions. The difference between the dispersion energies calculated with molecular and LMO polarizabilities is a manifestation of different expansions of the interaction operator truncated at a finite order. By comparing E6+E7 values with benchmarking symmetry-adapted-perturbation-theory (SAPT) dispersion energies, it is concluded that the dispersion expansion is not converged and at least the next term in the expansion, R^{-8} term, should be added.

The exchange repulsion Fock operator (V^{XR}) is derived by taking the variational derivative of the exchange repulsion energy between *ab initio* molecule and EFP potential (QM-EFP). The QM-EFP V^{XR} is added to the *ab initio* Fock operator during the self-consistent field iterations. The current implementation of QM-EFP V^{XR} and E^{XR} allows the presence of more than one EFP fragments. The agreement between QM-EFP and RVS exchange repulsion energies is within 4 kcal/mol for small clusters. The fully analytic gradients of QM-EFP energies with respect to both *ab initio* atom and EFP centers have been derived and implemented.

Currently EFP can only deal with closed-shell systems. The user makes the decision about the fragmentation when generating EFP potentials (MAKEFP). Each molecule in the system is typically treated as one EFP fragment.

Anionic water clusters $\left(H_2O\right)_n^-$, finite analogs of the solvated electron, are open-shell systems with rather diffuse excess electron density. Such systems are usually extremely difficult to deal with by fragmentation methods (a benzene ring should not be fragmented due to its delocalized π cloud). Moreover, the complexity of the potential energy surfaces of $\left(H_2O\right)_n^-$ grows rapidly. CIM, a local correlation approach, in

combination with CR-CC(2,3) provides a 'black-box' type calculation for $(H_2O)_n$. The CIM fragments are defined through LMO domains rather than atom domains. By reducing the threshold parameter ζ to 0.001 as a trade-off between accuracy and computational cost, CIM/CR-CC(2,3) approach can predict the vertical electron binding energies with the RMS error ~ 2.34 kcal/mol. The cluster size that can be studied by CIM/CR-CC(2,3) is significantly increased compared to full *ab initio* calculations with the same basis set.

Equilibrium structures and binding energies of gas-phase molecular complexes, SiH_4---BH_3, SiH_4---B_2H_6 and SiH_4---BCl_3, were determined using second-order Møller-Plesset perturbation theory (MP2) at aug-cc-pVTZ basis set. It was realized that the core electrons, especially outer core electrons, play a crucial role in predicating the structures and binding enthalpies for all three complexes. There are no transition states found for all three complexes at 0 K along the pathway of complex formation. The binding enthalpies of the three complexes were evaluated from 0 K to their respective dissociation temperatures. The binding enthalpies of all three complexes increase slightly followed by a monotonic decrease as the temperature rises.

As much as fragmentation approaches are advocated in this dissertation, it is important to realize the shortcoming and limitation of the approach. Approximations of different severity are applied to both the Hamiltonian and the wave function. Of course even the so called *ab initio* methods contain approximations. It is important to distinguish approximations and fitting: approximations are based on mathematical or sensible physical/chemical arguments while fitting is empirical even if the process of obtaining the fitted parameters is systematic. An extremely important attribute of EFP that

separates it from many other model potentials is that there is no fitting and all the terms are derived from first-principle with truncated expansions. Consequently EFP can be improved systematically, not through *ad hoc* attempts (e.g. the R^{-7} dispersion term is a systematic improvement). Another more subtle point is that clearly defined approximations allow users to decide whether a method can be applied to a specific system, e.g. EFP would not be employed for the SiH_4---BH_3 complex since the intermolecular interactions between core orbitals of different molecules are considered tiny and are neglected in EFP.

ACKNOWLEDGMENT

I would like to thank my family for all of their support throughout my life. Especially I would like to thank my parents for financially supporting my undergraduate studies in Australia and also supporting my decisions in life. Without their love and support, I would not be who I am today.

I would like to express my gratitude for my advisor Prof. Mark S. Gordon for guidance and support throughout my graduate years. I am very grateful to all the Gordon group members, both past and present, from many of whom I have learned a lot. I especially would like to thank Dr. Mike Schmidt and Dr. Federico Zahariev for many insightful discussions.

Last but not least, my special thanks to my husband, Dapeng, who has made my life complete.

This work was performed at the Ames Laboratory under contract number DE-AC02-07CH11358 with the U.S. Department of Energy. The document number assigned to this thesis /dissertation is IS-T 3117.